The University Of Sheffield.

Providing predictable and optimised traction and braking through tribo-chemical understanding of the wheel / rail interface

Thomas Reuben Kempka

Supervised by Professor Roger Lewis

A thesis submitted in fulfilment of the requirements for the degree of
Doctor of Philosophy

The University of Sheffield
Faculty of Engineering
Department of Mechanical Engineering

September 2019

Abstract

The chemical, physical, and tribological features of the wheel / rail contact are studied through a combination of environmental monitoring, chemical analysis, rheology, and tribo-testing. The work presents novel platforms for the combined analysis and physical testing of rail steel surfaces and oxide pastes, including friction mapping of surfaces, which have clear use in wheel / rail contact research as well as wider applications. X-Ray Diffraction identified eight iron compounds including iron oxides and iron oxide-hydroxides on the surface of operational rail-tracks. Trackside environmental monitoring revealed variation in conditions due to shaded areas and presence of vegetation. The railhead temperature is shown to lag behind that of the environment and occasionally below the dew point temperature; this is shown to happen most frequently in the early morning and can be related to the frequency of low adhesion events. A low adhesion condition was linked to the presence of wüstite, iron oxide-hydroxides, and small amounts of dew on the railhead. A newly proposed mechanism for the loss of traction due to oxides and debris on the railhead, in combination with small amounts of water, is supported by rheological and twin-disc tribo-testing which considers the extent of material entrainment as well as effect within the contact. Aqueous oxide pastes are shown to exhibit behaviours of Bingham-plastic fluids displaying both solid and liquid properties. High yield shear stress pastes are more entrained in the wheel / rail contact. High viscosity pastes more effectively transmit tractional forces through their layer and decrease the coefficient of traction less as a result. Results from the work provide new insights into how the surface of the railhead changes with environmental conditions as well as how oxide/water mixtures interact within the wheel / rail contact, including potential uses of viscous high shear stress pastes to control traction levels.

Acknowledgements

I graciously acknowledge the funding provided by the University of Sheffield Mechanical Engineering Department and LB Foster Rail Technologies (UK) Ltd. which made this doctorial project possible.

I would also like to express special thanks to my supervisor, Professor Roger Lewis, for their guidance and support which have proved invaluable to me throughout my studies.

Contents

1 Introduction

Railways play a significant role in the transport sector both in United Kingdom and internationally.

In 2015 approximately 62 billion passenger km were travelled on the UK rail network [1] and, in 2013, 21 billion tonne kilometres of freight where hauled on the UK rail network [2].

Rail transportation has distinct economical, technical and environmental advantages over other transport modes. Compared with road transport, rail can be economically competitive, significantly less energy and carbon intensive, and safer [3, 4].

Between the years of 2002 and 2014 the UK railways have seen a 70% rise in the number of passenger journeys [1]. This is expected to increase along with the use of the network for freight [2] as the demand for the railways continues to grow.

Control of adhesion is critical to the safe and effective operation of a railway because, for most railway vehicles, all the traction and braking forces are transmitted though the wheel / rail contact.

There are numerous benefits to making adhesion more reliable and predictable and it is important to ensure that levels are balanced for operation. If the coefficient of friction is too high, the loads applied at the contact are transmitted close to the rail surface and can lead to plastic shakedown – or a process known as 'ratchetting', if the ductility of the material is exhausted – which causes high wear rates, crack initiation and high costs for the operator [5]. If too low, braking and traction may be impaired leading to poor performance and safety issues.

Low adhesion events can also lead to unacceptable levels of wear on the railways. Loss of traction when driving leads to wheel spins which cause significant damage to the rail and when braking can lead to the wheels locking up and flattening of the profile. Wheel flats require re-profiling which is expensive and time consuming for the operator.

Infrastructure improvements achieving additional capacity for both passenger and freight operations is central to managing the UK rail infrastructure with greater traffic volume being increasingly demanded of existing railway lines. Network Rail's control period 6 Enhancements Delivery Plan (2019) sets out many strategies and projects to increase capacity as well as provide faster & more frequent services [6]. These changes put pressure on the accelerating and braking duty of the trains. By managing and providing predictable adhesion levels, the safety of the railways may be improved, fewer delays caused, journey times reduced, and there be less Signals Passed at Danger (SPAD) and station over-run incidents.

1.1 The wheel / rail contact

The wheel / rail contact is extremely complex and understanding the system is of great importance to effective operation of railways. The contact patch, where the weight of the vehicle is supported, as well as driving and braking forces are transferred, is typically $1cm^2$ in area per wheel [7]. Pressures in this region are usually within the range of 0.8-3GPa and typically are greater for freight rolling stock which tend to carry heavier payloads. A representation of this contact area is shown in Figure 1 for a typical wheel / rail contact where the contact is between the wheel tread and railhead.

Figure 2 shows three general positions that the wheel make take on the railhead which may vary depending on the curvature profile of the track; these may change the geometry of the contact. On straight track or high radius curves, position B is normal with positions A and C only experienced on tight curves.

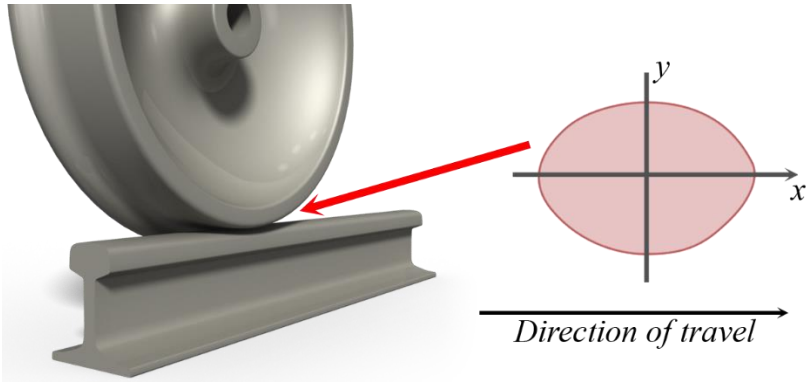

Figure 1, Representation of the wheel / rail contact geometry, presenting area of contact between the surfaces (red)

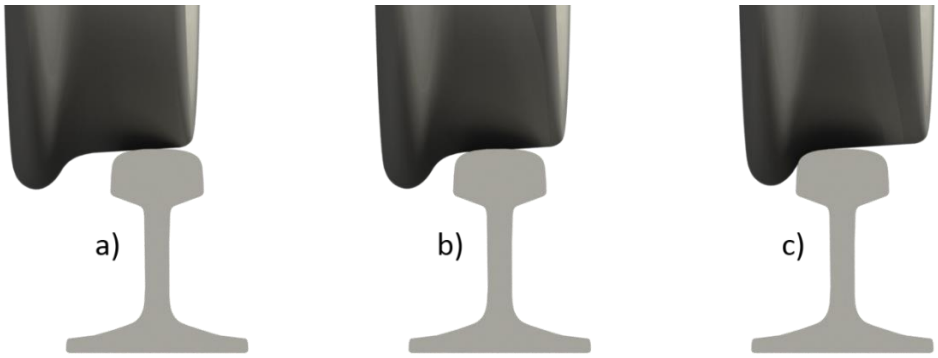

Figure 2, Wheel / rail contact positions: a, between the field side of wheel and rail; b, between the wheel tread and rail head; c, between the wheel flange and rail gauge corner

'Adhesion' in railway technology has a different meaning to the wider field of Tribology. Adhesion of a railway locomotive quantifies the forces applied at the wheel / rail contact as the ratio of tractive or braking forces (*F*) to the normal load (*N*). The coefficient of adhesion definition covers sliding, rolling, as well as rolling-sliding contacts. The adhesion coefficient (μ) is given as:

$$\mu = \frac{F}{N} \tag{1}$$

The wheel / rail interface can be classified as a 'rolling-sliding' contact. The contact between the wheel and the rail is divided into 2 regions: stick and slip. The longitudinal forces of traction and braking occur due to the slip that occurs in the trailing region and the relative areas of each vary depending on the force applied at the contact as can be seen in Figure 3.

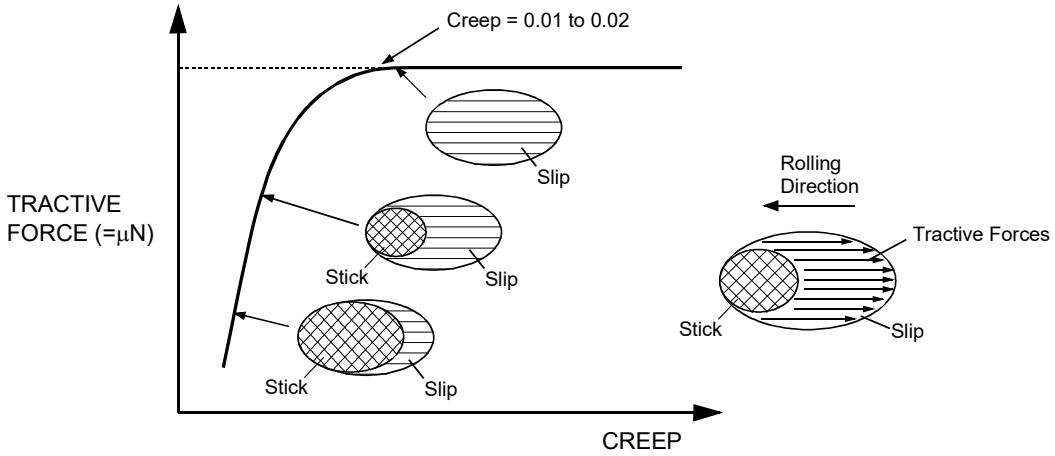

Figure 3, Creep curve and slip-stick contact diagram [5]

An important parameter to consider when defining the contact is 'creep', γ. This quantifies the relative speed of the surface of the wheel to the rail (sliding velocity, V_{slide}) as a fraction of the velocity of vehicle travel ($V_{vehicle}$):

$$\gamma = \frac{V_{slide}}{V_{vehicle}} = \frac{\omega_w r_w - V_{vehicle}}{V_{vehicle}} \quad (2)$$

where ω_w and r_w are the angular velocity and radius of the wheel respectively.

Under pure rolling, no tangential forces are transmitted by the contact and there is negligible creep. As the slip increases with the amount of tangential force, the tractive force reaches a saturation value where the entire contact is in the sliding region and transmitting force. This condition is typically reached at creep levels of 1-2% after which it falls due to thermal effects. The relationship can be seen on a creep curve which plots the traction force against the creep in the contact, an example creep curve (dry contact) is shown in Figure 4 and the condition of the contact illustrated in Figure 3.

The maximum level of traction able to be transmitted by the contact patch is taken as the coefficient of adhesion for that system and can be determined from the creep curve; exemplified in Figure 4 where it is shown to be 0.58.

Good levels of adhesion are in the regions of 0.3 – 0.35; operating with coefficients of adhesion in this range is said to not impact on driving or braking requirements [8]. In a study of adhesion on the British railway network the adhesion on rails was found to vary between 0.04 and 0.55, averaging around 0.3 in reasonably dry conditions [9].

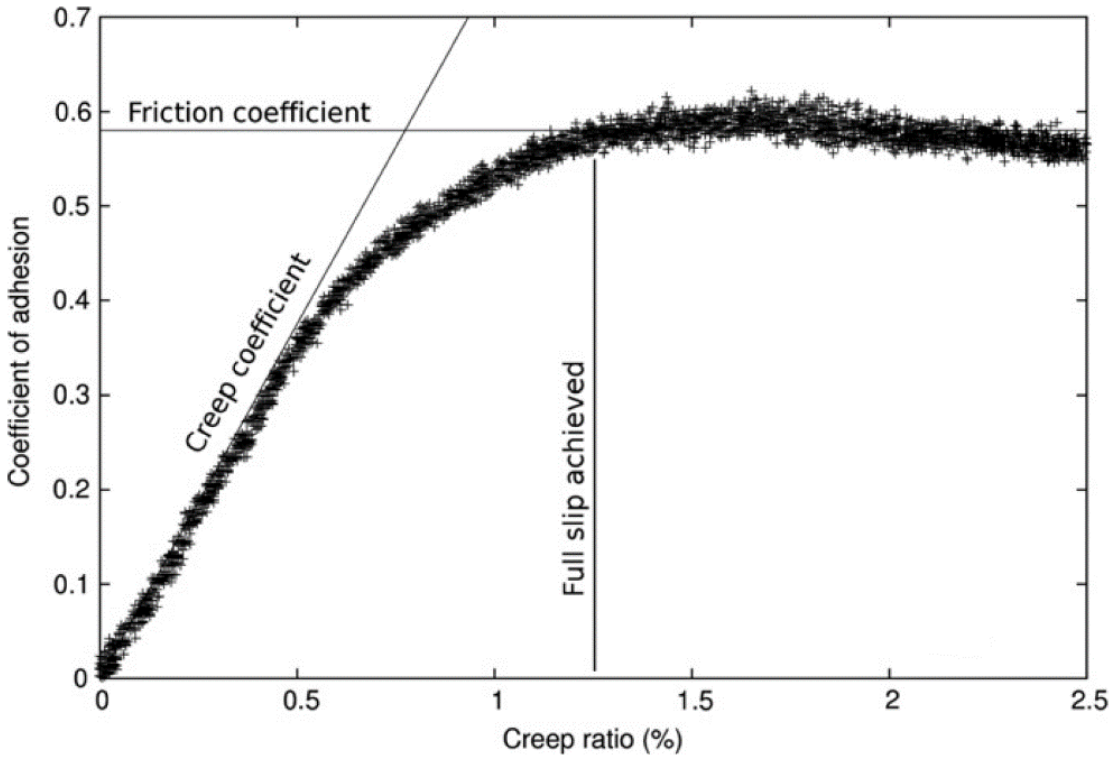

Figure 4, Example creep curve from twin-disc testing [10]

The following levels of adhesion levels are typically defined as [11] and are referred to within this thesis as such:

- Medium low: $0.10 < \mu < 0.15$
- Low: $0.05 < \mu < 0.10$
- Exceptionally low: $0.02 < \mu < 0.05$

The wheel / rail contact, in contrast to most other mechanical contacts, is an open system meaning that the interfaces are exposed to the wider trackside environment. Additional substances which may become present in the contact mix with wear particles to form a third body layer at the interfaces [12].

The third body layer is used to generalise the analysis and effects of contaminants in the interface. The layer has been categorised as either natural – caused by naturally existing materials like dirt, leaves or water – or artificial, where substances are purposefully added to the contact such as sand, grease or friction modifiers.

Third body thicknesses of 150µm to 200µm have been observed on wheels taken out of service and thicknesses around 15µm were observed on the rail; however, these figures are expected to vary considerable because of wide variations in the open environment of the wheel / rail system [13]. Descartes et al. [13] have also shown that the third body layer is capable of adsorbing and digesting certain solid and fluid contaminants, leading to complex rheological behaviour and very different friction values.

Traction has been shown to be both enhanced and diminished by the presence of other compounds in the wheel / rail contact as well as the environment the system is contained within. Traction effecting conditions are broadly grouped into the following: water, snow, ice and dew; oils and greases; iron oxides / rusts, inorganic materials / rocks; and leaves.

1.2 Traction management in the rail industry

Traction of railway locomotives has been managed since at least 1836 [14] in the form of sanders which apply sand to the rail in front of the driven wheels or into the contact. Such devices are widely used in the modern day, often alongside active control systems such as electronic traction control, but there are now a much wider variety of methods for managing traction.

In addition to sanding, there are other mitigative strategies to manage traction such as cleaning the rail surface which replenishes the surface and potentially removes the cause of low adhesion. A similar approach to sanding is also used in the form of traction gels which consist of hard sand-like particles in a gel suspension which is applied directly to the railhead and achieves a similar effect of increased adhesion. It must be noted that not all traction management of the railway aims to increase the available traction. Friction modifiers may be used to either increase or decrease friction and are typically used to reduce wear or noise but may include particles in the same way as the traction gels to increase traction.

Methods for the prevention of low adhesion are less understood and utilised by the rail industry than sanders although trackside management, such as ensuring a minimum distance between any lineside vegetation and the track, has been shown to be effective at combatting low adhesion caused by leaves. Chemical treatments of the railhead aiming to disrupt the formation of low adhesion conditions are in their infancy, primarily for the prevention of leaf layers, but how they function as well as their effectiveness is yet to be validated. The use of hydrophobic and hydrophilic compounds to disrupt other mechanisms of traction loss have been investigated but are also

uncertain as to their effects. It is clear from the wide variety of suggested chemical treatments that the mechanisms of traction loss are not well understood and research towards understanding these mechanisms can be of great value in the development of novel abatement strategies.

1.3 Approach and objectives

Managing traction and understanding low adhesion is of great importance to the railway industry to make passenger and freight operations safer and increase operating performance. It is therefore important to not only study the effects of conditions on traction, but identify the mechanisms by which traction is lost to allow both the prediction of problematic traction conditions as well as advancing knowledge to lead towards prevention of such conditions.

To narrow the wide scope of what is the open system of the wheel / rail contact, the research will focus primarily on iron oxides; however, throughout the study, other compounds will be discussed where relevant as it may be that the presence of numerous compounds causes synergistic effects on traction.

This study approaches the topics in three stages:

1. Understanding the railhead environment: The physical and chemical environment of railways is explored through environmental monitoring and chemical analysis to establish the environment experienced by the system which lead to both the formation of low adhesion areas and the conditions at the time of low adhesion events.
2. Iron oxide groups: A deeper analysis of iron oxide groups is performed to investigate how they form as well as their physical, rheological, and chemical properties.
3. Tribo-chemical properties: The effect of iron oxides and oxidation on the wheel / rail system is examined through various scaled experiments and using a full-scale wheel / rail rig to determine the mechanisms at play which affect traction properties.

The objectives of this study are to:

- Understand how conditions of the railhead lead to the formation of different oxide types on the railhead.
- Understand how environmental conditions at the trackside effect the wheel / rail conditions during train operations.
- Determine the mechanisms by which the presence of different types of iron oxides effect the available traction between the wheel and rail, as well as the magnitude of these effects.

1.4 Chapter Overview

This thesis is composed of 10 chapters, after the introduction the content of each chapter is outlined here as follows:

2. Literature review

A literature review was assembled to explore current knowledge related to low adhesion in the wheel / rail contact. The main topics include: the third body layer, documented causes of low adhesion, test methods, numerical models, and abatement methods.

3. Chemistry of the railhead

A comprehensive review surrounding the chemical make-up and formation of compounds generally found on the railhead. Organic and inorganic substances and their structures and chemical

components are identified. Known surface interactions between the chemical species identified and the surface of the railhead are studied including surface chemistry and organo-metallic interactions.

4. Hypotheses

Several hypotheses for the formation of low adhesion conditions as well as the mechanisms of traction loss are presented in this chapter.

5. Methodology

This chapter presents the design of experimental rigs, procedures, and equipment used in this thesis including novel railhead sampling and analysis techniques as well as a novel experimental procedure to produce friction mapping of surfaces.

6. Railhead analysis

Environmental monitoring around different features, sites, and seasons are performed to characterise trackside conditions. Railhead sampling and chemical analysis using X-Ray Diffraction identifies iron oxides present.

7. Synthesis and rheological properties of iron oxides

Iron oxides are synthesised on rail-steel substrates under laboratory-controlled conditions and their evolution examined visually as well as using X-Ray Diffraction and Scanning Electron Microscopy. The rheological properties of aqueous pastes of different oxide types and particle qualities are tested.

8. Tribo-chemical properties

The tribological properties of synthesised and deposited oxides are examined through a series of tribo-tests to assess how the oxides effect the wheel / rail contact. A UMT, pin-on-flat, tribometer was first used to perform a novel friction mapping technique and overlay friction maps onto sample surfaces. A twin-disc tribometer was used to explore the effect of oxide pastes of different types and concentrations in a rolling-sliding contact. Lastly, a full-scale wheel / rail contact rig was used for validation and confirmation of findings on a full-size contact, with some limitations.

9. Discussion

The discussion summarises the outcomes and findings of the work as well as proposes next steps for further understanding the formation of low adhesion conditions and mechanisms. Abatement strategies for low adhesion are suggested based upon the findings of the thesis.

10. Conclusions

Conclusions of the thesis are presented in this chapter and proposed further work is outlined.

2 Literature review

This chapter explores the wheel / rail contact through topics traditionally used to study the contact. These are: the properties of the third body layer, common causes of low adhesion, test methods for tribological as well as chemical analysis of the contact, some contact models for numerically simulating the traction coefficient, and abatement techniques.

A preliminary quantitative literature analysis is outlined to rank the current extent of research performed in topics within the scope of this work. The relevant literature is then presented.

2.1 Initial quantitative literature analysis

Initially, to identify the scope of low adhesion research as well as to guide the direction of thesis work, a quantitative literature analysis was performed to establish understanding of where there were gaps in current knowledge. The sources assessed were those published and available at the time, as of the first quarter of 2016. It must be noted that research has since advanced in these areas as outlined in the later sections of the literature review.

The papers were reviewed with regards to the extent research has been done relating to wheel / rail interface; where topics are covered that had not yet been applied to the wheel / rail interface this is reflected in their score. It must be noted that a low score does not indicate a poor-quality paper but rather that the topic has not been extensively explored in relation to low adhesion of the wheel / rail contact.

The categories explored were: causes, surface chemistry, test methods, numerical modelling and abatement. The scoring was standardised based on a rhetoric of 5 criteria in the form of “yes/no” questions as follows:

- Is the literature a peer reviewed publication?
- Is the theory in the source tested and supported by results?
- Are the conclusions in the work evidenced?
- Is a scale test used in the work?
- Is a full-size test used in the work (including railway operational data)?

Every ‘yes’ scores the source a point, these are summed to produce a final mark for the source. The literature is then graded and colour coded according to Table 1.

Table 1, Quantitative literature assessment scoring colour codes

Score	Rank	Colour Code
0 – 3	“Poor”	Red
4	“Average”	Orange
5	“Good”	Green

Each references’ number on the plot refers to its respective source listed in the references section of this report. Appendix A gives a template of the form used for the scoring and Appendix B provides a summary scoring table of the sources reviewed.

The graphical representation of the literature has been separated into the primary categories which cover different topics within the review. Figure 5 outlines the topic of causes, Figure 6 outlines the topics of test methods and numerical modelling and Figure 7 outlines the topics of abatement and surface chemistry.

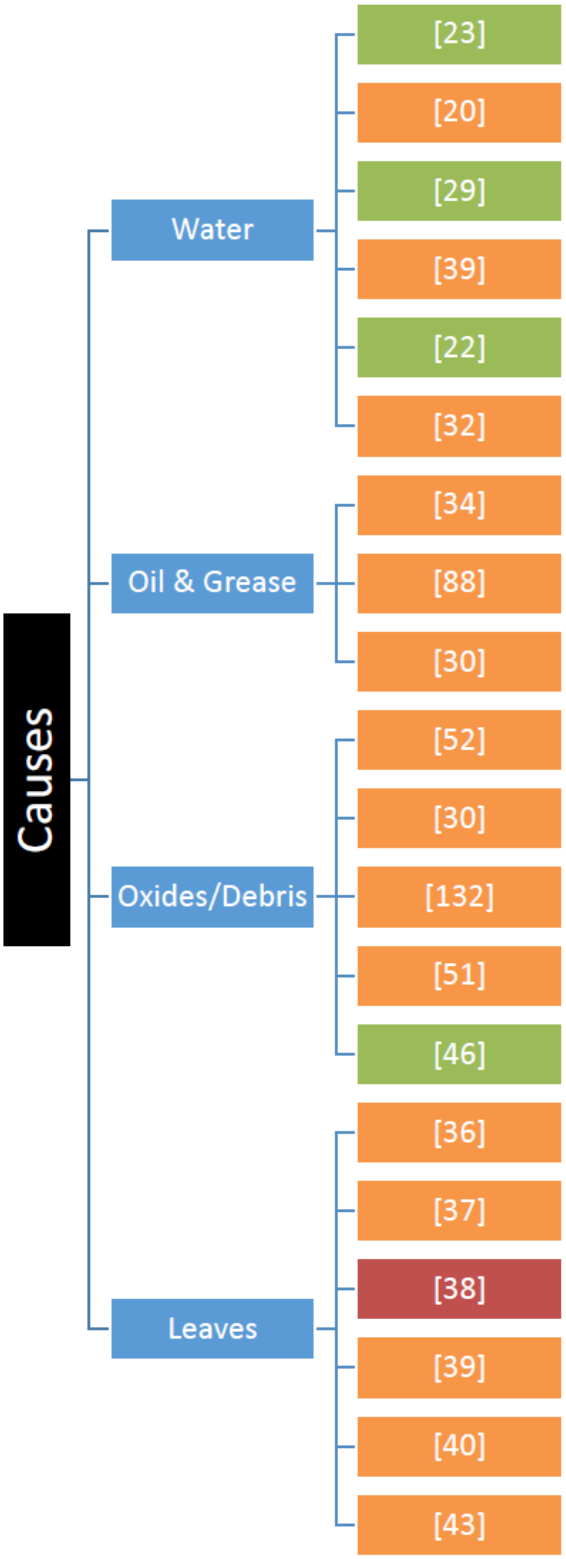

Figure 5, Quantitative literature map of low adhesion causes

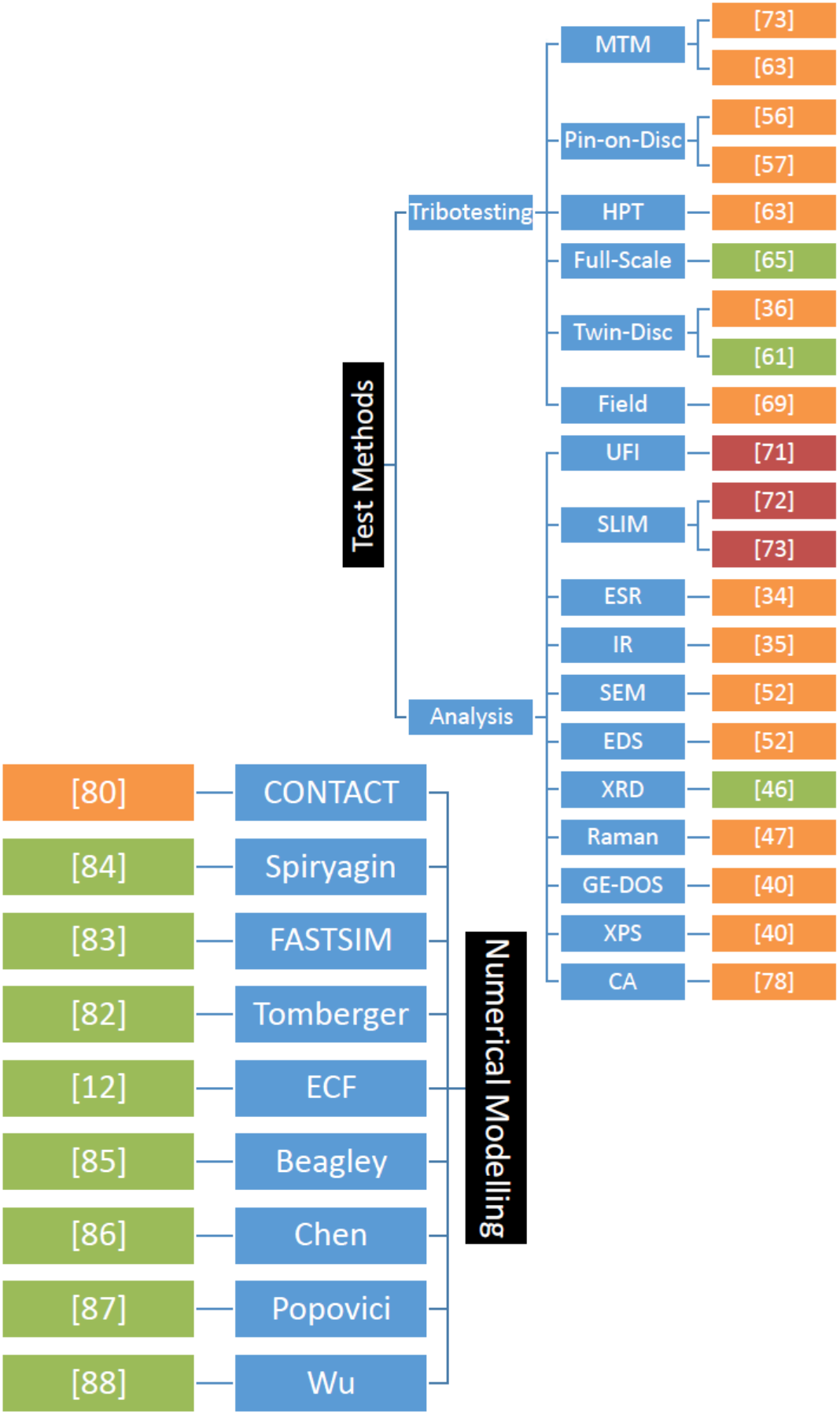

Figure 6, Quantitative literature map of low adhesion test methods and numerical modelling

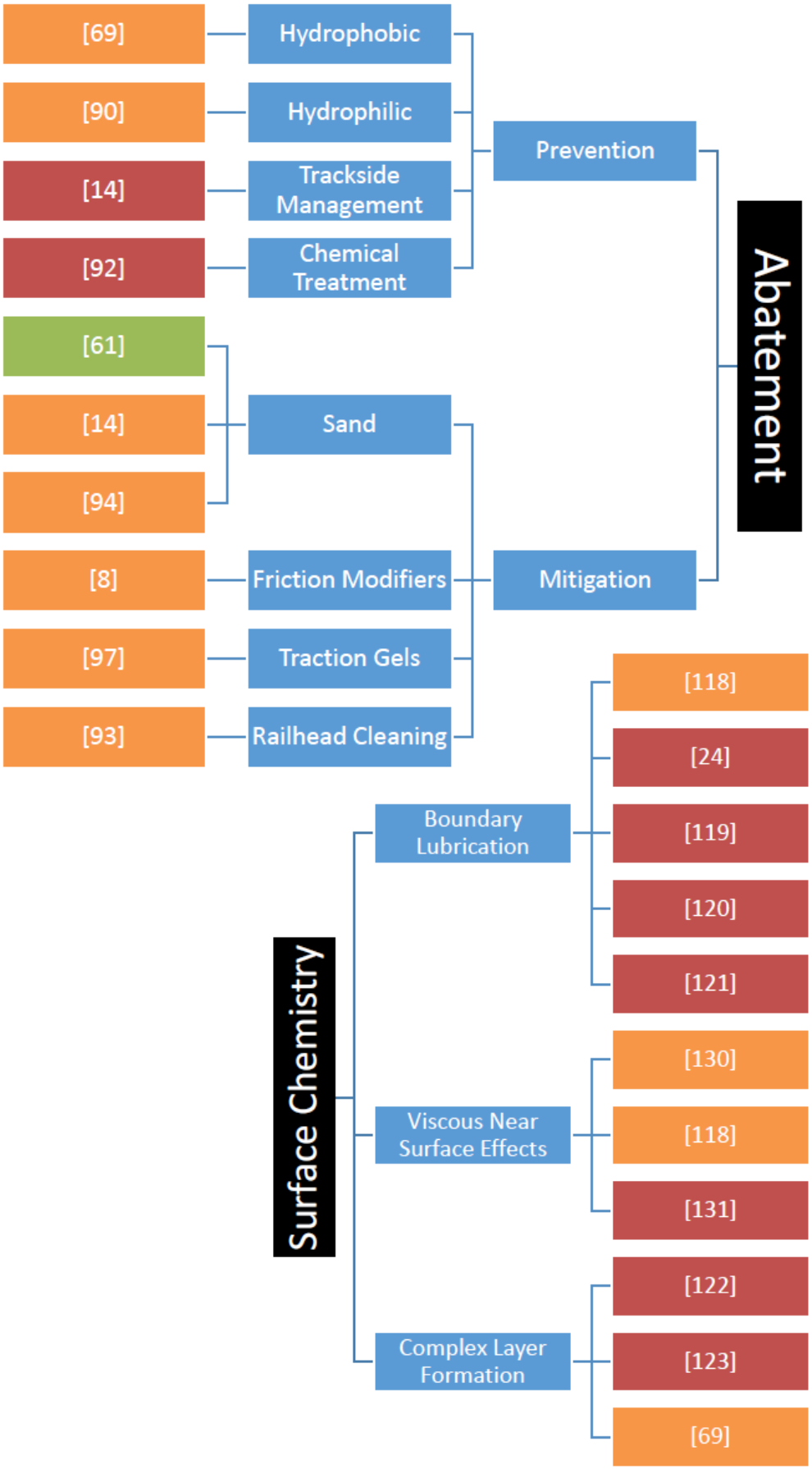

Figure 7, Quantitative literature map of low adhesion abatement methods and surface chemistry

From the quantitative literature analysis, it was revealed that water is a well-researched and established as a cause of low adhesion; it has been studied much in the laboratory and many of the smaller scale tests have been supported by full scale operating data. Oxides are also well-established as a cause of low adhesion, but less full-scale testing has been performed to understand them. Leaves as well as oil and greases both have many studies relating to them as causes of low adhesion; however, these studies frequently fail to incorporate either full-scale or operational data to validate lab-scale testing.

There had been various well-developed test methods for determining the tribological properties of the wheel / rail contact, most of which have been well validated with full scale tests. Powerful techniques for analysing the chemical and physical properties of the wheel / rail contact were seen; however, most of these had seen very limited use in studies.

The nine numerical models studied used underpinning experimental research as inputs into the models. Many of these models are validated with real operating conditions and most had validating test data for real operating conditions.

Techniques for the prevention of low adhesion were less researched and understood than mitigation; small scale tests have been performed but full-scale testing is generally lacking. Sanding is well understood as a mitigation method and many papers score excellent results for the quantitative literature analysis. Other mitigation techniques mainly lacked accessible supporting full-scale or operational data in the literature.

Most sources in the surface chemistry topics showed up as poor due to the lack of information directly relating to the topic of the wheel / rail interface and, as a result, it provides a gap and opportunity for future research in this area.

The largest gaps identified related to the chemical environment of the railhead, the contaminants present and the analysis in these areas. Chemical data, and the properties of these conditions had not been researched extensively with respect to the topic of the wheel rail contact; however, information of value may be obtained through applying other fields of study to the wheel / rail contact.

2.2 Third body layer

The wheel / rail contact, in contrast to most other mechanical contacts, is an open system meaning that the interfaces are exposed to the wider trackside environment. Additional substances which may become present in the contact mix with wear particles to form a third body layer at the interfaces [12].

The third body layer is used to generalise the analysis and effects of contaminants in the interface. The layer has been categorised as either natural – caused by naturally existing materials like dirt, leaves or water – or artificial, where substances are purposefully added to the contact such as sand, grease or friction modifiers. Its effect on adhesion is currently accounted for indirectly in dynamic railway models by a global wheel / rail friction parameter; however, this may be insufficient to account for local phenomena which may change the composition and physical properties of the layer [15].

In addition to friction modifying properties, electrical isolation of the wheel and the rails by the third body layer is a potential problem for track signalling which requires a good electrical contact between the rails to detect occupancy of the line, a process known as ‘shunting’ [16].

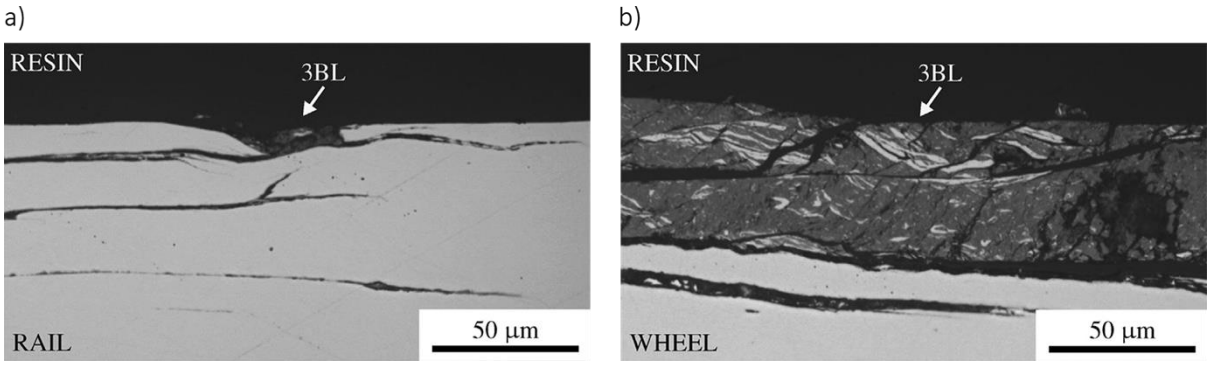

Figure 8, Optical analysis of the basic third body layer created on the rail (a) and wheel (b) discs by twin-disc experimentation [12]

Figure 8 shows a basic third body layer, consisting of particles stemming from the wheel and rail materials only, generated to observe its traction characteristics as well as analyse optically and through X-ray diffraction. The investigations revealed that the layer on the wheel formed up to 50µm thick made up of iron and iron oxide.

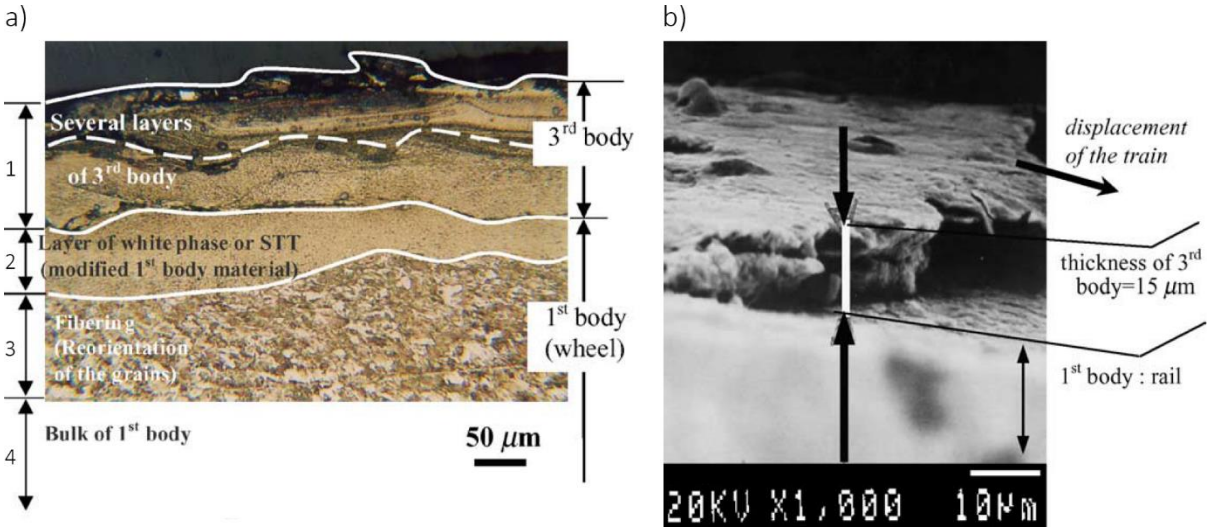

Figure 9, Third body layer of a locomotive wheel (a) and rail (b) [13]

Figure 9 is a similar analysis of the third body layers taken from a wheel and rail in service. Several layers are observed on the wheel to an overall third body thickness from 150µm to 200µm and a layer of 15 µm was observed on the rail surface which is far thicker than the surface roughness typically found on the wheel and rail. Descartes et al. [13] have also shown that the third body layer is also capable of adsorbing and digesting certain solid and fluid contaminants, leading to complex rheological behaviour and very different friction values.

Flows of the material in the third body layer have been studied in a paper by Berthier et al. [17] showing that material flows within the third body layer – described as 'local flows' – as well as flows of material into and out of the layer. The paper attempts to describe the influence of these flows on railhead traction and describes a third mechanism involving the removal and re-introduction of material into the third body layer or 're-circulation flow'. Due to the open system of the wheel / rail interface and the trackside environment, the third body layer is expected to be an extremely complex; even the material removal leading to wear debris and third-body particles is said to be one of the least understood areas in the field of tribology [18].

A more detailed review of common natural and artificial substances potentially present in wheel / rail system is provided in section 3 in the section on composition and formation.

2.3 Causes of low adhesion

The causes of low adhesion, for this review, have been divided into four sections: fluid lubricants, dry friction reducers, leaves, and oxides and wear debris.

2.3.1 Lubrication regimes: water, oils / grease

When two solids have direct contact with each other, without a separating layer, it is known as dry contact; in these conditions, the coefficients of friction are high ("dry friction"). However, in the presence of a fluid, lubrication occurs which can induce some form of hydrostatic or, when the surfaces are moving in relation to each other, hydrodynamic separation between the solid bodies [19]. Water in the wheel / rail contact has been shown to decrease the adhesion coefficient [20] and is found in abundance in the natural environment. Common sources include rain, drizzle (light rain), snow and dew. Other fluids have also been found in the trackside environment including oils and greases, which can cause similar effects, but most of the focus regarding fluid mechanisms in the wheel / rail contact have been based on studies of water in the contact.

Various lubrication regimes can exist in a contact depending on the system dynamics. The regime of lubrication can be determined from the Hersey number, *He*, given by:

$$He = \frac{\eta \cdot N}{P} \tag{3}$$

where: η = lubricant viscosity; N = relative sliding speed; P = normal applied load

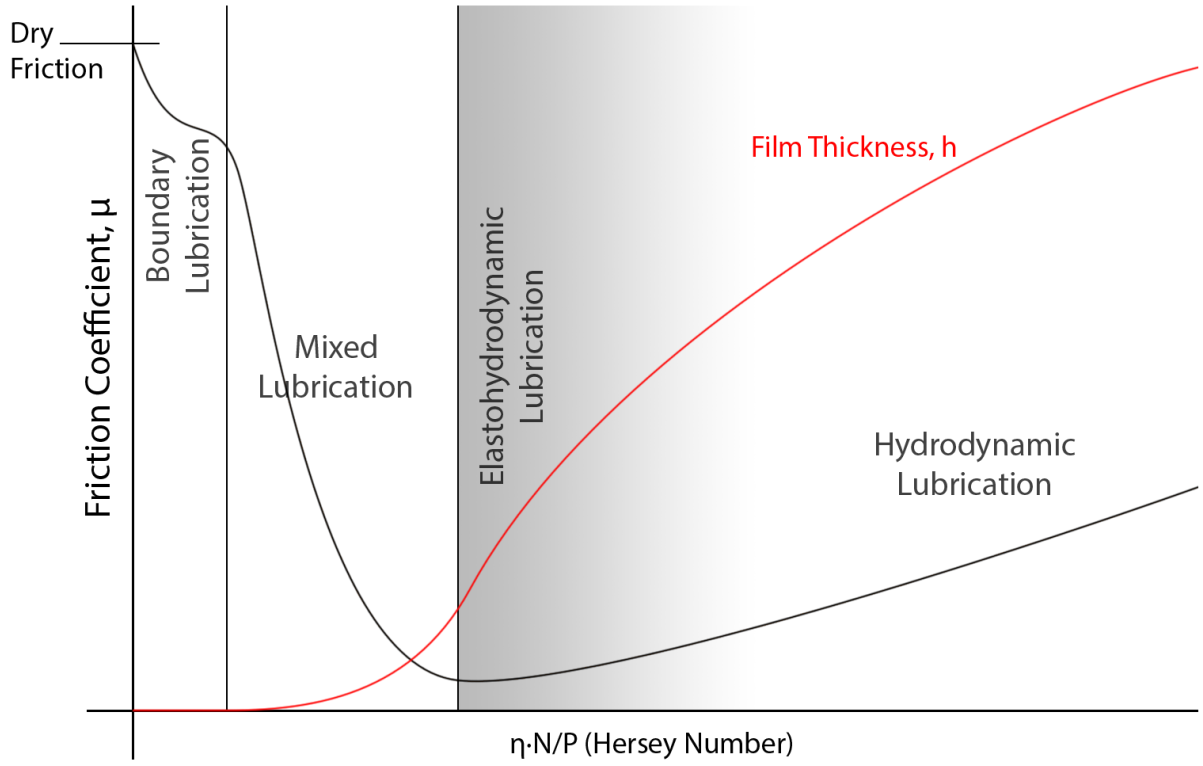

Figure 10, Stribeck curve showing lubrication regimes, adapted from Jan et al. [19]

The lubrication regimes can be found on the Stribeck diagram, shown in Figure 10, which plots the friction coefficient against the Hersey number. The effective lubricant thickness, *h*, is also plotted on

the diagram and shown to be proportional to the Hersey number. Four main lubrication regimes can be identified from the graph:

- Boundary lubrication – No liquid film is formed and the surfaces are in direct contact ($h \rightarrow 0$)
- Mixed Lubrication – The thickness of the formed film is approximately the same height as the surface roughness, R ($h \approx R$)
- Elasto-hydrodynamic lubrication (EHL) – The liquid film formed is marginally greater than the surface roughness ($h > R$) and there is full surface separation
- Hydrodynamic lubrication – The liquid film forms is much thicker than the surface roughness ($h >> R$) and there is full surface separation

At low Hersey numbers, the conditions are not present to permit the formation of a liquid film capable of significantly supporting the contacts, even partially, and is known as "boundary lubrication". In this regime thin molecular layers of substances on the surfaces are of great importance in determining the tribological conditions. Where there is incomplete coverage of a film in boundary lubrication, "dry contact" between the asperities of the solids may occur resulting in extremely high coefficients of friction.

As a fluid is entrained into a converging geometry a pressure is generated which forces the surface apart. This may cause separation if the hydrodynamic forces resulting from the pressure on the bodies is greater than the load applied to the components. This is known as hydrodynamic lubrication and, with complete separation, the frictional force experienced in these regimes results from shearing of the fluid between the surfaces. As the relative velocity of the surfaces increases the friction coefficient increases due to the higher shearing rates and thicker films of fluid being sheared between the solid surfaces [21].

Due to the great mass of railway locomotives and small contact area between the wheel and rail, it is generally accepted that significant or complete separation of the sliding bodies is not theoretically possible under the conditions; mixed or EHL models are typically used for simulating the contact under wet conditions [22, 23].

Elasto-hydrodynamic lubrication (EHL) is a special case of hydrodynamic lubrication which only becomes significant in specific conditions. EHL considers systems under extreme pressures and the phenomena expands the mechanism of hydrodynamic lubrication to include 2 additional factors:

- Variable viscosity
- Elastic deformation of solid surfaces around the contact region

These two phenomena allow components to be effectively lubricated by liquid film separation at far higher loads than hydrodynamic lubrication [24].

Hydrodynamic lubrication and EHL are associated with significant drops in friction coefficient due to complete surface separation by the lubricating film. Studies of rail adhesion do not report drops in traction coefficient with rolling speed to such a significant degree [25]; therefore hydrodynamic lubrication or EHL cannot be accountable. This is believed to be due to the high loads exerted on the small contact areas between the wheel and rail.

Mixed EHL (also known as 'partial EHL') refers to the regime between boundary lubrication and EHL. In this lubrication regime, the load is supported between the solid contact regions and the liquid film. EHL assumes that the surfaces are smooth but, in reality, the surfaces of the contacts are far rougher than the thickness of the liquid film that can be produced.

Mixed EHL contacts are usually modelled by integrating a statistical function accounting for the effects of surface roughness into EHL simulation – a concept known as load-sharing – which resolves both the asperities contacting with EHL and those directly contacting in boundary lubrication separately [26]. Mixed EHL is complex with various mathematical models developed to account for particular properties of the contact including the conformity of asperities between the surfaces [27, 28].

Authors have reported adhesion coefficients as low as 0.137 [20], 0.082 [29] and 0.2 [30] being achieved by the application of water alone on twin-disc testing rigs. Operating conditions of these rigs are around 17 tonnes of load or 1500MPa at 1% slip. The lower adhesion values of these tests are reported at high rolling speeds ($25ms^{-1}$) and the higher values at low rolling speeds ($1ms^{-1}$).

Lower values of adhesion have been achieved in similar experiments, but it should be noted that even in laboratory experiments, the nature of tribological testing inherently makes maintaining clean testing environments extremely difficult and therefore the testing of water contamination alone is unlikely. Oxides will always be present in the contact when there is water present.

At higher rolling speeds on studies utilising railway operational data from the Japanese Shinkansen high speed network, lower adhesion coefficients were also observed [31, 22]. The results are shown in Figure 11, a mixed lubrication regime model was used to estimate the adhesion coefficients at different speeds based upon boundary friction coefficients determined through twin disc experimental results (0.2 and 0.45). As the real operating case will have lower boundary friction coefficient due to additional contamination, the model over-estimates the adhesion coefficients. It should be noted that the Shinkansen network is an exceptional case due to very high rolling speeds and very smooth contacts making; therefore, it is more likely to experience hydrodynamic effects.

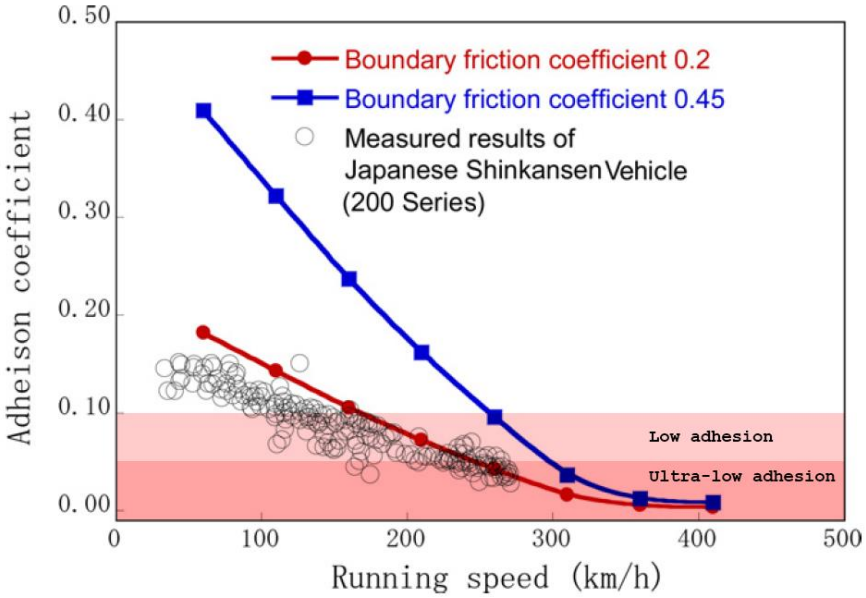

Figure 11, Wet condition adhesion coefficients plotted against the running speed for a mixed lubrication model and operating measurements [22]

Dry contact tests have also been shown to exhibit the same behaviour of decreased adhesion with increasing rolling speed and slip [20], but to a much lesser extent with its effect on adhesion only becoming significant past speeds of $300km.h^{-1}$ [32]. This is however, likely due to thermal effects resulting from increased slip in the contact which occurs at higher speeds.

The higher the temperature of the water, the greater the coefficient of adhesion [31, 22]. This relationship – which is possibly a result of falling viscosity – as well as the relationship with rolling speed, suggest that water can act to lubricate the wheel /rail contact in the mixed lubrication regime if the right conditions prevail.

Comparison of these results found in the literature has limitations due to different testing parameters and the amount of control which is possible to exercise in the gathering of the data, both in the field and lab; however, research into the wet rail phenomena has shown that water alone is unlikely to cause levels of ultra-low adhesion (<0.05). Higher viscosities or lower boundary friction coefficients are normally necessary to drop the levels of adhesion into the ultra-low levels.

Studies suggest that only a slight amount of water is required on the railhead in order to cause adhesion levels to drop significantly [20, 9]. Where greater amount of water is applied, the adhesion levels improve. Results of a questionnaire given to industrial stakeholders affected by the problem of low adhesion agree with this finding with 100% of stakeholders expressing importance of “Drizzle” on levels of adhesion and far fewer seeing heavy rain as having high significance [33].

2.3.2 Friction reducers

Where a thick lubricant film resulting from hydrodynamic lubrication is not able to be formed, chemistry and other properties of the surfaces may prove to be an important into understanding the tribological phenomena of the wheel / rail contact at the interfaces.

Under the great pressures exerted upon the wheel / rail contact by railway locomotives, it is hypothesised that hydrodynamic lubrication gives way to boundary lubrication. When these surfaces are physically in contact with each other, lubrication at the surface can still reduce the amount of friction which they experience; therefore, surface chemistry may play a significant role in many low adhesion events.

In the 1920s a quality of some lubricants was noticed and termed “oiliness”. This refers to the quality of a substance to act as a lubricant at slow sliding speeds, independent of its viscosity. The American Society of Automotive Engineers define the quality of oiliness as a “difference in friction greater than can be accounted for on the basis of viscosity when comparing lubricants under identical test conditions” [24]. Lubricants found with this quality were usually of natural origin (organic compounds) and had surfactant properties.

20-60% of oil sampled from rails at various sites was found to be surface-active chemicals such as acids, esters, ketones, amides and sulphur containing hydrocarbon compounds which can potentially interact with the railhead and wheels changing properties of the wheel / rail contact [34].

Figure 12 gives the results of a solution of leaf extracts applied to a ball-on-disc traction device compared with water. During the tests of the solution, black particles rapidly formed in the solution at the start of the test suggesting that the colour of leaf residue films is a result of the reaction between the steel surface and the water-soluble components of the leaf layer. This result is significant because it demonstrates that, from a leaf layer, solid material is not essential for a significant reduction in adhesion coefficient; however, it may not be as effective as with a full leaf layer present [35].

Surface agents in the form of acids or alcohols from organic matter, such as leaf residue or greases, are present in the environment wheel / rail interface; if allowed to disperse over the railhead they may form films on the surface leading to low adhesion conditions. The topic of surface chemistry with regards to the wheel / rail contact has been sparsely covered.

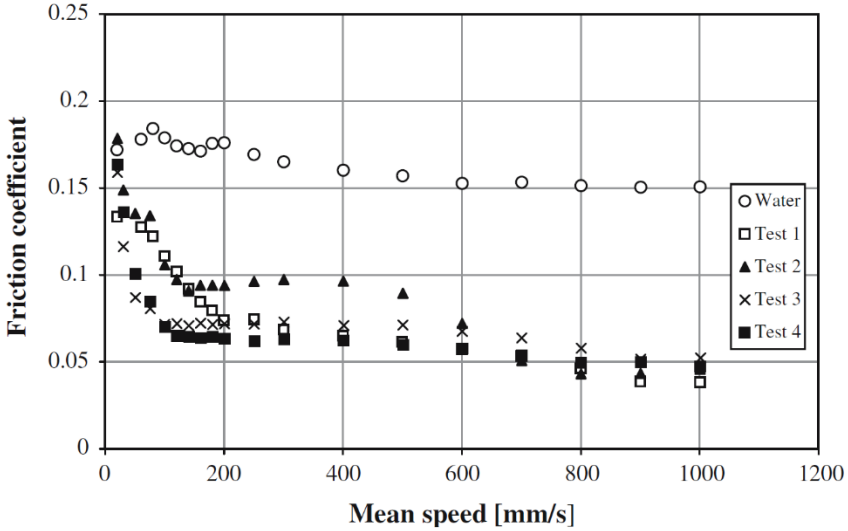

Figure 12, Friction curves for water-soluble leaf extracts [35]

2.3.3 Leaves

Leaves are one of the major contaminants often present in the wheel / rail interface. During the autumn, leaves present on the railhead pose considerable problems for the railways; around half of overrun incidents recorded in the UK in the autumn report leaf contamination present [33]. In addition to reducing the levels of adhesion on the rail, leaf layers can also be problematic for signalling by causing electrical isolation of the wheel and rail.

In studies comparing common railhead contaminants, leaves were shown to give the lowest adhesion values (within the ultra-low adhesion region); especially when water was introduced to the contact [36]. During the tests, leaf layers formed of compressed leaf material were formed on the surfaces. In wet conditions, two distinguishable layers were formed comprising of a soft dark upper layer and a hard compacted, difficult to remove, layer underneath; its similarity with leaf layers found on actual track is noted.

The film on the railhead is created rapidly, requiring only one train pass (16 axles) to develop a black durable contaminant layer; after which the layer remains for typically about 19 trains (300 axle passes) [9].

The friction coefficient of leaf slurry has been found to be in the range of 0.03 - 0.06 with a ball-on-disc test [35]. In this test, a black layer was also produced and in IR-spectroscopy tests, was found to contain pectin and cellulose derived from the leaf samples. Pectin is thought to produce a gel in the presence of metal ions and also cause cellulose fibres to agglomerate [35] which is what is hypothesised to be the black biomass film, giving a darkish colour to the leaf layer.

The typical chemical constituents of two common types of leaves are given in Table 2. Tribochemical reactions are expected to occur in the leaf layers and constituents be converted through chemical reaction to other organic forms. Research into the chemical composition of the leaf layers on the railhead is limited and the analysis done normally only identifies the presence of the leaf layer on the railhead. Fourier Transform Infra-Red (FTIR) spectroscopy is used in various studies [35, 37, 38, 39]; Cann's paper [35] analyses the spectra in detail for compounds and as a result is referenced in many other papers performing FTIR. The analysis in Cann's paper suggests the presence of both pectin and cellulose, but also suggested there are highly polymerised fatty acids, understood to be

effective lubricants [9]. Other analysis of the leaf layer includes Electron Spectroscopy for Chemical Analysis (ESCA) and Glow Discharge Optical Emission Spectrometry (GD-OES) which was used to determine the layers' presence and thickness [40].

Table 2, Percentage constituents of oak and hickory leaves [41]

Constituent	Hickory	Oak
Soluble reducing sugars	18.02 ± 0.87	11.13 ± 1.50
Soluble polyphenols	9.14 ± 0.98	16.24 ± 0.25
Hemicellulose	14.67 ± 0.30	16.44 ± 0.27
Cellulose	15.06 ± 0.43	18.39 ± 0.13
Lignin	10.01 ± 0.25	12.2 ± 0.46
Lipids	5.22 ± 0.30	4.90 ± 0.24
Nitrogen	1.48 ± 0.10	0.71 ± 0.03

Research concerning the detrimental impact of leaves to railhead traction has been conducted at The University of Sheffield [42]. A three-layer model of the leaf layer was explored with a top "tarnished" layer, a middle easily sheared friction reducing layer, and the bulk railhead layer. The cause of low adhesion by leaf layers is still not greatly understood and other work has suggested that compounds such as pectin may form lubricating gels that cause low adhesion [43].

A focus of some studies into the chemical nature of leaves as causes of low adhesion aim to determine bonding mechanisms between the leaf layers and rail-head [44]. Organic compounds from the leaf material was shown to have reacted with iron ions during the formation of the layers leading to an organo-metallic layer which creates a complex linking the leaf layer and the railhead surface. The chemical reactions which from these compounds result due to the pressures and temperatures of the wheel / rail contact. This research also identified the presence of graphite and phosphate compounds which are known to be lubricants [45]; however, unlike Cann's research [35], no substantial reduction in friction was noticed with leaf extracts only, suggesting that reactions leading to the formation of leaf layers are necessary for low adhesion due to leaves.

2.3.4 Oxides and wear debris

Oxides of iron are found on the rail and wheel surfaces and X-ray diffraction analysis have shown 2 common forms of iron oxides, Iron(II) Oxide (Haematite, red coloured) and Iron(II,III) Oxide (Magnetite, black coloured), make up a large portion of the 3rd body layer along with iron debris [30]. These anhydrous iron oxide compounds typically form a robust layer on the surface of the iron. Iron oxy-hydroxides, also known as rusts, have also been found on the railhead three forms of which have been identified as α-, β- and γ-FeOOH (goethite, akaganéite and lepidocrocite respectively) [46, 47].

Conditions greatly effect iron oxide formation; wet conditions, the chemical environment, and the cycling of such conditions result in both the rate and types of oxides formed [48].

Whilst the oxide layers have been studied in detail when on the rail, in the contact patch, little information has been gathered regarding the state of the layer. Iron oxides have many chemical and physical phases which are sensitive to changes in temperature and pressure. Thin iron oxide layers have been studied under different conditions and are shown to undergo reversible and irreversible reactions [49]. The properties of the iron oxide layer when under the pressures and temperatures within the contact is likely to differ in phase to that of the oxide layer found on the railhead.

Understanding this may potentially give insight into the mechanism of low adhesion due to oxides and debris on the railhead as well as potentially understand some of the mechanisms leading to the bonding of leaf layers to the railhead.

Table 3, Proportions of three types of oxyhydroxides present on the railhead under: accelerating (driving and braking), 1; free rolling, 2 and accelerating on guage corner of the high rail in curved track, 3 [46]

Running Condition	Rust	Initial State	1 Cycle	5 Cycles
No. 1	ß-FeOOH	10.2	5.1	No peak
	α-FeOOH	3.7	4.5	4.2
	γ-FeOOH	3.8	5.5	5.0
No. 2	ß-FeOOH	8.4	8.5	7.1
	α-FeOOH	4.9	5.3	5.9
	γ-FeOOH	7.5	9.7	9.1
No. 3	ß-FeOOH	16.3	6.8	No peak
	α-FeOOH	6.7	4.2	2.3
	γ-FeOOH	7.5	5.9	No peak

Table 3 gives the proportions of different types of iron oxyhydroxides on various positions of the railhead before and after train passes. The intensity of the Beta-FeOOH trace is reduced to negligible levels after five cycles on the accelerating railhead positions, it is suggested that this is caused by removal of the material. After one cycle the alpha- and gamma-FeOOH initially increased in their trace readings, this could be due to the revealing of the surface after removal of the beta-FeOOH or may be caused by a chemical change within the oxide; the specific cause has not been confirmed. Beta-FeOOH is understood to produce low friction coefficients [46].

White et al. [50] explored the wet-rail phenomenon through testing haematite pastes on a twin-disc tribometer. The experiment aimed to simulate a small amount of moisture generating oxide pastes which are hypothesised to lead to low adhesion [51], potentially owing to higher viscosity and a mixed lubrication regime. The results of the experimentation is given in Figure 13 showing a relationship that the higher concentration of oxide in the paste, the lower the coefficient of traction up to a point where as the oxide content approaches 100% it is marked by a steep increase in coefficient of traction. The significance of this result supports reports that small quantities of water lead to the wet-rail phenomena; very strong inversely proportional relationships have been found between the friction coefficients at the wheel / rail interface and the amount of water adsorbed in the debris at higher humidities [51]. With the application of further water, the paste is pushed away from the contact patch or potentially diluted, becoming ineffective in lowering the traction.

Iron oxides are abundant in the natural environment as well as on the railhead and can take on many forms depending on the conditions they are subjected to or formed under. Research has been done to characterise the oxides on the railhead and their effect on adhesion; however, current understanding of the reactions leading to the formation of the oxide layers and their intermediates, as well as the properties when subjected to the condition of the wheel / rail contact, is lacking.

Roughness of the surface of the railhead is shown to be linked to oxides as well as the running conditions and behaviour of the track. A newly ground length of track is shown to reach these values for roughness within a day and a half of operation suggesting that the removal and generation of oxide layers reaches an equilibrium [52].

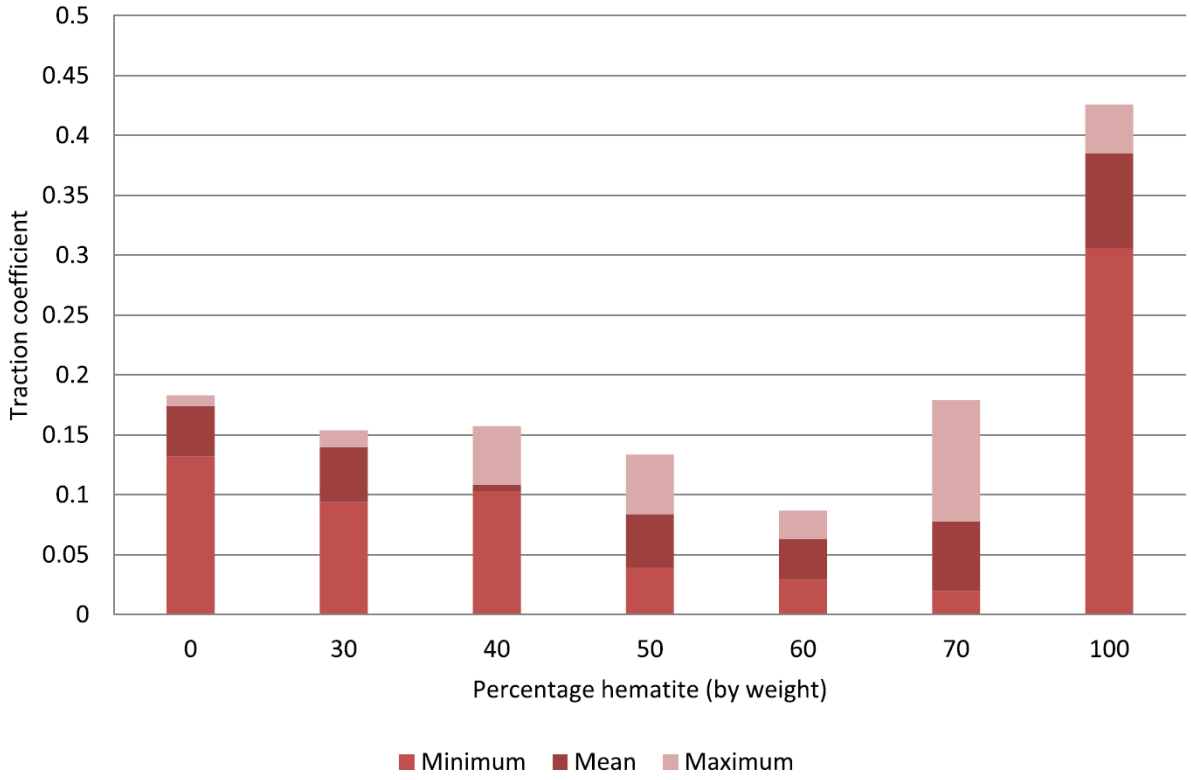

Figure 13, Traction coefficient values of twin disc tests with varying concentrations of haematite oxide pastes [50]

In dry conditions, thick oxide layers on rough surfaces have been shown to greatly increase levels of adhesion between the rail and wheel whilst thin oxides resulted in no significant change in adhesion in comparison to the control [52]. The same tests conducted in wet environment gave adhesion coefficients within a range of 0.14 to 0.2 and no significantly lower adhesion than the clean control. In the wet condition the initial adhesion of the rough thick oxide layer samples was high, but quickly reduced to the same range as the other samples.

It should be noted that the testing of the oxide layers was done under low rolling speeds; therefore, boundary lubrication or solid layer shear may be the only significant lubrication mechanisms.

Hardness of the oxides have been hypothesised to be important to the friction-modifying properties of the tribo-chemical system. Nakahara et al. [53] noted that an abrupt rise in traction coefficient may be caused by an increase in hard thin oxide layers but that an increase in soft oxides may prevent an increase in the traction coefficient.

Low adhesion caused by oxides on the railhead is notoriously difficult to reproduce in the laboratory [54, 55]. Studies have suggested that the reason for this is a very narrow band of conditions required to cause the phenomena.

2.4 Test methods

This section outlines some of the test methods used to study the wheel / rail contact as well as some proposed methods which hold potential to analyse the system. It is broken into two sections: Tribo-testing, which contains tests to study the tribological behaviour of the systems; and Analysis Techniques, which involve techniques for chemically and physically characterising the contact.

When selecting a tribotesting method, there is always a trade-off between complexity, time, cost and control.

Simple test rigs can provide data quickly and cheaply regarding one or two variables in the system. It is also easier to control the input parameters in the testing. In this study, the simplest are slow sliding-only tests.

More complex testing involves rolling-sliding contacts where more representative simulations of the wheel / rail contact can be made but some control over the individual parameters is lost.

The most representative data can be gathered by full scale or field testing which involved real operating conditions; however, costs are high and the control over most parameters is relinquished and unexpected and un-attributable errors to the data are introduced. Full scale field testing is normally reserved for validation of testing using the simpler methods.

Wherever possible, specimens are machined out of wheel and rail section material to give physical and chemical consistency with the steels used on the railway network.

2.4.1 Tribo-tests

Up until the mid-1990s British Rail conducted extensive testing of adhesion on a number of British Rail routes using a purposely designed tribometer train with instrumented wheelsets. Testing on operational track with a full-size railway locomotive provided extremely representative readings. Ever since the retirement of the tribometer train in 1996, researches have relied on data from portable hand-operated tribometers for field readings as well as various lab-based equipment to study the wheel / rail contact [9]. In this section some of these methods are reviewed.

2.4.1.1 *Pin-on-disc (PoD)*

A Pin-on-Disc tribometer simulates a sliding contact. The device consists of a horizontal rotating disc with a pin loaded against it. Contact pressures comparable to those experienced in the wheel / rail contact (900 MPa) have be generated with this equipment [56, 57].

Lyu et al. [56] have used this method within a climate-controlled environment, allowing manipulation of the temperature between -10°C to 20°C and humidity between 30-90%, to study the wear between wheel and rail.

2.4.1.2 *Mini traction machine (MTM)*

The mini traction machine consists of a rotating ball in contact with a rotating steel disc. The ball and disc can be driven independently and to create a rolling sliding contact. Due to the nature of the contact it can be used to determine the coefficient of adhesion between the two surfaces by varying creep levels and has been used to investigate the influence of various contaminants and surface roughness on the wheel / rail contact [58]. In the study, pressures of up to 1.25GPa were simulated.

The system can be enclosed in a temperature-controlled chamber and liquids applied to the contact allowing the study of contaminants under varying environmental conditions.

The MTM is often preferred to the pin-on-disc or pin-on-flat testing platform as it allows for a rolling-sliding contact [59] and the machine has been used to investigate various factors influencing wheel-rail adhesion [60].

2.4.1.3 *Twin-disc*

The twin-disc apparatus consists of two hydraulically loaded discs machined from the rail and wheel materials. They are driven separately, and their relative speeds adjusted to induce slip, simulating driving and braking forces [52, 50]. Such examples include SUROS (the Sheffield University ROlling – Sliding) machine [36] and full-scale wheel rigs [61].

The use of twin-discs for wheel / rail contact studies was first developed to simulate wear and fatigue but has since been used for adhesion and the testing of various contaminants including leaves, oils & greases and water [62].

2.4.1.4 *High pressure torsion (HPT)*

High Pressure Torsion testing of the wheel / rail interface has been developed by the University of Sheffield [63]. During the testing procedure, a specimen of wheel material with a machined raised ring area is compressed against a flat rail sample. Torque is then applied to slowly rotate the samples relative to each other at a constant speed.

The stress required to rotate the specimens relative to each other is plotted against the displacement. From this information, is it possible to predict the frictional properties of the wheel / rail system. Contaminants can be placed within the contact and studied. Buckley-Johnstone et al. [64] investigated the influence of concentrated oxide pastes on adhesion using this apparatus and found only a narrow range of oxide concentrations of the pastes reduced adhesion; however, sustained low adhesion was not achieved.

This testing procedure has been used to provide inputs into the Virtual Vehicle Research Centre's Extended Creep Force (ECF) model for use in multi-body dynamic simulations. The HPT has recently been used to simulate and assess the impact of oxides and water in the wheel / rail interface [64].

Due to its low-speed sliding-only operation, many lubrication effects of contaminants may not be studied; however, HPT testing is likely to be one of the more controllable methods for determining the rheological properties of solid third body layers, as well as the frictional behaviours of contaminants.

2.4.1.5 *Full scale rig*

Full scale rigs offer realistic contact geometry, loads and materials for the testing of the wheel / rail contact.

Various configurations of full scale rigs have been developed. Examples include a 2-axle high speed bogie on rail rollers capable of being excited, to simulate irregularities in the track [65], and a full-scale slow rolling/sliding rig operated at the university of Sheffield which uses a wheel on a short length of straight track [66, 67].

The larger rigs offer realistic testing conditions but are more complex systems to control and have limitations. An example limitation of the full-scale rig at Sheffield is that the same section of the wheel and rail contact on each cycle which may not allow for dispersion of substances on the railhead to be simulated realistically.

Instrumented wheelsets fitted to locomotives in operation are also used by train operating companies and researchers, providing direct representative data of real-world train operating conditions [68]. Whilst this data is valuable the implementation is both difficult to control and expensive.

2.4.1.6 *Field testing*

Portable tribometers introduced to replace the tribometer train are problematic and concern has been expressed after comparative testing studies demonstrated poor correlation between the mean values determined from the full sized wheel / rail contact and the handheld devices. The handheld devices tended to produce higher values. The cause of the discrepancy as a result of the scaling has been theorised to be a result of large debris, wear and surface roughness effects which are more significant with smaller geometries [9].

A pendulum test rig, traditionally used to assess the slip resistance levels of flooring in public spaces for health and safety regulation, has also been adapted to assess the levels of friction found on the railhead which provide results agreeable with those found using the twin disc method [69].

Newer 'hand operated' tribometers have been developed, improving on older 'push' tribometer units by offering more control over the testing; good agreement has been observed between instrumented wheelsets and values recorded on the new portable models developed [68].

2.4.2 Analysis techniques

Aside from properties directly relating to adhesion, other conditions of the wheel / rail contact such as the presence of a tribofilm or chemical compositions have been studied through use of various techniques. Some of the most relevant are detailed in this section.

2.4.2.1 *Fluorescence and electron spin resonance*

Fluorescence and Electron Spin Resonance (ESR) have both been used to investigate the properties of adsorbed layers of surfactant molecules to the solid-liquid interface. The polarity, viscosity, diffusion, solute partitioning and aggregation numbers can be determined through use of these techniques; thereby providing information of interest to boundary lubrication. These methods are highly sensitive to the environment but have been used to study layers of hydrocarbon chains adsorbed onto solid-liquid interfaces [70].

2.4.2.2 *Ultrathin film interferometry (UFI)*

Film interferometry is a technique used for studying tribofilms. It uses the principle of optical interference to superimpose light reflected onto a fixed surface and light reflected off a surface of which position varies based upon the thickness of a film. The augmented signal is then analysed to estimate the thickness of the film. A set-up similar to the MTM rig is used for this analysis with the main difference being the disc replaced by an optical slide and a microscope-camera focused on the reverse of the slide to the ball contact.

Its main use has been to study EHD films and this technique has been proved to measure lubricant film thicknesses between 1 and 500nm with an accuracy of ±0.5nm below 10nm and ±2 percent above 10nm [71].

2.4.2.3 *Spacer layer imaging (SLIM)*

Spacer layer imaging technology has been adapted onto the MTM tribometer to observe and determine the thickness of tribofilms formed between ball and disc surfaces. Unlike UFI, the tribofilm is observed outside the contact patch on the rubbing band of the ball's surface.

The device consists of a spacer layer coated optical slide which, when the device is stationary but before the surface is drained, is loaded onto the rubbing patch of the ball. Using a microscope with attached camera, the interference image is captured for the contact [72]. Analysis of the colour bands then allows for the estimation of the film thickness and a contour map of the contact to be generated.

SLIM is used in place of surface layer interferometry when a sliding or rolling/sliding contact is required as the rubbing of the surfaces abrades the optical coating used in interferometry. A limitation of this method is that the film can only be analysed stationary; therefore, no hydrodynamic lubrication effects may be observed.

It has been used to research ZDDP tribofilms which form on metal surfaces and are extensively used as anti-wear additives in engine oils [73].

2.4.2.4 *Chemical analysis*

Table 4 outlines chemical some main chemical analysis techniques which have been used to study the wheel / rail contact. Other techniques, relevant to topics of this research, are also included for consideration of further research regarding the low adhesion phenomena.

Table 4, Analytical chemistry technique overview

Technique	Description	Topics of interest	Example uses
Chromatography, Gas chromatography (GC), Liquid-Solid chromatography	Analytical chemistry techniques for the separation and characterisation of components in a mixture	Oils and greases, leaves, surfactants	Separate and determine fractions of chemicals present in oily contamination on the railhead. GC [74] and Liquid-Solid chromatography [34].
Mass Spectrometry **Secondary Ion Mass Spectrometry (SIMS)**	Analysis technique which determines ions based on their weight, it is often combined with gas chromatography.	All	
Infra-Red (IR) and Fourier-Transform Infra-Red (FTIR)	Spectroscopy measuring the absorption or transmittance of infrared radiation vs frequency or wavelength	Oils and greases, leaves, surfactants, oxides	Determination of fractions of chemicals present in oily contamination on the railhead [34]. Leaf layer analysis to determine the bonding within organic compounds present in leaf layers [35, 37, 39]. Unsuccessfully used to detect the presence of hydroxide anions on the surface of iron oxide (too thin layer) [75].
Scanning Electron Microscopy (SEM)	Electron microscope using focused beams of electrons for imaging. Can be combined with other X-Ray analysis methods.	Railhead surface	Surface topography analysis of railhead and oxides [52].
Energy-dispersive X-Ray spectroscopy (EDS)	Can be combined with SEM to provide elemental analysis or chemical characterisation of a sample.	Oxides	Elemental analysis of oxides on the railhead [52].
X-Ray Diffraction (XRD)	The physical interaction between x-rays and material are observed using	Oxides	Determining composition, type,

Also Synchrotron X-ray Diffraction	XRD and may be used to determine crystal structure as well as the chemical composition.		and structure of oxides on the railhead [46, 76].
Raman Spectroscopy **Also: High Pressure Raman Spectroscopy**	Similar to IR, observes the interaction between radiation and matter to study chemical composition of compounds and their functional groups.	Oxides, oils and greases, leaves.	Used successfully in the detection and characterisation of iron oxyhydroxides on rail surfaces [47].
Glow Discharge Optical Emission Spectrometry (GD-OES)	A destructive analysis technique which analyses the elemental composition of materials. Can also be combined with mass spectroscopy.	All	Along with electron spectroscopy for chemical analysis (ESCA or XPS), used to determine the elemental composition of the top of the railhead as well as a five micrometre depth profile into the railhead [40].
X-ray photoelectron spectroscopy (XPS), Electron spectroscopy for chemical analysis (ESCA)	Analyses surfaces in a high vacuum to accurately determine the elemental composition and chemical state of a material.	All, Surfactants	Characterising monolayers on stainless steel surface [77, 78, 79, 40].
Contact angle measurement	Quantifies the thermodynamic wettability of a surface	Surfactants, surface characterisation	Characterisation of surface properties and determination of monolayer presence [78].
X-ray Adsorption Spectroscopy (XAS) and X-ray Adsorption Near Edge Spectroscopy (XANES) – also known as "Near Edge X-ray Adsorption Fine Structure" NEXAFS	Signals can be extracted from surface monolayers or buried layers in the presence of a large background signal. Powerful technique for organic and inorganic chemical structure analysis which allows the examination of molecules adsorbed on surfaces.	All	

2.5 Numerical modelling of the wheel / rail contact

RSSB Report 1077 reviews as well as quantitatively assesses and ranks mathematical models for simulating the wheel / rail contact [33].

There are three classes of friction force models for tangential contacts divided by complexity [80]:

- The least complex are approximate approaches including lookup tables which are used for fast calculations but are unsuitable for detailed studies of the contact required for simulations running at – or close to – the adhesion limit such as traction control [81].
- Half-space models use simplified geometry but are more complex and use physical principles to compute the contact outputs.
- The most complex models use comprehensive finite element approaches that are appropriate for studying detailed geometries and effects in the contact but are computationally intensive making them unsuitable for dynamic simulations.

The extent of simplifications to the models depend strongly on their intended use [82].

Friction force models are used to simulate the wheel / rail contact and provide understanding for complex system behaviour. The models allow for simulation of experiments as well as be able to conduct parametric studies and optimise the system. Vehicle dynamic simulations incorporate the wheel / rail contact models as an essential part of larger model simulations which are increasingly being used in vehicle design, track engineering, wear/damage models and serious incident investigations [80].

2.5.1 CONTACT

Contact is a half-space based approach. It has been extended to include further relationships, including a third-layer rheological law, friction memory and falling friction effect. These aim to describe the effects of surface roughness, temperature effects and a third body layer; however, the third body layer is generalised formula and the effect of liquid lubricants are only included within this empirical relationship [80]. Results generated from the model have been shown to agree well with experimental results taken from the Bombardier locomotive in wet conditions.

2.5.2 FASTSIM

FASTSIM is a simplified theory of rolling contact with a similar derivation as CONTACT. It is faster to compute due to its simplicity and relies on empirical correlations to approximate the system properties [83].

2.5.3 Polach

The Polach model is an empirical model based on Kalkers's linear theory and is used as an alternative to FASTSIM. It has been developed for dry and wet contacts taking into account the shape of the contact amongst other parameters [81]. The Polach model was determined to be the most suitable model in the RSSB T1077 report for modelling the influence of water on wheel / rail adhesion levels due to its representative results under water lubricated conditions as well as being computationally efficient and empirically extendable. In addition, it has already been implemented in Multi-Body simulation software [33].

2.5.4 Spiryagin

The Spiryagin model is another model based on FASTSIM and extends it to fit more closely to observed traction curves by employing an initial slope reduction and decreasing friction coefficient at high creepages [84].

2.5.5 Tomberger

Based on the FASTSIM, the Tomberger model incorporates other models for lubrication conditions into the calculations, including a temperature and a micro-contact model [82]. The Tomberger model also considers surface roughness and its effect on adhesion levels under dry and wet conditions (boundary and mixed lubrication conditions).

2.5.6 Extended creep force model (ECF)

Based on the Tomberger (FASTSIM) model, the Extended Creep Force (ECF) model adds more complexity in the form of a temperature and normal stress dependent elasto-plastic third-body-layer model. This allows the effect of solid interfacial layers on the traction characteristics to be studied [12]. Non-linear traction characteristics also allow for the simulation of liquid lubricants within the contact.

In RSSB report T1077, the ECF was identified as one of the most suitable models for studying the "Wet-Rail" phenomena [33]. In addition to this, High Pressure Torsion experiments for determining the frictional behaviours of wheel / rail systems, accounting for the presence of contaminants, have been conducted at the University of Sheffield and have been used as inputs into the ECF model.

2.5.7 Beagley

Beagley's model, which considers both solid and liquid railhead contamination, is based on two phenomena: the shearing of a solid contaminant layer and viscous lubrication effects of solid/liquid mixtures of the contaminants [85].

2.5.8 Chen

A 2D model based on elasto-hydrodynamic lubrication and contact theory of rough surfaces [23] was extended into a 3D model. Its main applications are at high rolling speeds where lubrication effects are expected to become significant [86].

2.5.9 Popovici

Poppovivi's extensive model has been developed based on mixed lubrication with rough surfaces. The layer between the wheel and rail is modelled as a viscoelastic lubricant. Extensive field testing and validation of the model was conducted and shown to have good correlation for a wide range of lubrication (mixed and EHL) regimes and temperature conditions [87].

2.5.10 Wu

Wu et al. [88], factors EHL into a numerical model considering small pockets of water and oil which can be stored between the asperities on the wheel / rail due to the roughness of the interface being of the order of several microns. The study shows that the adhesion coefficient is reduced to the lowest levels when a mixed environment of oil and water is present as a contaminant on the line; more than oil or water alone. Higher train speed is also presented to cause a significant reduction in adhesion through the EHL mechanism. The oil fraction and it's positioning in the contact was also studied and shown to influence the adhesion coefficient.

2.5.11 Water-induced low adhesion creep force model (WILAC)

The WILAC model can simulate the wheel / rail traction coefficient in dry, moist, and wet conditions; however, it puts special emphasis on moist conditions (humid conditions and during the onset of rain) [89]. The model is an extension of the Polach model incorporating numerous linear regression models which modify the parameters of the underlying model based on the normal force and rolling speed to encounter for a wider range of operating conditions. The model simulates the creep curves for four different scenarios (dry, wet and two 'damp' conditions) and allocates a weighting for each of the scenarios to the current computation determined by the water flow rate.

2.5.12 Model suitability

In this study of low adhesion, research is likely to be done on a fundamental chemical or physical level; therefore, the approximate approach models such as the ones based on FASTSIM are not ideal

for exploring the causes of low adhesion at this level. CONTACT, Beagley and Chen are all good candidates for predicting the effect of physical or chemical influences at the wheel / rail contact.

A secondary intent of the research is to be able to provide predictable adhesion levels. Whereas, the ECF and WILAC models may be unsuitable for studying the fundamental mechanisms leading to low adhesion, they are extendable, the ECF model has been implemented in simulation packages and they are developed to accept input from tribo-testing lab results; therefore, either are good options for integrating the outcomes of this research into vehicle dynamic models to improve the reliability of simulations.

2.6 Abatement

Control of the levels of adhesion on the railway has been divided into two categories in this section: prevention and abatement. Prevention control methods aim to eliminate the problem by removing the conditions required for low adhesion to form. Mitigation methods, on the other hand, work to reduce the impact of low adhesion after it has developed or had the opportunity to form.

Active control systems, such as electronic traction control or magnetic train brakes, have been omitted from this study as they do not deal directly with the conditions between the physical and chemical connections of the wheel / rail system.

2.6.1 Prevention

2.6.1.1 *Hydrophobic*

The formation of dew on the railhead can be controlled somewhat by the application of a hydrophobic product forming a water-resistant surface on the head of the rail.

Lewis et al. [69] study the effect of applying a hydrophobic liquid product to the rail-head surface in order to attempt to prevent the formation of dew on the railhead. Enhanced coefficients of friction are reported under “misted” conditions; however, when the surfaces are wetted, the treated rails are shown to have lower coefficients of adhesion than with water alone. This suggests that the chemicals are acting as lubricants when in solution.

The study demonstrates that hydrophobic treatment with chemicals similar to those tested can make a rail more resistant to adhesion loss, but in limited conditions, and worsen the effect in others.

Other alternative chemicals, such as non-organic hydrophobic agents which may have the desired water-resistance properties yet not exhibit lubricating effects, may worth investigating.

2.6.1.2 *Hydrophilic*

Use of hydrophilic agents have been the focus of some low adhesion studies [90, 91]. The theory behind hydrophilic chemicals is that they may reduce the amount of water which can be supported on the railhead by preventing beading and encouraging dispersion over the surface; essentially draining the contact. The study demonstrates the effectiveness of using dioctyl sodium sulfosuccinate as a coating for increasing the affinity of water to the rail surface and promoting dispersion. The effect of this is increased friction levels for dry and “moist” conditions but lower friction where there is a greater quantity of water on the railhead.

It should be noted that the tribo-testing has been performed using a pendulum tester with a rubber contact which complicates the system and that there may be unaccounted interactions with the coating which would not be present in a steel-steel contact.

2.6.1.3 *Trackside management*

Preventing ingress of contaminants onto the railhead may allow for better control of trackside conditions and reduce impact on adhesion. These methods primarily target leaf contamination but may also reduce dust or debris contamination. Such management strategies include [14]:

- Vegetation management – ensuring a minimum distance between any lineside vegetation and the track.
- Rail leaf guards – involving barriers to influence the flow of air around the rail, reducing the entrainment of leaves onto the railhead through turbulence created by passing trains or crosswinds.
- Trackside leaf fence – providing a barrier to prevent leaves and other debris from the wider environment entering the trackside region.

These management strategies may be limited due to cost of maintenance, environmental legislation, or the design/layout of the railroad area. For instance, the extent of management of rail side vegetation on UK railways is often limited due to the role trees play in ensuring structural stability of embankments.

2.6.1.4 *Chemical treatment of the railhead*

Characterising leaf contamination, primarily what binds the leaf layers onto the railhead, has been recommended for further research by the Rail Safety & Standards Board (RSSB) [9].

The mechanism by which leaves chemically bond to the railhead to form a layer causing low adhesion has been studied through the discipline of chemistry and biochemistry [92, 42, 44].

The exact mechanisms have not been validated but, proposed hypotheses are drawn up, most of which involve iron ions. It is suggested that the formation of leaf layers can be prevented by the use of chemicals which suppress the formation of iron ions and, in turn, halt the formation of problematic leaf layers on the railhead.

The prevention options proposed include:

- Neutralisation of “free” iron by chelators
- Use of Enzymes
- Soapy hydrophobic solutions

2.6.2 Mitigation

Methods to increase adhesion to acceptable levels when encountering low adhesion after its formation.

2.6.2.1 *Sand*

The process of applying sand to the wheel / rail interface is known as Sanding. Sanding is the oldest and most common [61] method employed to tackle low adhesion and railway locomotives have been fitted with sanders since 1836 [14].

The sand is applied to the wheel / rail interface by being blown from a hopper mounted under the train using compressed air. Sanding is rarely used in normal operation but is applied during emergency braking. It is effective and easy to use but can lead to complex and costly problems with the rail or wheel surfaces and has been shown to increase the wear rate of both the rail and wheel materials by up to an order of magnitude [93]. Sand has also been shown to cause track surface electrical isolation [94].

For leaf and grease contaminated contacts, the application of sand has been shown to be effective in recovering adhesion; however under dry and wet conditions it was shown that sanding initially reduces adhesion through the creation of a low-shear-strength solid layer which prevents direct contact of the surfaces until the layer is broken and adhesion levels recover [61].

Alumina particles have been found to be more suitable for improving traction than the traditionally used silica sand as it is shown to subject the wheel and rail surfaces to less wear for the amount of adhesion recovered [8].

2.6.2.2 *Friction modifiers*

The aim of a friction modifier is to be able to have control over the friction coefficients of the wheel / rail interface by either increasing or decreasing it. The first friction modifiers were developed as solid stick application products to lower corrugation and squeal noise and do so by reducing the traction coefficient [59]. Increasing the traction coefficient is the objective of other friction modifiers which may be necessary in places that regularly suffer from low adhesion to enhance the adhesion, for emergency braking situation for instance [5].

Friction modifiers can be either water [59] or oil [95] based and often include particles in suspension. They can be applied by brush or spray to the railhead in a suspension to form a thin film. Application is important when applying oil-based friction modifiers as too much can result in very low adhesion levels [95]; however, water-based friction modifiers are less sensitive to overdosage [59]. Another method of application is to use an abrasive block made from a synthetic resin which is pressed against the wheel and applies the particles to the wheel surface in a controlled manner [8]. Some friction modifiers provide the required traction with no solid particle suspension,

Non-particulate based friction modifiers are mainly used to reduce wear and fatigue or to control noise. In doing so they can occasionally cause adhesion levels to drop to levels unacceptable for braking or traction [96]. Typically, solid particles are present in suspension when an increase in traction is required.

2.6.2.3 *Traction gels*

Traction gels, also known as traction enhancers, are a particular type of friction modifier which has been developed in the aim of replacing sanding as the primary adhesion control solution. They consist of a solid/liquid suspension of sand particles within a gel base and are designed to be applied either by a vehicle mounted system or a pumping from trackside devices.

A commercially available traction gel has been tested with the aim of recovering adhesion levels with leaf contamination [97]. It has been shown to enhance the rate of adhesion recovery and lead to lower wear rates compared when compared with sand; however, immediately after application there is a reported drop in adhesion and some electrical isolation. This suggests that a vehicle mounted system may be problematic but applied to the track it may be a viable substitute to sanding.

2.6.2.4 *Cleaning of the rail surface*

Where a layer of leaves has built up they can be physically removed from the railhead using various methods [93]:

- Water Jets
- Sandite blasting (mixture of sand and aluminium oxide particles)
- High power laser cleaning

The removal of the leaf layer may eliminate the cause in that situation; however, this method is expensive and difficult to apply extensively on the rail network.

2.7 Summary of literature

Providing predictable and optimised traction and braking of the wheel / rail contact presents great difficulties. The causes of adhesion loss are well documented; however, the mechanisms by which traction is lost are not fully understood and replicating the effects of documented causes has only achieved limited success in the lab.

Very high rolling speeds such as those associates with high speed trains have been shown to be able to produce traction coefficients within the 'ultra-low adhesion' regime. Slower trains sporadically also experience low adhesion but the mechanisms leading to this phenomena are less clear but believed to be associated with small amounts of water such as from the onset of rail (drizzle) or dew on the railhead.

Current numerical models effectively predict traction of locomotives over most operating conditions and incorporate extensions to account for narrow water-content conditions which are shown to produced reduced traction, but these are often based on empirical relationships rather than from first principles.

Much of the research into the material components which result in low traction conditions regard leaves and leaf layers which are only present during half of the incident during the autumn period; other components such as oils / greases and iron oxides are less covered. The literature exploring these materials in the context of the wheel / rail contact is also often of high level and rarely explore the chemistry of these components. It is clear that this lack of chemical analysis is a large gap in current knowledge which the work of this thesis will aim towards addressing.

Abatement techniques for tackling low adhesion reflect the current lack of understanding for the chemistry and mechanisms of low adhesion incidents, often resorting to the almost 200 year old method of sanding as a design basis.

Overall the literature shows a need for further understanding of the chemical and physical conditions and behaviours of the railhead which may be instrumental in identifying mechanisms of low adhesion and designing new methods to counteract its development and impact.

3 Chemistry of the Railhead

The third body materials of the wheel / rail system are diverse but have been grouped into two categories to explore in this chapter: inorganic and organic compounds. This chapter seeks to firstly identify and then explore these compounds, through the literature, in greater detail than they have been studied directly in the context of the wheel / rail contact. The physical and chemical properties of these materials and their interactions are explored here mainly through the fields of chemistry and materials science.

The chapter is separated into three parts: inorganic compounds; organic compounds, including structures and chemicals in leaves; and documented chemical and physical surface interactions.

3.1 Composition and formation

The typical grade of steel used on railways is a pearlitic steel, composed of finely laminated structures of ferrite and cementite. By weight it is approximately 0.6% carbon [98]. The wheels are steel, manufactured to various grades via hot forging and rolling, varying slightly in chemical composition and mechanical properties [99].

In addition to the materials of the wheel and rail, compounds found in the wheel / rail contact system originate from the trackside environment which can vary widely in climate conditions and materials present.

3.1.1 Inorganic compounds

Oxides are always going to be present to some extent on the railhead and will therefore make up the majority of inorganic compound research in this chapter. The oxides mainly originate from the corrosion of the rails. Other inorganic compounds that may be present include ores, from mining / quarrying and transport of materials; dirt and stones, from the trackside environment and ballast; and sand from the practice of sanding to improve traction of locomotives.

Iron is a transition metal and as such can exist in many states of oxidation which are changeable over time if exposed to different environmental conditions. In typical conditions, where oxygen and water are present, three groups of compounds may form: Iron Oxides, Iron Hydroxides and Iron Oxide Hydroxides. These common compounds are given in Table 5.

These iron compounds have different material properties and therefore have a direct impact on the mechanical tribology of the wheel / rail interface [100]. Their chemistry is also of interest as the compounds may interact differently with organic materials and other contaminants on the railhead.

Table 5, Overview of common inorganic compounds [101]

	Iron Oxidation State	**Formula**	**Morphology**
Iron oxides	2	FeO	
	3	Fe_2O_3	alpha
	3	Fe_2O_4	gamma
	2,3	$FeO.Fe_2O_3$	
Iron hydroxides	2	$Fe(OH)_2$	
Iron oxide hydroxide	3	$FeO(OH).n(H_2O)$*	alpha
			beta
			gamma
			delta

*alternatively: $Fe(OH)_3$

Iron, as a transition metal, can have many oxidation states, but typically takes on one of two under conditions where oxygen is present: ferrous (Iron II-, or Fe^{+2}) and ferric (Iron III-, or Fe^{+3}) [102]. Most of the iron will be found in the ferric state due to the relative abundance of oxygen in the atmosphere. All compounds covered in this section consist of iron with these two oxidation states.

Iron (II) oxide, or wüstite, is a rare form of iron oxide which exists in a cubic lattice. Its presence usually indicates a heavily reducing environment. It was not identified on the railhead by the in-situ X-ray diffractometer [46] and is not mentioned often in the very few other studies into iron oxides.

Iron (III) oxide is found in 2 common phases: α-hematite and γ-maghemite. α -iron (II) oxide is more common, but γ-iron (II) oxide may be formed through the thermal dehydration of α-iron (III) oxide hydroxide [101].

A final common iron oxide composed of both ferrous and ferric oxidation states, iron (II, III) oxide is magnetite.

Most iron hydroxide compounds exist as Iron oxide-hydroxides, but a less stable iron (II) hydroxide may be possible; however, in the presence of oxygen it rapidly oxidises into iron (III) oxide hydroxide. This compound is also an intermediate product of rusting [101] but due to its stability, the concentration on the railhead is unlikely to be more than a trace.

Iron (III) oxide hydroxide can be found in either anhydrous or hydrated forms depending on moisture present. Four different structures occur naturally of this compound: α-goethite, ß-akaganéite, γ-lepidocrocite. The final δ structure, feroxyhyte is not stable under atmospheric pressures, but is found to form in high pressure environments such as deep sea conditions; the pressures experienced in the wheel / rail contact may potentially permit its formation but, as it would have to be analysed in-situ, detecting it is likely to require extreme technological difficulties.

“Rusting” is a complex electrochemical process by which there is successive oxidation and reduction reactions occurring at the surface of the metal along with an electrolytic solution, the solvent of which is typically water. The liquid film on the metal surface is often microscopic, but is almost always present due to moisture in the environment. Rusting of the railhead is a continuously ongoing process, therefore it is important not only to consider the end products of the reaction, but also intermediate compounds formed temporarily during the process.

The three major compounds involved in the rusting mechanism are iron, oxygen and water. Other ions may occasionally be involved such as calcium and chlorine; they may act as catalysts, speeding up the reaction, or form compounds in addition to the common rust compounds [101].

The first stages to the reaction are the oxidation of iron from the surface of the metal whereby the electrons are transmitted through the electrically conductive metal; the iron ions formed are soluble and enter into the solution. At the same time, water and dissolved oxygen are reduced into hydroxyl ions at a separate surface site:

$$Fe \rightarrow {Fe^{2+}}_{[aq]} + 2e^- \quad \text{[A]}$$

$${O_2}_{[aq]} + 2H_2O + 4e^- \rightarrow 4{OH^-}_{[aq]} \quad \text{[B]}$$

Some of the iron may be oxidised further by the oxygen dissolved in the solution:

$$4{Fe^{2+}}_{[aq]} + {O_2}_{[aq]} \rightarrow {Fe^{3+}}_{[aq]} + 2{O^{2-}}_{[aq]} \quad \text{[C]}$$

Iron hydroxides / oxide-hydroxides are then formed from disassociation of water molecules and ionic attraction to the hydroxyl ions:

$$Fe^{2+} + 2H_2O \leftrightarrow Fe(OH)_2 + 2H^+ \quad [D]$$

$$Fe^{3+} + 3H_2O \leftrightarrow FeO(OH) \cdot H_2O + 3H^+ \quad [E]$$

These compounds may precipitate from the solution and exist to varying degrees of hydration whereby water molecules are physically adsorbed to the compounds.

Over time these compounds undergo dehydration, precipitating water to form iron oxides:

$$Fe(OH)_2 \leftrightarrow FeO + H_2O \quad [F]$$

$$Fe(OH)_3 \leftrightarrow FeO(OH) + H_2O \quad [G]$$

$$2FeO(OH) \leftrightarrow Fe_2O_3 + H_2O \quad [H]$$

It should be noted that many reactions which occur during the rusting mechanism are reversible causing the chemical composition to vary with the conditions. The phases of the compounds, which are associated with the crystal morphology, are also transient and different structures of the oxides and hydroxides may vary with the railhead conditions.

3.1.2 Track ballast

The track ballast which is placed and packed to form the track bed upon which the railway sleepers are laid varies depending on requirements and available material. Crushed hard stones must be used for new or replacement ballast laid in maintenance in the UK [103]; however, old materials such as ash and sand may still be present on the network as well as a vast variety of materials internationally. Granite is the most common choice of material, but occasionally hard limestone or steel slag may be used [104].

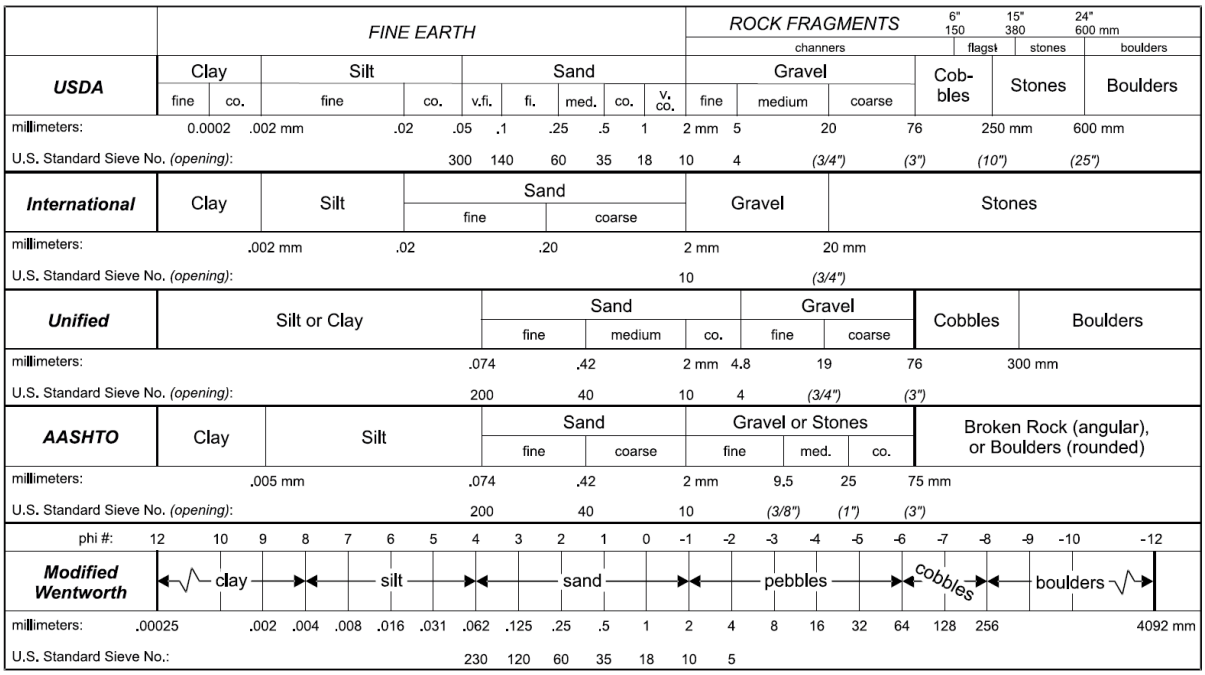

Figure 14, Soil particle size classifications [105]

Quarrying, natural geological features and human activities ultimately give rise to a vast diversity of trackside materials and soils. The great variety of debris and soils has resulted in many systems to

attempt classify their chemical physical and biological properties [106]. Of these systems, particle sizes are of great interest, as can be seen in Figure 14 which set out the categories of clay, silt and sand for fine earths [105].

Soil texture classes and subclasses have been further defined by the United States Department of Agriculture as combinations of these particle sizes as can be seen in Figure 15.

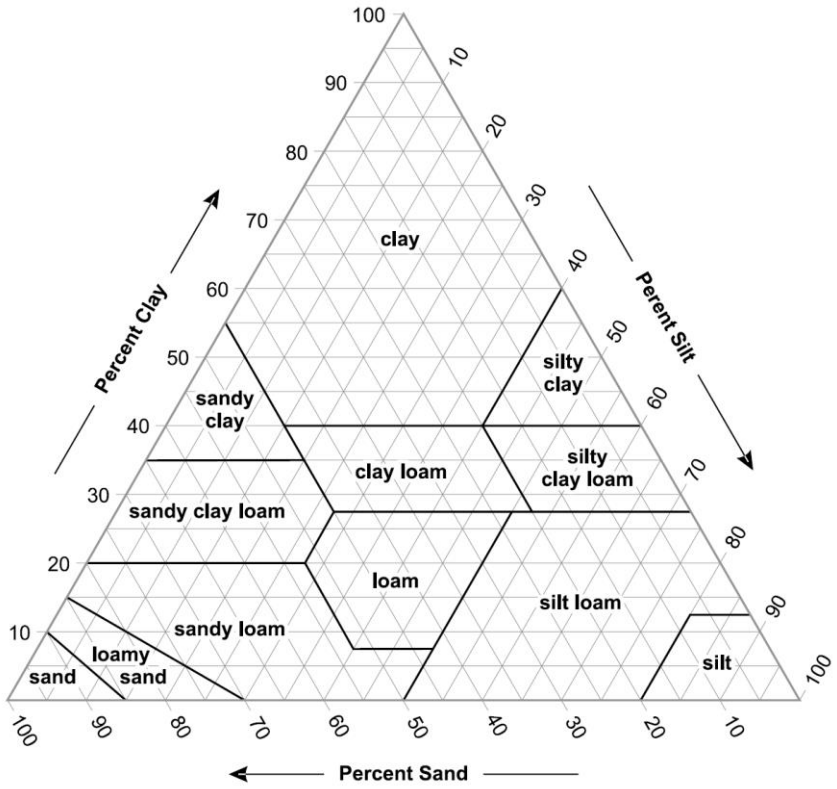

Figure 15, USDA texture triangle for soil classification [105]

3.1.3 Organic compounds

Oils and greases are present on the railhead in small quantities. Even though they may not be as abundant as other kinds of contaminant their presence has been shown to control adhesion. Their composition, chemistry and effect on railhead adhesion is therefore important to understanding railhead chemistry.

Typical oil contamination levels found on rails from organic chemicals extracted from rust scrapings have been found to be around 2 – 7µg per square cm. Analysis of this contamination has shown that the majority of the oils found can be grouped into three fractions, summarised in Table 6.

Table 6, Content summary of oily railhead contamination [34]

Fraction	Composition, %	General chemistry	Example compounds
A	30 – 65	Mixture of mainly branched aliphatic hydrocarbons, C_{18} and higher	squalene
B	2 – 6	Viscous large aromatic compounds, C_{20}-C_{36}	none mentioned
C	20 – 60	Mixture of large molecules containing C=O grouping as well as amine and sulphur containing compounds. Highly surface active.	acids, esters, ketones, naphthenic acids

The oils may originate from oils and greases on the locomotives or rail infrastructure; they may also originate from lubricants or friction modifiers which often use an oil additive in addition to particles to control levels of traction on flanges or in the wheel / rail interfaces in curves [107, 108].

Leaves are a major contaminant of the wheel / rail interface and account for approximately half of the safety incidents in the United Kingdom during the autumn period [109].

The number of unique compounds found within the structure of the leaf is great, but this section will only include the most abundant chemicals and structures found within leaves as well as those that have been identified as of interest in the context of the wheel / rail contact.

The leaf has been simplified into 4 parts shown as a cross section in Figure 16: the inner mesophyll, the epidermis surrounding it, a covering surface waxy cuticle layer and veins (not shown here).

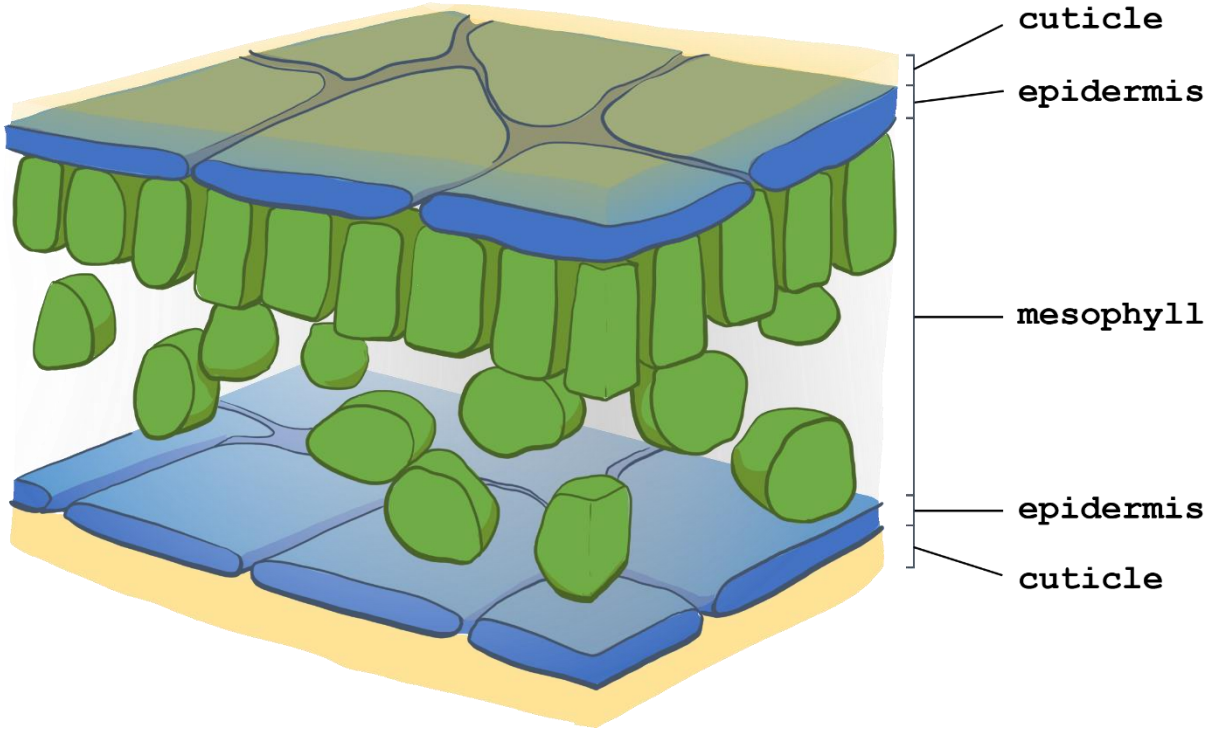

Figure 16, Diagram of leaf cross section, adapted from [110]

The cuticle is a layer of waxy film covering epidermis cells on the surface of leaves or other parts of a plant which are not covered in bark. It consists of insoluble lipid polymers and waxes synthesised by the cells in the epidermis. This waxy layer is moulded to fit tightly into and around the spaces between the cells and bonded to it with a thin pectin layer.

The epidermis is a single layer of cells covering the leaf organ. It forms a boundary between the plant and the external environment as well as synthesising the chemicals of the plant cuticle.

The tissue in the middle of the leaf is called the mesophyll and normally consists of 2 layers: a thin upper surface of 1 or 2 densely packed vertically elongated cells where the majority of photosynthesis takes place, and a less densely packed layer below with air pockets to facilitate the transfer of gasses within the leaf. It is in these cells of the mesophyll where chlorophyll is most abundant.

Veins within the leaf are made up of a vascular bundle containing a core of 2 cell types, xylem and phloem, which transport water and minerals, and sap with dissolved sucrose respectively. Surrounding the vascular tissue is a sheath of lignin which strengthens the structure of the leaf.

The plant cells in a leaf all share a similar general structure and are 'knitted' together by their cell walls. An illustration of a cell is given in Figure 17. The main parts of the plant cell include the cell wall, a membrane, cytoplasm fluid inside, a vacuole, the cell nucleus and plastids which can serve a variety of functions.

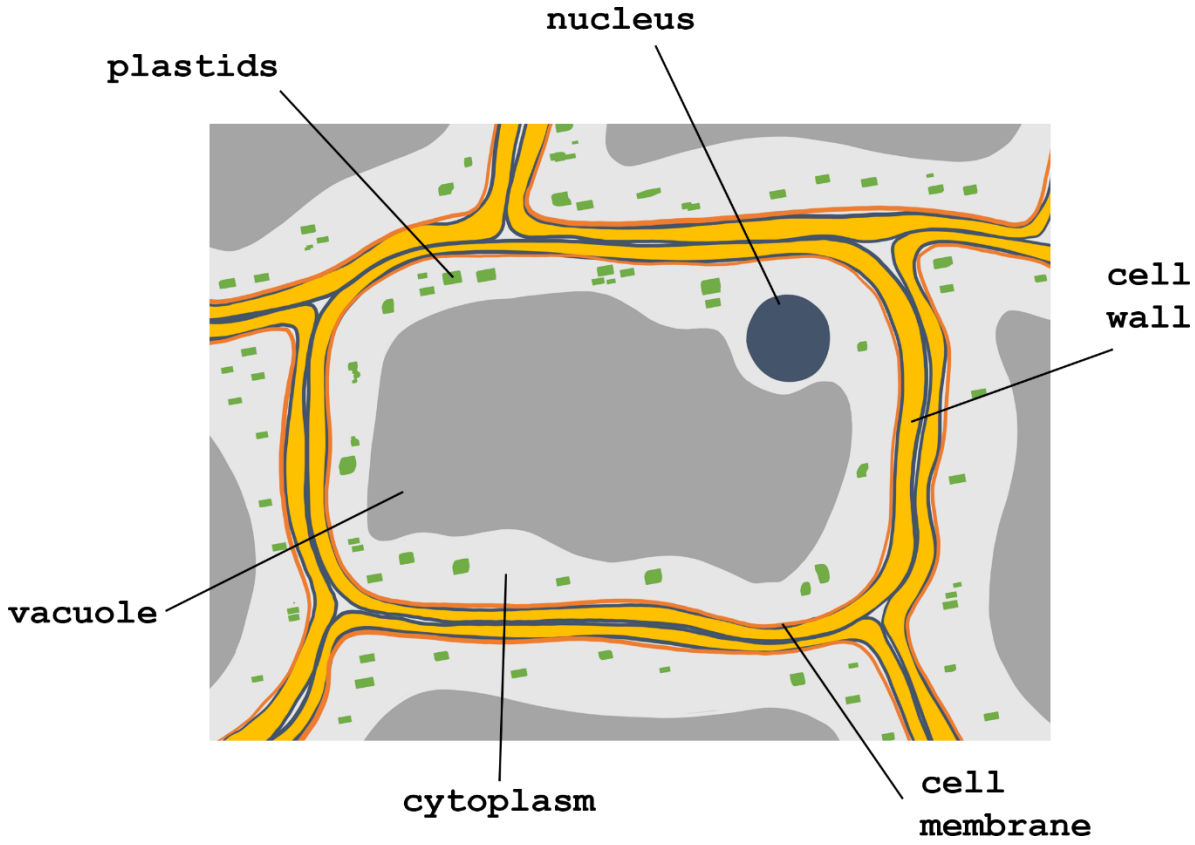

Figure 17, Simplified leaf cell, adapted from [110]

The structure of plants is formed from networks of cells working together. Plants do not have skeletons like animals and therefore rely on the rigidity of this network of cells to support the entire organism. The cell walls are what enable this rigidity and their strength comes from organic fibres.

The bulk of the cell walls are composed mainly of micro-fibrils of cellulose "tethered" together by hemicelluloses. Lignin fills some of the spaces between the micro-fibrils, reducing the porosity as well as strengthening the structure. Pectins and other plant proteins form a matrix which the structure resides within [111]. The plant cell walls can be thought of as an interwoven network of fibres held together by the presence of thin strands which bond to the fibres and themselves, this is shown in Figure 18.

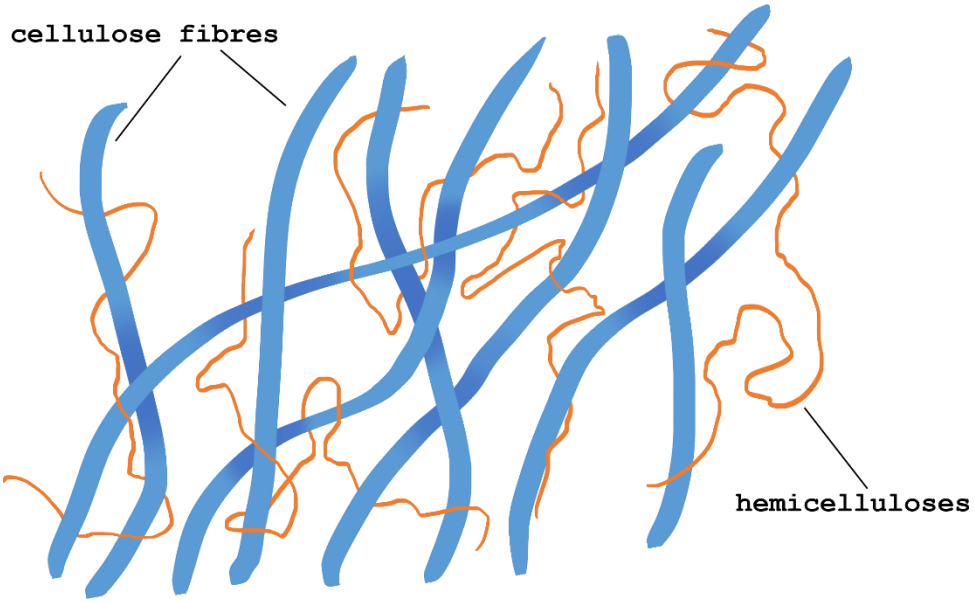

Figure 18, Plant cell wall general structure

The fibres are a multi-scale structure of mainly cellulose, but with trace amount of hemicellulose between the larger scales. The elementary fibril from which the larger strands are formed, known as the micelle, is composed of a parallel bundle of crystalline cellulose molecule chains. It is the connected network of these fibres which give the plant its structure.

Between the cell walls is a discontinuous layer called the middle lamella, forming the interface between plant cells and gluing them together. This middle lamella consists of pectin, lignin, and some proteins.

The cell wall is often porous to many substances, but the cell membrane, attached to the inside of the cell wall, regulates material transfer into and out of the inner cell. The membrane consists of a phospholipid bilayer, illustrated in Figure 19, with various types of proteins which aid the membranes' selective permeability function [110].

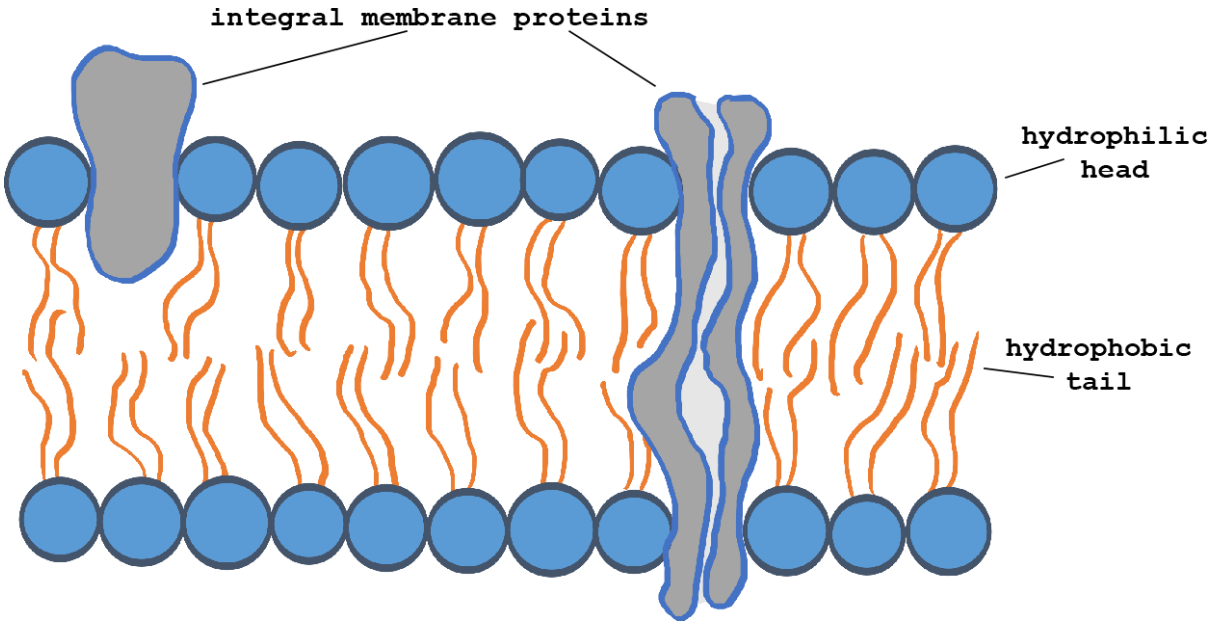

Figure 19, Phospholipid bilayer

Chloroplasts, a type of plastid abundant in leaves, contain the chlorophyll and carotenoid. Within them they synthesise glucose from photosynthesis. Other plastids can store products such as starch, or synthesise other compounds such as proteins. Plastids in the epidermis cells synthesize fatty acids and enzymes to form the plant cuticle.

Cytoplasm is the main liquid making up the cells. Mainly composed of water but can include other compounds such as inorganic compounds, starch, glycogen and lipid droplets.

The nucleus is a membrane enclosed organ which contains a complex mix of proteins. It also contains membrane materials similar to those within the cell membrane.

The vacuole within a cell is a compartment of fluid enclosed within a membrane. In the leaves it supports the structure of the cell by exerting a pressure but may also serve other functions including the store of enzymes, waste products, water and other small molecules. Polyphenols are also present within the vacuole and have a significant composition (9% hickory and 16% oak) [41], but normally only found in other parts of the cell when it is ruptured (when the cell is destroyed). Its membrane can be thought of as similar to the cell membrane in composition.

A major component of leaves is water and depending on the species, it may vary from between 98% for turgid (saturated) spring leaves, to around 40% in desiccated leaves. Wilting leaves typically have a relative water content of around 60-70% [112].

The chemical compounds are grouped into three groups of discussion: sugars, starches, polyphenols and structural polymers; carboxylic acids, cutin matrix and lipids; and chlorophyll and seasonal changes in the compounds which make up leaf plant cells.

Many compounds are based on the glucose monomer with the general formula of $C_6H_{12}O_6$, existing as both a straight chain form as well as the more abundant various cyclic isomer forms shown in Figure 20. These compounds are known as sugars or saccharides and are an important source of energy for plants cells. They may be in the form of monosaccharides, composed of only a single monomer (like glucose); disaccharides, consisting of 2 monomers; or longer polysaccharides, consisting of long chains of monosaccharide units in linear or branched configurations bound together by glycosidic bonds [113].

There are two general classifications of polysaccharides: storage-related, such as glucose and starches intended to store energy, and structural polysaccharides such as cellulose which have a stronger form of glycosidic bonding and are not hydrolysed easily.

Reducing sugars, unlike many polysaccharides, are sugars which can act as reducing agents due to the presence of free aldehyde or ketone groups. Glucose and all monosaccharides are within this classification. Many disaccharides and some polysaccharides are also reducing sugars. These sugars are found in concentrations of roughly 18% and 11% in hickory leaves and oak leaves respectively [41]. For the purpose of this study, they differ from starches by their solubility in water: starches are insoluble in cold water and the more simple sugars, including glucose, have good solubility in water.

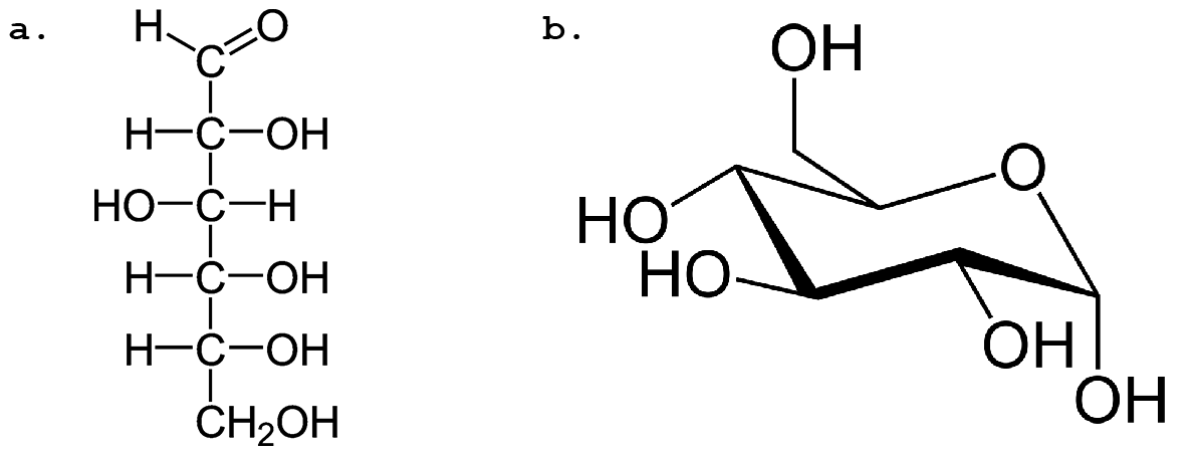

Figure 20, Molecular diagrams of glucose; a, open-chain form; b, cyclic form

When stored in starches, glucose monomers are joined by glycosidic bonds (covalent bonds between a hemiacetal or hemiketal group and a hydroxyl group of another molecule). The starch molecules are composed of two main types, an amylose (linear) form and a more abundant (75-80% typical) amylopectin (branched) form. The general structures of these can be seen in Figure 21. Starch content within leaves varies throughout the course of the year. A study into the starch content of pear trees showed that the starch in the leaves increases in concentration towards the end of the year after harvesting of the fruit. The concentration was shown to be 4% of dry weight in the leaves towards the end of the monitoring period [114].

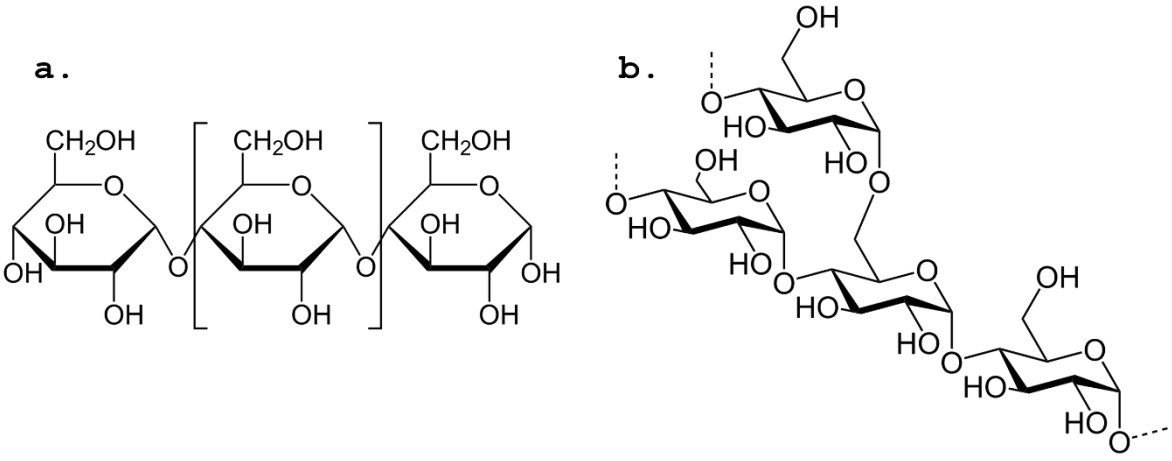

Figure 21, Skeletal diagrams of amylose (a) and amylopectin (b) starch forms

Structural polymers are compounds predominantly found within the cell walls. Whereas the monomers in the storage-polymers are bound by easily hydrolysed alpha-glycosidic bonds, structural polymers are bound by stronger bonds such as beta-glycosidic bonds which are more resistant to hydrolysis.

Cellulose is a 1,4-ß-poly-anhydroglucose polysaccharide. It is a homo-polymer of glucose, meaning that it is composed entirely out of glucose monomers. It can also be thought as a polymer formed from monomers of cellobiose which structure can be seen in Figure 22; a disaccharide molecule formed from 2 glucose units.

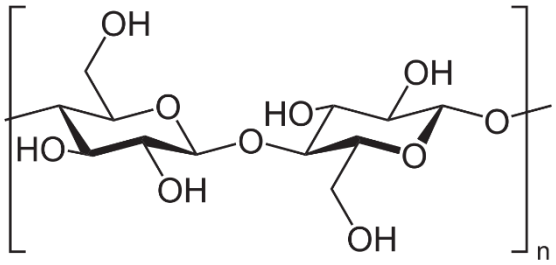

Figure 22, Cellulose monomer skeletal formula (n = 2000-6700 typical)

The compound is a major chemical constituent of plant tissue varying between 50-70% overall; however, the cellulose content of leaves is usually significantly less than in other parts of trees. Depending on source, the molecules are usually formed in lengths of between 2000 and 6700 units.

Cellulose is an unbranched highly crystalline polymer and is capable of a high degree of hydrogen bonding which gives the microfibrils their strength.

Hemicelluloses, unlike cellulose, are hetro-polymers and composed of various monomer units including glucose, glucuronic acid, xylose, arabinose and galactose. They are branched polymers. Within this classification are the compounds xylan, galactan, araban and pectins. Usually consisting of between 500 to 3000 monomer units, hemicelluloses are typically shorter molecules than celluloses and due to their random amorphous structure, they have little mechanical strength and may be hydrolysed easily. Hemicelluloses are about as abundant in leaves as celluloses [41] and the composition of the hemicelluloses present varies widely according to the plant source.

Determination of the type of hemicellulose is done by identifying the number of carbon atoms in monomer structure. Xylan is the most abundant of these hemicelluloses, one possible structure can be seen in Figure 23.

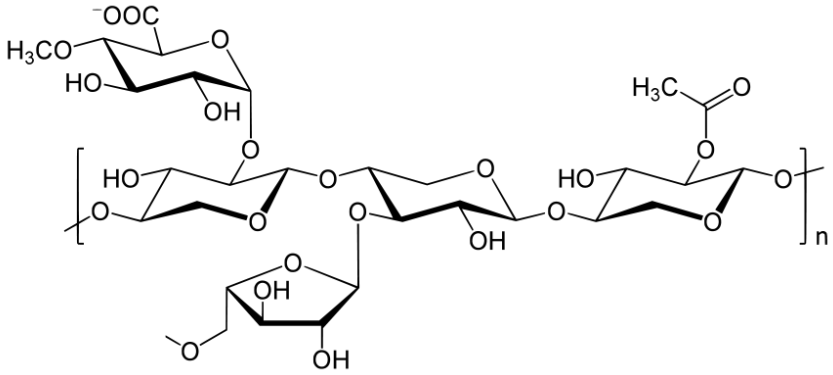

Figure 23, A possible configuration of xylan molecular structure (n = 500-3000)

The hemicellulose, pectin, has a complex irregular backbone chain of monomers derived from d-galacturonic acid (homogalacturonan) and occasionally a rhamnose monomer (1-4%). The structures of glucuronic acid and rhamnose are given in Figure 24. The main chain of the polymer appears to contain groups of similar modifications. A significant portion of the galacturonic acid groups have been esterified to contain methoxy groups and some containing acetyl groups. The length of the polymer is composed of distinct regions dominated by homogalacturonan (smooth) and regions dominated by side groups (hairy) as shown in Figure 25. Common side groups include xylose, arabinose and galactose sugars.

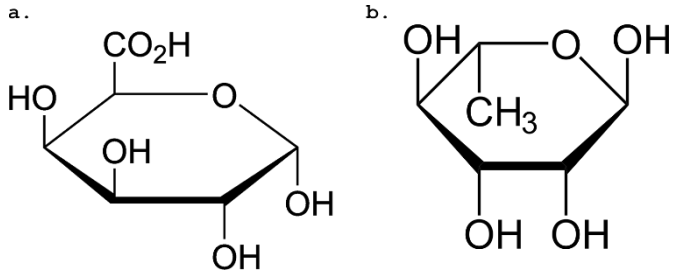

Figure 24, Skeleltal molecular diagrams of galacturonic acid (a) and rhamnose (b)

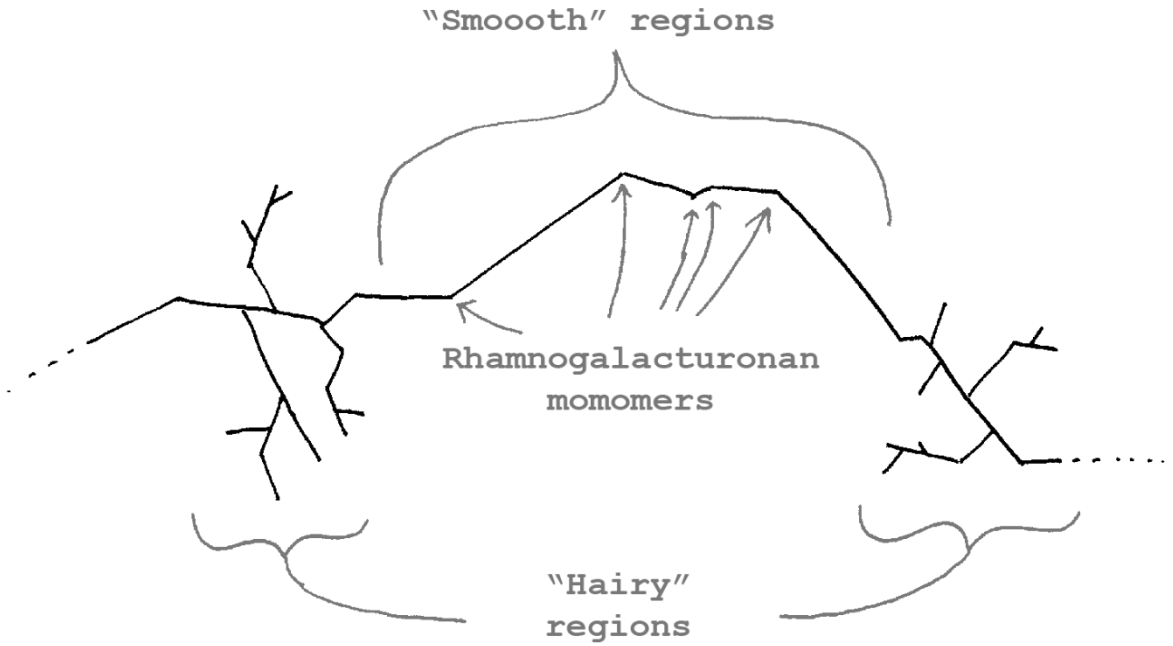

Figure 25, Pectin primary structure showing smooth unbranched regions and hairy regions, rich in sugar side chains

Pectin is typically found in and between the cell walls of plants. Its presence helps bind the cells together as well as allow for cell growth and extension.

Like all hemicelluloses, their various components making up the polymer vary depending on their source. For instance, citrus peel pectin is low in galactose and arabinose. Molecule sizes vary widely and molecular weights have been observed between 60 to 130 000g.mol.$^{-1}$ [113].

The last major structural polymer is lignin which, unlike cellulose and hemicellulose, is not a polysaccharide composed of glucose monomers but a polyphenol. Polyphenols are a class of aromatic compounds composed of many multiple phenol units in their structure. Lignin is insoluble but soluble polyphenols also exist which constitute to around 9% of the composition of hickory leaves and 16% of oak leaves.

At the basic level Lignin can be considered to be a polymer of coniferyl alcohol shown in Figure 26. Related aromatic compounds and a representative structure of the polymer can be seen in Figure 27. Similar to cellulose, lignin is less abundant in the leaves than in "woody" parts of the tree organism, this is in part due to its mechanical structural role in the organism.

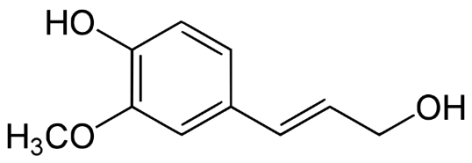

Figure 26, Coniferyl alcohol structure

Lignin fills in the spaces between other components in and around the cell walls offering rigidity to the organism as well as controlling water permeability due to its hydrophobic nature. Unlike many other chemicals within the cell walls it forms covalent bonds with hemicellulose and cross-links molecules, further strengthening the organism. Due to this tight bonding of lignin to other compounds, extraction processes cause a breakup of the polymer making examining the size and structure of lignin difficult.

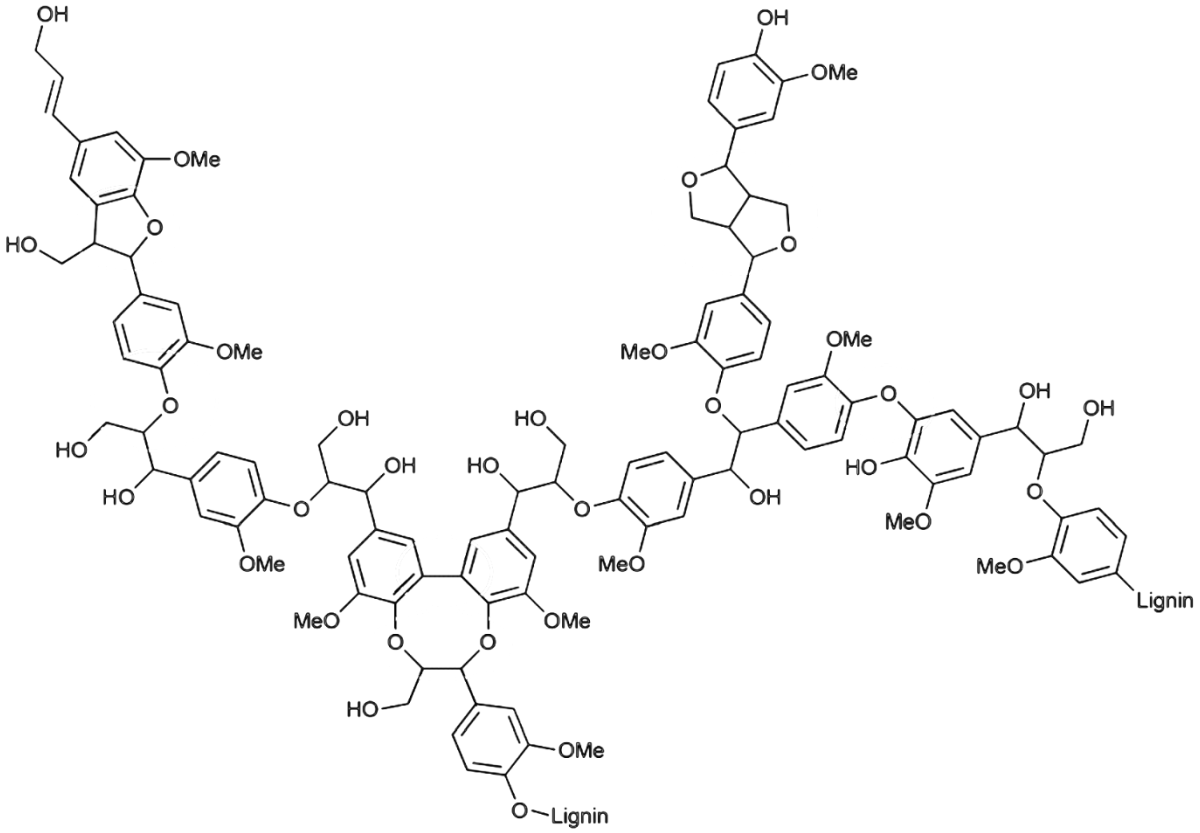

Figure 27, Representative structure of part of a lignin polymer [115]

Lignin does not rot easily and therefore extends the life of the structure by “sealing” other compounds cross linked to the lignin by making them inaccessible to enzymes, thereby slowing degradation.

Tannins, including tannic acid, is another an example of polyphenols found within leaves. In plants they serve many functions including acting as UV screens to protect against ionising radiation, as a signalling chemical interacting with morphology and hormones, and deterrence of microbes and herbivores due to their toxic properties. They are typically contained within the vacuoles of the cells.

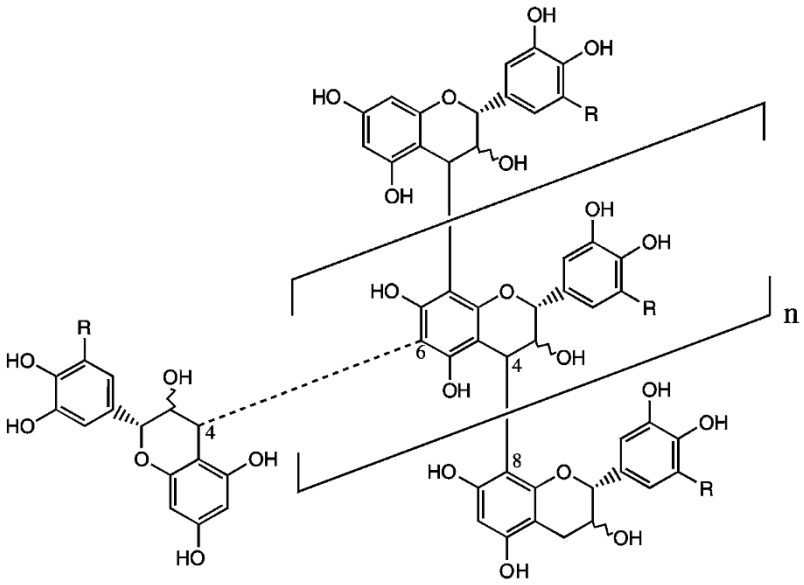

Figure 28, Structure of condensed tannin, n < 18 typical for soluble varieties [116]

Condensed tannins are the most abundant type of polyphenols. The general structure of this group of molecules is given in Figure 28, typical soluble molecules of tannins consist of between 2 and 17 monomer groups.

In the plant cuticle, epicuticular wax coats the outer surface of the leaf attached by a pertinacious glue layer. Cutin and cutan are the two polymers responsible for this layer. The compounds are solids at ambient temperatures and have melting points above 40°C. They are soluble in organic solvents including hexane. Thicknesses of the layers varies by species and has a coverage of between 20 to 600 µg per square cm of surface area.

The most abundant chemical found within the cuticle is cutin, a polyester polymer composed of straight chain carboxylic acids. The monomers are in two families of 16 and 18 carbon chain length omega hydroxyl acids and their derivatives. The acid and hydroxyl groups on the monomers react to produce ester bonds and form an amorphous polyester coating of molecules of extensive sizes. Lipid monomers of this polymer may also be found within the layer. For some plants, a different molecular structure called cutan may be found; unlike cutin, which is a polyester containing ester and epoxide bonds, cutan is a hydrocarbon polymer. Cutan is more resistant to degradation due to its absence of ester groups which can be hydrolysed.

Fast growing parts of the plants tend to have higher quantities of the C16 family of monomers in their cutin; this includes leaves which are approximately 65% C16 polymer. The most common major components in the C16 family are 16-hydroxyhexadecanoic acid and 9 or 10, 16-dihydroxyhexadecanoic acid which are liberated when the ester bonds of the polymer are hydrolysed. Their structures are given in Table 7.

Figure 29 gives a general polymerised form of the cutin components which may cross link due to the monomer's multiple hydroxyl groups.

The C18 family of monomers has similar molecular shapes but also includes some epoxide group molecules as well as unsaturated carboxylic acids (enoic acids) and trihydroxy – acids. Bonding in the formed polymer is, alike C16 cutin, dominated by ester bonding.

Table 7, Major C16 components of cutin

Name	Structure (skeletal)
16-hydroxyheadecanoic acid	
9,16-dihydroxyhexadecanoic acid	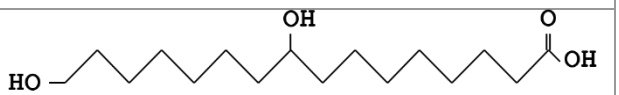
10,16-dihydroxyhexadecanoic acid	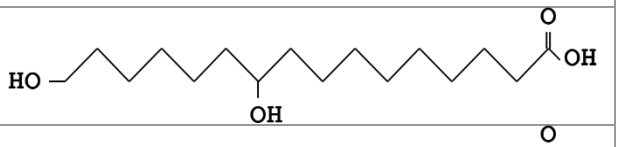
Hexadecanoic acid	

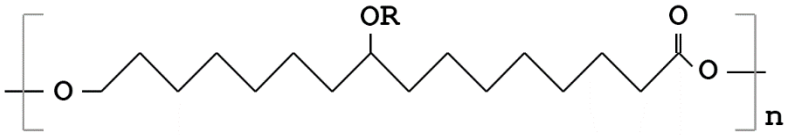

Figure 29, General structure of plant cutin based on 9,16-dihydroxyhexdecanoic acid, R may represent a cross-link between polymers or a hydrogen atom

Also present within the cuticle are lipid molecules which are the monomers making up the epicuticular waxy layer. These are fatty acids such as those given in Table 7 but, unlike cutin, remain unpolymerized.

The structure of the cutin monomers are similar to molecules found within the thin membranes of the cells, called lipids which are surface agents enabling them to be self-assembling. These thin membranes separate the interior of the cell from the external environment, as is the case with the cell membrane, but also enclose and isolate parts of the cell such as the nucleus, plastids and vacuoles. These biological membranes are mainly of the form of phospholipids composed of double chained hydrophobic fatty acid chains of 16 to 18 carbon atom lengths joined by a glycerol molecule containing a phosphate group which is hydrophilic.

Chemicals are present within leaf layers with specific functions serving processes within the organism. These include photosynthesis, membrane selectivity, plant metabolism and growth.

Proteins are naturally occurring polyamides and diverse in variety. They are also referred to as polypeptides due to the peptide bond (or amide linkage) which joins the amino acids. The two major groups of proteins are fibrous proteins and globular proteins; fibrous proteins being long molecules which are held together in coiled immiscible chains by hydrogen bonding between the molecules. Globular proteins are held in spherical or elliptical shapes by intramolecular hydrogen bonding and are soluble in water with low salinity.

Chlorophyll is the substance within a leaf which is responsible for the primary function of the leaf of photosynthesis. Two main types exist within terrestrial plants, shown in Figure 30; however, they have similar physical properties.

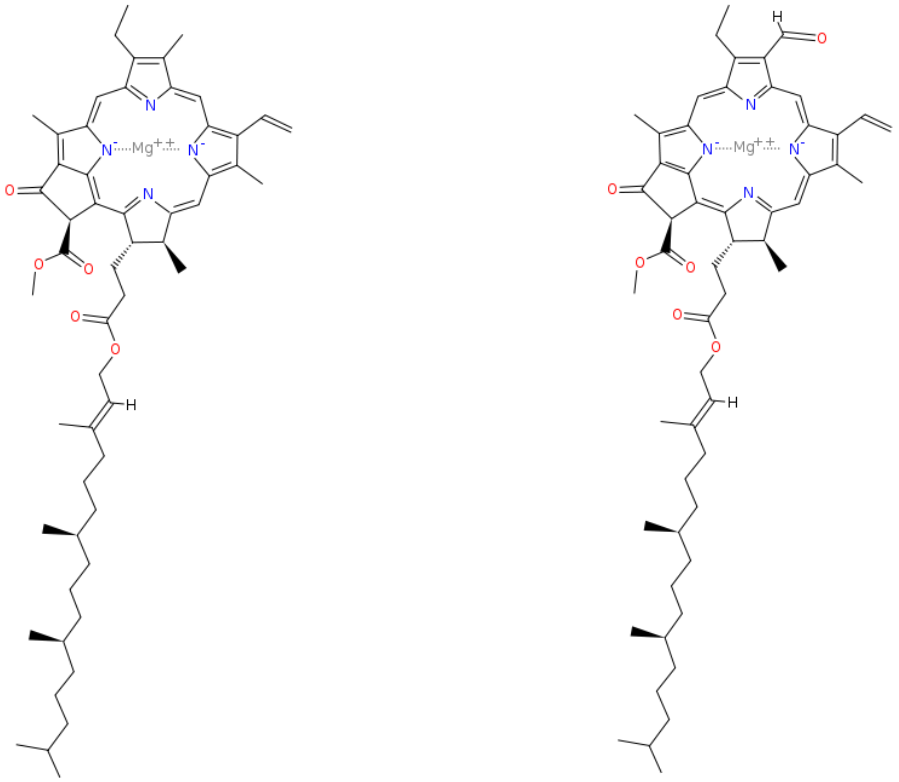

a b

Figure 30, Structure of chlorophyll a and chlorophyll b

Chlorophyll is responsible for the strong green colour in leaves and varies in concentration over the course of the year. Leaves of deciduous forests have been shown to contain, at their peak, approximately 50µg chlorophyll per square cm, accounting for approximately 0.6% of the leaf's dry content.

Carotenoids are also an important chemical for photosynthesis, aiding the reaction and protecting the chlorophyll from light damage. They are found at about 1/5th the concentration of chlorophyll in green leaves.

Much of the information compiled within this review considers 'green' leaves; however, during the problematic season of autumn, leaves have undergone changes in a process known as leaf senescence [117]:

- Chlorophyll is expended yet the carotenoids are more stable causing the pigmentation within the leaves to change, revealing autumnal colours.
- Sugars and starches are withdrawn from the leaves into other organs of the tree.
- A cork-like growth develops at the base of the leaf to isolate and separate it from the branch.
- Moisture in the leaf is no longer retained and it begins to wilt.
- Microorganisms begin to degrade the leaf.

The cell walls cannot be metabolised easily and so remain mostly unchanged. The plant cuticle is also mostly unaffected due to it being located external to the leaf; however, it is degraded by microorganisms more rapidly due to this position.

3.2 Compound and surface interactions

This subsection considers the chemicals discussed in this chapter with regards to their chemical interactions and mechanical properties which may be relevant to railhead traction.

3.2.1 Boundary lubrication and adsorbed films

Under the great pressures exerted upon the wheel / rail contact by railway locomotives, it is hypothesised that hydrodynamic lubrication gives way to boundary lubrication. When these surfaces are physically in contact with each other, lubrication at the surface can still reduce the amount of friction which they experience.

Surface agents are chemicals which interact with interfaces and may result in a change of physical or chemical properties. Two major basic types of interactions are physisorption and chemisorption.

Physisorption, or physical adsorption, is the process where a molecule is adsorbed to a surface, but the electronic structure of the adsorbed species or substrate is not strongly altered by the adsorption or desorption process. This is mainly characterised by a relatively low binding energy between the adsorbed species to the substrate and is mostly associated with intermolecular van der Waals forces, polar forces and hydrogen bonding.

A theory of a monolayer boundary lubrication was proposed and developed by Hardy [118], by which the sliding surfaces are held apart by monolayers of physically adsorbed and orientated polar molecules such as alcohols or acids. These monolayers form a plane of low shear strength, reducing the friction between the surfaces, as illustrated in Figure 31.

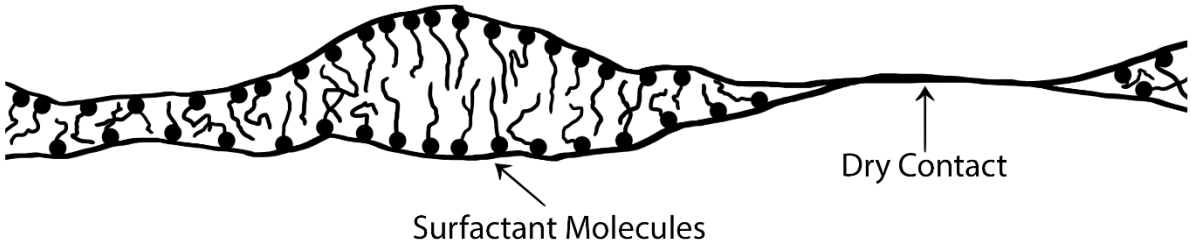

Figure 31, Illustration of physically adsorbed monolayer boundary lubrication

Monolayers have been shown to reduce the friction coefficient of interacting surfaces by orders of magnitude. Figure 32 shows the effect of the concentration of a polar surface agent (hexadecanol) in a steel-steel sliding system. It can be seen that at a certain concentration, the surface is saturated and no further reduction in friction can be achieved by increasing the concentration of surface agent.

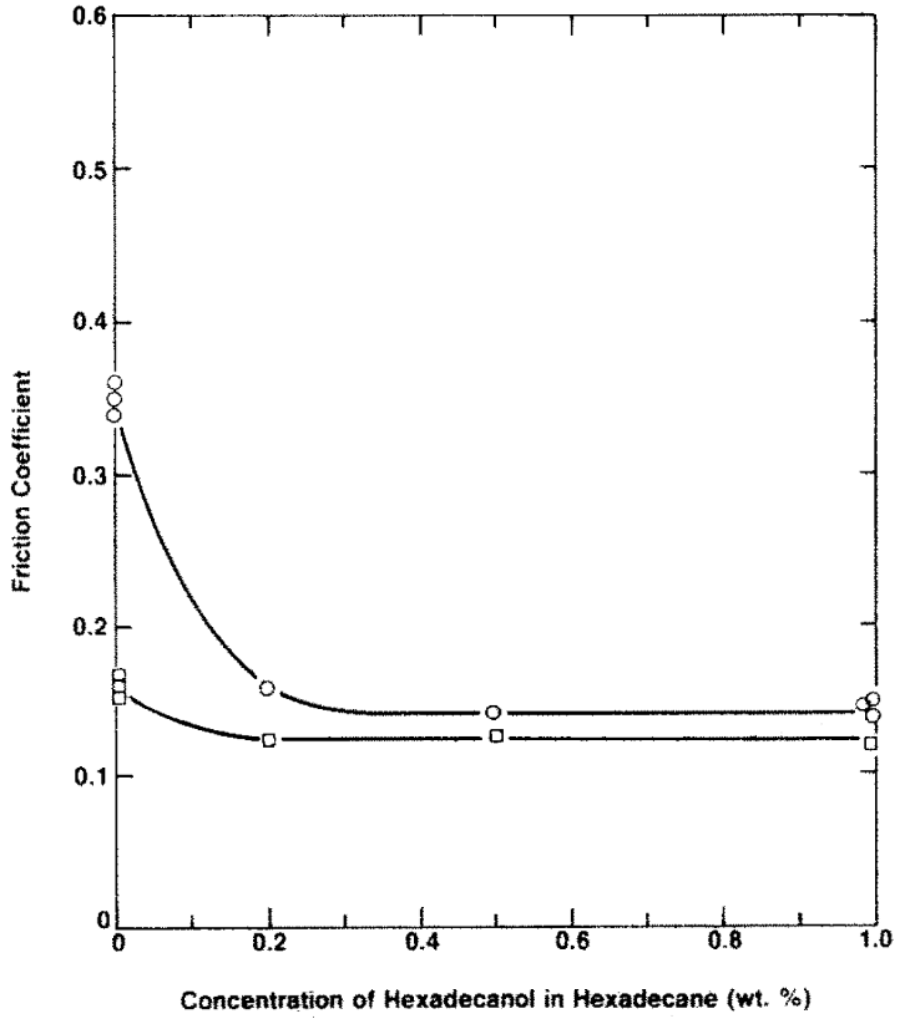

Figure 32, Effect of Hexadecanol concentration in Hexadecane on Friction Coefficient using Steel ball on cylinder testing, 5 × 10^{-4} ms^{-1} (○) and 1 × 10^{-2} ms^{-1} (□) [119]

Gregory [120] also demonstrated that with only small amounts of surface agent (0.001% dodecanoic acid solution), it was possible to achieve significantly reduced coefficients of friction; however his work also demonstrated that the adsorption of a sub-monolayer quantity of acid onto the sliding surfaces is a slow process by taking hours to attain a value comparable to the saturated cases.

Whilst over-saturating the interface with the active surface agents does not achieve an initially lower friction coefficient, it has been shown to increase the robustness of the effect either through the existence of redundant layers or a rapid reformation of the film. This can be seen in Figure 33 which shows the friction of stainless steel surfaces with stearic acid films of varying monolayer thicknesses. Whilst a single monolayer is quickly worn away after just a few passes, the lowered friction behaviour is prolonged greatly with more layers.

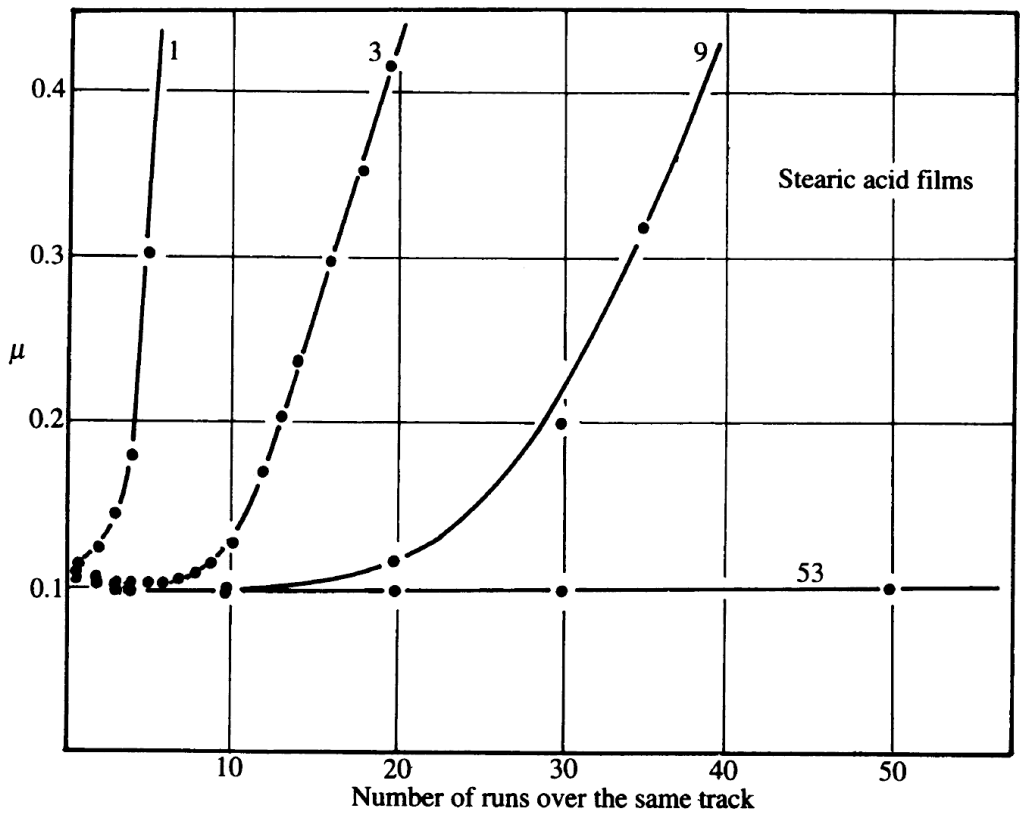

Figure 33, Friction of stearic acid films on stainless steel surface of varying number of monolayers [121, p. 187]

The effectiveness of a boundary lubricant is highly dependent on how strongly the protecting molecules adhere to the contact surfaces. In the monolayer theory, this bonding is predominantly physical with the polarity of the surfactant's active group being the source of the attractive force. Chemical bonding is also shown to occur between some more reactive additives and metal surfaces to form a chemically bonded protective film of low adhesion; this is chemisorption.

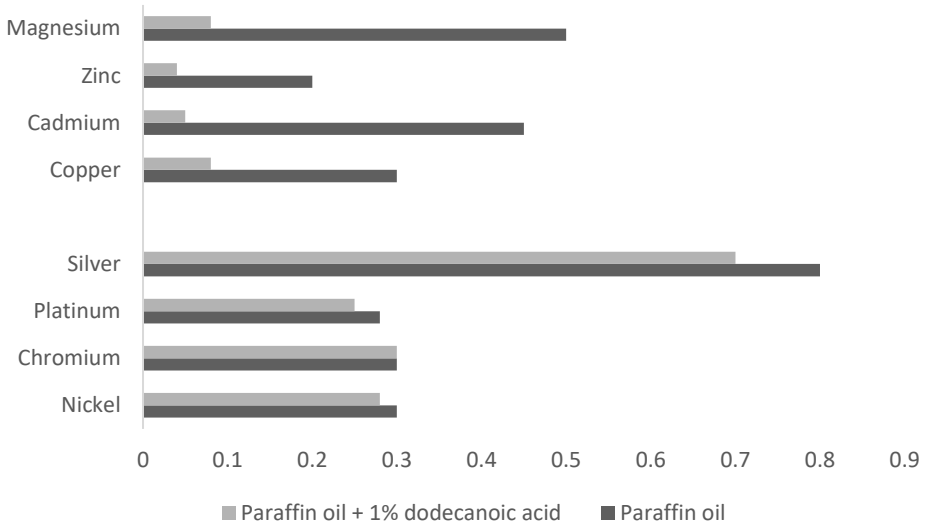

Figure 34, Kinetic coefficients of friction of reactive and unreactive metals in the presence and abscence of dodecanoic acid additive in paraffin oil (adapted from [121])

Figure 34 compares the effect of a boundary lubricant additive, dodecanoic acid, on the sliding coefficients of friction of various metals. The lower set of metals are relatively unreactive and show little change in frictional properties with the additive. The top group, on the other hand, are more reactive metals and expected to interact chemically with the acid in the solution. We can see from the results that the sliding coefficients of friction are greatly reduced, indicating the formation of a low shear stress layer on the surface of the metals.

Strong evidence is presented to suggest that lubrication of the contacting surfaces is unaffected by the presence of the active chemicals (usually fatty acids) themselves, but as a product of the reaction between them and the surfaces [121]. This is referred to as a metallic soap.

The expected chemical reaction between a general reactive metal (*M*) and dodecanoic acid is given as:

$$M + C_{12}H_{23}OOH \rightarrow [C_{12}H_{23}OO^{-}][M^{+}] + H_2 \qquad [I]$$

and in the case of copper (*Cu*), this is:

$$Cu + [C_{12}H_{23}OOH]_2 \rightarrow [C_{12}H_{23}OO^{-}]_2[Cu^{2+}] + H_2 \qquad [J]$$

Copper dodecanote is insoluble and therefore may build up to form a thin layer on the surface of copper metal after reaction.

Layers formed by this mechanism are said to act in the same way as solid lubricants. This is evidenced by the effects of temperature on the lubricants and also by comparison to solid lubricants themselves. The effect of Dodecanoic acid was observed under a range of temperatures on two surfaces: copper and platinum. Results are show in Figure 35. From this study we can see evidence that solid copper dodecanoate is the effective lubricant in both cases. The effect of applying copper dodecanoate to the platinum surface reduces the friction to almost the same level as applying a solution of dodecanoic acid to the copper surfaces. For both, the coefficient of friction is shown to rise rapidly at the softening point of copper dodecanoate.

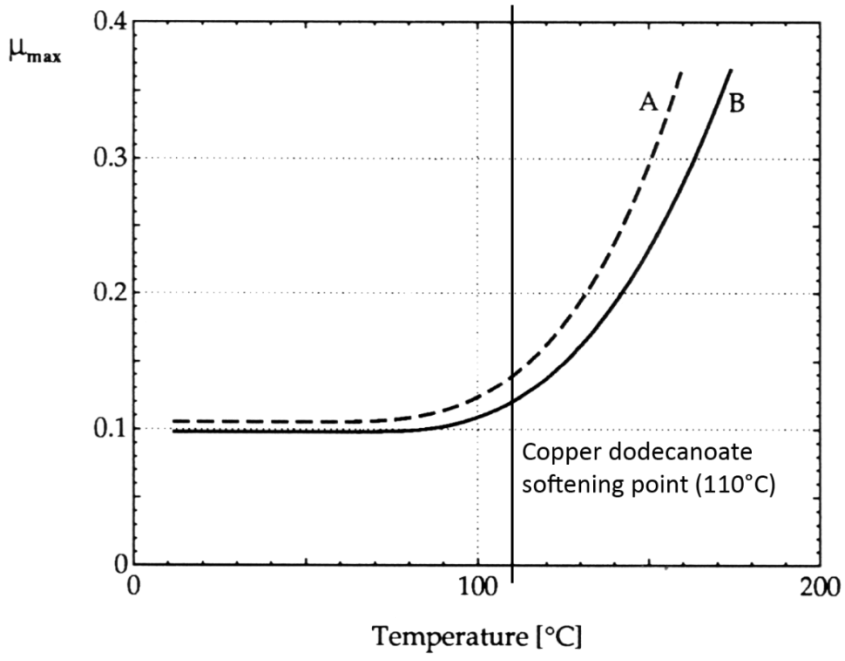

Figure 35, Effect of temperature on the coefficients of friction of platinum lubricated by solid copper dodecanoate (A) and 1% dodecanoic acid in paraffin oil on copper surfaces (B) (adapted from [118])

The cause of the rise in adhesion at the melting point or softening points of the surface chemicals is that the layers are less effective in maintaining mechanical separation of the surfaces and therefore are not as effective lubricants.

Chemical reactions at the interface can lead to the formation of complex films. One such example is the oil additive Zinc dialkyl-dithophosphate which, at high temperatures, synthesises a complex layered film of polymer strings and polyphosphate glass [122, 123]. The formation of the Zinc dialkyl-dithophosphate tribofilm has been studied using the same apparatus as has been used for rail adhesion testing [73].

Each case studied is very specific and out of the scope of this research; however, it is important to be aware of the existence of complex tribo-chemical surface interactions in addition to physical or chemical adsorption of surfactants when considering the chemistry of the wheel / rail interface.

Surfactants which may physically or chemically adsorb onto the railhead interfaces may form part of more complex systems by promoting the adhesion of other organic compounds to the railhead which are not able to adhere to the railhead themselves. Chemicals which aid bonding between hydrophobic organic films and hydrophilic metallic surfaces are termed “molecular adhesion promoters” and have been developed in the pharmaceutical industry to aid biocompatibility applications [77] where the properties of surfaces need to be significantly modified.

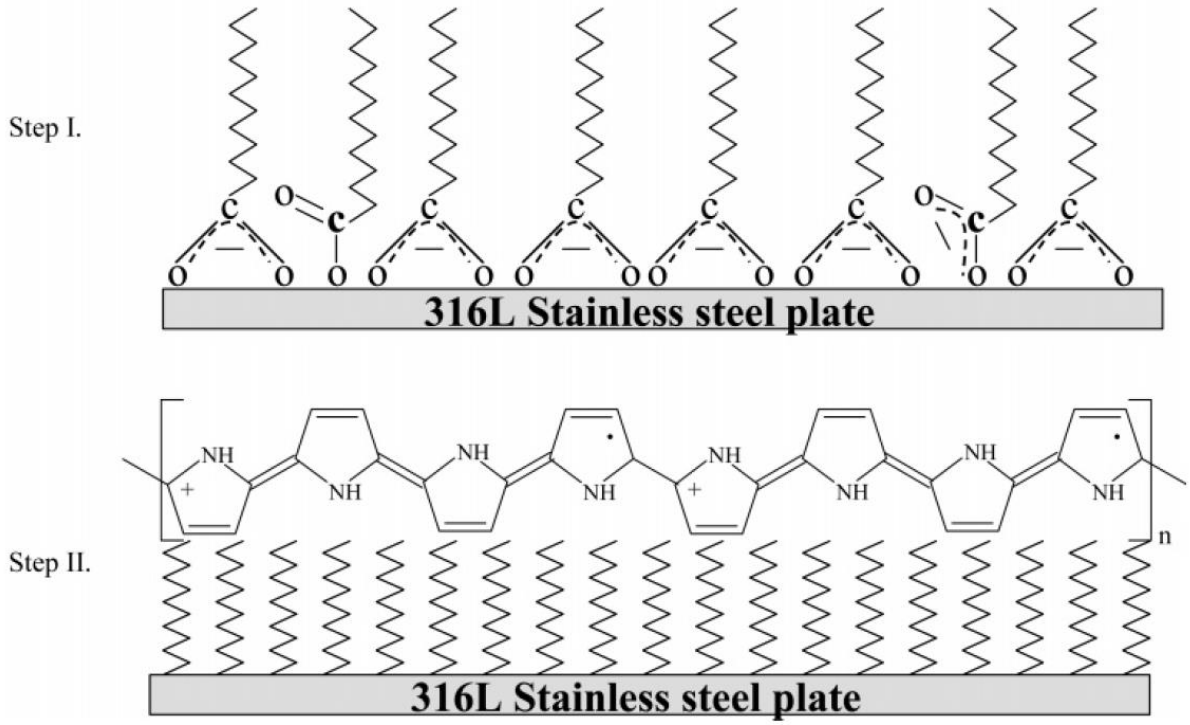

Figure 36, Steps to the formation of an organic coating on stainless steel [77]

Figure 36 shows the formation of an organic layer on a stainless steel substrate. Firstly, a self-assembled monolayer on the surface consisting of the surfactant molecules forms. This then provides a suitable chemical environment to allow the other organic molecules to adhere. Compounds shown to act as these adhesion promoters are similar to substances found on the railhead and this mechanism may contribute to the bonding or formation of leaf layers.

The geometry of iron oxide surfaces has been shown to change the way many chemicals interact with the surface; however, for most iron oxides, the interactions are similar.

Two types of interaction have been observed and studied via molecular calculations and chemical analysis. The first type concerns physisorption of the molecule onto the surface whereby the molecule remains intact. When water is present it often is adsorbed onto the surface in this manner whereby the oxygen atom's charge is attracted to the iron in the oxide lattice and / or the hydrogen ions are attracted to the oxygen within the lattice [124]. Ultrathin surface layers of water have been shown to be adsorbed onto the surfaces of oxides in this manner. As this method of adsorption relies on intermolecular forces, the molecules are only weakly bound to the surface and are easily removed.

The second and more commonly observed mechanism of adsorption for most oxide types occurs when the adsorbing species comes into contact with the oxide surface and disassociates. The disassociated molecule may form strong bonds with the oxide surfaces. In the case of water, the molecule is disassociated into a hydroxyl group and a hydrogen atom which are bound to adjacent vacant sites on the iron oxide mesh.

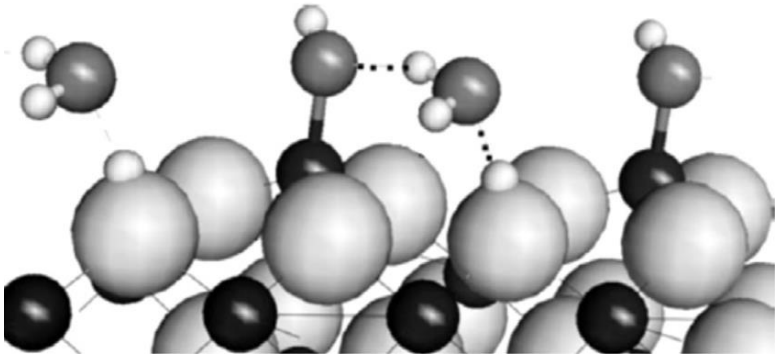

Figure 37, Schematic of disassociated water adsorption and physiosorbed water on iron oxide interactions [124]

A combination of the adsorption types may also occur, as is shown in Figure 37, whereby the disassociated molecules adsorbed onto the surface of the iron oxide may provide sites of origin for further intermolecular physisorption.

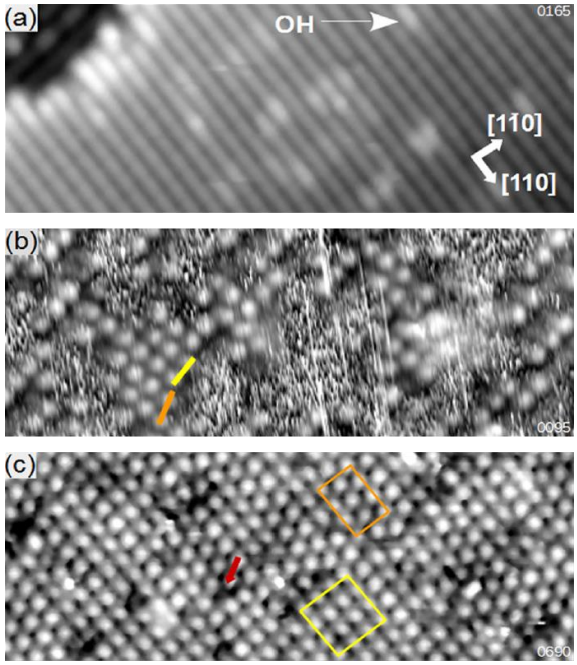

Figure 38, Tunnelling microscope images of a surface of iron oxide. Clean, a; after low exposure to formic acid, b; and after longer exposure to formic acid, c [125]

The simple carboxylic acid, methanoic acid (C1) has been observed, using tunnelling microscopy, making tightly bound monolayers on the surface of iron oxides in what is proposed to be a bidentate configuration. This is shown in Figure 38 whereby two oxygen atoms in the carboxylate anion are bonded to an adjacent iron atom each.

Alcohol groups, have also been shown to interact with and bond to the surface of iron oxide in a dissociative manner and it is likely that this is the mechanism by which many organic compounds present on the railhead may interact with the iron oxide surfaces.

It may be important to note the catalytical properties of these types of interaction. When molecules are desorbed from the surface they may reform with other compounds to the species they were originally bonded with, resulting in chemically different reformed products [124].

Oils present in low concentrations on the railhead have been tested and the relatively low concentration of this type of contamination when compared to other groups of contaminants along with their high surface activity has led researcher's to study their effects as boundary lubricants [34]. Oils extracted from rail rusts scraped off the surface of running rails were tested on rolling disc tribometers alongside known compounds and are shown to dramatically reduce the coefficients of friction in only small concentrations as shown in Figure 39.

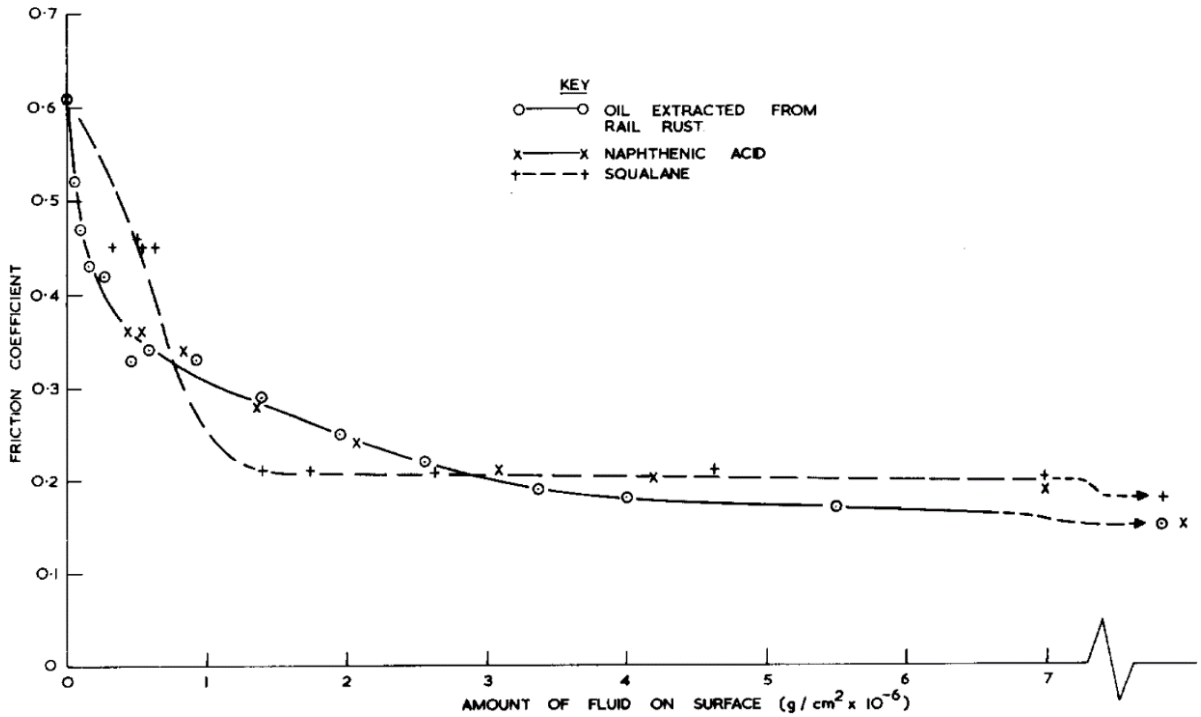

Figure 39, Effect of oils extracted from rail dust on friction [34]

Their presence on the railhead in small amounts even on apparently uncontaminated rails suggest that there will always be some form of oily contamination adsorbed in the contact which is irremovable with rainfall washing.

3.2.2 Rheology

Rheology is a branch of study into the deformation and flow of matter. It is an important consideration for railhead traction as the shearing of solid matter provides a disconnect between the driving surfaces.

Pastes of material can be formed from water and solid particles present on the railhead such as oxides, sand or ballast debris, or organic matter. These pastes of highly concentrated suspensions of fine solid particles, display properties which can be likened to a Bingham plastic fluid which behaves as a solid up to a finite load or stress can be applied after which continuous deformation of the fluid can occur [126].

Table 8, Summary of oxide appearance and physical properties [127]

Oxide name	Chemical Formula	Appearance	Density, $g.cm^{-3}$	Mohs' Hardness
Wüstite	FeO	Gray	6.02	5 – 5.5
Haematite	Fe_2O_3	Red / reddish brown	5.0 – 5.3	5 – 6.5
Maghemite	γ-Fe_2O_3	Brown / brick - red	4.86	5
Magnetite	Fe_3O_4	Black	5.175	5.5 – 6.5
Goethite	α-FeO(OH).n(H_2O)*	Yellowish to reddish brown	4.28	5 – 5.5
Akaganéite	β-FeO(OH).n(H_2O)*	Yellowish brown / rusty brown	3.75	-
Lepidocrocite	γ-FeO(OH).n(H_2O)*	Light reddish to reddish orange	4.09	5

*alternatively: $Fe(OH)_3$

The material and physical properties of particles within a suspension greatly influence the properties of the fluid. Newly formed iron oxide may have crystalline morphology and debris may be ground by mechanical action to smaller particles. Higher hardness of particles in oxide pastes has been proposed to influence the shear thickening behaviour of suspensions due to effects on the stress-bearing hydroclusters within the pastes; harder particles have been observed to not achieve the shear thickening behaviour exhibited by softer materials [128]. Different oxide types and morphologies have been shown to exhibit differing mineral harnesses which have been compiled in Table 8.

Gutsulyak et al. [129] observed the effect of materials of different hardness combined with water in a rolling-sliding interface using a twin-disc rig; these results are presented in Figure 40. It was observed that materials with lower hardness exhibited lower minimum traction levels in the contact. This was speculated by the authors to be caused by stable low shear pastes causing separation of the discs during the runs. High hardness materials were proposed to be less prone to the formation of these shearing pastes.

Leaf layers may also exhibit similar complex rheological behaviours to inorganic particle suspensions.

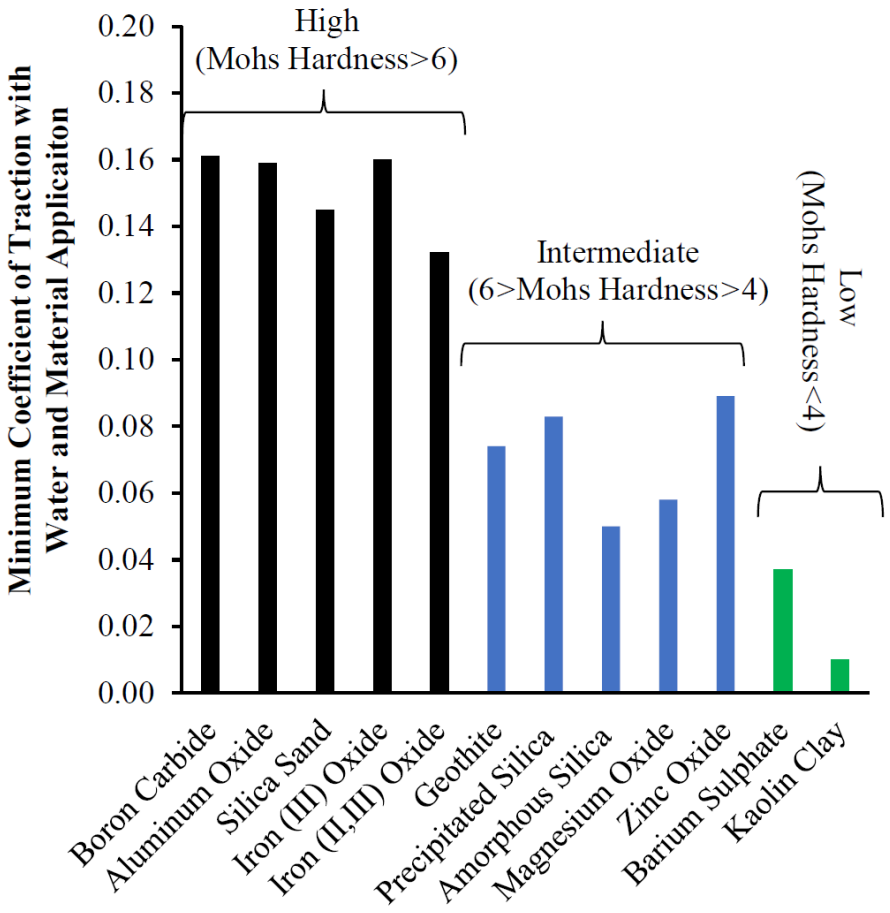

Figure 40, Bar chart showing the minimum coefficient of traction values from twin disc testing of various materials mixed with water, grouped by their hardness [129]

3.2.3 Viscous near surface effects

The most widely accepted theory of lubrication from additives is the for-mentioned thin-layer boundary lubrication; however, there has been much research to suggest a second mechanism may cause some reduction in friction between the surfaces. It has been noticed that the properties of a fluid close to a surface can be considerably different to that of the bulk with some studies showing the effective viscosities of thin liquid films to be of several orders of magnitude higher than the bulk viscosity within two molecular layers of the surfaces [118]. This effect may be enhanced by the presence of other chemicals which can migrate to the interfaces or be formed there.

Using ultrathin film interferometry, the formation of EHL films has been studied in the presence of various additives and under different chemical conditions.

Figure 41 summarises some of the findings of Ratoi et al. [130] in which the logarithm of the film thickness is plotted against the logarithm of the mean rolling speed. At sufficient separation of the surfaces, all the tests showed the same linear relationship; however, where an additive was present, non-linear behaviour was observed at thin film thicknesses implying that the viscosity of the fluid near the surface is different to that of the bulk. In Figure 41 b, arachidic acid shows non-linear behaviour at film thicknesses less than 10nm.

The testing was also conducted in wet solutions (Figure 41 c and d) where some water was blended with the hexadecane prior to testing. The presence of this water appears to be very significant in the formation of the film. Arachidic acid with the presence of water is shown to form a film of up to 20nm before the linear behaviour of the solvent was attained.

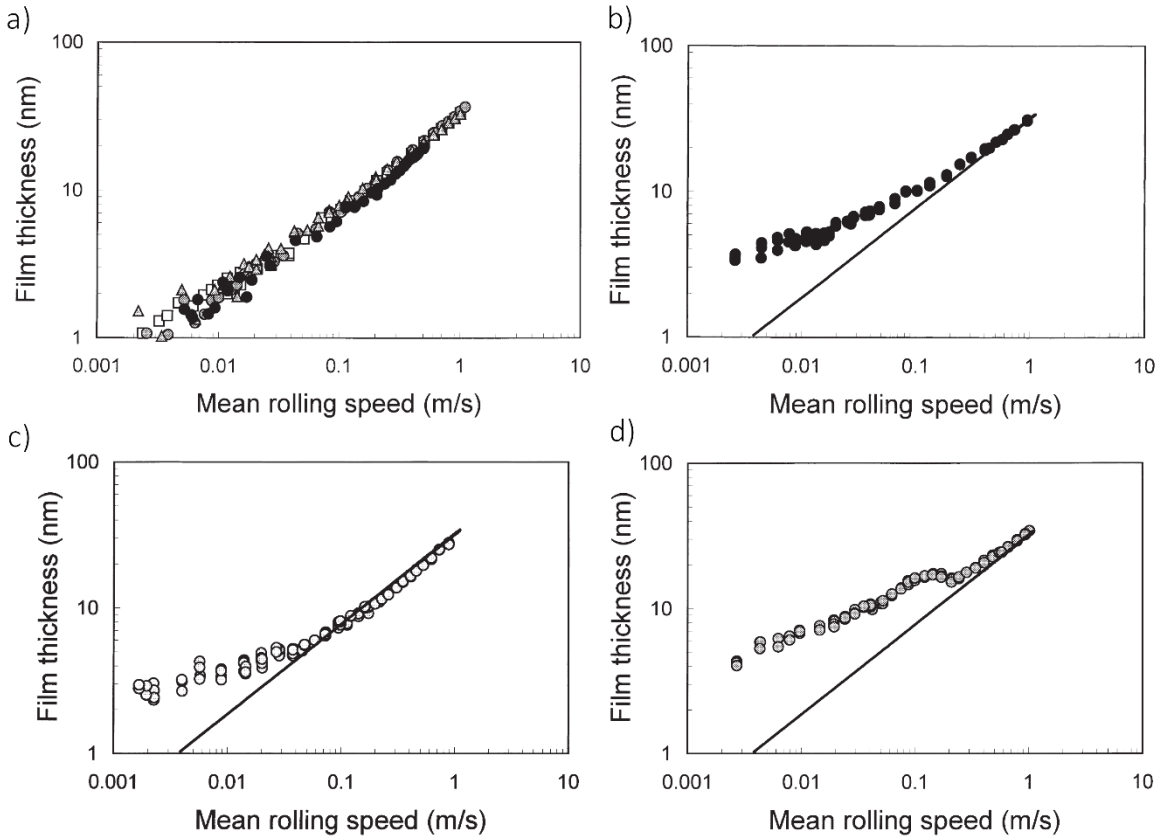

Figure 41, EHD film thickness measured by ultrathin film interferometry a) purified hexadecane, b) dry 0.1% arachidic acid c) wet hexadecane, d) wet arachidic acid [130]

In addition to the rolling film thickness, the amount of separation that was maintained when the bearing was stationary but loaded was also recorded. These findings are compiled alongside the rolling film thicknesses in Figure 42. From this we can see that in the absence of water no film persists under a stationary contact; however, in the presence of moisture and arachdic acid, a film of 2-4nm continues to separate the surfaces. This suggests either that the film is more strongly chemically adsorbed to the surfaces or, more likely, that oxidation has formed a thin solid layer which continues to support the stationary load. This is evidenced by the persistent separation of the tests where water is present in the contact.

Water is believed to promote the oxidation of iron to the Fe(II) and Fe(III) states which is required for the formation of a metal-carboxylate salt and thereby enhancing the effectiveness of carboxylic acid as a lubricant to form thicker films than what is present in the acid-only cases.

Other acids (stearic and oleic) were also tested and shown to exhibit the same behaviour as arachidic acid in wet and dry contacts.

Interestingly the tests were repeated with a less chemically reactive stainless steel ball bearing rather than the standard bearing steel ball bearing. Results comparable to that of dry purified hexadecane was found where only a thin boundary film was formed. This indicates that the enhanced lubrication results from the reaction between the carboxylic acids and the steel surfaces.

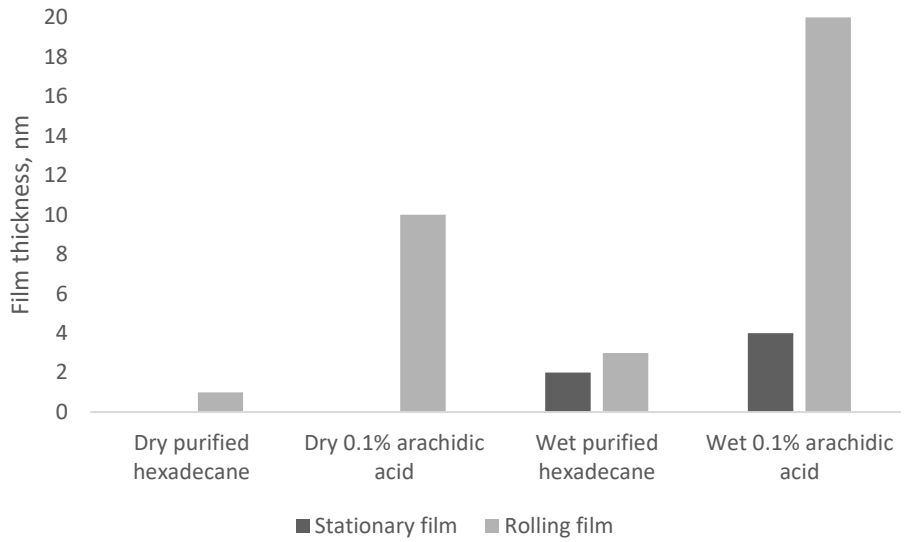

Figure 42, Film thicknesses under different chemical conditions determined using ultrathin film interferometry of a rolling steel ball bearing on glass [130]

Metal (steel) hydroxides and oxides have also been shown to react with surface active chemicals, notably fatty acids, resulting in the formation of these films. The generalised reactions are given as:

$$Metal\ Oxide + Acid \rightarrow Salt + Water \quad [K]$$

$$Metal\ Hydroxide + Acid \rightarrow Salt + Water \quad [L]$$

Mechanical agitation and heat both promote the formation of these layers [131]. Other chemical reactions which may occur between the oxides and organic compounds have been studied [132]. It was also noted that the amount of 'soap' required to form a lubricating film is very small.

Although the films in this study were tested under elasto-hydrodynamic lubrication, which may be unachievable in the wheel / rail contact, enhanced viscosity from these films may have a significant impact of the adhesion in the mixed EHL lubrication regime, the more likely state of operation.

Chemical reactions which change the viscosity of an interfacial fluid through chemical modifications to leaf matter alone are known which involve the degradation of polymers. The reactions concerned are challenging to study but have been documented for cellulose, hemicellulose and starches by changes in physical properties including viscosity, solubility and the synthesis of gels [133].

A phenomenon called starch gelatinisation can occur when the intermolecular bonds are broken down in the presence of water and heat (60-80°C). This causes an irreversible swelling of the starch granules, increased hydrogen bonding with the water, and possible solubilisation of amylopectin, resulting in a paste of high viscosity [134].

3.3 Summary

The railhead is a complex diverse and varying chemical system. Oxides are always going to be present on the railhead and may vary in physical properties which are determined not only by the conditions of formation but also at the time of analysis. In addition, the railhead is an open system thus enabling a great host of other organic and inorganic compounds to be present including from leaf matter and other features of the local area.

Structural polymers such as cellulose and hemicellulose constitute a large percentage of leaf organic matter; however, the leaf cuticle and other structures within the organism also contain highly surface-active chemicals which are known to interact with metal surfaces. Oils and greases typically found on the railhead have also been identified as containing high proportions of surface-active chemicals.

Surface active chemicals similar in composition to the ones identified in leaves and railhead oils / greases are known to interact with metallic iron and iron oxide surfaces. The mechanisms by which the chemicals interact are shown to reduce the coefficient of friction through boundary lubrication; more complex bonding mechanism and other interactions are also shown which may form a layer of lubricant on the surface of the railhead through chemical reaction with the surface.

The mechanical and chemical action of the wheel action over the railhead surface may chemically and physically alter the properties of both organic and inorganic components on the railhead through hydrolysis reactions or mechanical breakdown of the material. One of these ways is a change in viscosity of a contaminant film.

Pastes of inorganic particle suspensions and leaf layers have complex rheology which are affected by the properties of the containing particles.

Many interactions between chemicals derived from materials present in the locality of the trackside are possible which may cause loss or gain of wheel / rail traction. Due to the interactions between the components, it is a challenge to isolate any particular potential cause of loss of traction; however, the mechanisms investigated appear to be based on either boundary lubrication, the presence of an enhanced interfacial lubricant or the rheological properties of a thick layer generated within the wheel / rail contact.

4 Hypotheses

Although they may vary slightly in their exact elemental composition, almost all railway wheels and rails worldwide are manufactured out of steel. As a result, the components have a thermodynamic affinity for each other which leads to a high bonding strength when the metals are in direct contact. Starting from this simple principle, we can infer that any compound present within the wheel / rail system, which reduces the area of true steel – steel contact, that does not introduce another mechanism increasing traction, will lead to reduced overall bonding strength and ultimately a lower traction coefficient. Other widely known ways of reducing friction and traction include lubricating the surfaces, altering the roughness of the surfaces, and reducing the loading forces on the contact. It is important to consider all these system modifications, which often do not have trivial results; for instance, increasing the roughness of surfaces often increases friction, but in some cases, affords the opposite effect due to reduced surface contact.

The main reported causes of low adhesion are water, leaves, iron oxides, and oil and greases. Contemplation of the features of these causes reviewed in sections 2 and 3, whilst acknowledging common ways of reducing friction or traction, allows for some initial deliberation into how they may reduce wheel / rail traction. Water, a fluid, may act as a lubricant. Oils and greases are also potential lubricants to the wheel / rail system; however, they may also interact with the railhead surface, forming thin films and reducing the overall bonding strength between the surfaces. Leaves are also shown to contain many surface-active chemicals, but are also composed of solid matter too; the significance of this is that the surfaces of the wheel and rail may be separated by a thicker solid third-body-layer. To simplify the broad category, oxides and debris, it will be considered within the hypotheses as matter which is unbonded to – and largely loose on – the railhead.

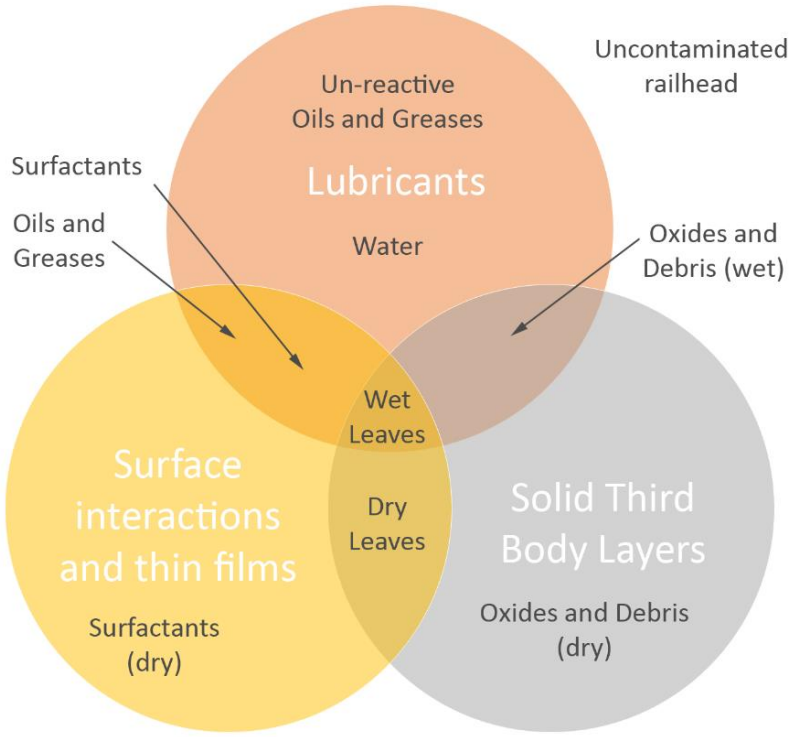

Figure 43, Proposed relationships between reported causes and effects (regions) relating to low adhesion

Figure 43 loosely combines the reported causes of low adhesion with the proposed effects discussed. For example, 'Oxides and Debris (wet)' causes solid third body layer effects due to its solid component but also may act as a lubricant due to the wet component. It must be noted that the

'effect' regions outlined on the diagram are not completely discreet due to complex behaviours of materials such as solid lubricants. The effect of changing roughness is also not included on the diagram; however, will be considered within the hypotheses.

4.1 Condition formation mechanisms

This first category of hypotheses relates to how the railhead surface changes under different physical and chemical conditions. Here we explore how various substances interact with the railhead surface and not the actual mechanisms that lead to low adhesion.

4.1.1 Surface interactions

Many substances found on the railhead, mostly oils and greases but also those derived from naturally occurring matter such as leaves, contain organic molecules with chemically active functional groups such as alcohols, amides, and acids. These can act as surfactants and may self-arrange form monolayers on the surface of the railhead, exemplified in Figure 44, through a process known as physisorption. In a similar way, some functional groups are also capable of bonding with iron oxide surfaces on the railhead through dissociative bonding which is a stronger – chemical – bond than the physical molecular adsorption of physisorption; known as chemisorption.

When substances are adsorbed onto the surface of the railhead, they effectively create a very thin barrier that acts as a boundary lubricant.

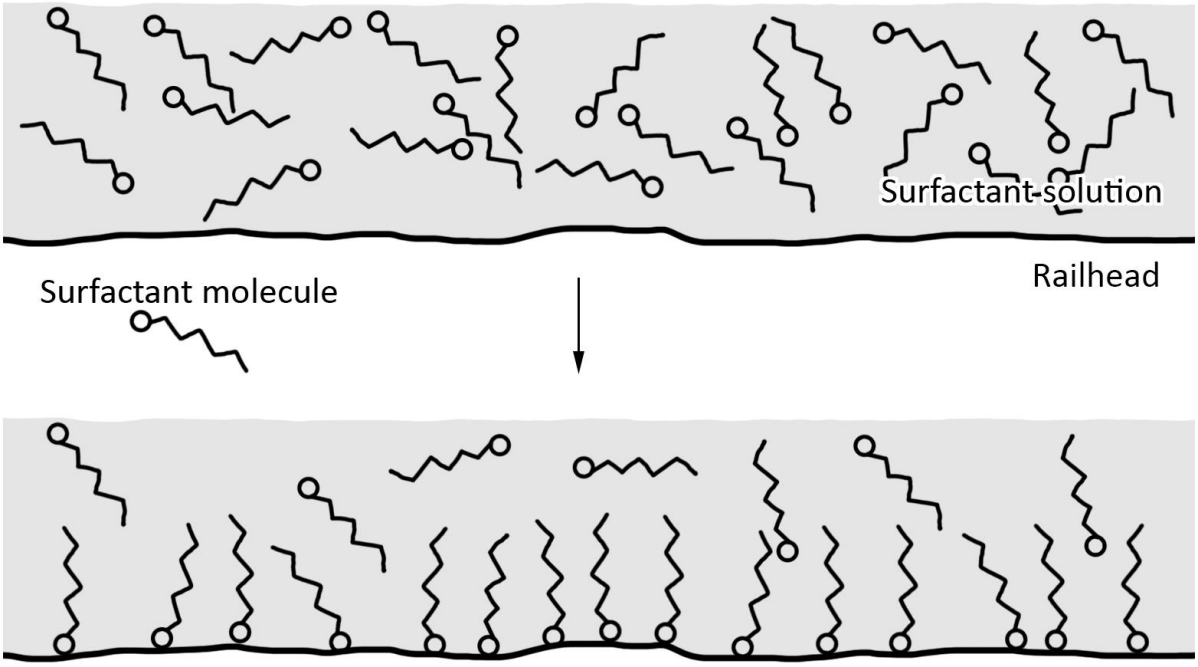

Figure 44, Formation of monolayers on railhead (circular heads represent active functional group which bonds to the railhead surface)

The rate of monolayer formation is dependent on the concentration of the active agents and the temperature. Chemisorption and physisorption are both surface interactions and, as such, would be limited to just a few tens-of molecular layers on the railhead making the surface treatment very susceptible to almost instantaneous wearing out under the contact conditions of the wheel / rail contact; however, they may be heavily instrumental in the formation of thicker and more robust tribofilms with other compounds present as shown in Figure 45.

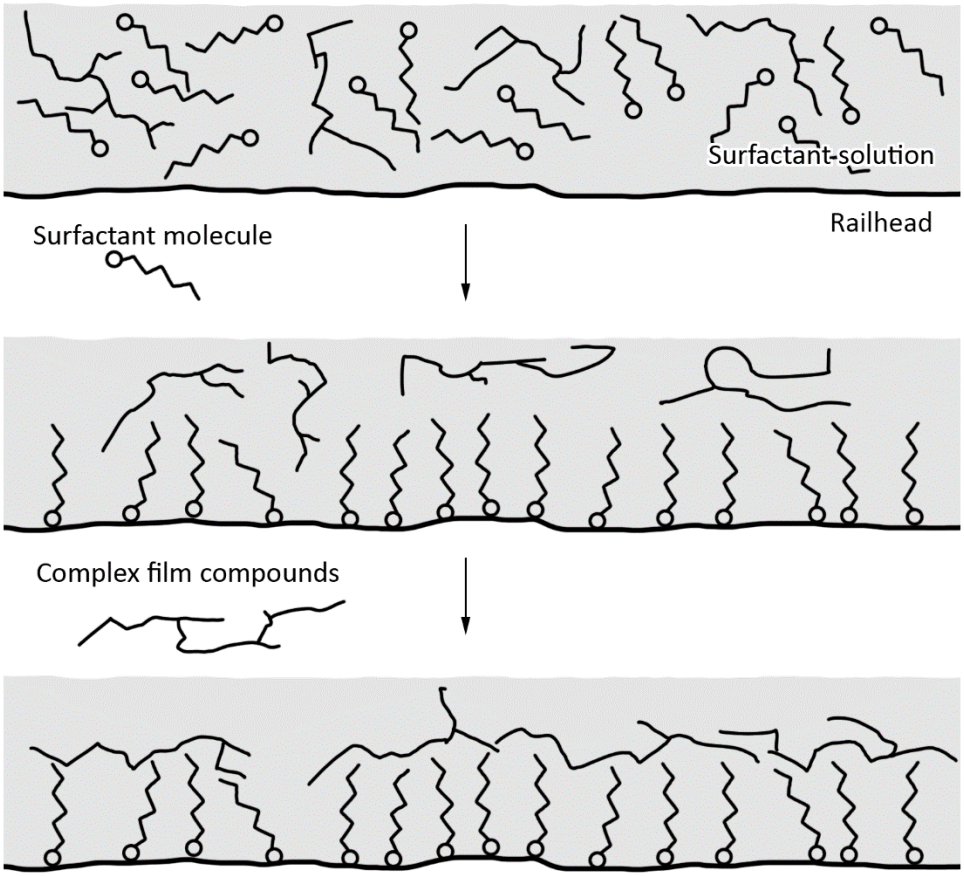

Figure 45, Formation of tribofilm promoted by chemically or physically adsorbed surfactants

4.1.2 Formation of complex leaf layers

Leaves are comprised of an extensive variety of chemical compounds and can form very robust layers on the railhead. Through reviewing literature in section 3 and scrutinising not only the chemical components of leaves but the overall structure of the plant cells, it is apparent that there are two main sources of highly surface active chemicals present within the structure of the leaves:

- The cuticle containing cutin, and
- The plant cell vacuoles which contain tannins and enzymes.

Cutin may be hydrolysed in acidic or caustic environments, or enzymatically with cutinase, resulting in its monomers with active functional groups. The general reaction is given as:

$$RCOOR_I + H_2O \leftrightarrow RCOOH + R_IOH \quad [M]$$

Iron ions may also interact with cutin though ligand substitution and become incorporated into the leaf layer as given in the following equation:

$$RCOOR_I + MOH \rightarrow RCOOM + R_IOH \quad [N]$$

The vacuoles of the plant cells, containing the tannins and enzymes, normally confine the contents within but release them when the cells are ruptured. A wheel-pass over rails with fallen leaves would be enough to break apart the cells and rupture the vacuole, releasing the highly active chemicals within.

These compounds may react with the railhead and form bonds between the railhead / oxide surface and the strong fibrous material of the leaves. These bonds as well as the incorporation of iron ions

into the leaf material may form a transitional layer allowing the leaf material to adhere more strongly to the railhead surface. An illustration of this structure is given in Figure 46.

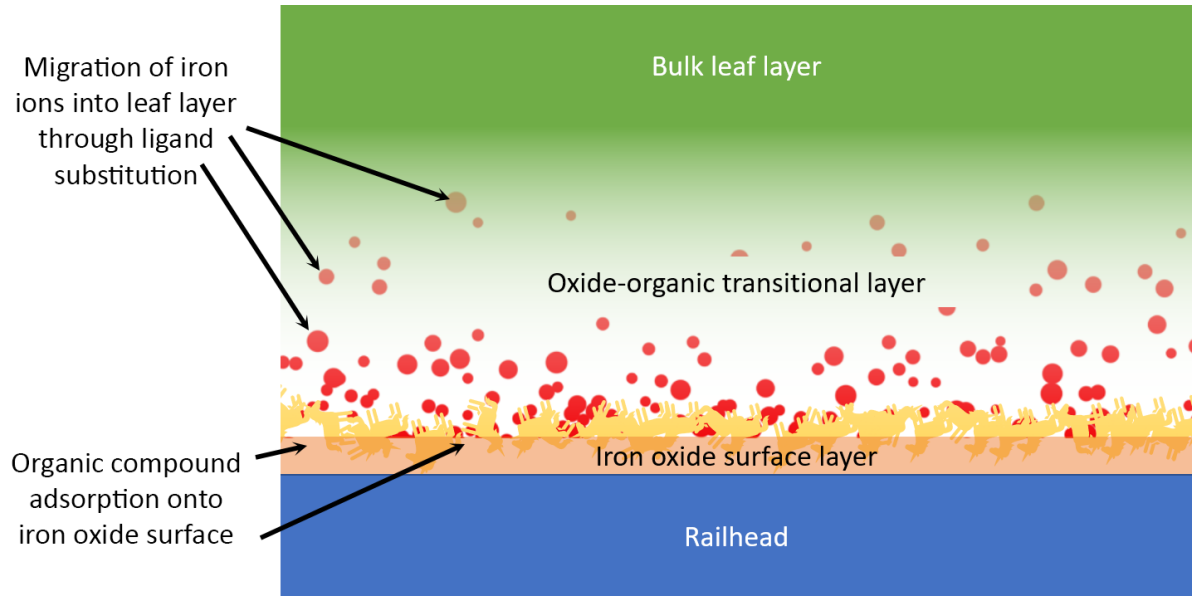

Figure 46, Hypothesised leaf layer bonding mechanisms presenting adsorption of organic compounds to the railhead surface and integration of iron ions into the leaf layer to give an oxide-organic transitional layer

4.1.3 Formation of viscous compounds

More viscous compounds may be formed through reactions on the railhead with organic compounds.

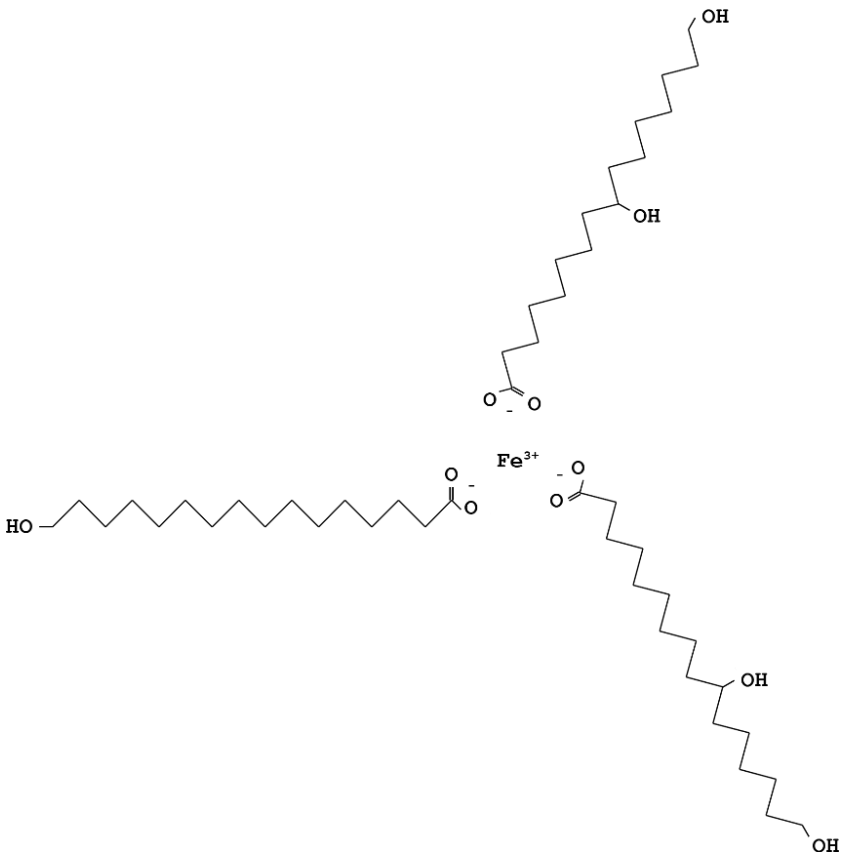

Figure 47, Iron tripalmate skeletal structure

Carboxylic acids and other active chemicals present can interact with iron hydroxide compounds in acid / base reactions effectively substituting the hydroxyl ligands bonded with the iron and forming an iron – organic complex:

$$Fe(OH)_3 + 3ROOH \rightarrow Fe(ROO)_3 + 3H_2O \qquad [O]$$

The form of the compound produced will depend highly on the carboxylic acid(s) involved in the reaction. Free carboxylic acids may form complexes such as that shown in Figure 47 (iron tripalmate formed from reaction between ferric hydroxide and palmitic acid).

These compounds are often known as metallic soaps. They can act as boundary lubricants but can also become suspended in water and increase the viscosity of water films. The mechanism by which they could form on the railhead is given in Figure 48.

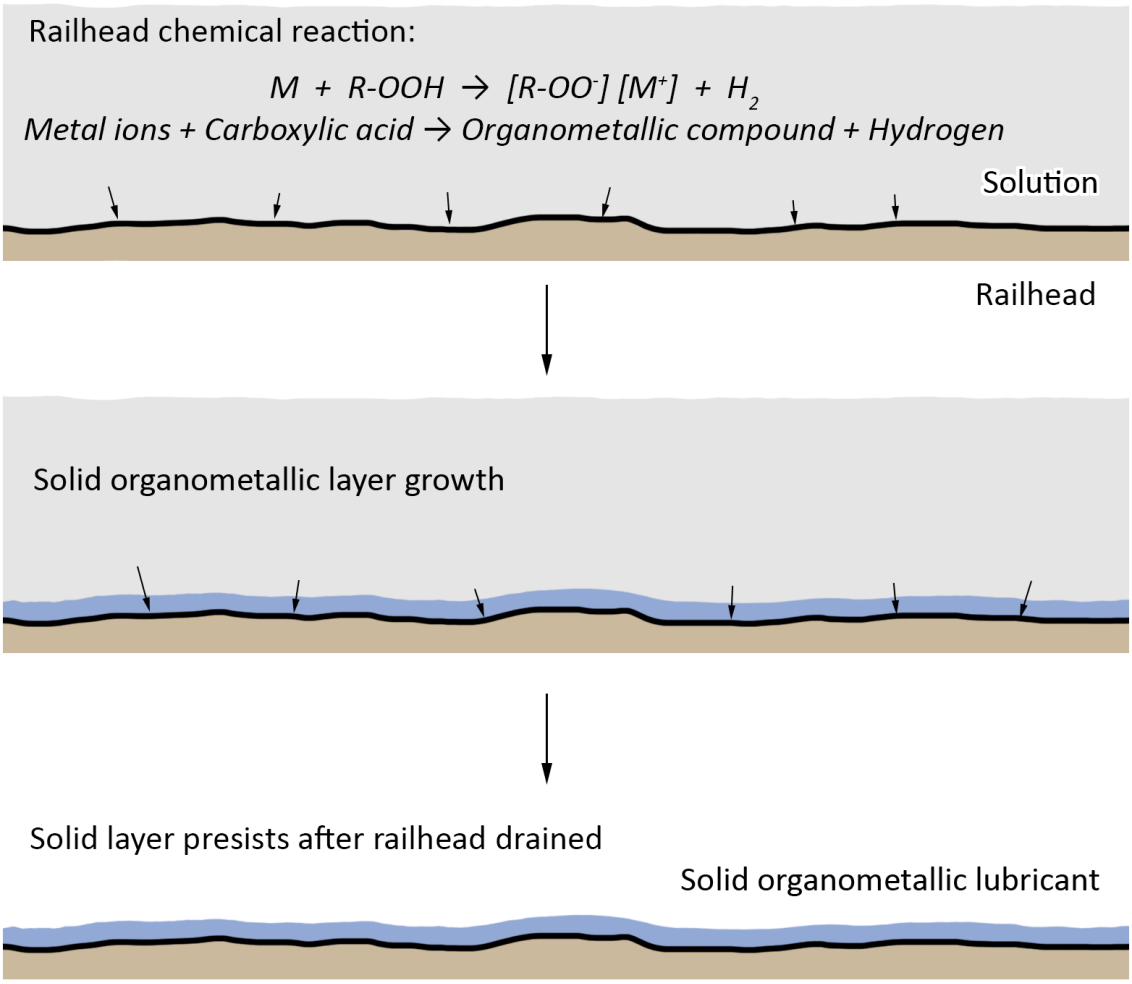

Figure 48, Formation of solid organometallic lubricating layers on railhead

4.1.4 Oxide formation and build-up

Different environmental conditions result in the formation of different iron oxides and therefore, since different oxides have different physical properties, the tribological properties of the railhead surface is likely to be affected by the conditions prior to train movements.

A general hypothesis that is proposed is that drier conditions, where water arrives on the railhead due to condensation will develop a surface composition of high iron oxide concentration (magnetite,

haematite, and wüstite), whereas rails which experience regular rainfall will develop surface compositions of high iron oxide-hydroxide concentration (goethite, akaganéite, and lepidocrocite).

4.2 Traction loss mechanisms

The second category of hypotheses proposes mechanisms which may cause a loss of traction, whether driving or braking.

4.2.1 Boundary lubrication

Compounds may be chemically or physically adsorbed onto the surfaces of the rail and / or wheel forming thin films. These layers can cause the surfaces to exhibit much reduced coefficients of friction leading to reduced traction.

The mechanism by which this is achieved is that the layers cause less of the contact to be supported by areas of dry contact; instead the surface is supported by indirect contact on the layers of adsorbed compounds as shown in Figure 49. This leads to lower shearing stresses between the two surfaces and reduced traction.

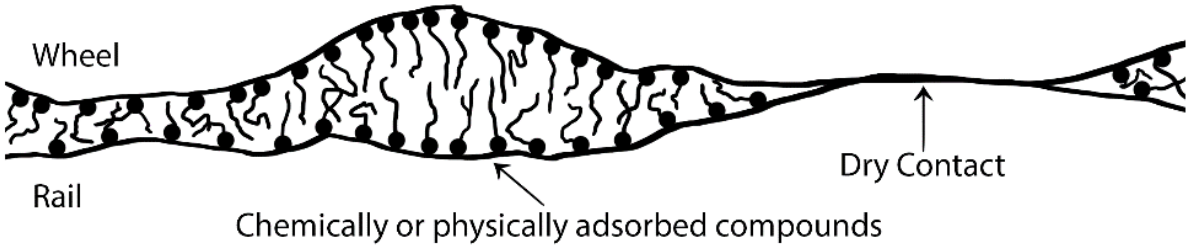

Figure 49, Boundary lubrication mechanism hypotheses illustration

4.2.2 Shearing of solid layers

The second traction-loss hypotheses relate to thick solid third body layers. The materials considered being capable of forming shearing solid layers include thick oxide and debris layers, and leaf layers composed mainly of the pulp of the leaf, rather than soluble compounds.

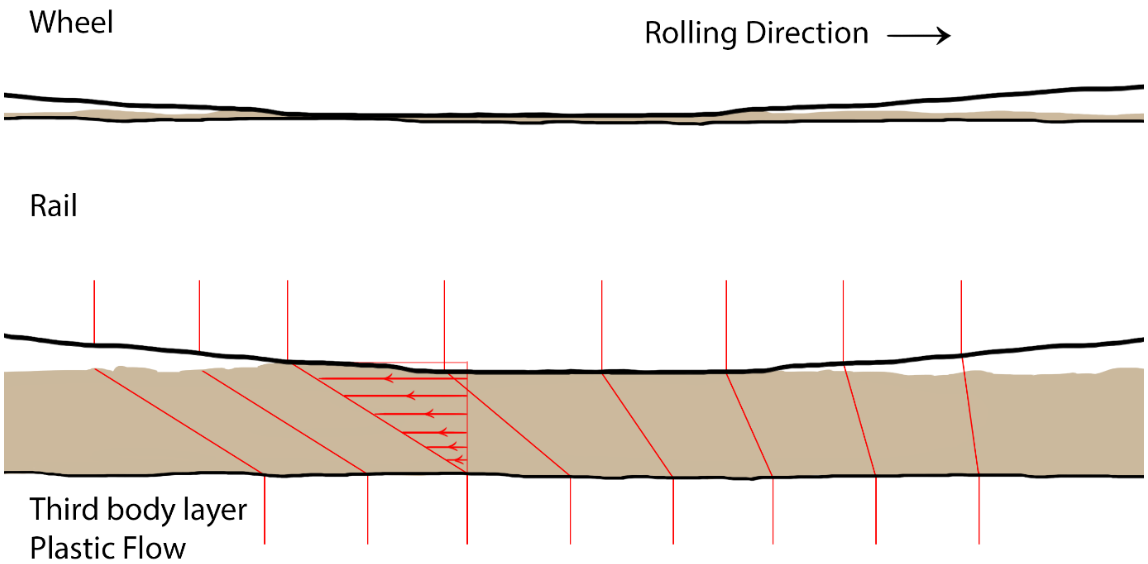

Figure 50, Diagram showing the shearing of a third body layer during driving

Figure 50 outlines this hypothesis. When the longitudinal forces of traction or braking are applied to a solid layer supporting the contact, they impart a shearing force on the material. Traction is lost in this instance due to plastic deformation in the solid layer as the material is sheared and the forces are unable to be transmitted through the contact effectively.

Unlike a liquid lubricant, such as water, the layer thickness is less influenced by the speed of rolling and therefore is possibly a significant mechanism leading to low adhesion at slow speeds or creep if the force is sufficient to cause shearing of the solid layer in the contact patch.

4.2.3 Liquid film lubrication enhancement

Water in the wheel / rail contact may form a liquid film which acts to cause 'patchy' separation of the surfaces through application of a hydrodynamic load. In the contact the pressures are so great that it is not possible for a liquid film thicker than the surface roughness to be generated under operating conditions; therefore, full hydrodynamic separation cannot occur. As a result, the lubrication regime that the wheel / rail contact condition is likely to be within is either boundary lubrication or mixed lubrication.

The wheel / rail contact may be supported by microscopic areas of elasto-hydrodynamic lubrication between the asperities of the contacts as well as solid-solid contact of the wheel and rail surfaces. This hypothesis is outlined in Figure 51.

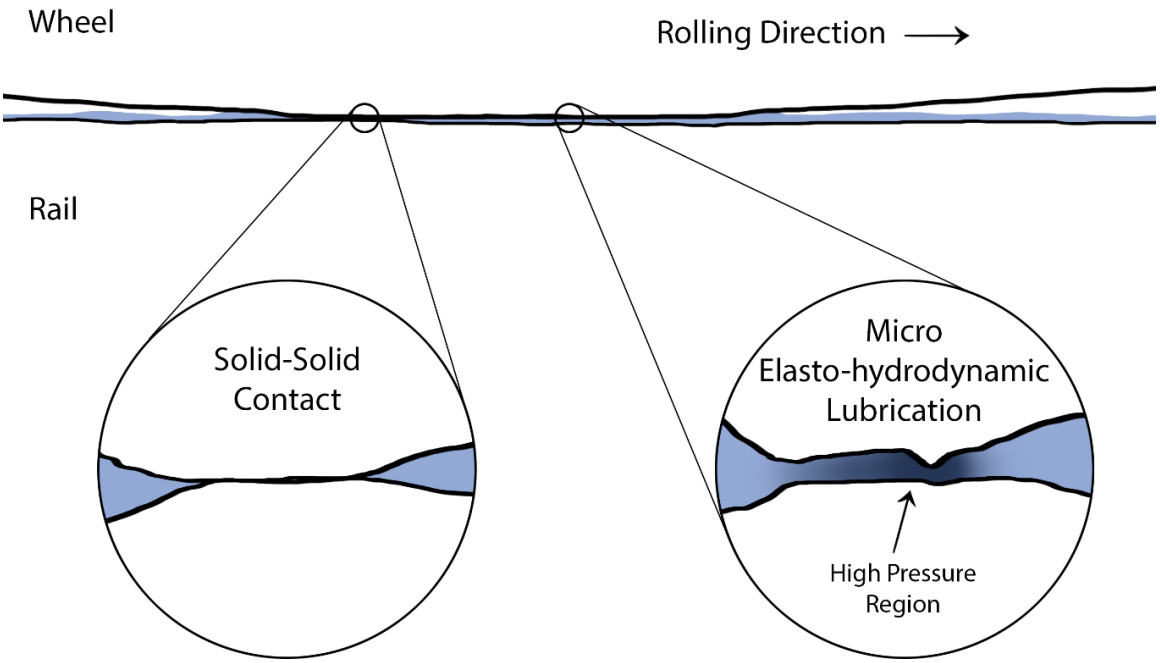

Figure 51, Diagram of mixed lubrication showing solid-solid contact areas and micro elasto-hydrodynamic regions

It is unlikely that this effect, concerning water alone, is responsible for many cases of low adhesion due to the fact that railway locomotives operate largely without issues in wet conditions; therefore, this hypothesis also suggests the presence of substances on the railhead which increase the viscosity and therefore enhance the lubricating effect of an interfacial water film.

The first proposed lubrication enhancement, illustrated in Figure 52 a) and Figure 53 results from physical or chemical interactions at solid / liquid interfaces which can greatly influence the properties of fluids close to surfaces. This may be the migration or orientation of polar molecules within close proximity of the interface. A result of this is that within tens of nanometres of the

interfaces the properties of the fluid, including viscosity which can be of an order of magnitude higher than the bulk fluid. This enhanced viscosity phenomena could potentially change the lubrication profile of very close contacts and thereby allow very thin fluid films to support more of the load through micro EHL behaviour.

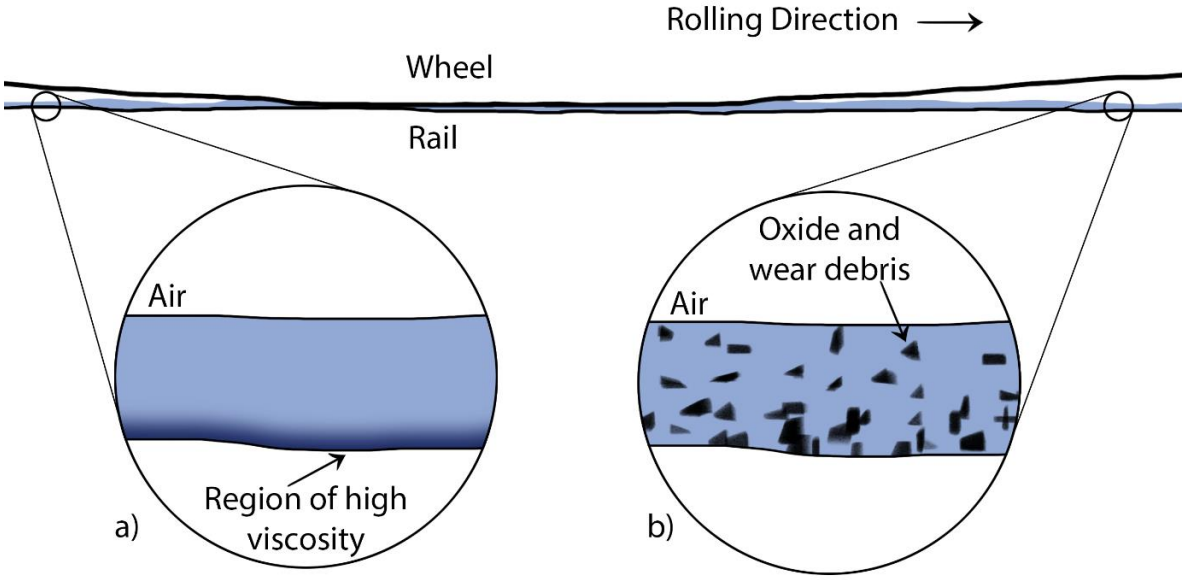

Figure 52, Enhanced viscosity mechanisms: a, regions of high viscosity close to solid - liquid interface; b, solid - liquid slurry suspensions

Figure 52 b) illustrates the second lubrication enhancing hypotheses. Slurries or pastes can be formed when solid particles are present within the lubricant. Generally, the higher the solid content within the lubricant, the higher the viscosity.

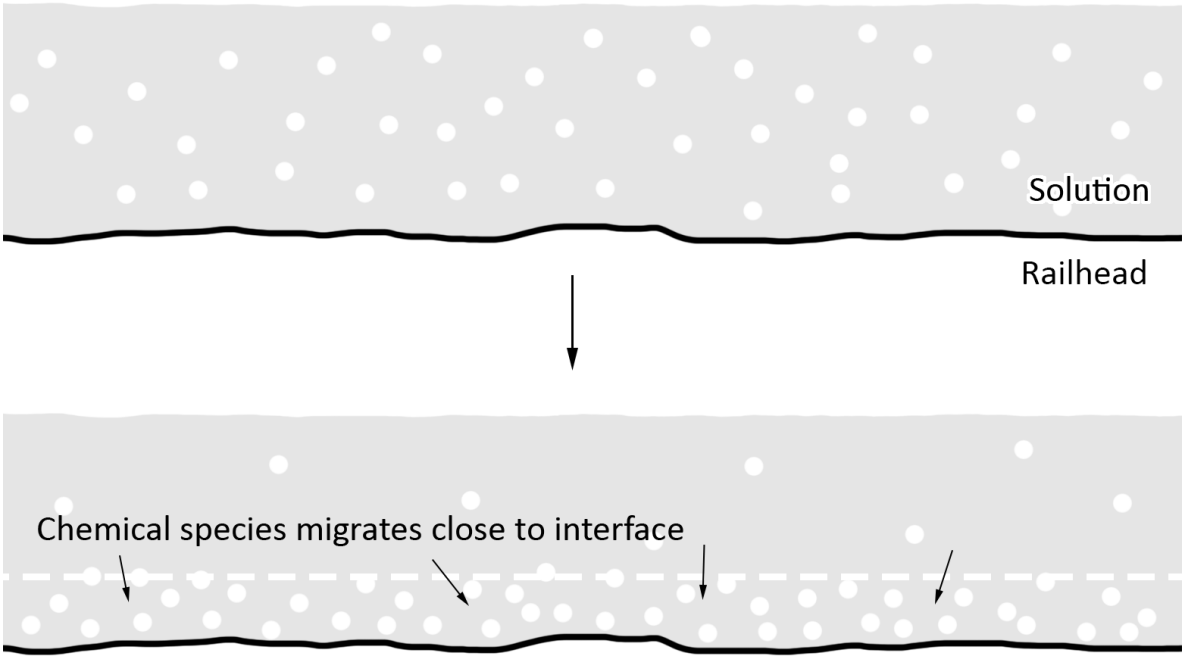

Figure 53, Formation of viscous near-surface layers

The effect of increasing the viscosity of the lubricant on adhesion at the wheel / rail contact is shown on a Stribeck diagram in Figure 54. The drop of friction caused by increasing viscosity through the

mechanisms discussed is caused by the regions of micro EHL supporting more of the load and reducing the normal force on the areas of solid-solid contact.

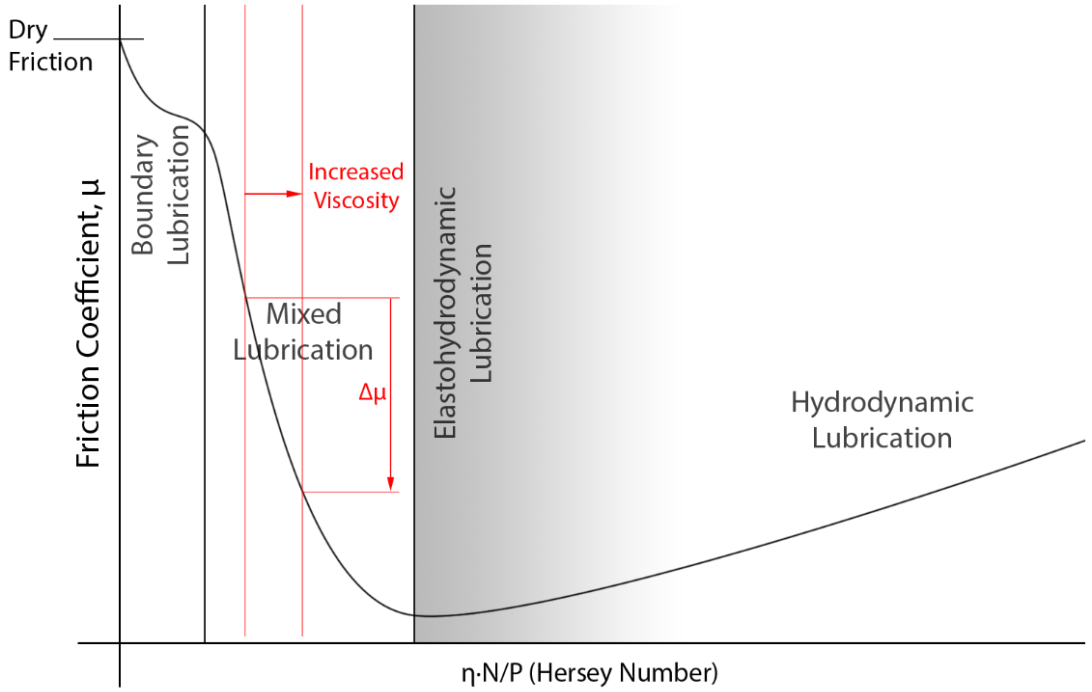

Figure 54, Stribeck diagram showing the effect of increasing viscosity on the friction coefficient

4.2.4 Quazi-solid / fluid rheological properties of railhead debris

Oxide pastes have been shown in the laboratory under rolling-sliding tests on twin-disc tribometers to achieve ultra-low adhesion levels but due to the extremely high contact pressures of the wheel / rail interface, it is unlikely that a lubricating fluid would be able to support the great forces acting on it when unconfined; however, some solid-liquid suspensions – oxide pastes included – behave as Bingham-Plastic fluids. This means that they have a yield shear stress which is a finite shear stress level required to be exceeded before the fluid begins to flow; below this yield stress, the material behaves as a solid and resists deformation.

Aqueous debris pastes on the track can behave as Bingham plastic fluids, they may therefore exhibit properties pertaining to both solid layers and liquid lubricants. This final hypothesis relates to this ability.

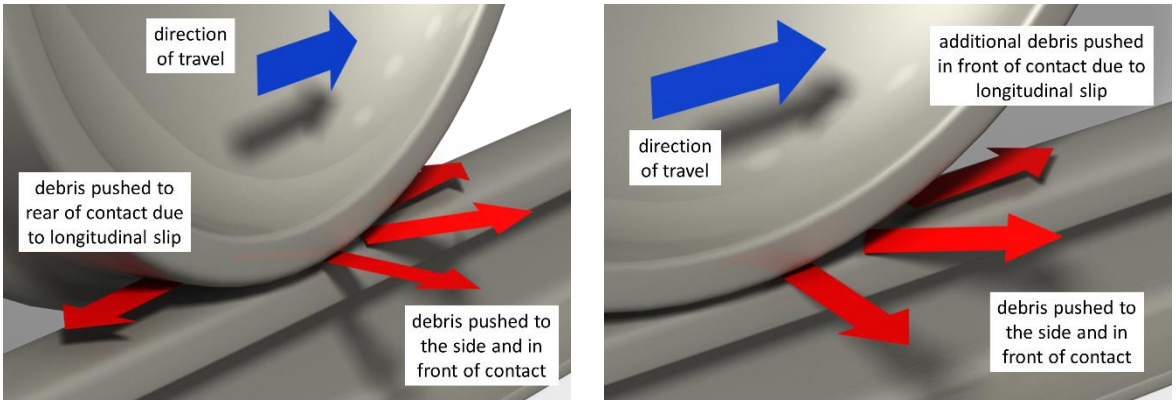

Figure 55, Proposed movement of debris on the railhead due to driving and braking in the wheel / rail contact

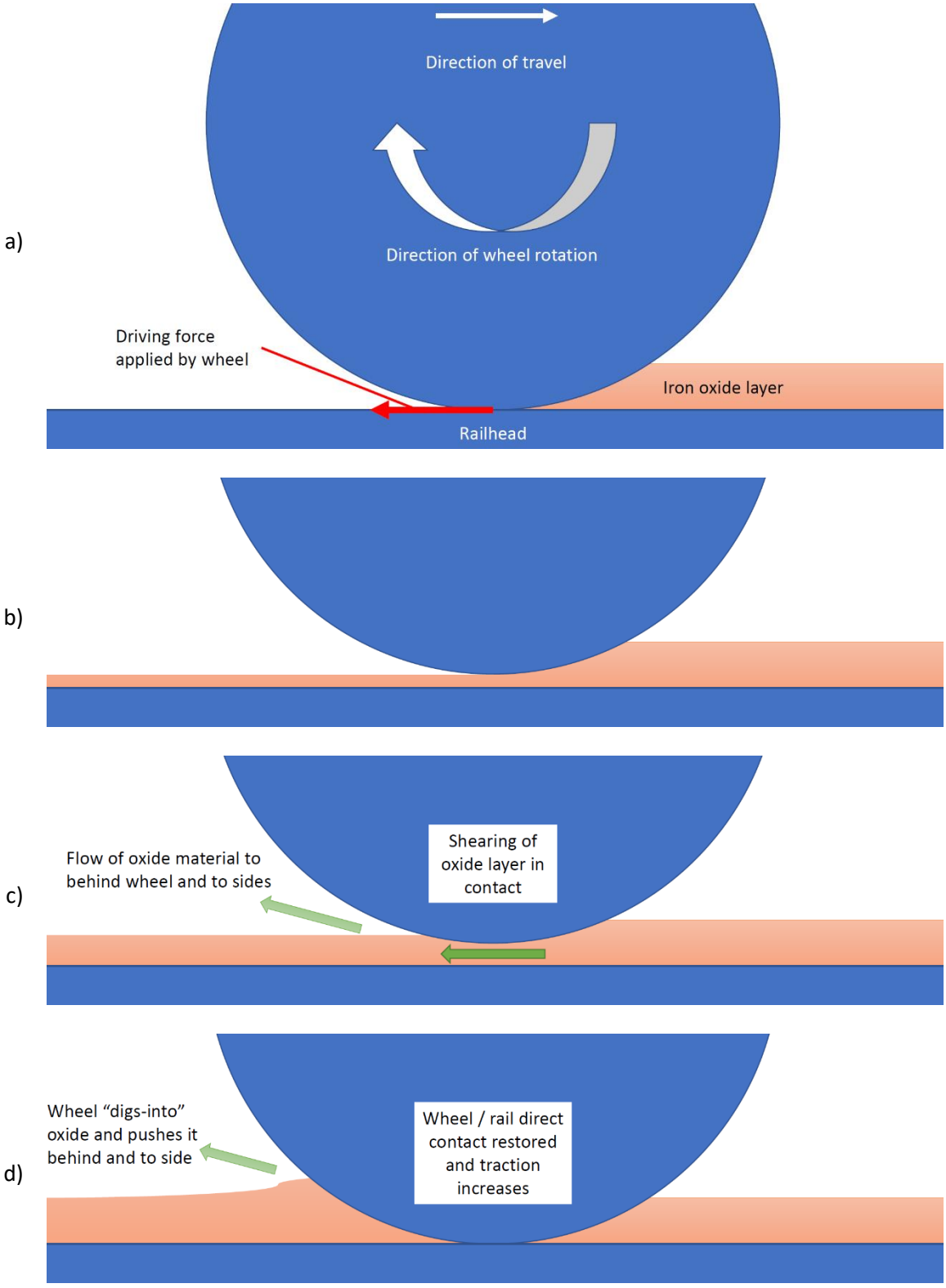

Figure 56, Quazi-solid / liquid rheological mechanism of adhesion loss under driving showing stages: a to b, gradual increased support of the wheel vertical load by the oxide paste layer; c, yield shear stress of layer reached and flow of material in layer; d, recovery of wheel traction due to expulsion of material from contact and restoration of solid-solid contact. Relative thickness of oxide layer greatly exaggerated.

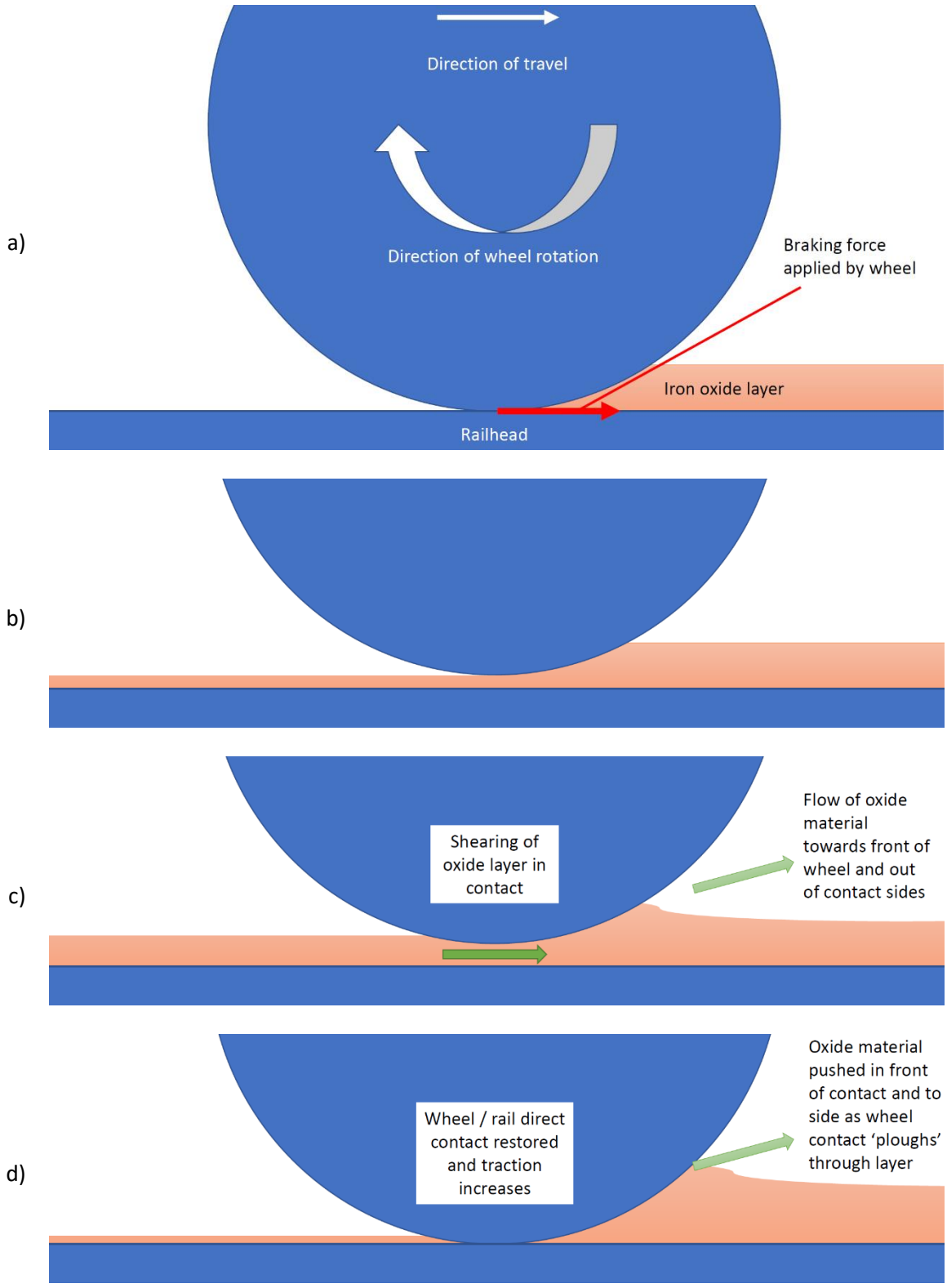

Figure 57, Quazi-solid / liquid rheological mechanism of adhesion loss under braking showing stages: a to b, gradual increased support of the wheel vertical load by the oxide paste layer; c, yield shear stress of layer reached and flow of material in layer; d, recovery of wheel traction due to expulsion of material from contact and restoration of solid-solid contact. Relative thickness of oxide layer greatly exaggerated.

Visualisation of the wheel / rail system during lateral load application reveals two possible scenarios relating to the movement of oxide pastes and layers around the contact which may be significant for the proposed mechanism; these are presented in Figure 55. For both driving and braking, the force of the impending wheel is likely to cause debris to be pushed in front of and to the sides of the contact. When driving, the surface of the wheel slips backwards relative to the direction of travel over the railhead and as a result, material within the contact may be pushed out of the back of the contact due to the sliding of the wheel and shearing of the debris layer. When braking, the opposite is true; the surface of the wheel moves forwards in relation to the direction of travel over the railhead resulting in additional material being pushed out in front of the contact.

The ability for the debris / oxide paste to act as a solid is significant as, when under compression, it enables for the normal load of the wheel to be supported by the layer.

The hypothesised mechanisms are given in Figure 56 for driving and Figure 57 for braking. As the wheel is rolling gradually more of the contact is supported more and more via the oxide / debris layer (a to b). Full separation of the physical wheel and rail solid-solid contact may not occur but is shown on the diagrams to better illustrate the mechanism. The oxide / debris layer initially effectively transmits the longitudinal forces of the contact through it; however, once it reaches shearing stresses greater than the yield stress (c), shearing of the layer commences and the layer begins to behave as a fluid. This shearing diminishes the ability of the contact to transmit lateral forces between the wheel and rail causing loss of traction. The amount of force which can be transmitted through the contact recovers as the shearing of the layer causes material to be pushed away faster than material is able to be entrained into the contact (d), this increases direct wheel / rail contact and thus restores traction. It is hypothesised that this mechanism may cycle as material becomes entrained in the contact during 'normal' rolling / sliding behaviour (as the paste exhibits the properties of a solid) and expelled from it during the layer shearing (when fluid behaviour is observed).

The main differences between the driving and braking mechanisms are that with traction, sheared debris is pushed out of the trailing end of the contact and away; whereas, during braking, the sheared debris is pushed out of the leading end of the contact potentially becoming re-entrained in the contact.

4.3 Summary

The wheel / rail contact is a complex system. A variety of mechanisms attempting to describe the how traction is lost in the wheel / rail system are proposed and many of the compounds found in and around the railhead are theorised to be able to display these behaviours.

Surface active chemicals are hypothesised to contribute to both the formation of different surface conditions as well as have direct effects on traction through boundary lubrication; however, due to their effect on the contact being confined to a few molecular depths in thickness from the surfaces, their impact on railhead traction when considered on their own is likely to be small as a result of their fragility.

Lubrication and thick films are a feature of a few of the presented hypotheses and may be presented by both iron oxides, debris, and leaf layers.

The complex rheological behaviours of debris pastes, particularly iron oxides due to their abundance on the railhead, appears promising to allow both entrainment and shearing within the contact.

Due to their presence on the railhead and complex behaviour, this thesis will pursue the hypotheses relating to the formation and behaviour of iron oxides and water within the wheel / rail system, outlined in sections 4.1.4 and 4.2.4. The decision to investigate these hypotheses over those concerning leaf layers was also partly made due the current lack of knowledge in literature regarding the chemical composition and iron oxides present on the railhead prior to the formation of the leaf layers; as a result, accurately simulating leaf layer formation under similar conditions to those found on operational railways would require pre-conditioning of the railhead substrate. Research performed to understand the formation of iron oxides on the railhead, as has been done in this thesis, may therefore support future work aiming to explore the formation of leaf layers.

Research has been performed regarding the tribological properties of iron oxides and their pastes within the wheel / rail contact; however, very little was discovered about how they are formed on the railhead and most iron oxide testing in the literature used crudely synthesised oxides or purchased material of a standard oxide type. The analysis programmes and testing platforms chosen for the work of this thesis, outlined in section 5, were chosen to be able to exhibit more control over the chemical analysis, formation of, and testing of the chemical, rheological, and tribo-chemical properties of various types of iron oxides.

5 Methodology

To develop understanding and test the hypotheses discussed, the wheel / rail contact will be explored through a series of monitoring and experimental campaigns. These intend to record the environmental conditions surrounding the system and then simulate them within a laboratory setting to test the hypothesised mechanisms of traction loss.

This chapter initially outlines the field monitoring techniques utilised in this thesis, it then describes how samples were prepared from environmental simulation in the lab environment after which the surface chemical and physical analysis approaches are given; lastly, the mechanical tribo-testing methods are described.

5.1 Field testing

The field-testing methods were designed to analyse the trackside environment and explore the transient conditions of the open system. Both physical environmental data as well as chemical swabs of the surface of the railhead were taken.

Sites of this trackside monitoring and analysis were approached based on accessibility and opportunity. The sites which formed the field testing were:

- Quinton Rail Technology Centre test track, Long Marston, Warwickshire, England.
- Rail Bridge No. 194 near Royston, Barnsley, South Yorkshire, England. (53°36'52.7"N 1°26'54.8"W).
- Two test locations in British Columbia, Canada. (Measurements taken by Don Eadie, Rail technology consultant)

5.1.1 Track swabbing

The concentration of iron oxide compounds present on the railhead have been shown to vary [46]. The composition of the railhead has been analysed though the use of a trackside X-Ray diffractometer by Suzimura et al. [46]. Unfortunately, this technique requires complex equipment rarely available. The alternative which this project explores is to utilise a sampling technique to then later perform ex-situ examination of the railhead compound.

Swabbing of the railhead surface was performed using swab cloths made from cellulose and glass microfibre filter papers. Glass microfibre paper was used in addition to the cellulose filter paper due to its greater hardness and abrasiveness which allows for greater material pick-up in many cases; particularly when material is bonded strongly to the railhead surface.

The cellulose filter paper used was a 90mm circular plain disc format grade 51 ashless hardened quantitative filter paper and the glass microfibre paper a grade 259, 55mm diameter, circular borosilicate glass paper. Both of the filter papers were obtained from fisher scientific.

The filter papers were stored in sealed plastic sample bags before and after sampling. Clean gloves were worn when handling the filter papers to minimise contamination and to protect the user against sharp fragments of rail steel which may have spalled off the railhead surface.

The circular filters were folded in half into a semi-circular shape before taking the swabs. Each of the filter papers were used to take 2 samples. The positions on the filter paper where these samples are to be taken are shown in the Figure 58 below.

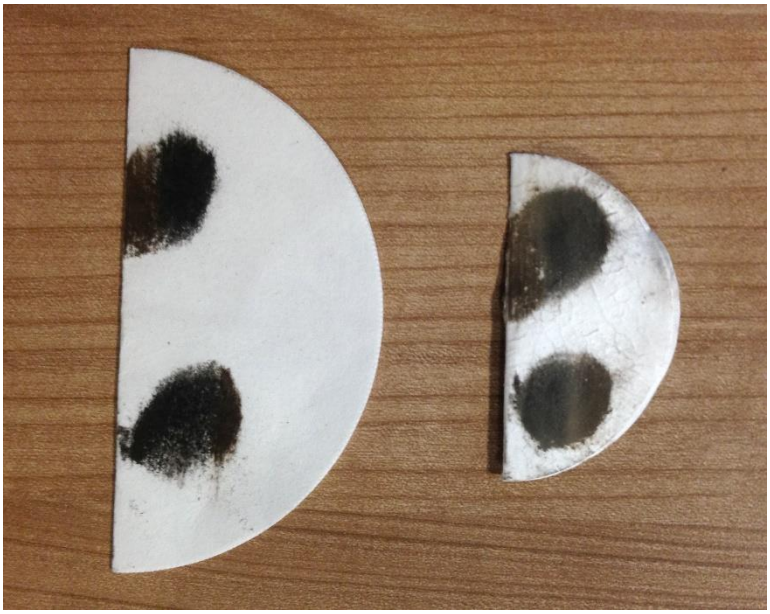

Figure 58, Photograph showing positions of sampling on the filter paper of ashless filter paper (left) and glass fibre filter paper (right)

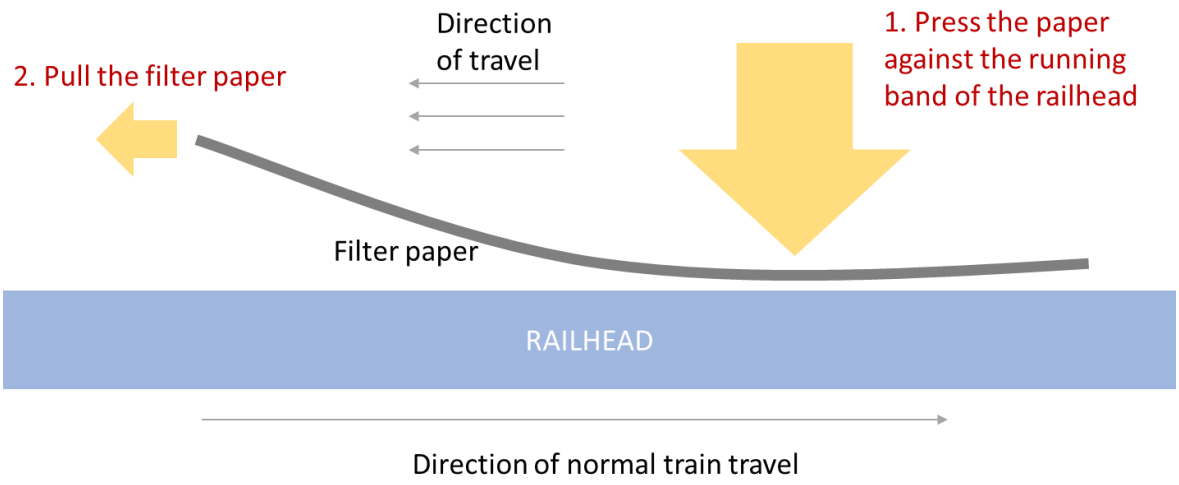

Figure 59, Diagram detailing the sampling procedure

The general procedure taken when sampling is annotated in Figure 59. After the filter paper had been folded it was held near to one of the corners and placed against the running band of the railhead. Moderate pressure is applied to a position on the opposite half of the filter paper to where is held and pressing against the running band of the rail. The pressure was such that as much force was to be applied to it as possible whilst the filter is dragged without causing the filter paper to tear.

The ashless cellulose filter paper was dragged in the direction opposite to the normal travel of trains along the running band with the pressure applied. The distance of dragging was about 40cm per swatch for the cellulose paper and for the glass fibre filter paper this distance was reduced to 15cm due to the fragility of the medium.

This procedure should be repeated for the other side of the filter paper using a fresh section of railhead where no sampling has been taken on that occasion or tribo-testing done.

After sampling the sample was returned to the sampling bag and information recorded detailing the date and time, location, conditions at time of sampling, and a comment containing other significant information pertaining to the sample collected. It was normal practice to pre-label bags containing the samples with unique id's, for example: GF01 – 30 for the glass fibre and FP01 – 30 for the ashless filter papers.

Analysis of the swabs was performed as soon as practical after collection; however, preliminary tests were done to determine differences between swabs analysed within 2 hours of collection and a month after analysis. It was found that there were negligible composition changes between the swabs during that time; however, the stability of all compounds considered in this thesis on the swabs have not been fully determined.

5.1.2 Environmental monitoring

A data logging device was designed and constructed to record a variety of environmental parameters at the trackside. The environmental monitor is based on an Espressive Systems ESP8266 microcontroller, the schematic can be seen in Figure 60 and photograph of the logger in Figure 61.

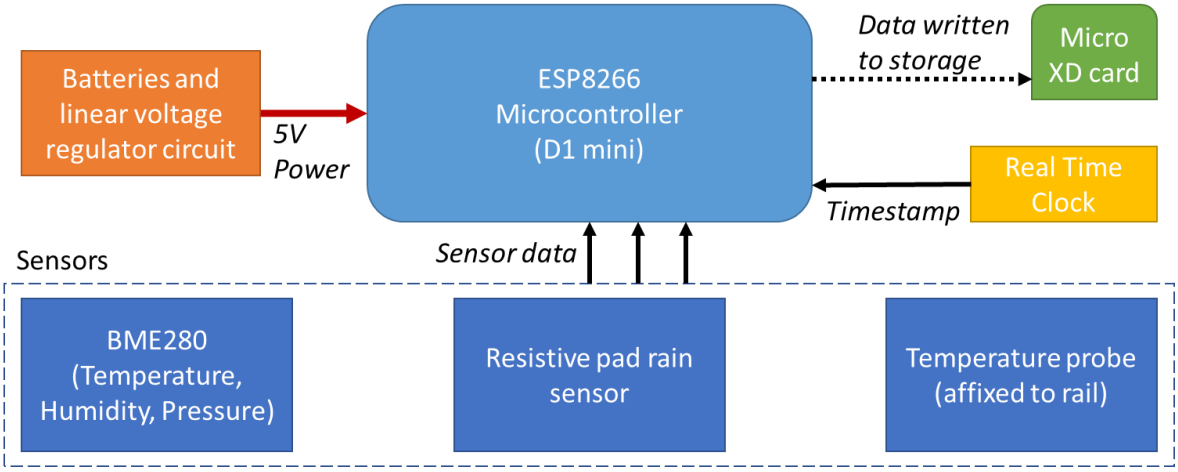

Figure 60, Environmental monitor schematic

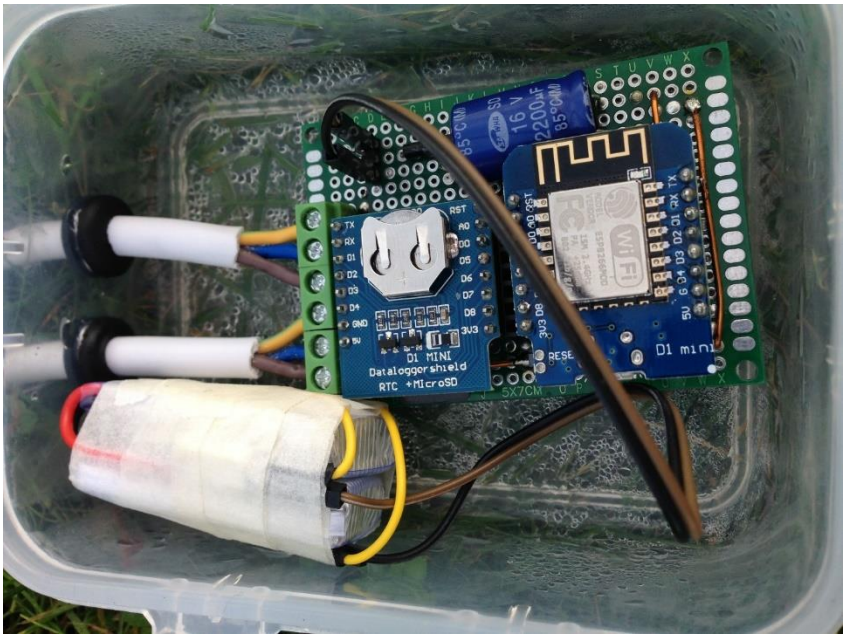

Figure 61, Environmental monitor photograph

The ESP8266 microcontroller was chosen as it offers very low power operation through a “deep sleep” mode allowing the device to remain in a standby state until reawakening and performing the data-logging activities using the microprocessor’s low power internal clock. This “deep sleep” period was configured such that the device would take readings every 2 minutes. Using this frequency of readings, a relatively small battery of 400mAh was allowing for up to 2 months continuous monitoring. The high frequency of sampling of every 2 minutes was decided upon in order to be able to visualise the rapidly changing environment events of the trackside.

Each reading taken by the monitor records the following values:

- Date and time
- Ambient temperature, humidity and pressure
- The temperature of the railhead via a temperature probe
- A rain sensor reading (Resistive element sensor recording the presence of droplets of water)

From these values, an approximation for the dew-point temperature is calculated when the data is being processed for analysis using the Magnus formula, equation 4 [update # before submission].

$$Dewpoint = \frac{c \cdot \gamma}{(b - \gamma)} \tag{4}$$

$$\gamma = \log(Humidity) + \frac{b \cdot Temperature}{(c + Temperature)} \tag{5}$$

where: b = 17/62 and c = 243.12

Data was saved to comma separated variable (CSV) files on a micro-SD memory card with one file being created at the start of each day and being appended by each subsequent reading. Files were downloaded directly from the card and processed into charts in batches using a Matlab program.

5.2 Sample preparation

Different surface treatments were applied to rail steel for chemical analysis via XRD and tribo-testing through pin-on-flat friction analysis on the UMT tribo-tester. These samples were prepared from a 4mm thick section of R260 grade rail steel, cut from rail stock close to the top of rail. Two sizes of samples were cut from the material: small 10mm square sections and 42mm diameter discs which can be seen in Figure 62.

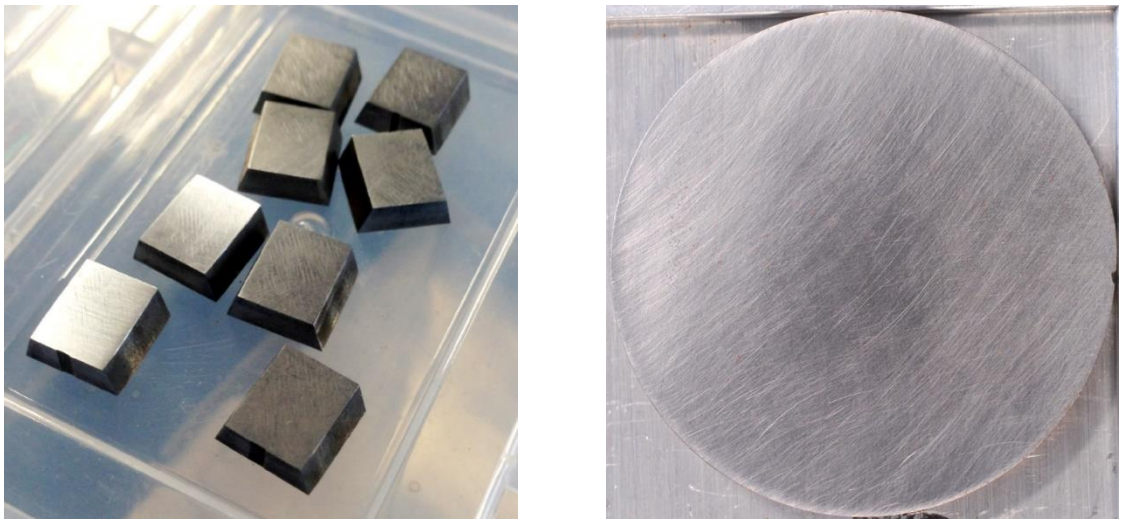

Figure 62, Sample substrate pictures

The larger disc sample geometry was chosen to be the largest sample size which could be placed in into the X-Ray diffractometer, this allowed for a large area of irradiation and greater strength signals from the diffractometer.

Before each substrate was prepared for testing, the surface was ground using progressively fine silicon carbide paper up to 1500grit achieving a surface roughness of around 0.2µm. The final stage of grinding was done in isopropanol before the surface was rinsed with isopropanol.

Samples were then subsequently prepared for testing in two ways: simulation of the environmental conditions observed to induce the oxidation of the sample surface and the deposition of oxide powder onto the surface of the disks to provide more control over the chemical environment on the sample surface.

5.2.1 Oxide synthesis

Oxide synthesis was performed in a series of environmental chambers of which shown schematic is given in Figure 63, which simulated the physical environmental conditions observed at the trackside. Within the chambers saturated brine solutions of specific salts were placed to regulate the humidity. The sample substrates were places on a mesh platform held above the brine solution. These containers were then placed in two different areas where the temperature was controlled: a refrigerator set to 7°C and in an air-conditioned room (20°C).

A body of water and the air directly above it undergoes mass transfer of water through evaporation and condensation, eventually reaching an equilibrium state at corresponding concentrations of water within the liquid state and the gas (humidity). This equilibrium is also dependent on the temperature of the system and the water - affinity of the gas and brine solution. By adding an excess of salt into a saturated brine solution, a buffer is created, maintaining the saturated condition and a corresponding stable humidity above the brine. By utilizing salts which have higher and lower affinities for water, saturated brine solutions were employed to generate stable regions of humidity into which the samples were placed.

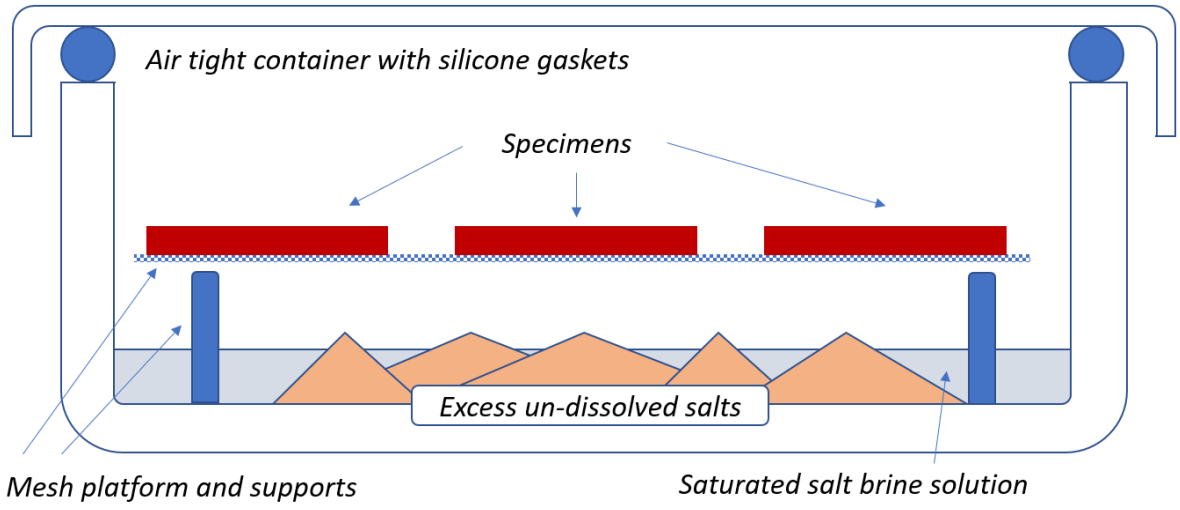

Figure 63, Schematic of environmental chamber layout

Salt solutions and their target humidity are given in Table 9 and a BOSCH BME280 digital humidity sensor was used to confirm the conditions, which is the same sensor used for the environmental monitoring in the field. Using these humidity chambers, as well as the two temperatures environments, the various sample preparation treatments for oxide synthesis are given in Table 10. In addition to varying the temperature and relative humidity, some of the treatments include the

spraying of water to simulate dew, this was performed using a spray bottle / atomiser to deliver a controlled amount of distilled water to the surface of the substrates from 10cm away which achieved an even distribution.

Table 9 List of saturated salt solutions used for simulating environmental conditions.

Saturated solution salt	Humidity above solution surface (% RH)	Condition simulated
None (Distilled water)	100	V. high humidity
Potassium Chloride	85	Normal humidity
Sodium Chloride	75	Medium low humidity
Sodium bromide	60	Low humidity

Table 10 Descriptions of simulation conditions, after which the samples are placed with the control sample until testing.

Treatment	Description
A – Control	Control – Stored at room temperature (~20°C) and at 85%RH
B – Dew	A condensation cycle – Cooled to 7°C at 60% for 3 hours then placed in 100%RH container at room temperature for 5 hours to induce dew formation.
C - Drizzle	Sample sprayed with 0.1ml of distilled water which is left to evaporate.
D – Mixed	As for B but sample is sprayed after 30 minutes of being placed in 100%RH container.
E – Flooded	5ml of distilled water placed carefully on the substrate surface to flood the surface.

The samples generated in this way served two purposes: to investigate the nature of oxides formed on the surfaces through different conditions and to observe the effects of the oxides on the tribo-properties of the surfaces.

5.2.2 Oxide deposition

The second sample preparation technique used is the direct deposition of different oxide types to the surface of the substrate, thereby allowing investigation into the effect of individual oxide types on the tribo-properties of the surfaces.

Two different carrier mediums were used to deposit the oxides on the surfaces: distilled water and isopropanol; this was decided upon after initial testing of depositing via distilled water caused noticeable oxidation of the surface of the substrates. Magnetite, haematite, goethite and lepidocrocite powder obtained from the Sigma Aldrich and Alfa Aesar suppliers with particle sizes of approximately 50-100nm, 0.1-5µm, 1-2µm and 1-5µm respectively were dispersed in the solvents for deposition. Only the larger, 42mm diameter, disc samples were used for the oxide deposition.

The first batch of samples was prepared using distilled water as a solvent. $1 g.dm^{-3}$ concentration suspensions of the oxides were deposited in volumes of 5ml per sample. The second batch was prepared using isopropanol as the solvent. $1 g.dm^{-3}$ was used again; however, due to the lower surface tension, only 2ml could be applied per disc to avoid overflow.

The general procedure for the deposition requires firstly that the suspension is well agitated prior to deposition to ensure good entrainment of the oxide particles throughout the suspension. A pipette is then used to dose the required amount of suspension evenly onto the disc surface. Surface tension of the liquid will contain the material on the top surface of the substrate as shown in Figure 64. The substrate is then left until the liquid has evaporated leaving a coating of the oxide on the substrate surface as can be seen in Figure 65.

The layer mass density of the deposited oxide on the surface of the substrate is calculated by difference in mass of the sample before and after the oxide deposition and the layer thickness determined through removing part of the layer with a scalpel and using an optical surface profilometer.

Figure 64, Drop deposition showing the suspension as initially deposited on the substrate

Figure 65, Photographs showing the drying of a goethite oxide dispersion in isopropanol on a sample substrate, left; and the dried sample surface, right

5.3 Chemical analysis

The oxides both formed on the substrate and collected in field track swabbing were analysed predominantly through XRD due to the strength of this technology in being able to identify crystalline substances such as the oxides. Scanning electron microscopy and visual analysis based on the colour of the observed oxides were also incorporated into the chemical testing to cross-analyse the XRD results.

5.3.1 XRD

A PANalytical X'Pert-3 powder X-Ray diffractometer mounted in glancing incidence geometry and equipped with a copper anode was used to analyse the synthesised oxide samples. The steel substrates were mounted in bulk sample holders and placed in the sample cassette as shown in Figure 66.

Continuous scans of each sample were performed between the 2θ angles of 20 to 65 degrees using a step size of 0.02 degrees and incident angle of 14° with a solar slit of 2° to maximise the x-ray beam intensity. The sample stage was rotated during scans and 4.664 seconds exposure taken per step.

A different configuration was used to analyse the track swabs. The filter paper medium was pressed into 'zero-background' sample holders so that the surface of the swab was flat on the plane of irradiation as shown in Figure 67. Out of the two patches of debris which were captured on each swab, the swab which visually appeared to contain the most material was selected for the analysis. Due to the lower quantity of material present on the swabs than on the bulk samples, the reflection geometry instead of glancing incidents was used.

The data produced from the scans of the track swabs resulted in a combined XRD spectrum of the sampled material as well as that of the swab material. Initially it was planned that XRD spectrums

from the blank filter papers could be subtracted from the signals from the swabs, but due to the complex artefacts of this base signal due to the obscuring of the signal due to material on the swabs, it was not possible to do this. Instead, a baseline curve of the signals was estimated in software and subtracted from the signal to obtain a clear spectrum with a flat baseline. The glass microfiber paper did not have any strong peak signals due to its structure being amorphic and therefore, for samples using GF filter paper, the subtraction of the baseline curves was enough processing to obtain a clean spectrum for the samples.

Figure 66, Samples mounted in bulk specimen holders

Figure 67, Mounting of filter medium (track swab) into zero-background cassettes

The scans from both the synthesised oxides and the processed signals from the track swabs were then analysed against powdered samples of pure phases of iron oxide as well as the ICDD PDF-4+ database [135]. The positions and relative intensities of the peaks from the scans were matched to the peaks of these known compounds to identify the chemical makeup of the surfaces and swabs analysed.

5.3.2 SEM

A Hitachi tm3030 plus scanning electron microscope was used to closely observe the structures of the deposited layers as well as investigate the morphologies of the oxides synthesised.

Three magnifications were used as standard amongst the micrographs: 1000x, 2500x and 6000x; to achieve a range of scales of which to view the specimens.

5.4 Surface imaging and roughness

An Alicona SL optical profilometer was used for both determining the roughness of surfaces of the substrates for tribo-testing as well as for calculating the thickness of deposited surface layers from a topological profile recorded by the instrument. Figure 68 gives an example of how this oxide layer thickness was found using an area of the substrate where the layer has been removed with a scalpel.

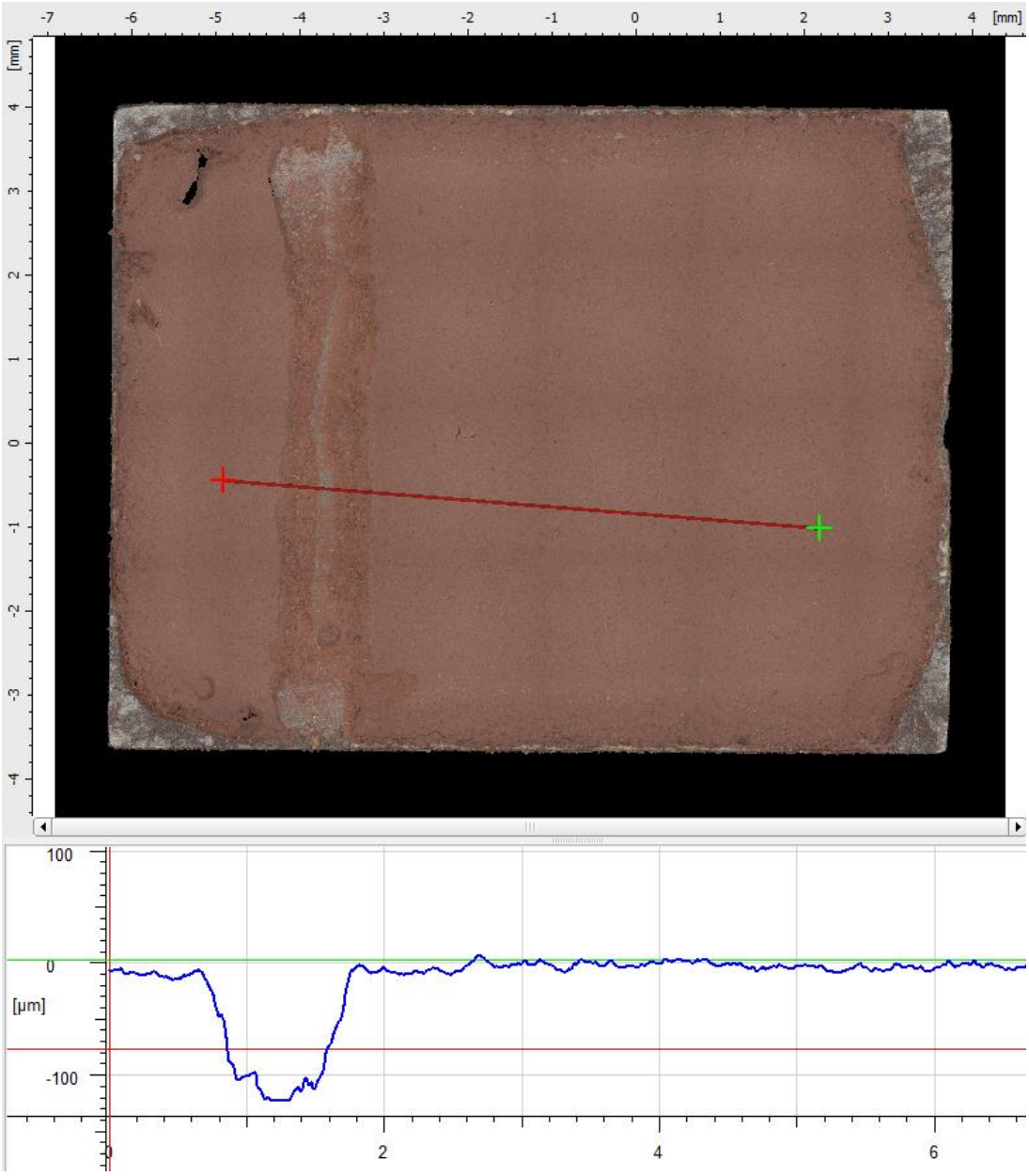

Figure 68, Example of the measurement of surface topography to determine oxide layer thickness

5.5 Physical testing

A variety of physical mechanical testing apparatus was used to analyse the samples. The different methods were used to test different types of contact simulation and explore different mechanisms which are not possible with a singular test. The UMT, pin-on-flat testing is a pure-sliding test platform whereas the SUROS utilises a rolling-sliding contact. The full-scale rig was used to validate the testing done on the smaller contacts and the rheometer testing explores the material properties of oxide suspensions to look more closely into the mechanisms of iron oxides with water within the wheel / rail contact.

5.5.1 UMT

The mechanical testing of the synthesised and deposited oxide samples was performed using a Bruker UMT tribo-tester set up in a pin-on-flat testing configuration. As the pin-on-flat test explores only pure-sliding contacts, this experimental setup simulated the portion of the wheel / rail contact in full-slip and hence at a maximum traction scenario.

Three different geometry sizes were used with this testing.

The first consisted of a 5.6mm stainless steel ball upper specimen and the small machined rail steel metal blocks approximately 10mm square, held in place with a larger machined part as can be seen in Figure 70. A contact force of 2N was used to load the ball against the plate corresponding to a contact area radius of 0.033mm and a maximum contact pressure of 860MPa as can be seen in the contact pressure-displacement model in Figure 70.

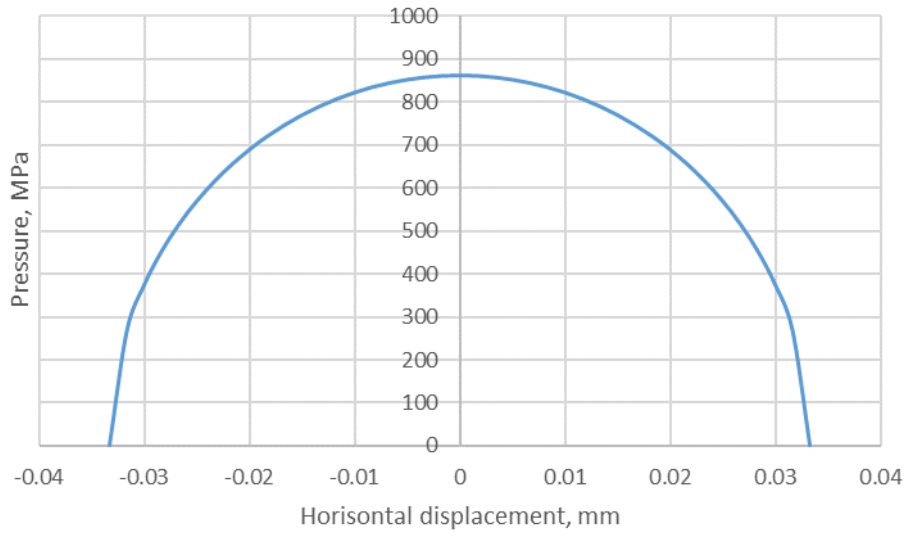

Figure 69, Small 5.6mm stainless steel ball contact pressure-displacement model

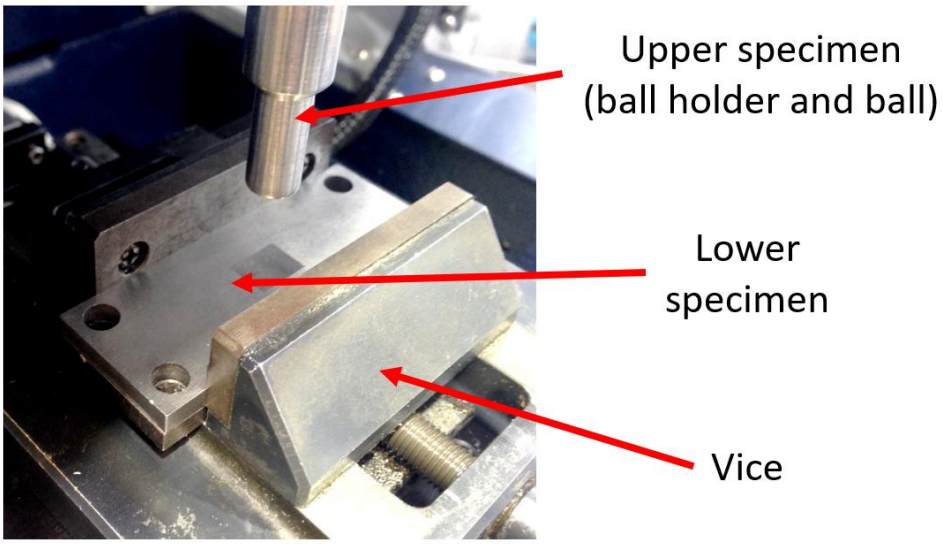

Figure 70, Photograph of the small 5.6mm stainless steel ball and small square rail steel UMT set-up

The larger 42mm disc samples used a larger 10mm diameter stainless steel ball as the upper specimen. The ball is loaded against the sample surface at with a force of 7N to achieve a mean

contact pressure of 590MPa and Maximum Hertzian contact pressure of 890MPa as shown in the model of Figure 71. Under these conditions the ball initially contacted the plate with an approximate diameter of 0.12mm.

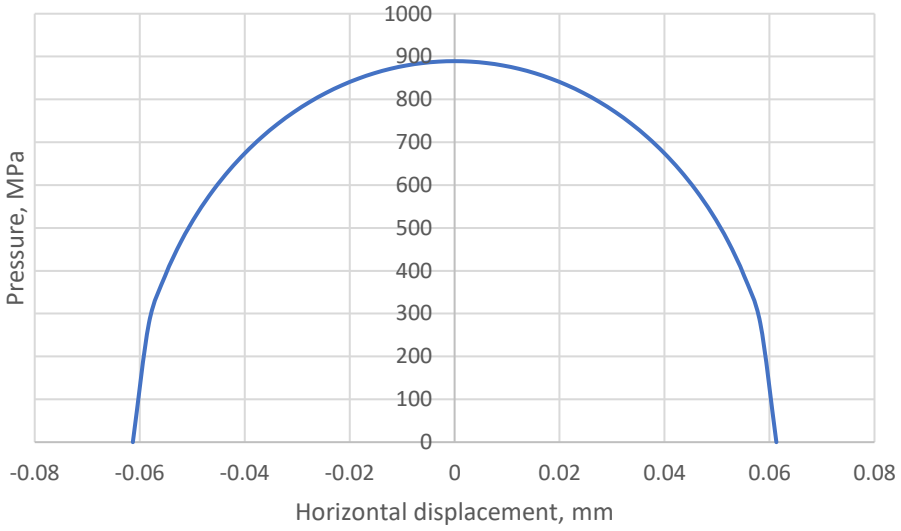

Figure 71, 10mm stainless steel ball contact pressure-displacement model

The largest of the three contact conditions, also utilising the 42mm discs as lower specimens had a larger upper sample consisting of a pin machined with a projected curvature of a sphere of 100mm; the stock material for these pins was 0.5" bright steel rod. The reason for investigating this larger geometry was to obtain a greater contact surface on the samples to make the contact geometry of a greater physical size than the pitted areas of oxidised sample substrate. For this larger contact, a larger contact force of 20N was used to achieve a mean contact pressure of 180MPa and maximum Hertzian contact pressure of 270MPa which can be seen in Figure 72. Initially a greater force of 50N was intended to be used; however, lower forces were used due to concerns that the vice holding the lower samples would be unable to hold the samples tightly enough for the large lateral forces.

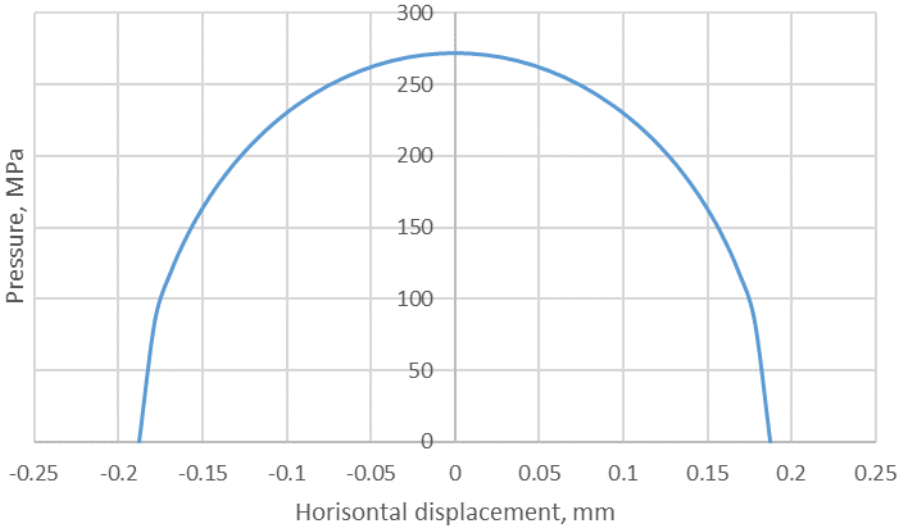

Figure 72, 100mm bright steel curvature contact pressure-displacement model

For all tests, a contact track in a single-pass grid pattern was traced over the surface of the samples at a speed of 20mm per second. The path traced by the contact was such that it does not reciprocate and continually traces on fresh surface during each run as shown in Figure 73. This new technique allowed for an individual-pass reading to be taken; observing the tribo-properties of the layer at various stages of being broken down by mechanical action. Cartesian co-ordinates are also logged with the load cell data to allow for a COF map of the sample surface to be generated.

The programs to guide the movement of the top sample over the specimens were writted such that the space between the paths was roughly twice the space between the tracks as the track width itself so as for the contact tracks would not interfere with each other. For the larger, circular samples, a different contact path given in Figure 74 was employed to utilise a greater area of the sample surface than what a rectangular pattern area would allow.

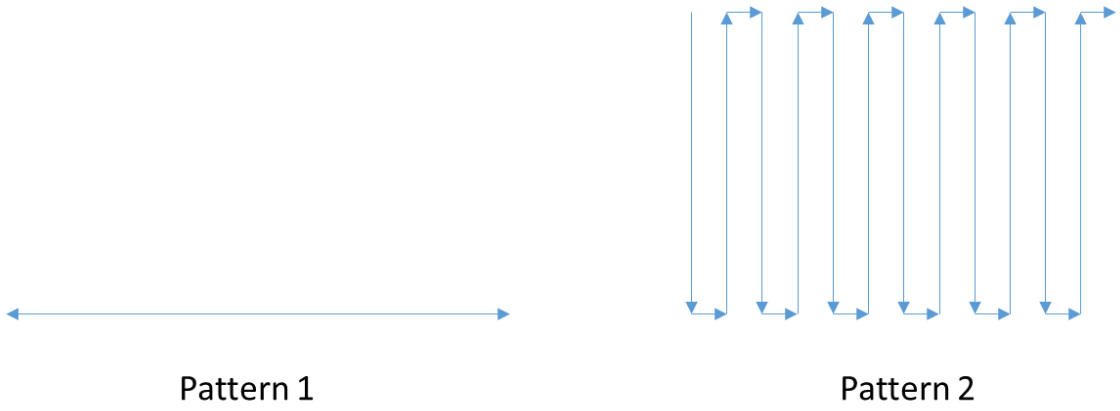

Figure 73, Contact paths of traditional reciprocating pin-on-flat (pattern 1) and single pass COF mapping track (pattern 2)

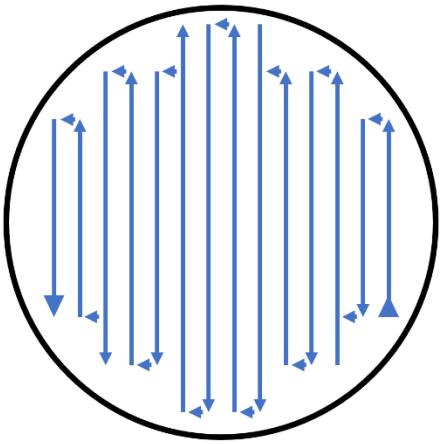

Figure 74, Single pass COF mapping track for 42mm circular specimens

Tests are either conducted dry or with distilled water applied using a spray bottle at the start of the run. The program take is approximately 5 minutes to complete all steps of each run for all the patterns.

The data collected from the runs was processed using a program written in MATLAB. For each of the runs the program outputs a mean and standard deviation value for the COF over the surface of the specimen as well as a histogram showing in greater detail the statistical distribution. From each run, a COF colour map is also generated which can be used to identify physical regions over the surface of the specimens of high or low friction; this information can then be overlaid onto images of the

sample surfaces as a valuable tool to understand the effect of different surface conditions on the frictional properties; photographs of the sample surfaces were taken before and after runs to aid with this analysis.

5.5.2 SUROS

The SUROS or "Sheffield University ROlling Sliding" rig is a twin disc apparatus. The machine consists of a metalworking lathe and AC motor which provide the rotation and tangential forces for the wheel and rail respectively, a schematic of this setup is given in Figure 75. A hydraulic piston, which applies a load to the shaft of the lower wheel specimen, loads the wheel and rail specimens together with a force up to 29kN. Load cells are used to measure the torque generated between the discs and confirm the normal force applied. A computer running LabVIEW is used to operate the rig; the rotational speed of the lathe is controlled relative to the speed of the AC motor to induce a controlled amount of slip / creep between the wheel and rail specimens.

The parameters are logged every second and from these values, the traction coefficient was calculated as the ratio of the tangential force to the normal load applied.

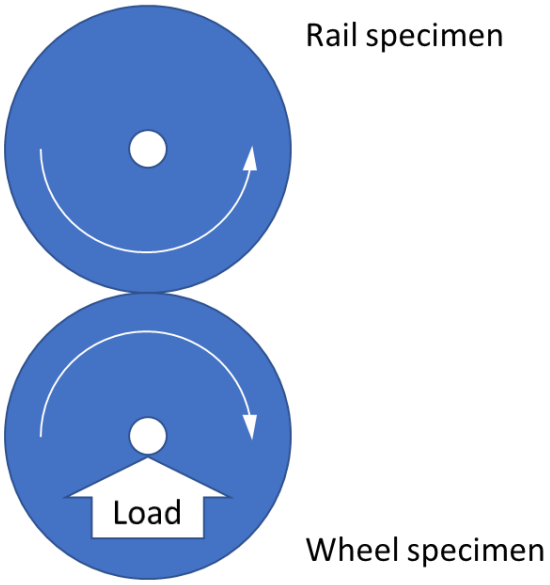

Figure 75, Schematic of SUROS twin disc tribometer

The specimens – both wheel and rail – used in the testing were cut from R260 rail steel and wheel steel. All specimens were machined to 1cm thick discs and surface finished with a cylindrical surface grinder to final diameters of 45.47mm.

Each of the run was performed at 400RPM, 900MPa and 2% slip. The force required by the hydraulic arm to load the specimens together was calculated in the LabVIEW software of the rig.

The oxide pastes consisted of powders of haematite, magnetite, goethite and lepidocrocite, made up to compositions of between 30 and 60% oxide with distilled water. Control samples of distilled water and dry contacts were also tested for comparison. The pastes were prepared by weighing out approximately 1g of oxide powder then adding distilled water to achieve the desired consistency. The exact mass fractions of the iron oxides in these pastes was determined gravimetrically. Oxide mixtures of an easy to apply viscosity were initially prepared and the mass ratios later used as a guide for varying the ratios of oxides to water to prepare samples of a suitable range for the testing. This is because very high viscosities resulted in difficulties when applying the paste.

To test the effect of each oxide paste on the traction performance, the oxide pastes were applied in drops at a rate of around 2ml per minute via a drop pipette to the top of the rail specimen which would then be carried into the contact. After three or four drops, a bead of the paste developed around the contact and the application would then be ceased and the contact allowed to dry out. The drying out of the contact was monitored both visually and by observing the traction coefficient resulting in a steady decrease in traction followed by a steep increase; once this steep increase was noticed, the application of oxide paste would resume once again for multiple cycles for 2 to 5 minutes depending on the availability of oxide pastes. By observing this "drying out" relationship and identifying the minima, judgements regarding the effect of each oxide could be made.

5.5.3 Full Scale Rig

The full-scale wheel / rail test rig utilised was a re-commissioned rig originally built and used for work at British Rail Research; now serving as the University of Sheffield's Full-Scale Test Facility.

The apparatus consists of a locomotive wheel mounted to a pivoted loading frame above a rail specimen positioned on a linear actuator as shown in Figure 76 [67]. A load is applied to the wheels axel from a hydraulic press acting on the frame and the wheel is free to rotate along the rail as it is pulled beneath it. A chain connects the rim of the wheel to another hydraulic piston which is used to induce slip in the system by pulling the wheel and increasing its speed above that of the rail.

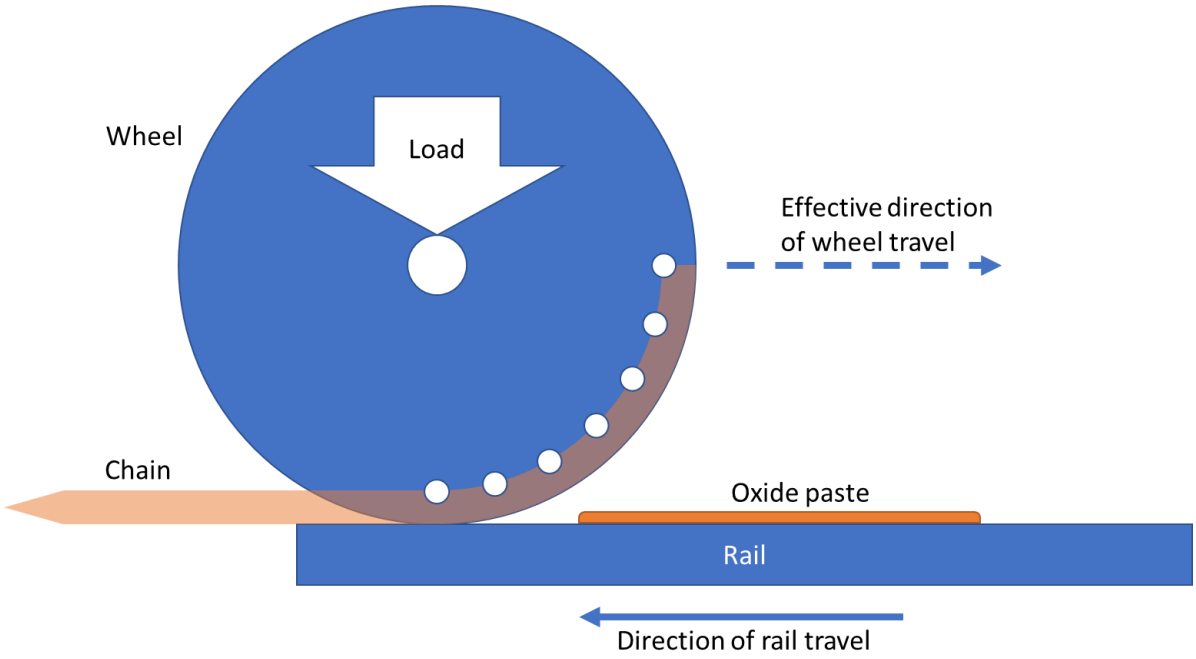

Figure 76, Full scale rig schematic

A maximum load of 180kN can be applied to the rail by the wheel. The maximum travel distance of the rail is 600mm and at a maximum speed of 100mm.s^{-1} during which the wheel can be rotated to cover a distance of 710mm, thus inducing a slip of up to 110m. The parameters chosen for the testing were a rail speed of 100mm.s^{-1} along 300mm and slip of 2mm/s or 2%. The vertical load applied was 75kN and a preload which was determined from 10kN to 20kN depending on conditions was applied to remove slack from the chain and actuators.

Oxide pastes were synthesised by mixing oxide powders with distilled water to a 1:1 ratio. These samples were applied directly to the railhead in the running band before testing as shown in Figure

77 with 15ml of paste applied each run. Haematite and goethite oxides were both explored against wet (distilled water) and dry runs.

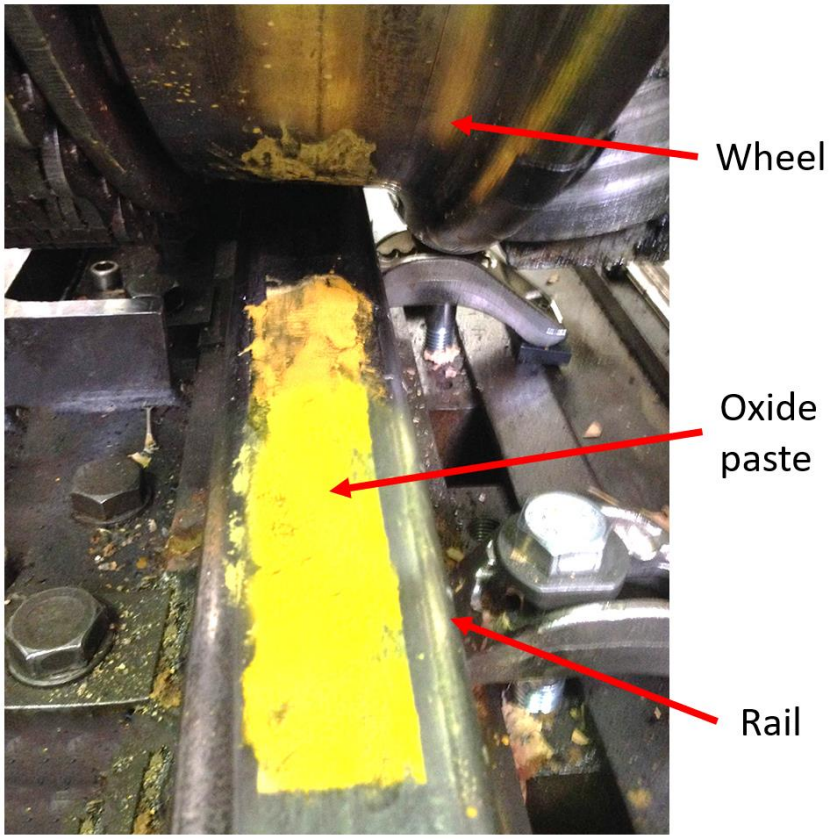

Figure 77, Goethite paste deposition on full scale rig

After the surface treatment had been applied to the railhead, each run commenced as soon as possible. The program ran 6 cycles with 4 steps:

1. The wheel was lowered onto the railhead and force increased to 75kN
2. The chain was pre-tensioned with 10-20kN
3. The rail was pulled 300mm and a slip of 2% was induced in the wheel
4. The wheel was raised, and the system returned to its original position

Lateral and vertical forces were recorded during all cycles from which a plot of the coefficient of traction could be obtained. The first cycle of each run was always problematic due to an unwanted artefact of the rig; because of this the second, third, fourth, fifth and sixth runs were used to generate a statistical analysis of the coefficient of traction.

5.5.4 Rheology

For the rheology testing, a TA Instruments AR2000 Rheometer was used to measure the material properties of various oxide pastes consisting of varying oxide concentrations.

The rheometer shown in Figure 78, is a parallel plate type fitted with a 4cm diameter flat plate and uses an air bearing to provide close to friction-free force application. Due to this air bearing, the normal force that could be applied was limited and a maximum of 1N force exerted on the bearing was decided.

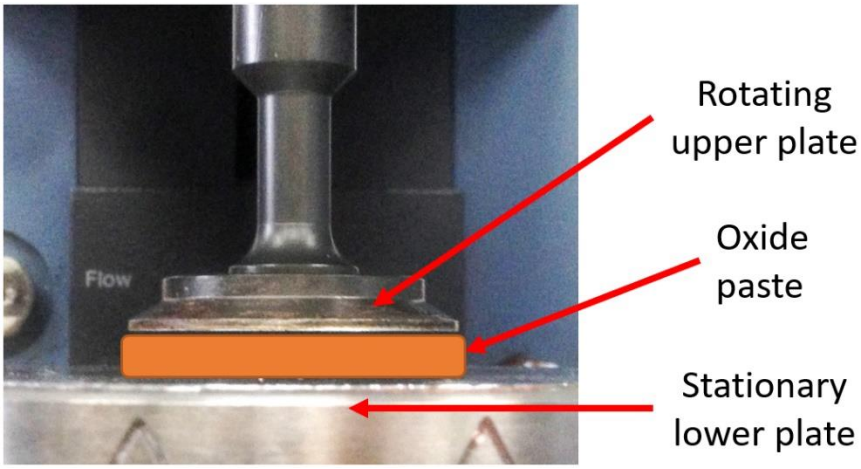

Figure 78, Rheometer geometry

Each sample of oxide to be tested was first measured dry in a small vile so that when 1ml of water was added, the mass fraction of oxide would be within the target oxide concentration range and the mass of the sample recorded; the vile would then be sealed until final preparation. A few minutes before testing each vile would be reopened and 1ml of distilled water accurately deposited with a volumetric pipette and the paste prepared through mixing with a glass rod.

A program was prepared for the runs in which the top plate would be lowered onto the paste, spreading it to cover the entire volume between the plates and compressing the paste. The maximum force exerted by the weight of the instrumentation and the lowering force of the machine was around 1.8N resulting in a compression pressure of around 1.5kPa. The gap between the top and lower plate at this point was between 500 and 800µm. Once the normal compression force was reached the program then proceeded with a linear continuous shear rate ramp from stationary to a rate of $100s^{-1}$ over a period of 5 minutes. After completing the ramp another linear continuous ramp was programmed to bring the shear rate of the system back to stationary over a further 5 minutes.

During the runs the shear stress, shear rate and normal stress was recorded from which the viscosity could be calculated as a function of time.

A key value used to compare the oxides is the yield shear stress. This is the stress required to deform the material from stationary. It must be noted that the yield shear stresses in this thesis were recorded at normal compression values of around 1.5kPa and before any lateral plate movements as in the testing, after shearing begun, the shear stress and normal forces acting on the paste dropped rapidly.

6 Railhead Analysis

This chapter presents environmental monitoring and chemical analysis of the railhead to provide further understanding into how conditions experienced at the trackside affect the surface of the railhead. Bespoke environmental monitoring stations have recorded the physical conditions at the trackside and a combination of visual and X-Ray diffraction analysis is used to investigate the surface of the railhead and identify chemical species present. Relationships between patterns and variations in the environmental conditions to the surface railhead condition is explored in this chapter.

6.1 Environmental monitoring

Monitoring stations were set up in select locations around the UK as well as abroad to monitor, to a high time-resolution, the environmental conditions on or around the railhead.

6.1.1 Station overviews

Stations were set up and weather conditions logged in a variation of locations as well as times of the year to investigate conditions throughout the year and in different places. Three major locations were the sites of the stations: Quinton Rail Technology Centre (QRTC) in Warwickshire, UK; a infrequently used wooded railway cutting near Royston in Yorkshire, UK; and a location in Surrey in British Columbia, Canada.

Overview graphs of all data obtained from all stations are given in Appendix C; their content is summarised in this section.

QRTC, 10th October – 12th October 2017:

Figure 79, Photograph showing position of station 1 at QRTC

Three stations were set up to run during a three-day preliminary testing campaign. The stations were positioned in different locations on the site as can be seen in Figure 111 on page 114. The first, station 1 shown in Figure 79, was on a raised set of steps in the open about 10 meters from the track. The second, station 2 shown in Figure 80, was located above grass by the track with a temperature probe connected to a rail section placed by the side of the track. The third, station 3 shown in Figure 81, was positioned in an area where the track passes through a tree clearing; the area is sheltered by mixed woodlands and a fence on the south east and parked rolling stock on an adjacent track to the north west; the ground on which it was placed was a harder compacted ground with mosses, dry grass and leaf debris.

Figure 80, Photograph showing position of station 2 at QRTC

Overviews of the environmental data obtained from these stations are given in Figure 167 through to Figure 171 in appendix C.

The environment temperatures recorded at the stations reached 18 to 20°C during the day on the first two days and 15 to 18°C on the last day. During the night, temperatures fell as low as 13 or 14°C on the first night and 6 to 8°C on the second night. Rainfall was recorded around 1500hrs to 1800hrs on the second day (11th October), this was accompanied by a change from a falling to a rising pressure associated with a cold front. The humidity varies between the stations which will be discussed further in the next section but overall, the relative humidity remained tended to increase towards 90% for all stations during the nights and fall during the day to 70-80%.

Figure 81, Photograph showing position of station 3 at QRTC

QRTC, 22nd January – 11th February 2018:

Two of the environmental monitoring stations were set up once again to run for 3 week. The stations set up were station 2 (located above grass by the test area) and station 3 (positioned in an area where the track passes through a tree clearing) as they were in the previous monitoring campaign at QRTC. Station 3, in addition to station 2 on this occasion, was equipped with a temperature probe attached to a section of rail placed beside the operational track to log the apparent railhead temperature.

An overview of the environmental data obtained from these stations is given in Figure 172 Figure 167though to Figure 175 in appendix C.

The differences of the conditions observed between the two stations are discussed in the following section. The temperature observed over the monitoring campaign fell from daytime temperatures of 10 to 12°C to around 3 to 5°C for station 3 and night temperatures of 7 to 8°C to as low as -5°C towards the end of the campaign. Humidity was high at night, for both stations around 95% and station 2 occasionally reaching saturated conditions. The pressure and rain sensor measurements indicate that there were at least 18 weather fronts passing over the location during the monitoring campaign resulting in regular rainfall.

Royston Rail Bridge 194, 10th October – 19th December 2017:

A monitoring station was placed for 10 weeks on a scarcely used route near Barnsley shown in Figure 82 and Figure 83 near a road bridge. The location is in a ground cutting surrounded by trees. The

route is operated by Northern Rail for driver training and occasionally operates goods trains serving the glass factories nearby.

An overview of the environmental data obtained from this station is given in Figure 176 Figure 167though to Figure 178 in appendix C.

Two outages of the station were logged. On the first, which was a few days after the station was set up, it was revealed that a man living in a property close to the station frequently walked their two dogs, grey whippets, alongside the track and that one of the dogs had urinated on the weather station causing the rain sensor to short-circuit and the microcontroller to malfunction ultimately draining the battery as a result. This was rectified with the help of the dog walker who trained their dog to avoid the spot as well as replacing the batteries in the station. The rain sensor was, however, destroyed as a result and there was no further data on rainfall recorded for the station. The second outage occurred halfway through monitoring due to freezing temperatures affecting battery performance, this was fixed by replacing the lithium-polymer batter with a lithium-ion battery more suited to the low operating conditions.

The daily temperatures fell over the course of the monitoring period from daily highs of 20°C down to 0°C and lows from 14°C down to -7°C. The pressure chart indicates that over 30 weather fronts passed over the station during this time. The relative humidity throughout the majority of each days was 100% likely due to the position of the track being within a low-lying ground cutting within the shade for the majority of the day. Occasionally the humidity would fall as low as 75% during the early afternoon before returning to saturated conditions later in the evening.

Figure 82, Photograph showing position of station at bridge 194 in Royston, Barnsley

Figure 83, Photograph showing the area surrounding bridge 194 in Royston, Barnsley

Surrey B.C. Canada, 13th February 2018 17 – 3200hrs UTC (09 – 1500hrs local):

A final environmental monitoring station was posted to a researcher in British Columbia to monitor conditions during the testing of a new portable railhead tribometer. Tests were carried out on a single day in February.

An overview of the environmental data obtained from this station is given in Figure 179 and Figure 180 in appendix C.

Temperatures began at around 2°C in the morning and increased over the day fluctuating with conditions and reaching a maximum temperature of around 13°C in the afternoon. The humidity rapidly dropped from around 70% RH in the first hour to fluctuating between 35% and 50% during the rest of the day. Pressure was dropping steadily over the course of the monitoring.

Monitoring was once again conducted on the 26th April, later in the year in the same spot during another trial. The researcher did not affix the railhead temperature probe this time. The day was hot and dry, increasing from the low twenties to the low forties during the day with the relative humidity gradually increasing from 23% to 32%.

6.1.2 Regular patterns and phenomena

The general pattern observed during the course of the day is a rise in temperature from the morning through to the late afternoon. Occasionally it was noticed that the railhead temperature would fall below the dewpoint temperature.

During the experimental trials at QRTC it was noticed in the morning of the 12th October 2017 that a thin film consisting of a mixture of orange / brown and silver / grey oxide had formed on the railhead along with a thin film of water as shown in Figure 84. The driver of the test locomotive at QRTC also noted that the operating conditions of the locomotive at that time were of very poor traction. The environmental monitoring stations revealed that between 2300hrs on October 11th to 0830hrs on October 12th that the temperature of the railhead had fell below that of the dew point and thus may have led to the inclement traction conditions.

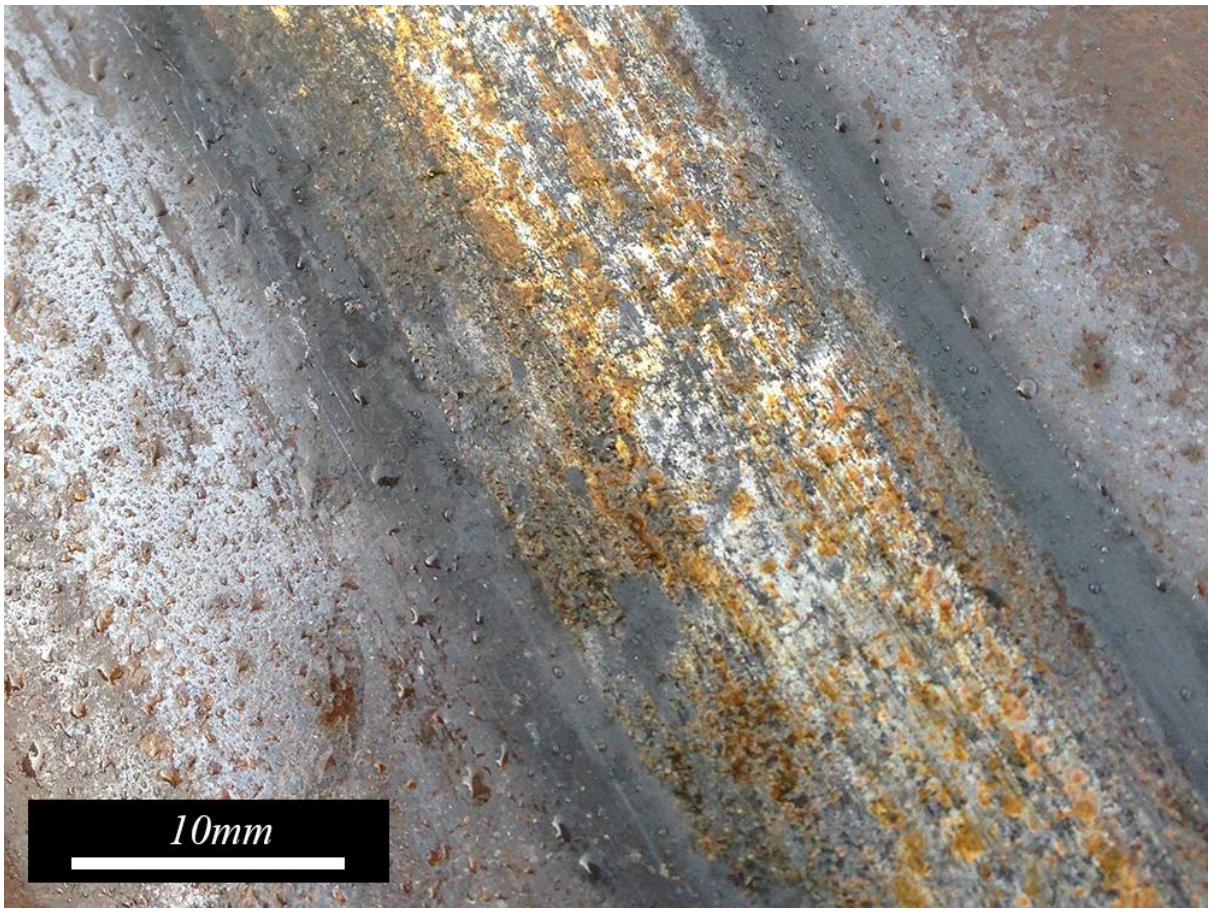

Figure 84, Railhead condition observation at QRTC on 12th October 2017 morning

The data from the weather stations reveals how the relationship between the railhead and its surrounding environment may contribute to scenarios which could allow the railhead temperature to drop below that of the dew point. The first of these situations regards the thermal mass of the railhead in comparison to the surrounding environment.

The volumetric thermal mass of steel is millions of times higher than that of air. This causes the railhead to behave as a great bulk thermal mass in the environment which resists changes in temperature. This can be seen in Figure 85 which shows the railhead temperature lag between one and two hours behind the temperature of the environment leading to around one to two degrees Celsius of temperature difference between the two values during the periods when the environment temperature is changing most rapidly. It should be noted that the example given was that of a monitoring station within the shaded tree clearing as the temperature of the railhead rises rapidly when exposed to direct sunlight – this will be discussed in the next subsection.

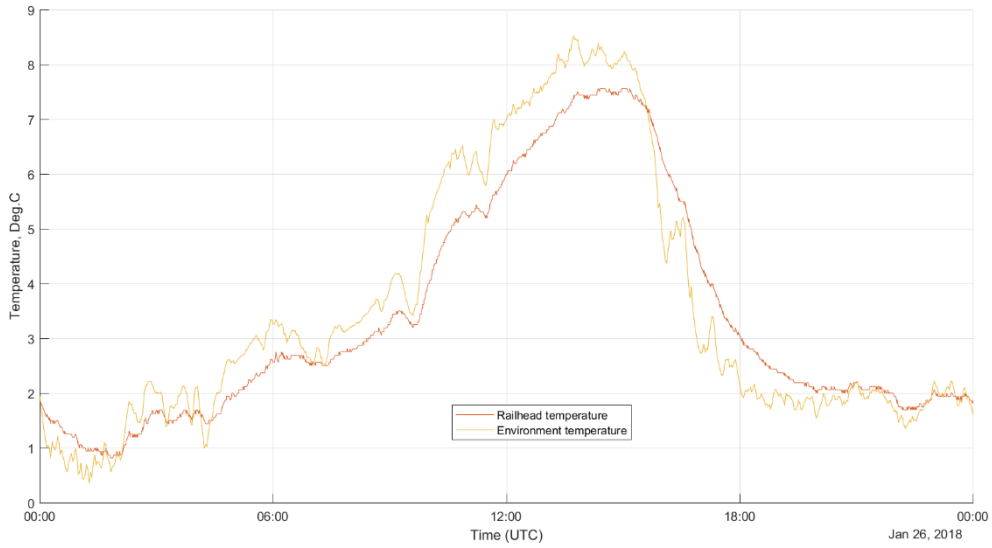

Figure 85, Chart showing the temperature of the railhead and environment of weather station located in shaded area

These sudden increases in temperature, especially during periods of high relative humidity, such as in the morning, may cause the temperature of the railhead to lag behind that of the environment long enough to cause it drop below the dew point temperature and therefore induce net condensation of water onto the surface of the railhead. This is shown in the morning of February the 8th in Figure 86.

Rain and sudden increases in humidity may also lead to the situation where the temperature of the railhead drops below that of the dew point. This is shown at approximately 2200hrs on February the 8th on Figure 86. Rainfall is shown to happen, followed by a decrease in both environment temperature and railhead temperature. The humidity also increases resulting in an increase in the dew point temperature, bringing it above the temperature of the railhead. A result of this mechanism is that after the rainfall, net condensation on the surface of the railhead may allow for a more persistent film on the surface as well as allowing the liquid film to spread greater over the surface due to evaporation and condensation mechanisms.

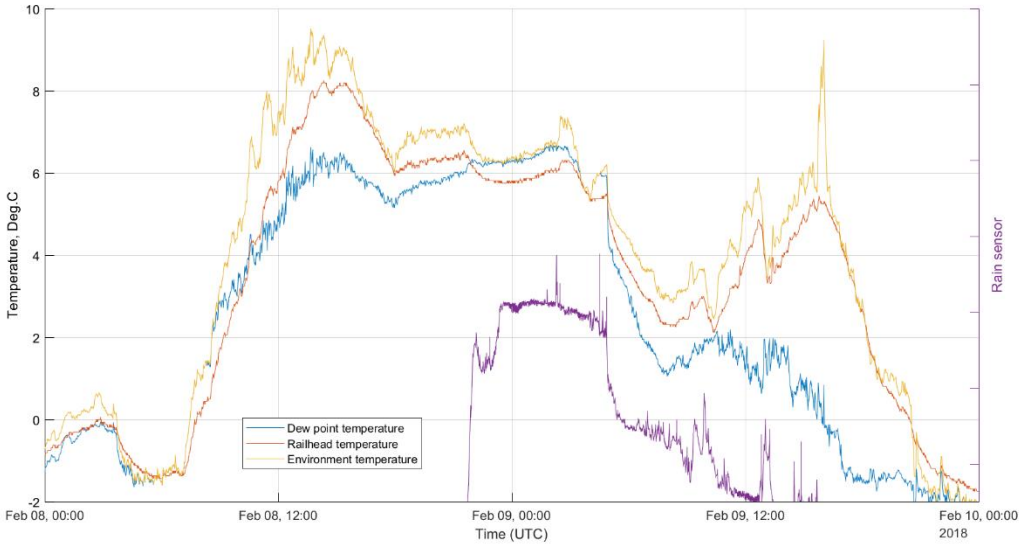

Figure 86, Chart showing the railhead, environment and dew point temperatures as well as rainfall (given in arbitrary units) of station 2 at Long Marston

The frequency of events when the railhead temperature of the railhead falls below that of the dew point temperature have been plotted by time of day in Figure 87. The pattern of number of events by time of the day closely matches the relationship between time of day and normalised frequency of low adhesion related events [109]. The general pattern indicates a high frequency of this phenomena in the morning hours, likely due to railhead thermal lag and another moderately high frequency around 2200hrs possibly due to rainfall around this time of the day.

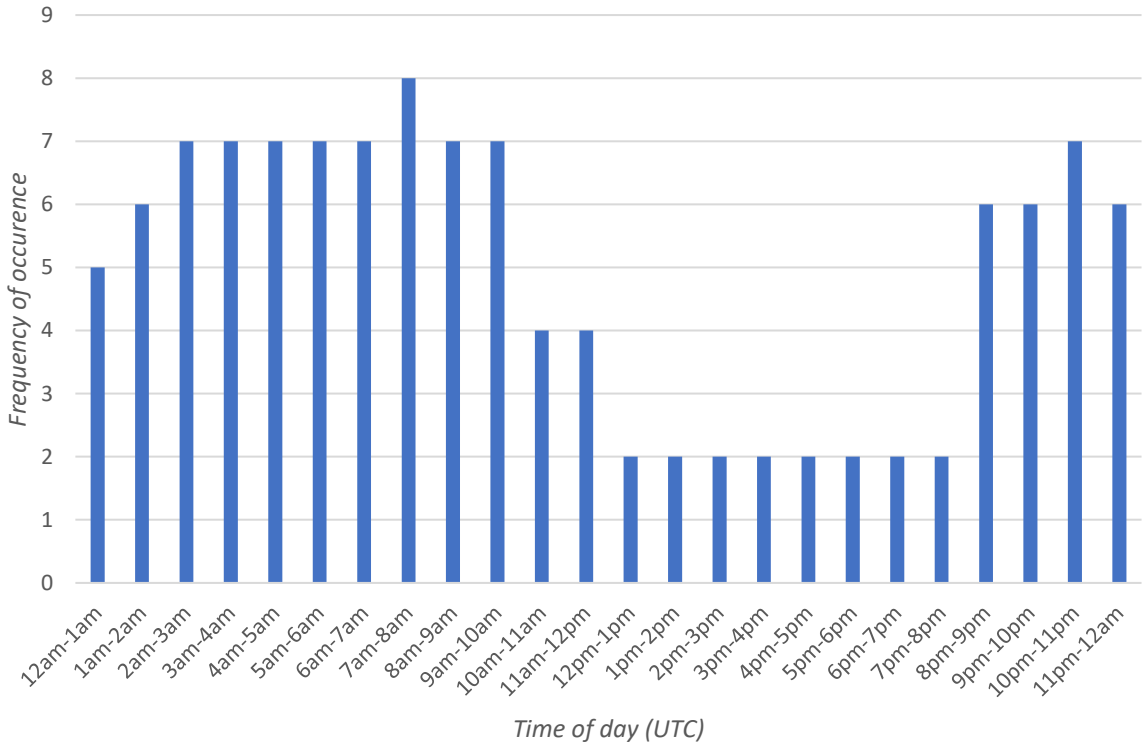

Figure 87, Histogram displaying the frequency of occurrence by time of day of the railhead temperature being lower than the dew point temperature, data from station 2 of QRTC monitoring campaign Jan / Feb 2018

6.1.3 Locational variability

The patterns of railhead and trackside conditions appear to vary with location. Sheltered areas prevent direct irradiation of the railhead by sunlight resulting in lower daytime railhead temperatures. This can be seen clearly in Figure 88 where on some days (presumably sunny) the railhead temperature in the open by the test area reaches values far greater – often by 10°C – than that of the rail in the tree clearing. However, this is not the case on some days and the daytime temperatures are similar throughout the day, presumably due to the lack of clear skies.

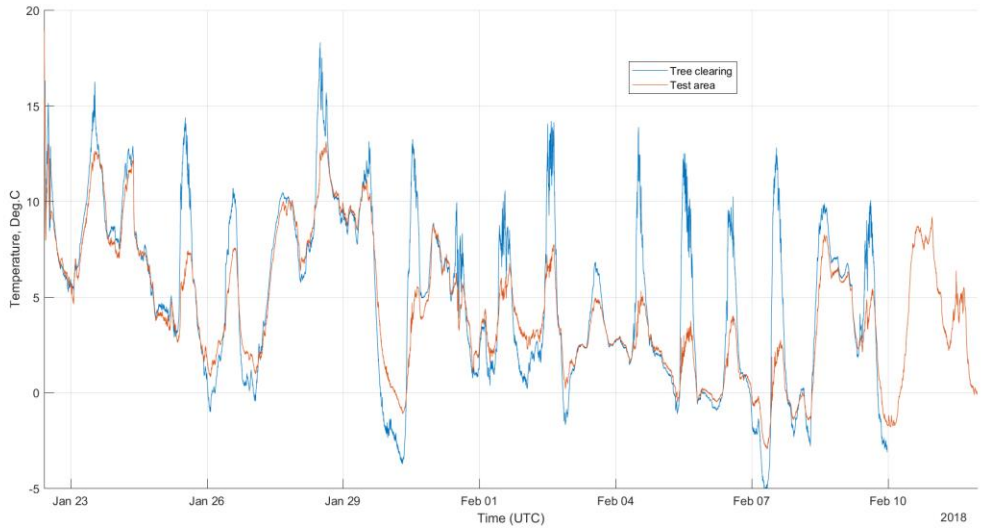

Figure 88, Railhead temperature comparison between sheltered track (tree clearing) and open track (test area)

The ground that the railhead lays on appears to have a direct influence on the humidity of the air above. Figure 89 plots the relative humidity for three stations at QRTC over the same period. The highest humidity was experienced by the station at the test area which was located on long grass likely due to transpiration from the vegetation. The station positioned in the tree clearing typically displayed a lower relative humidity as a result of being placed on drier ground with less vegetation in the shade of the trees.

In the monitoring period of early 2018, station 3 in the tree clearing was moved to be out of the way of security patrols due to its low profile and thereby reducing chances of it being tripped over. This new location, shown in Figure 90, was in a longer growth of vegetation which is less dry and nearer to the boundary fence. The resulting effect on humidity is shown in Figure 91 which reveals that its humidity is greater than that of the station at the trackside. During this time, the area under the tree cover had a much damper appearance than in October suggesting seasonal variations in both covered and uncovered conditions; however, such seasonal variation cannot be concluded by the limited data recorded in this study.

The station to display the lowest relative humidity the majority of the time and did not reach 100% relative humidity was station 1, which was positioned on a raised steps platform in the open near the test area. The reason for the relatively lower humidity is likely due to the station being in a raised position in relation to the other stations and the ground.

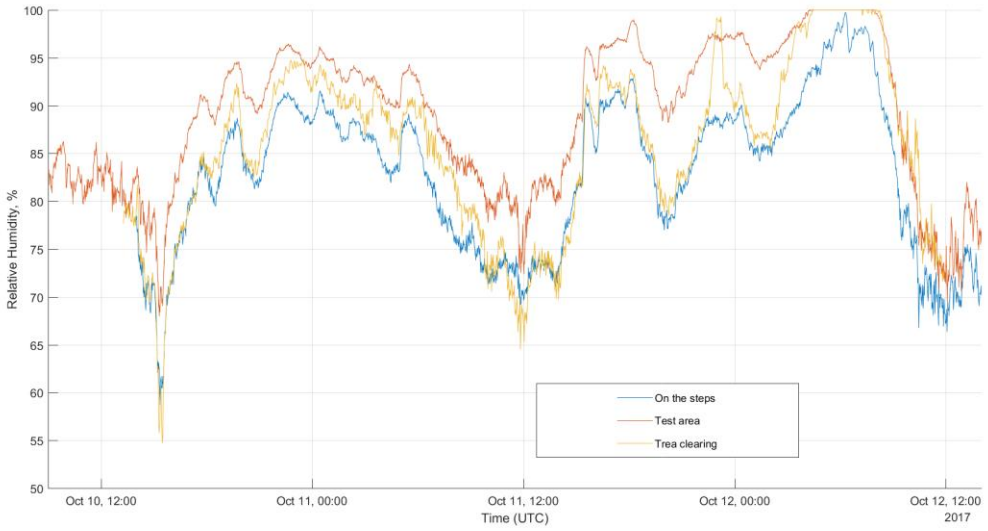

Figure 89, Relative humidity of stations 1, 2 and 3 recorded at Long Marston in October 2017

The station positioned in a railway cutting in Barnsley, Yorkshire, Exhibited an almost constant high humidity throughout the monitoring during October, November and December 2017. This is likely due to the station being located in a low spot of the land excavated for the railway to be laid.

Figure 90, Moved location of weather station 3 in the tree clearing during early 2018

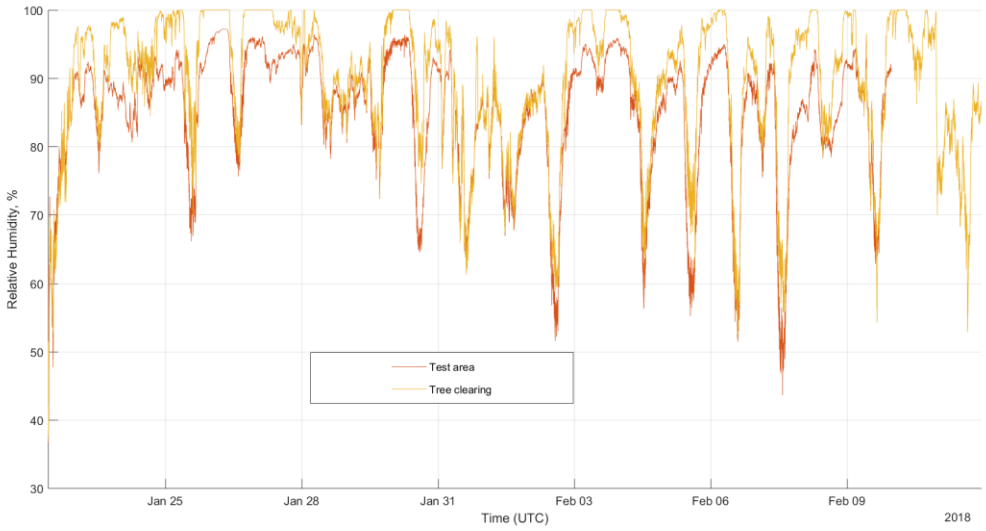

Figure 91,Relative humidity of stations 2 and 3 recorded at Long Marston in January / February 2018

The station briefly set up in British Columbia, Canada, recorded a much drier environment than conditions monitored in the UK with relative humidity falling from 70% to around 30-35% during the day for the monitoring in February and remaining constantly lower than 35% in April throughout the day; this resulted in the railhead temperature remaining substantially greater than the dew point temperature for both days. Due to the very short period of monitoring, as well as the station not being left to monitor overnight, there is not enough data to understand the daily patterns of trackside conditions at the location, but due to the great temperature increases from 1°C to almost 15°C during the day, it is likely that greater fluctuations in environmental conditions between night and day can be expected from this location.

More data is clearly needed to build up a comprehensive picture regarding seasonal fluctuations in conditions which may lead to the formation of railhead conditions affecting wheel / rail traction; however, much supporting data has been collated from the environmental monitoring stations to suggest correlations between conditions experienced and the formation of low adhesion conditions.

6.2 Chemical analysis

In addition to the environmental monitoring, XRD and visual analysis was also performed during some of the monitoring campaigns to determine the chemical make-up of the railhead surface.

6.2.1 Standards, controls and identified oxides

This section explores the stability of oxides on the swabbing material as well as how to maximise the clarity of the XRD signals from the material obtained from the track swabs. This was accomplished by appraising different available filter media for their background signal flatness and taking reference spectra from oxides purchased as test samples. From these starting blocks and using the ICDD PDF-4+ database of XRD spectra, oxides were identified from the spectra of the sample swabs; examples of each of the oxides identified from the chemical analysis are given.

Initially two filter paper mediums were tested: a cellulose based ashless filter paper and glass microfiber, their spectra can be seen in Figure 92 and Figure 93 respectively. The ashless paper is shown to give a strong signal around 23° and a further smaller peak at 34.5° which results in a complicated background signal that is difficult to compensate for whereas the glass fibre displays a much flatter spectrum with a relatively low intensity broad peak centred around 24° which is easier to process. Attempts were made to subtract this background signal from spectra of the track swabs to isolate signal of the collected material with some success; however, the signal from the swab medium contributing to the background of the swabs varied according to numerous factors including the type and thickness of material collected on the swab as well as the incident and reflection angles. As a result, a simpler signal processing was used whereby a moving average intensity of 5 degrees was calculated and subtracted from the spectra as a form of high pass filter. Figure 94 demonstrates this processing applied to the blank glass fibre swab. An undesirable artefact created from this processing is overcompensation of the signal close to intense diffraction peaks; however, as these peaks tend to be far shorter than the moving average compensation, they are shown clearly in the processed data. The objective of the processing was to enable identification of oxides more clearly from small traces and, even though after data processing the relative intensities of peaks relate to the relative composition of the oxides, this approach is unsuitable for rigorous quantitative composition analysis.

In Figure 95 through to Figure 98, the XRD spectra of the purchased standard oxide powders deposited on glass microfiber filter paper are given. These oxides were magnetite, haematite, goethite and lepidocrocite. Photographs of these swabs, exhibiting the colours of the oxide powders, can be seen in Figure 99.

Cross referencing all of the track swab spectra against the standard oxide swabs and the ICDD PDF-4+ database resulted in the identification of nine compounds:

- Haematite
- Magnetite
- Maghemite
- Goethite
- Akaganéite
- Lepidocrocite
- Iron
- Wüstite
- Soot / graphite

Examples of track swabbing spectra which exhibited the spectra of these compounds are given in Figure 100 through to Figure 108 with the positions of the intensity peaks of the named oxide overlaid onto the spectra. Photographs of the example track swabs are given in Figure 109.

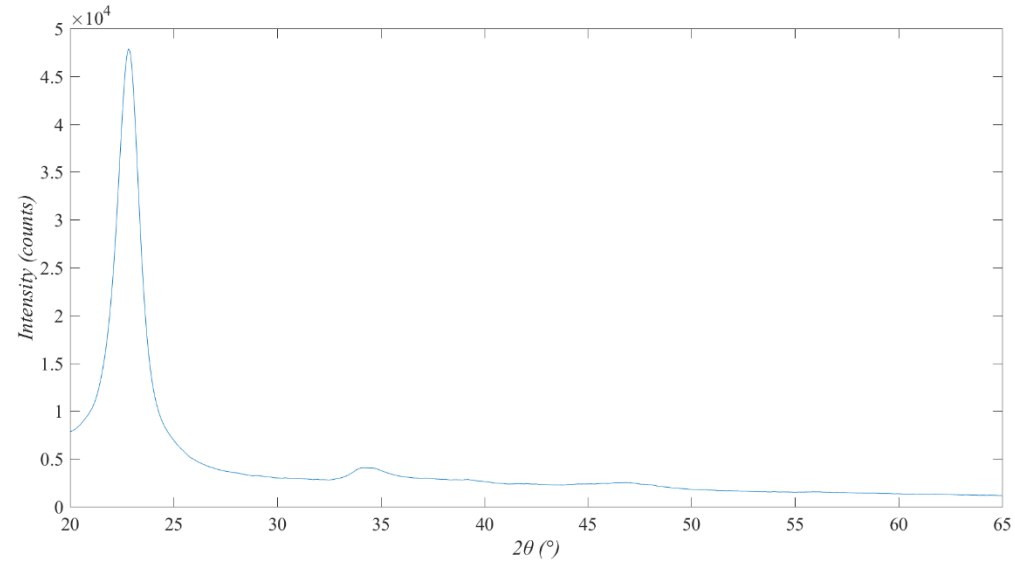

Figure 92, Blank ashless cellulose filter paper XRD spectra

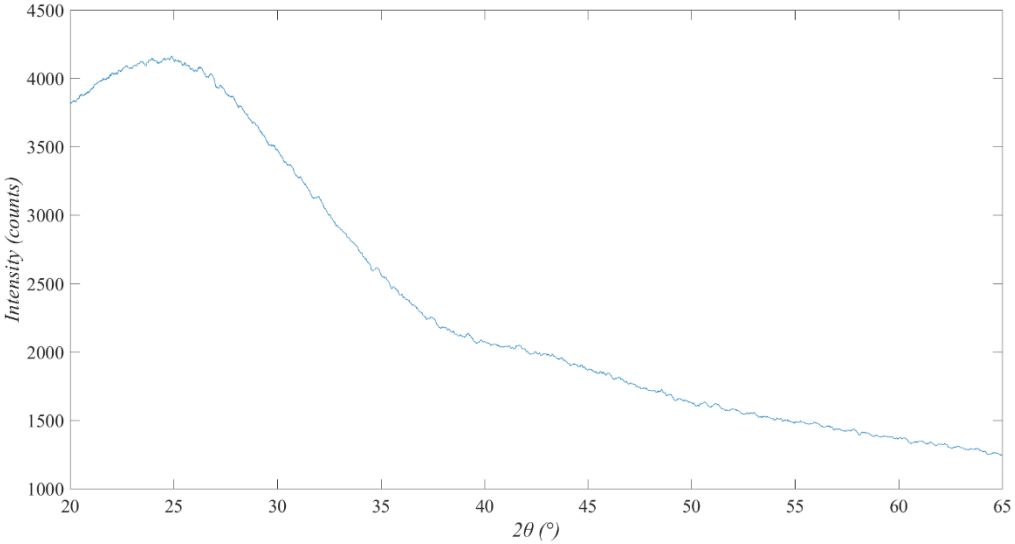

Figure 93, Blank glass microfiber filter paper XRD spectra

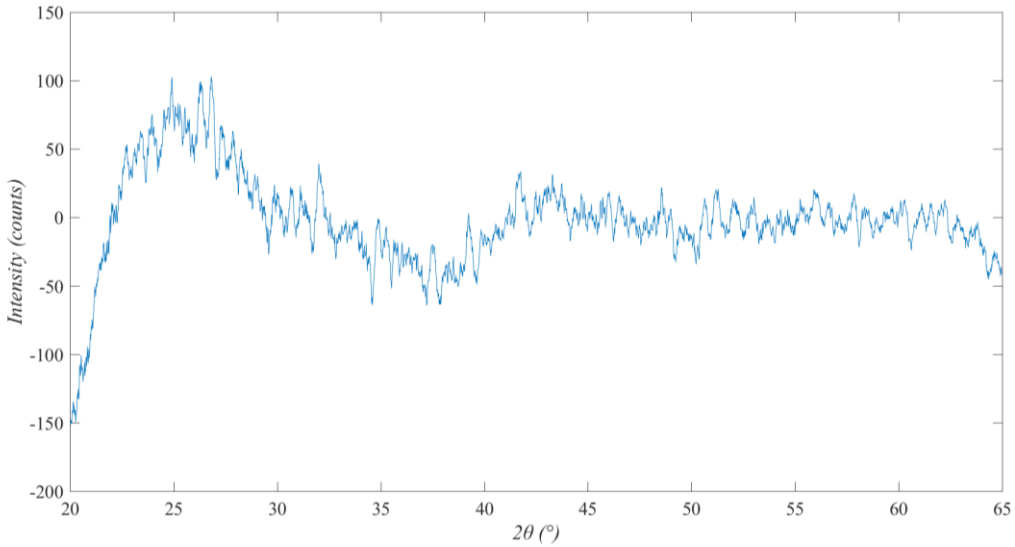

Figure 94, Blank glass microfiber filter paper XRD spectra processed using high pass filter

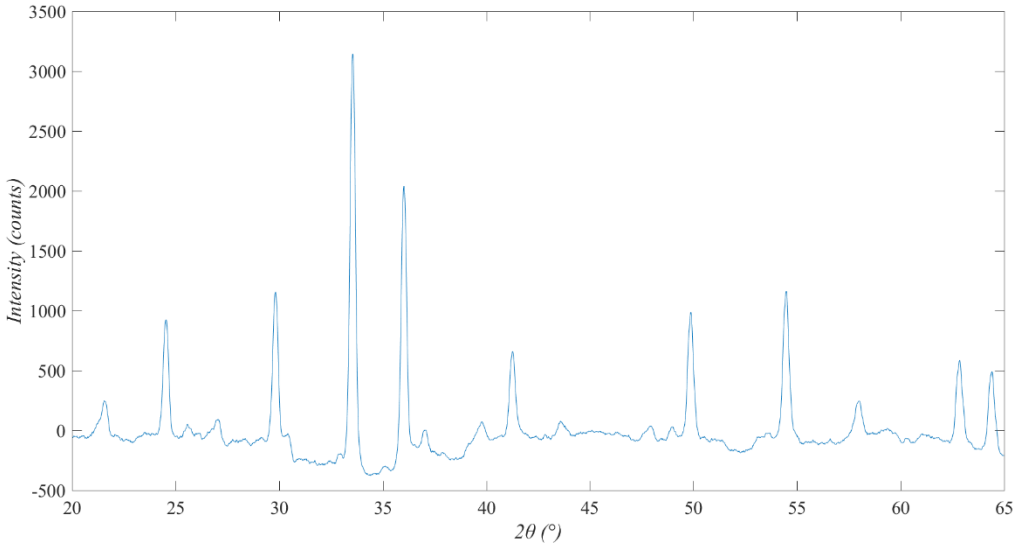

Figure 95, Haematite

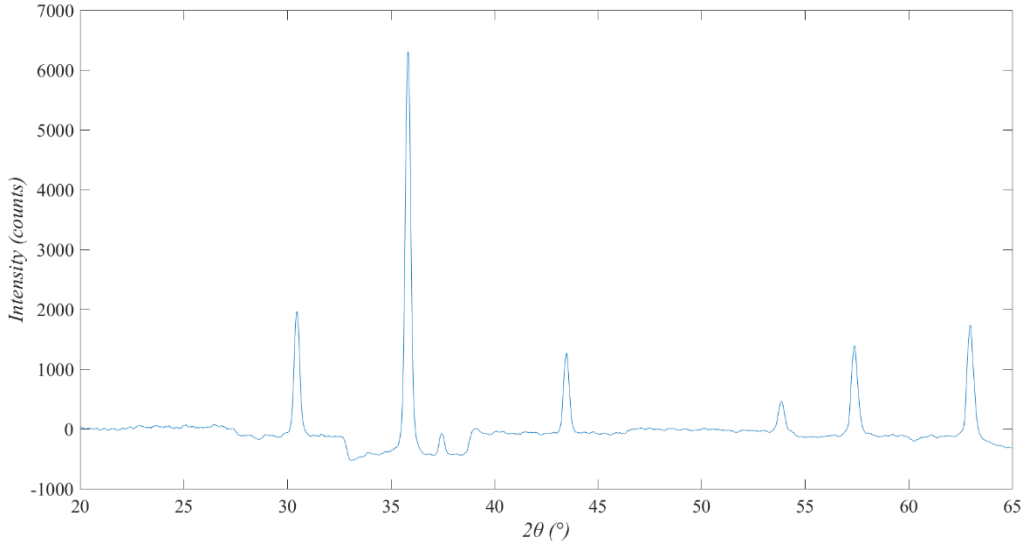

Figure 96, Magnetite

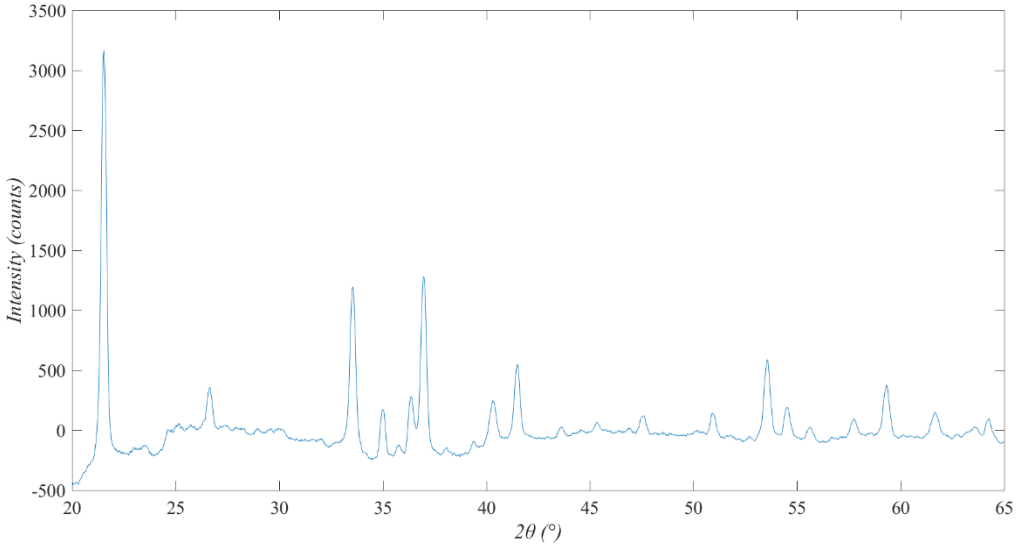

Figure 97, Goethite

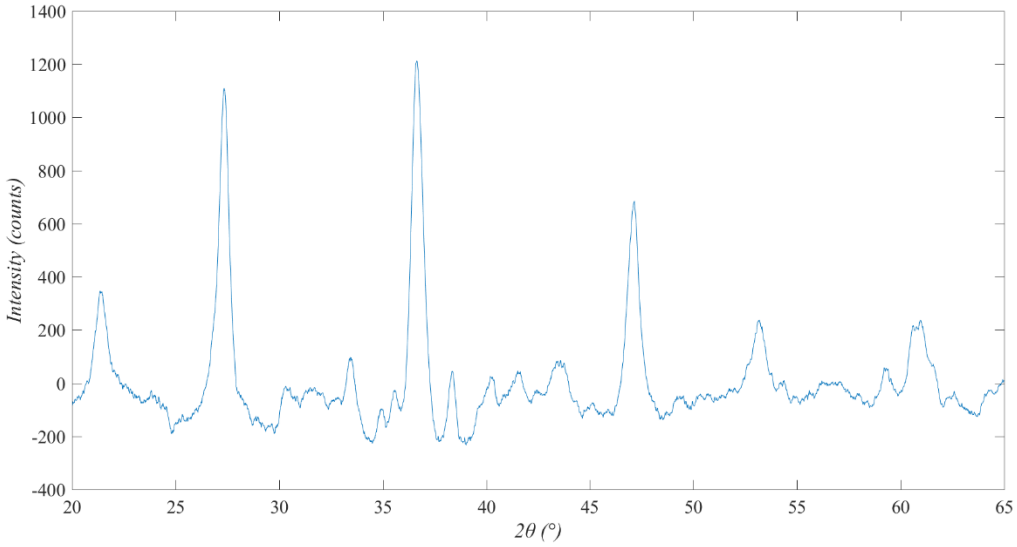

Figure 98, Lepidocrocite

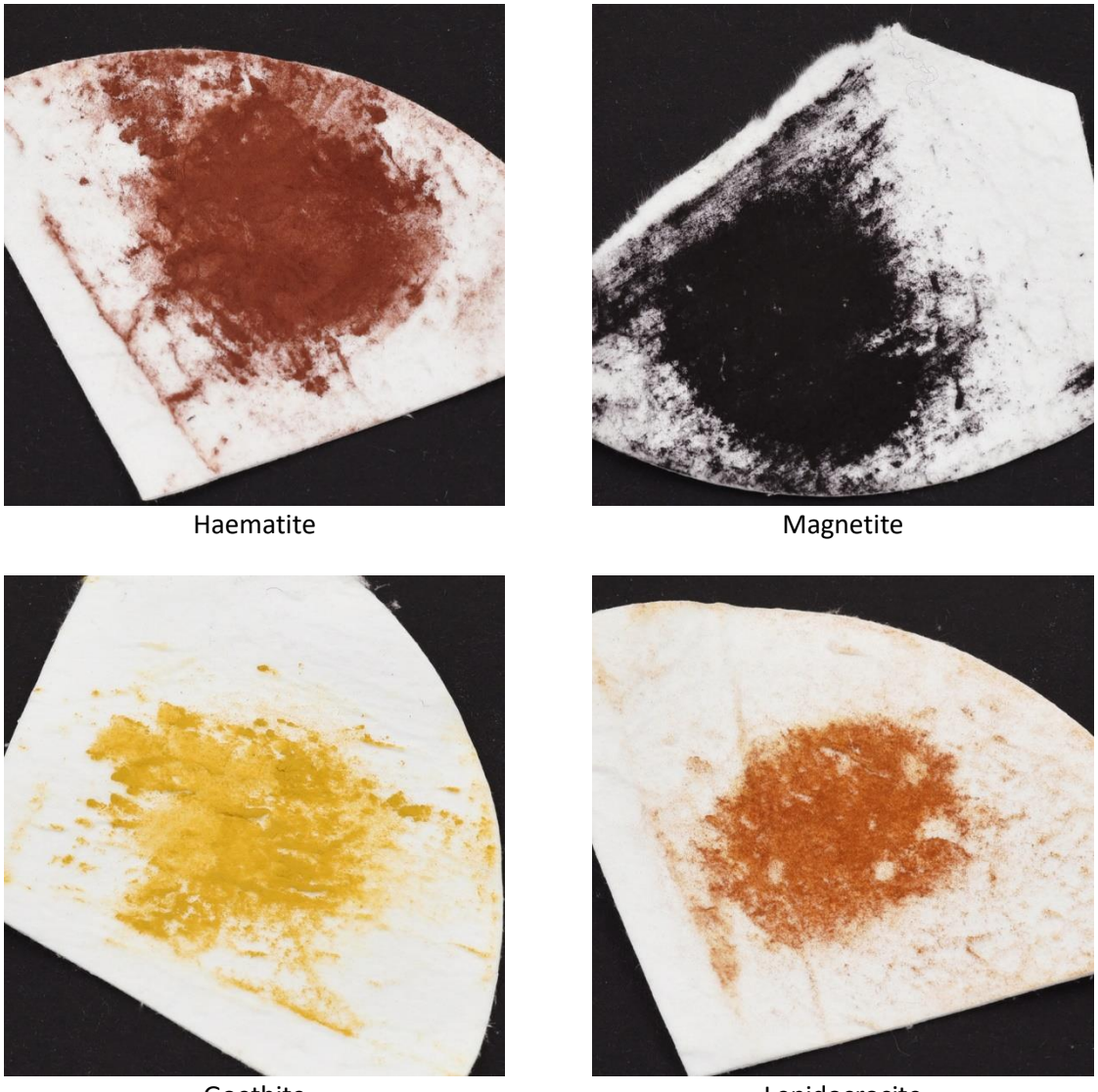

Figure 99, Photographs of control swabs

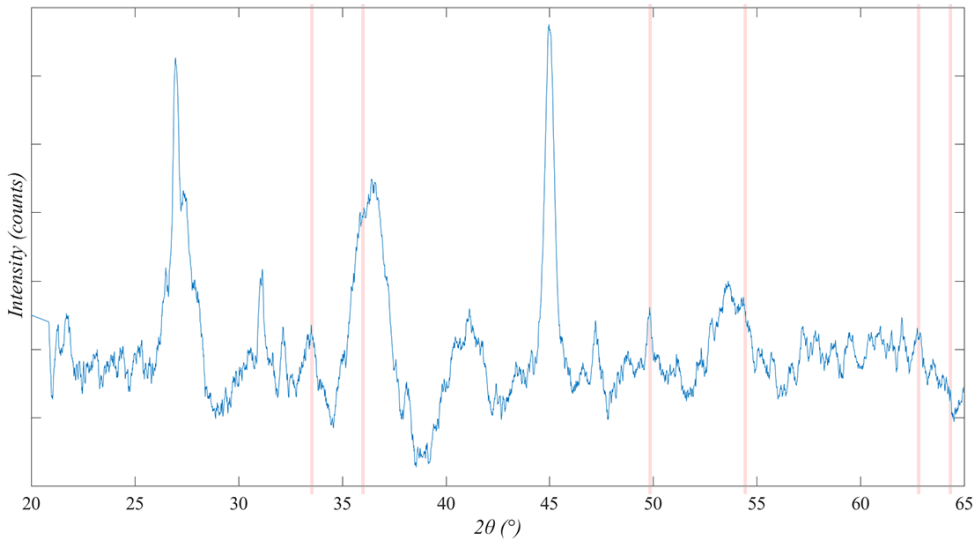

Figure 100, Example of presence of Haematite, GF3 of the QRTC loop monitoring campaign

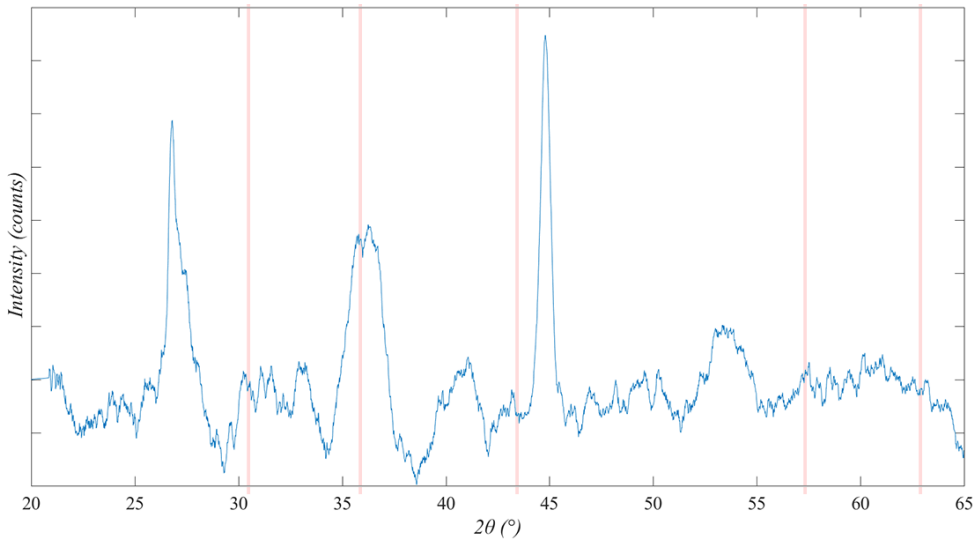

Figure 101, Example of presence of Magnetite, GF9 of the QRTC loop monitoring campaign

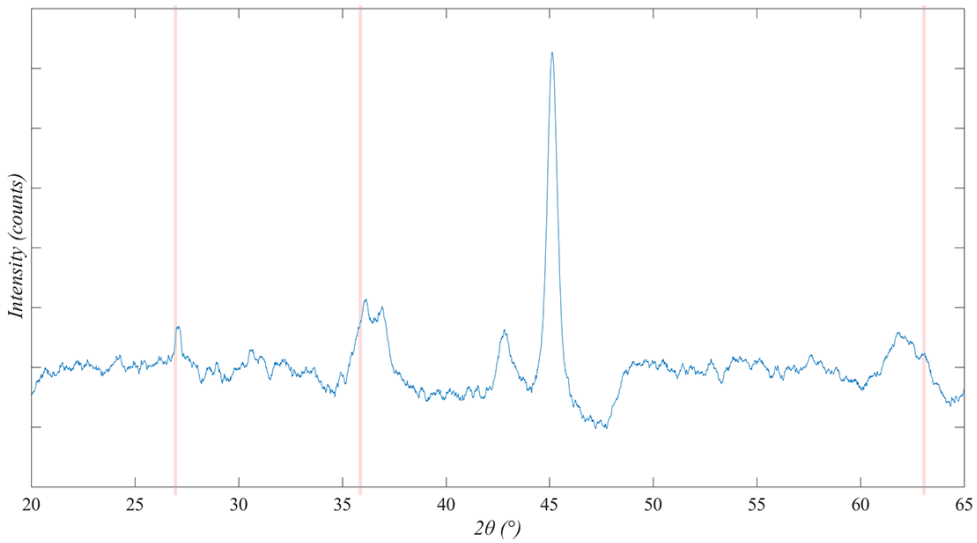

Figure 102, Example of presence of Maghemite, GF4 of the QRTC initial monitoring campaign

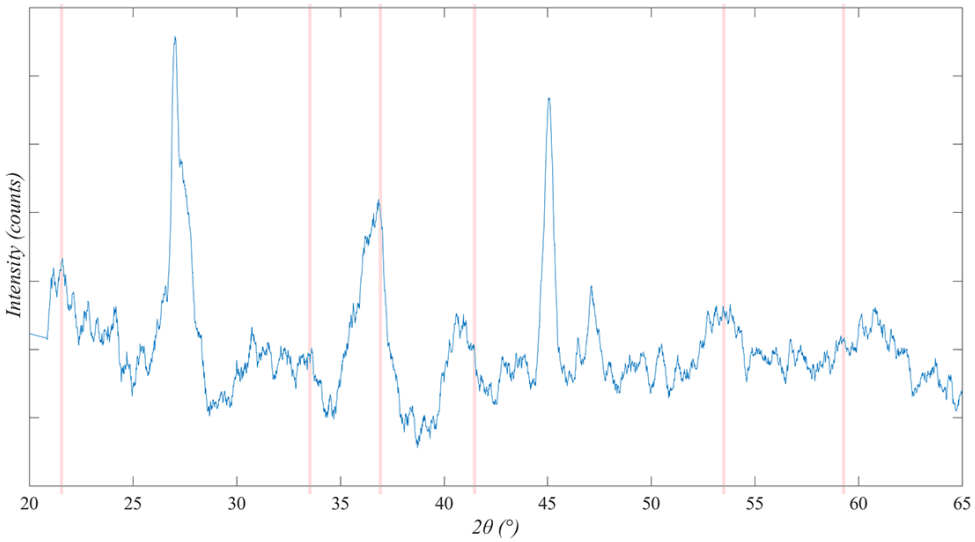

Figure 103, Example of presence of Goethite, GF2 of the QRTC loop monitoring campaign

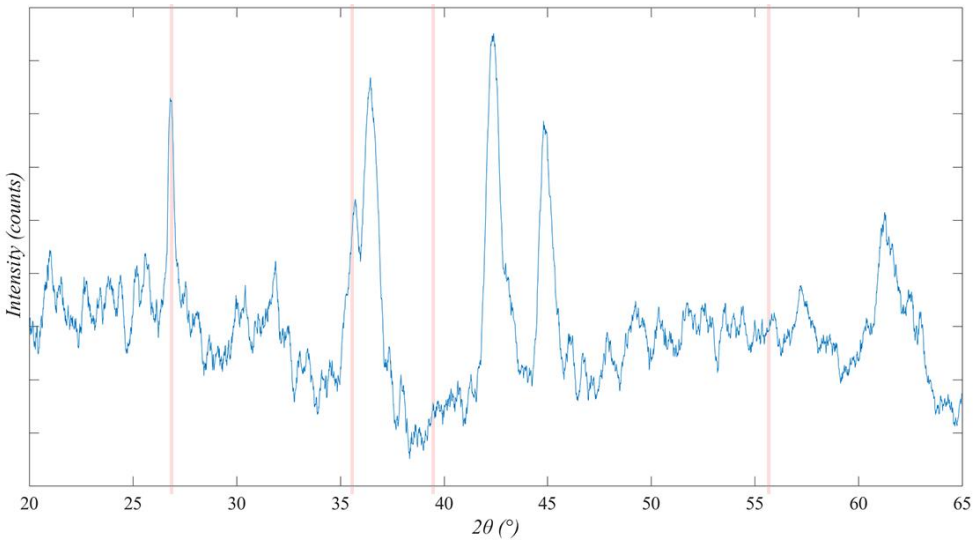

Figure 104, Example of presence of Akaganéite, GF1 of the QRTC initial monitoring campaign

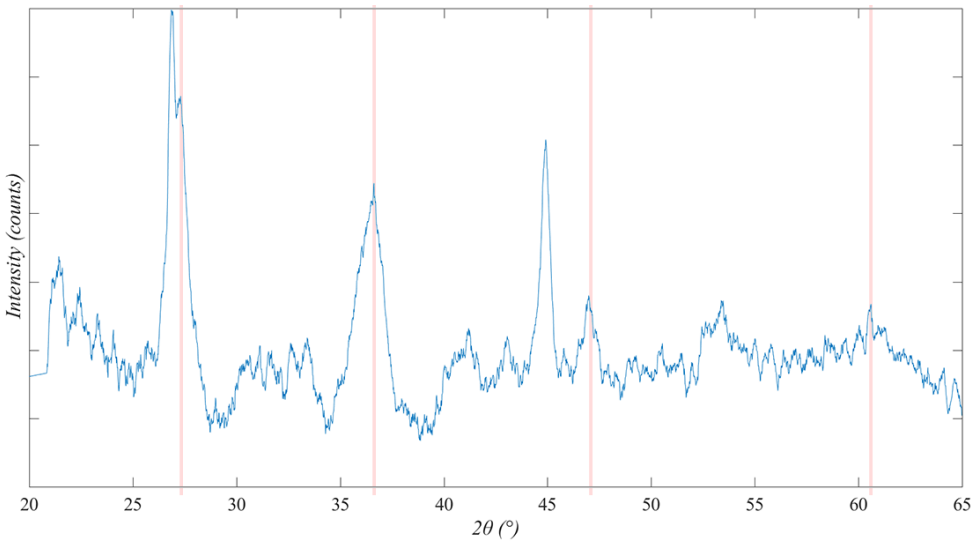

Figure 105, Example of presence of Lepidocrocite, GF7 of the QRTC loop monitoring campaign

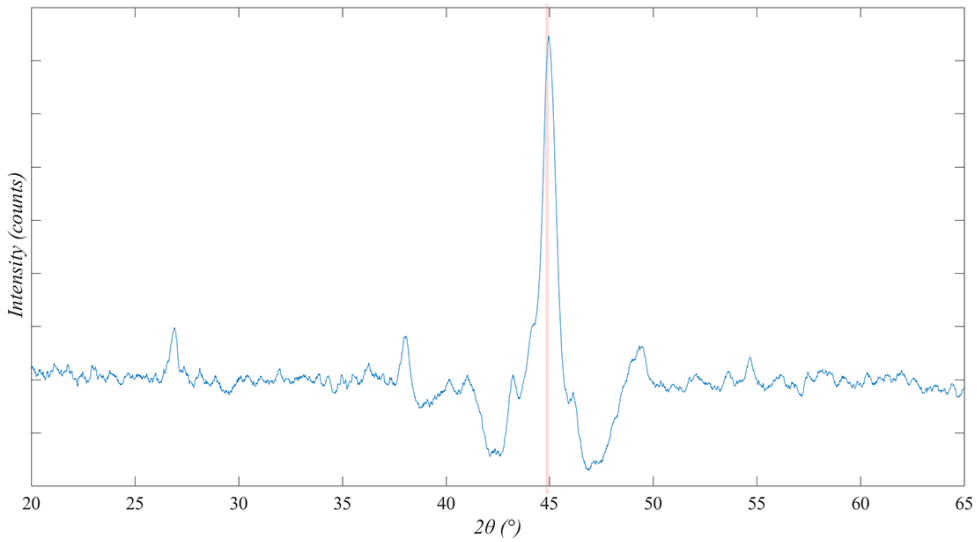

Figure 106, Example of presence of Iron, GF6 of the QRTC initial monitoring campaign

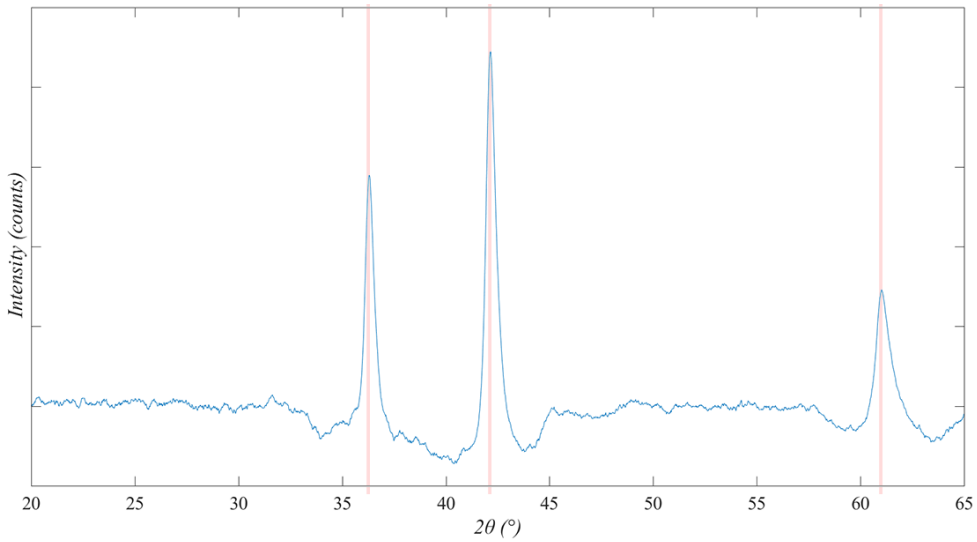

Figure 107, Example of presence of Wüstite, GF18 of the QRTC initial monitoring campaign

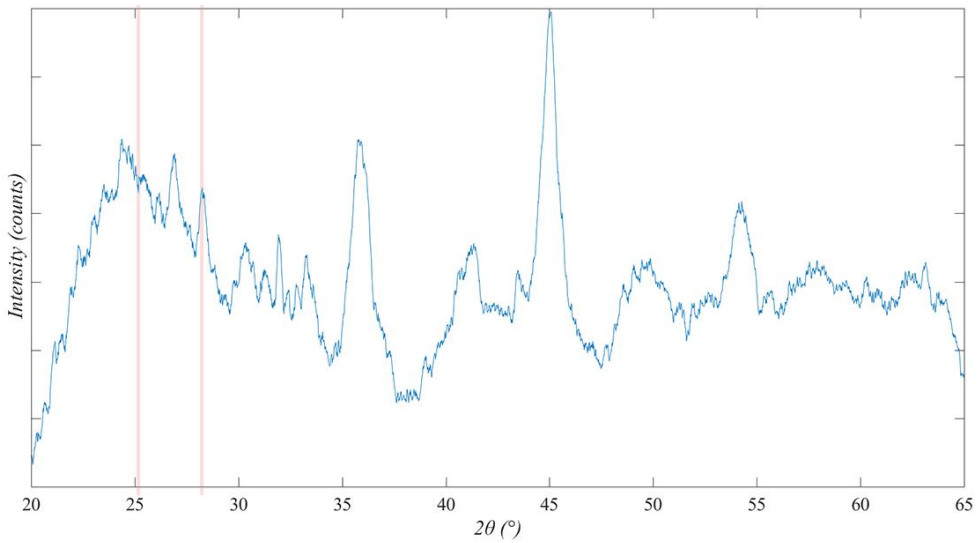

Figure 108, Example of presence of Soot, combined XRD spectra of the first British Columbia monitoring campaign


Haematite

Magnetite

Maghemite

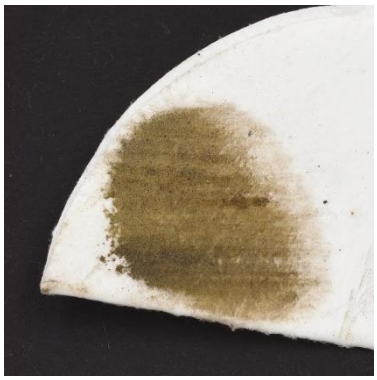
Goethite


Akaganéite


Lepidocrocite


Iron


Wüstite


Soot

Figure 109, Photographs of example swab photographs showing exemplified compound identified in the XRD spectra

6.3 QRTC October 2017

The period of track swabbing done in October 2017 was conducted in a time of changeable weather conditions as shown by the environmental monitoring, discussed in section 6.1.1. The track swabs, along with their sampling time and other relevant condition descriptions are given in Table 11. The table also outlines the compounds identified on the individual swabs from their XRD spectra.

All of the identified compounds were observed to varying extents on this swabbing campaign.

On a select few swabs, wüstite was found to be present. The presence of this oxide is unusual because the signal was very prominent in the spectra whereas in other swabs on this monitoring campaign, as well as all the other swabbing dates, this pattern was absent.

Table 11, Results of XRD analysis of track swabs taken from the initial QRTC monitoring campaign in October 2017

ID	Date (yyymmdd)	Time (UTC)	Description	Oil / Soot	Maghemite	Magnetite	Goethite	Haematite	Lepidocrocite	Akaganéite	Iron	Wüstite
GF 1	2017 1010		Straight, Top of Rail before vehicle movements with slides		m		m		y	y	y	
GF 2	2017 1010		After second run with w/s - taken in patch of slide		y	y		m		m	y	m
GF 3	2017 1010		after run and after slight onset of shower - longer braking distance		y	y	y		y			
GF 4	2017 1010		After slight rain, after run		y	y		m	y	m	y	y
GF 5	2017 1010	2pm	After lunch and before train pass	y	y	y					y	
GF 6	2017 1010		after first train pass		m	y		y	m	m	y	
GF 7	2017 1010		Before wet runs	m	y	y		m	m	m	y	
GF 8	2017 1010		After first wet run			m						y
GF 9	2017 1010		After all 5 wet runs taken in dry part of wheel slide	m							y	y
GF 10	2017 1011		Before any train movements of day		m	y	m	y		m	y	m
GF 11	2017 1011		After first run with possible wheel flat		m	y					y	y
GF 12	2017 1011		After wet run		y	y		y	m	m	y	m
GF 13	2017 1011		After 4 coasting passes		y	y	m	y	m	m	y	y
GF 16	2017 1012		Before first run of day			m					y	y
GF 17	2017 1012		Away from leaf layer / braking zone		y	y		y	y	y	y	
GF 18	2017 1012		After lunch before first track wetting								y	y

y = clear pattern identified for oxide, m = spectra patterns identified, but not clear

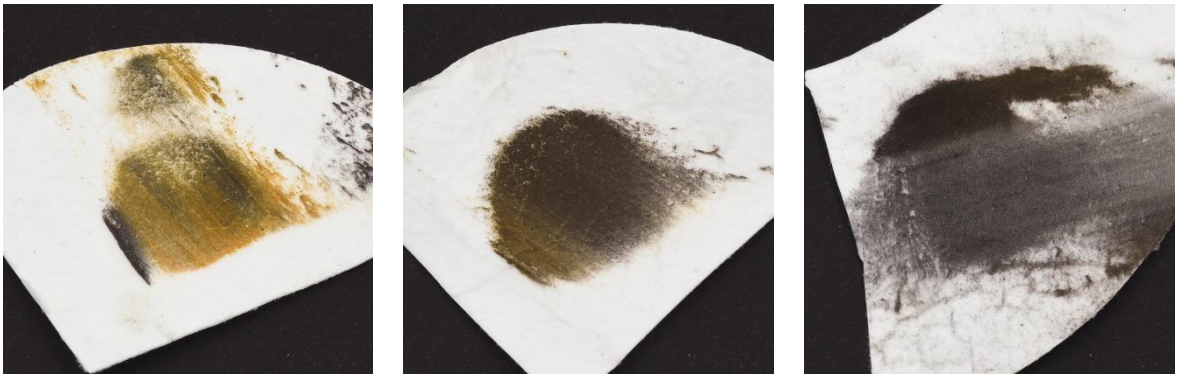

GF16 GF17 GF17

Figure 110, Photographs of track swabs taken on the 12th October 2017 when lowered traction conditions reported by the test driver

It was noted by the test driver that on the 12th October the traction conditions were particularly bad. Three swabs were taken this day the photographs of which are shown in Figure 110 and the railhead condition can be seen by the photograph in Figure 84 in the previous section. The colour of the first railhead swab appears to show two compounds, a vivid ochre orange-yellow and a dull grey. The two colours appear to have originated from the orange / brown and silver / grey oxide films on the railhead respectively. The XRD spectra of the swabs reveal that wüstite is present on the first and last swab and a great variety of oxides are present on the second, GF17, however the pattern for wüstite cannot be seen.

It is possible that the compound causing the orange / yellow colour is in not abundant enough on swab GF16 to display a strong enough fingerprint signal and allow it to be differentiated from the background noise.

This brown / orange compound may be maghemite. It is shown that magnetite decomposes over time into maghemite [136] and this may be a process going off on the railhead surface. Magnetite, being a harder material, may not have been picked up by the swab in this occasion as it might be more difficult to transfer onto the filter medium.

6.4 QRTC Loop test 20th April 2018

Sampling was conducted on the 20th April 2018 once again at the QRTC test track. Swabs were taken in five locations around the track circuit loop to explore the oxide composition at different sites around the loop. Locations of these sites are given in Figure 111; sites were chosen to represent different combinations of straight and curved track as well as covered and uncovered sections. Swabs GF6 to GF10 were taken around location A in a variety of locations on the railhead with different visual appearances to attempt to identify a wider variety of oxides that may be present on the railhead; all other swabs were taken in the running band of the railhead in patches which were visually representative of their locations.

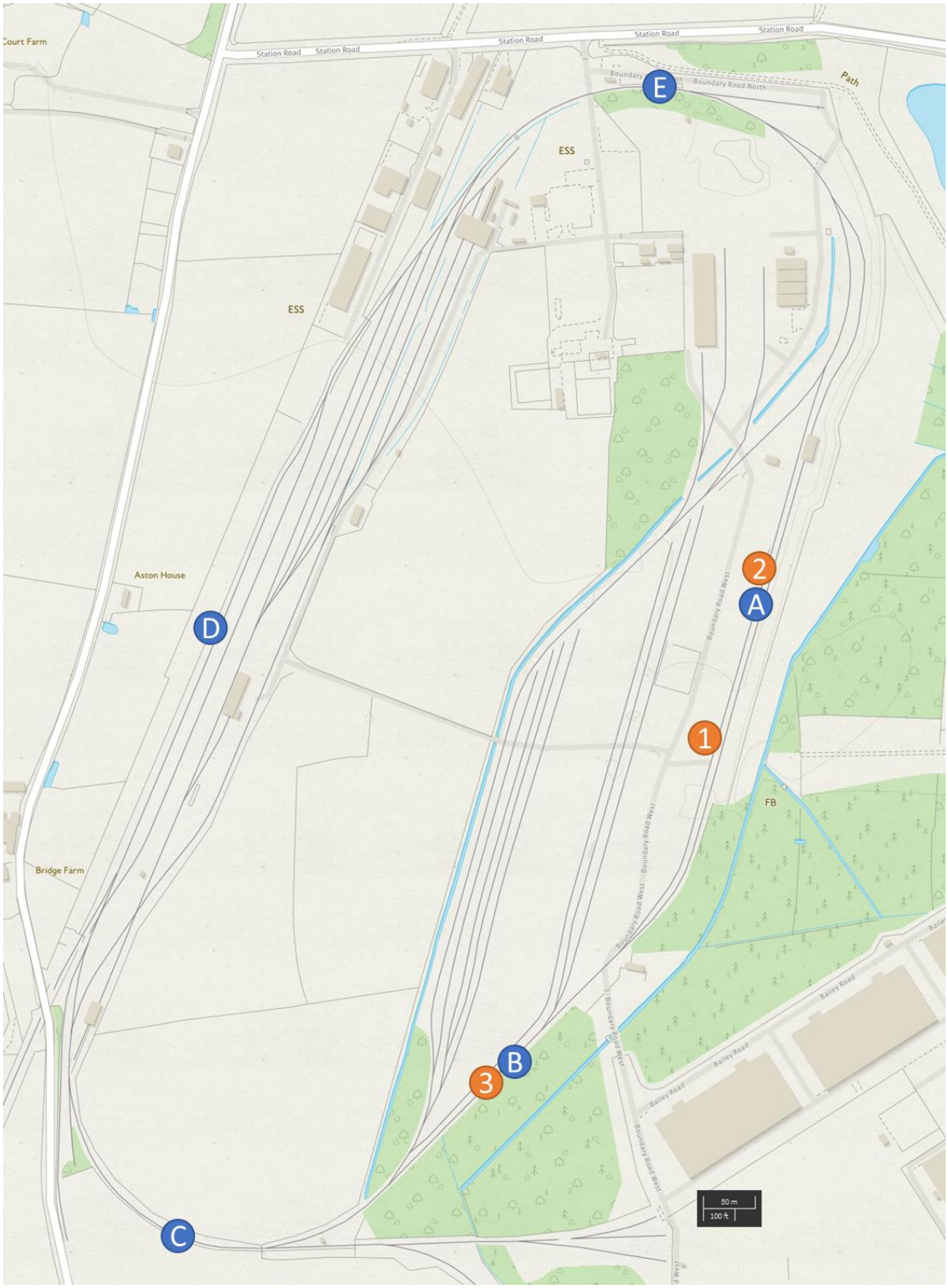

Figure 111, Map of Long Marston test track facility (QRTC test track) displaying environmental monitoring stations (orange) and swab locations (blue): A, uncovered straight section by testing area; B, straight section in tree clearing; C, uncovered curved section; D, uncovered straight section; E, curved section in tree clearing [137]

Table 12, Results of XRD analysis of track swabs taken from the QRTC loop test monitoring campaign in April 2018

ID	Date (yyymmdd)	Time (UTC)	Description	Oil / Soot	Maghemite	Magnetite	Goethite	Haematite	Lepidocrocite	Akaganéite	Iron	Wüstite
GF 1	2019 0420	1020	Before train movements, **location A**	m	m	y		m	m	y	y	
GF 2	2019 0420	1030	**location B**	m	m	m	y		y	m	y	
GF 3	2019 0420	1045	Became V. sunny before this swab, **location C**	m	y	m			m	y	y	
GF 4	2019 0420	1055	**location D**	m	m	m	y	y	y	y	y	
GF 5	2019 0420	1110	**location E**		m	m			y	y	y	
GF 6	2019 0420	1126		m	m	y	m		y	y	y	
GF 7	2019 0420	1145					y		y	y	y	
GF 8	2019 0420	1155				y	m		y	y	y	
GF 9	2019 0420	1206			m	m		m	y	m	y	
GF 10	2019 0420	1220		m	m	y		m	m	y	y	

y = clear pattern identified for oxide, m = spectra patterns identified, but not clear

The identified compounds found on the swabs is given in Table 12. A variety of compounds were observed during the sampling. On most swabs akaganéite and lepidocrocite were present. The weather conditions changed over the course of the sampling from being overcast to being clear and sunny; train movements also commenced during the sampling and as a result the conditions during each swab sampling could not be ideally controlled.

Goethite was observed in straight section B, in the tree clearing, and uncovered straight section D. It was not seen in curved sections C and E as well as section A. The appearance of this oxide in these locations may be due to the locations being neither typically used for braking or traction and sections being straight; as a result, the forces applied to the rails at these sections is minimal and may allow the build-up of oxides which are susceptible to being worn away when lateral force is applied to the rails.

6.5 Other sampling

Tracks swabs were also taken from both British Columbia in Canada during winter and summer 2018, as well as a line in Northern England in Autumn 2017.

Swabs taken for the two times in British Columbia, Canada were analysed using X-Ray diffraction and can be seen in Table 13. In comparison to the other track swabs collected, typically less material was collected on the swabs. The material retrieved from the swabs when analysed, typically showed the presence of iron oxides, such as haematite and less instances of iron oxide hydroxides were

identified. This is likely due to the dry conditions experienced at the time of swabbing resulting in a relatively clean railhead with the absence of iron oxide-hydroxide compounds.

At the start of the day in February, track swab GF01 displays the presence of more compounds showing that more compounds are more present at the start of the day.

Table 13, Results of XRD analysis of track swabs taken from British Columbia in Canada in February and April 2018

ID	Date (YYYYmmdd)	Time (UTC)	Description	Oil / Soot	Maghemite	Magnetite	Goethite	Haematite	Lepidocrocite	Akaganéite	Iron	Wüstite
GF 01	2018 0213	1050	Tangent south rail	y	y	y		y		m	y	
GF 02	2018 0213	1015	Tangent north rail									
GF 03	2018 0213		-									
GF 04	2018 0213	1145	-		m	m		m		m	y	
GF 05	2018 0213	1145	Top of Low rail, (Severe RCF)					m		m	y	
sta mp	2018 0213		Postage stamp image check									
FP 01	2018 0213	1050	Tangent south rail							m	y	
FP 04	2018 0213	1145	Top of Low rail, (Severe RCF)		y			y		m	y	
GF 09	2018 0420	945	North (high) Rail, Top of Rail			y		y				
GF 10	2018 0420	948	North (high) Rail, Gauge corner (?)		m	y		m			y	
GF 11	2018 0420	952	South (Low) Rail, Top of Rail	m		m				m	y	
FP 09	2018 0420	[094 8]	North (high) Rail, Gauge corner (?)			y		y				
FP 10	2018 0420	955	South (Low) Rail, Top of Rail	m					m		y	
FP 11	2018 0420	1505	South Rail, tangent (Top of Rail) (possible oil)	m				y			m	
GF 14	2018 0620	1405			m			m		m		
GF 15	2018 0620	1420			m			y				
GF 16	2018 0620	1430										
FP 12	2018 0620	1400			m					m	y	

y = clear pattern identified for oxide, m = spectra patterns identified, but not clear

Photographs of the track swabs taken in autumn in the tree clearing are shown in Figure 112. The track at the time was heavily contaminated with leaf matter and the photographs show the resultant track swabs. Swabs a and b display a light silver ochre colour which may be the initial formation stages of leaf layers and swab c gives a darker, more resinous pattern which is similar in appearance to fully formed leaf layers.

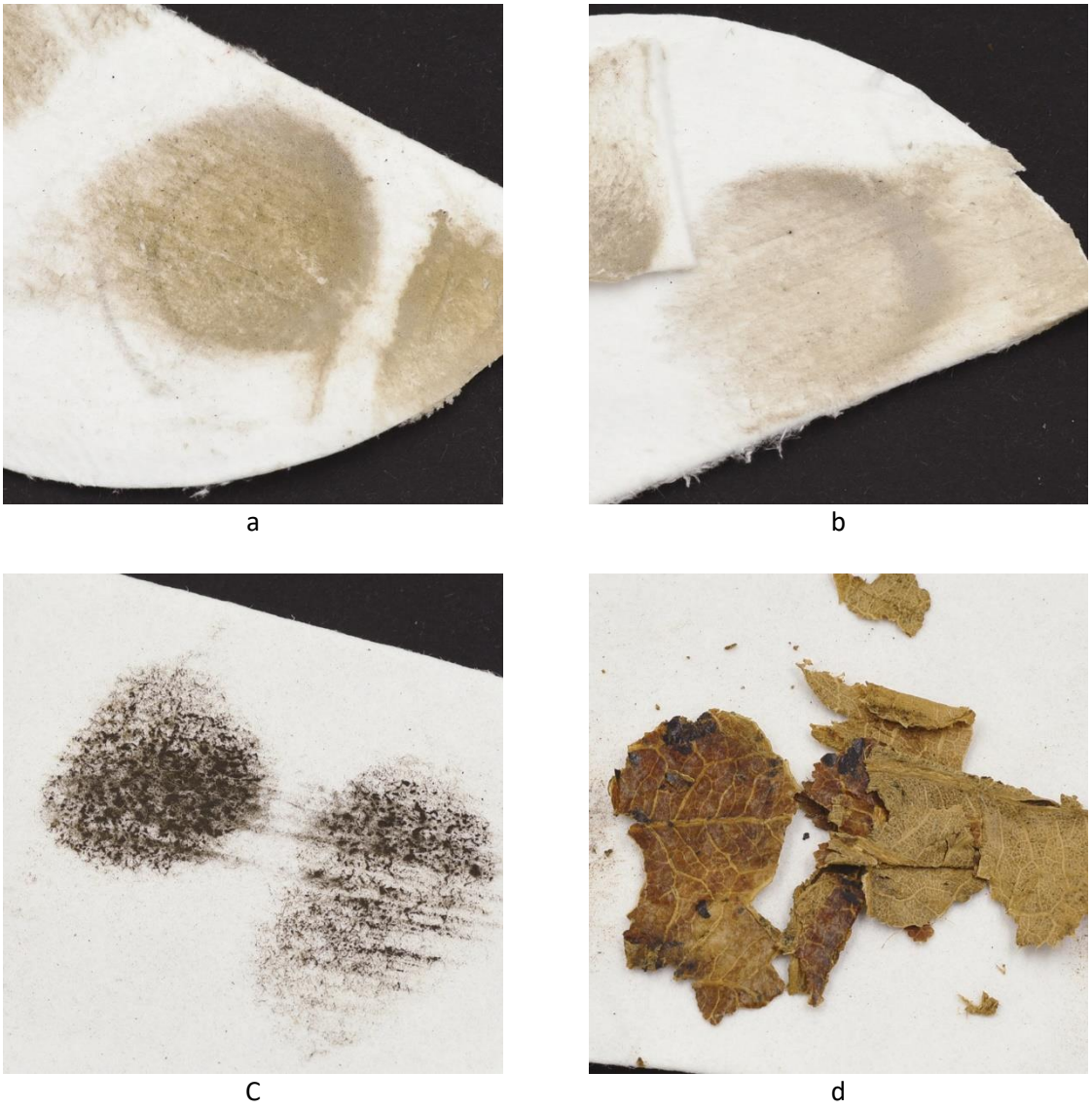

Figure 112, Track swabs taken from the line in Northern England near Bridge 194 in 2017 including photographs of bulk leaf material extracted from the track surface

6.6 Summary

The importance and effectiveness of the environmental monitoring stations designed for this project has been shown from the results. Clear daily relationships and variations in conditions have been identified from the work; in particular the thermal lag of the railhead temperature behind that of the environment and the resulting fall of the railhead temperature below the dew point. The occurrence of this phenomena by time of the day is shown to strongly correlate with reported incidents of low adhesion reported by train operating companies.

The environmental monitors have also shown the very strong influence of the very local features of the trackside to the conditions experienced by the railhead including the influence of structures which shade the track as well as vegetation effecting local humidity levels.

Surface analysis of the track swabs has identified nine compounds through X-Ray diffraction. The chemical make-up of the railhead surface was shown to vary considerably between location to location, times and seasons.

The environmental conditions and compounds present on the railhead are shown to effect the visual appearance of the swabs taken. Other compounds present on the railhead which could not be identified from X-Ray diffractometry of the track swabs may be identified visually from the swabs.

Wüstite was discovered during a period and location where the driver of a locomotive exclaimed that traction conditions were low. Clear, strong signals of this compound were given in the swab spectra whereas during other sampling campaigns the signal for this compound was completely absent. The appearance of Wüstite at this time suggests that this compounds is either responsible for the low adhesion conditions, or an intermediate chemical species in the stages leading to low adhesion conditions.

Iron oxide-hydroxides were identified on the railhead swab spectra primarily in wet and humid conditions such as those taken at QRTC. Swabs taken from British Columbia in which the conditions at the time were very dry show very little presence of the iron-oxide hydroxide components, but still display the presence of iron oxide components such as haematite and magnetite (but not wüstite). In these conditions very little material was able to be sampled from the railhead onto the track swabs indicating a very clean railhead condition.

Chemical conditions have been shown to vary along the railhead in a very short distance and with different trackside features in the QRTC loop sampling campaign; however not enough control over the sampling was possible during this study to clearly display the effect on chemical make-up of the railhead surface of the very localised features of the trackside.

To the knowledge of the author, this is the first time that study has been performed to investigate relationships between trackside features, locations, environmental conditions and the chemical composition of the railhead surface and has brought about some interesting insight into the importance of railhead chemistry to the physical operating conditions of the railways; however, only a limited sample set of the examples explored within the scope of this work and a greater amount of monitoring work would be helpful to verify the findings of the work as well as explore further complex environmental, chemical, physical and tribological relationships.

7 Synthesis and rheological properties of iron oxides

Iron, as a transition metal, may take on many oxidation states. This property of the metal contributes towards its ability to take on many forms with limited additional elements. As was seen in section 6.2, many different inorganic compounds were identified on the surface of the railhead.

This chapter explores some chemical and physical properties of these oxide compounds. It also examines oxidation of the surface of rail steel in controlled conditions to observe their formation.

For simplicity, and to allow for greater control over the synthesis of oxide on the surface of the railhead, the only substance introduced to rail material in this testing was distilled water which was either sprayed directly onto the surface of the specimens or through induced condensation.

7.1 Oxide synthesis

An initial crude oxide synthesis was performed to determine the extremes of oxide synthesis and identify some compounds formed as a result.

The control offered by the initial oxide synthesis programme was lacking due to uneven conditions within the environment chamber of the ultrasonic humidifier. A more controlled approach to the oxide synthesis was devised using humidity chambers of saturated salt solutions to control the relative humidity as well as different temperatures. Conditions were cycled through to achieve the desired treatment. The overview of this treatment regime is given in section 5.2.1 of this thesis.

A final treatment program was undertaken to explore the effects of cycling the treatment conditions B and C (dew and drizzle).

7.1.1 Initial synthesis

An initial oxide synthesis programme was performed in an ultrasonic humidifier which produced a fine mist of water droplets along with an environment of 100% relative humidity. Rail steel samples were placed in this environment for 4 days to generate a visible level of surface oxidation showing small scattered patterns of oxide no bigger than 1mm across. Heavier oxidation was achieved by 7 days in the environmental chamber. Results of this surface treatment can be seen in Figure 113.

Freshly ground surface | 4 days treatment | 7 days treatment

Figure 113, Images of sample surfaces after initial treatment program in ultrasonic humidifier

The freshly ground surface contains no visible oxidation. It's XRD spectra can be seen in Figure 114, from this we can see the clear peaks for iron around 45° and 65° two clear peaks for iron carbide can also be seen at around 38° and 48°; these peaks are from cementite in the ferrite / cementite pearlitic structure of railhead steel. A third peak, present at 43° suggests the presence of magnetite and some degree of oxidation of the suface.

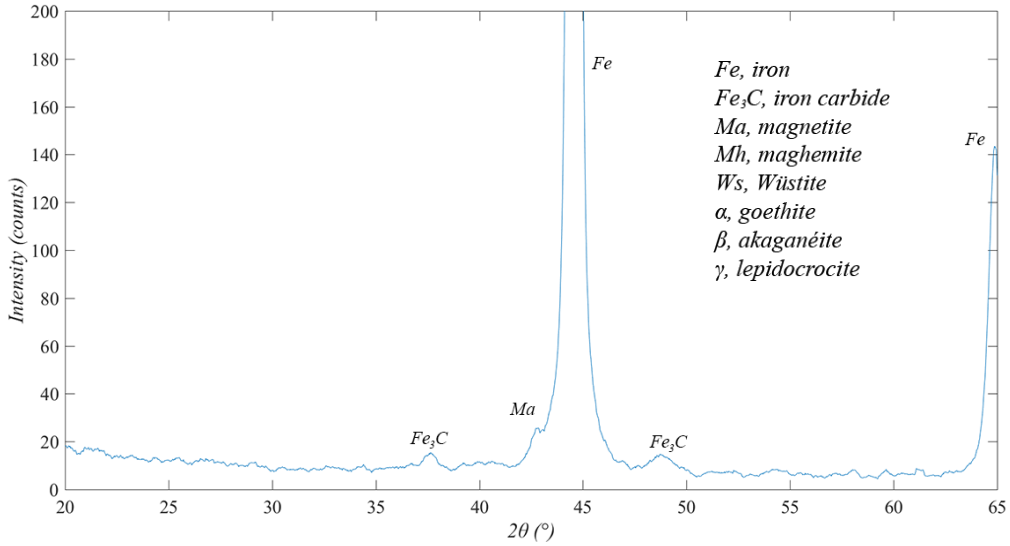

Figure 114, XRD spectra of freshly ground rail material surface

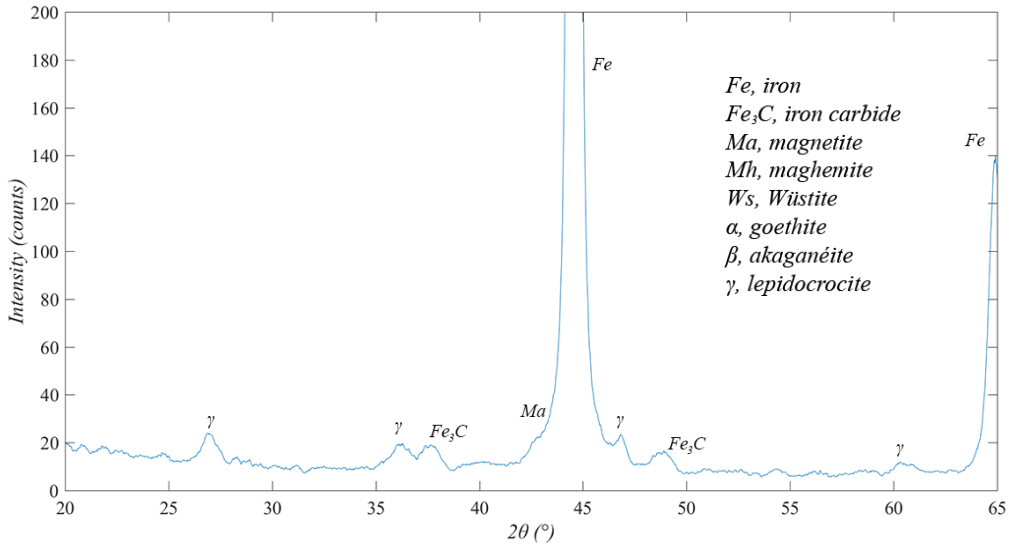

Figure 115, XRD spectra of 4 days surface treatment of rail material

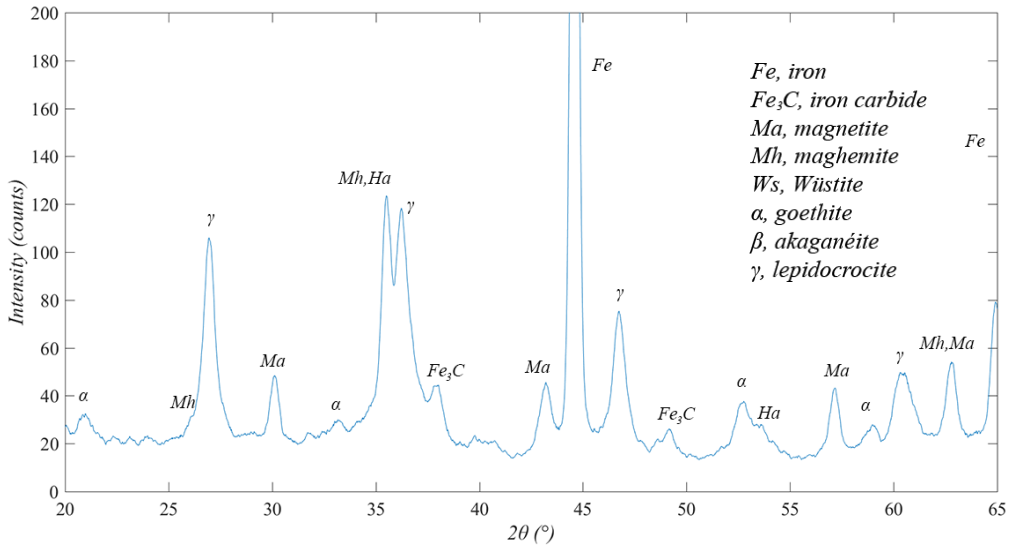

Figure 116, XRD spectra of 7 days surface treatment of rail material surface

After 4 days of treatment, visible patches of oxidation less than 0.5mm across cover the surface the specimen; the XRD spectra for this sample can be seen in Figure 115. The spectra displayed the presence of the same compounds as the freshly ground surface, but also displayed peaks around 27, 36 and 61° which correspond to lepidocrocite. As this is an iron oxide-hydroxide, this indicates that there has been further oxidation of the surface due to the influence of water.

After 7 days, large patches of oxide, greater than 5mm in diameter can be seen covering the surface. It is easier to distinguish different shades of orange and brown in the oxide, however these were also present in the 4-day treatment samples. The XRD spectra for this surface can be seen in Figure 116 and show the presence of a greater variety of compounds than the less oxidised surfaces. The signal from the iron substrate is much lower due to the build-up of other compounds on the surface attenuating x-rays before reaching the base material. In this spectrum, peaks corresponding to haematite, maghemite and the iron-oxide hydroxide, goethite, are present in addition to those discovered in the less treated surfaces. The signal for lepidocrocite is also far more intense on this sample.

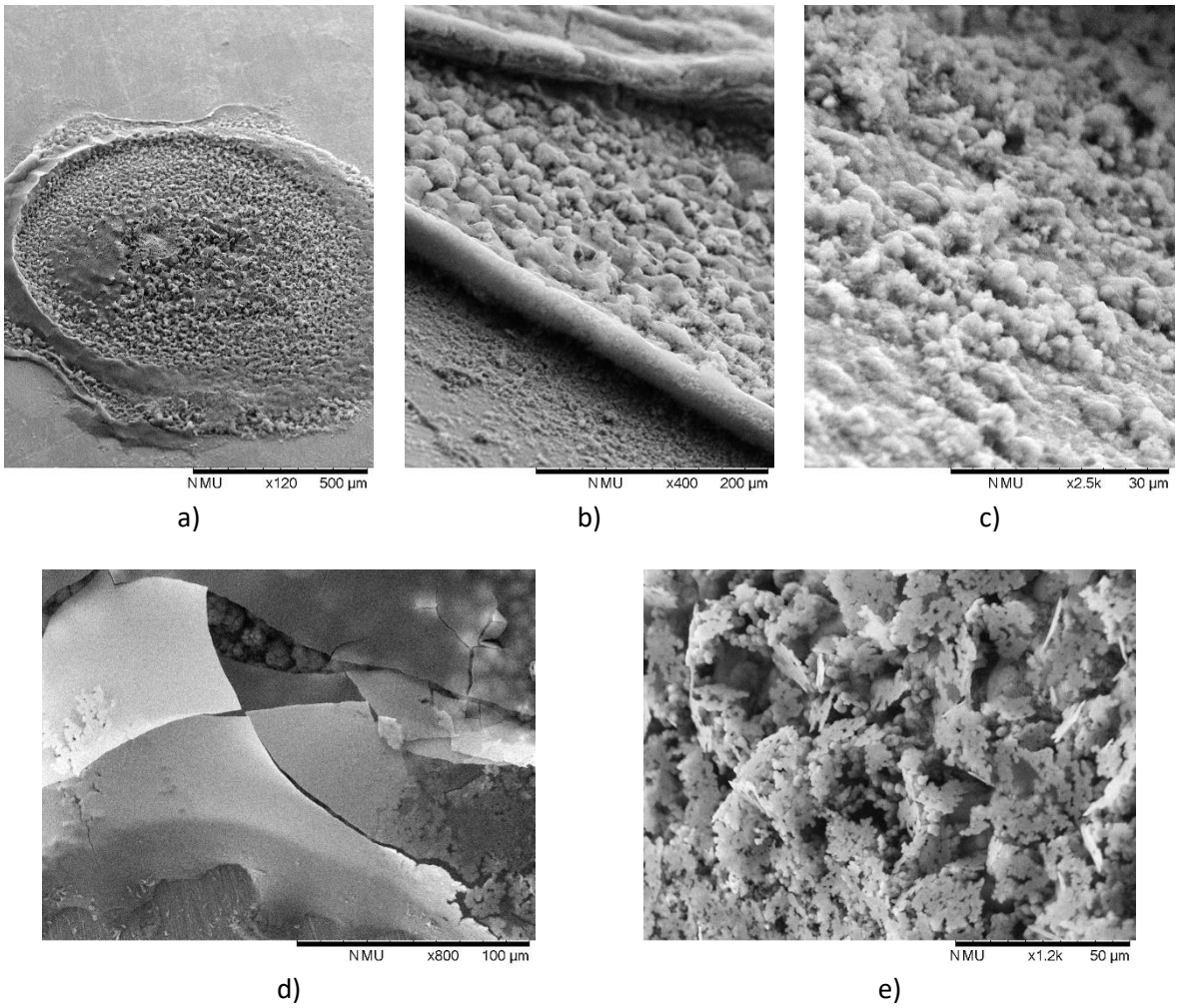

Figure 117, Microscopic structures of oxidised railhead surface. a, overview of patch of oxidation; b, edge of patch of oxidation; c, oxidation present outside main patches of oxidation; d, plate-like structure close to edges of main patches of oxidation; e, loose structure present in centre of patches of oxidation

Scanning electron micrographs were taken of the samples with the 4- and 7-day treatments to determine the features of the oxidation patches; these are presented in Figure 117. The oxide patch structures shown in a) were observed to be of sizes varying from 0.1mm to centimetres across.

Figure 117 b) shows the edge of an oxidised area. At the bottom of the micrograph, material is seen on the surface of the substrate outside of the main oxidised areas and an example of this material more magnified is given in image c).

Inside the main patches of oxidation, a fragile thin film roughly half a micron in thickness appears to be present in the location where water droplets contacted with the air; this is shown in Figure 117 d). The presence of this film may be due to dissolved ferrous (2+) ions reacting at the surface of the droplet to form an insoluble crystalline compound; this compound is likely to be iron (II) hydroxide (ferrous hydroxide) or lepidocrocite [138] due to the reaction with hydroxide ions formed at the air/water interface as shown in reaction equation M. Due to the low solubility of ferric (3+) ions, the initial layer is unlikely to be iron (III) hydroxide (ferric hydroxide).

$$Fe^{2+} + OH^- \leftrightarrow Fe(OH)_2 + 2H^+ \qquad [P]$$

Figure 117 e) shows the centre of a main oxide patch. The film described in the previous paragraph appears to have collapsed inwards and lost its uniform surface. This may be due to insufficient mechanical structure strength when a supporting body of water dries out and / or the film reacts further producing other compounds. Possible reactions include the oxidation of ferrous hydroxide to ferric hydroxide (given in reaction equation O) and subsequent dehydration to iron oxide hydroxides and other compounds as outlined in equations F to H in section 3.1.1.

$$Fe(OH)_2 + OH^- \leftrightarrow Fe(OH)_3 + e^- \qquad [Q]$$

Figure 118 shows the SEM micrographs taken of the surface underneath the film, in the centre of the oxide patches. In these images, a variety of crystal morphologies are displayed which are characteristic of compounds such as goethite (left image); however, much of the surface appeared to display a mixture of shapes with no defining geometric features.

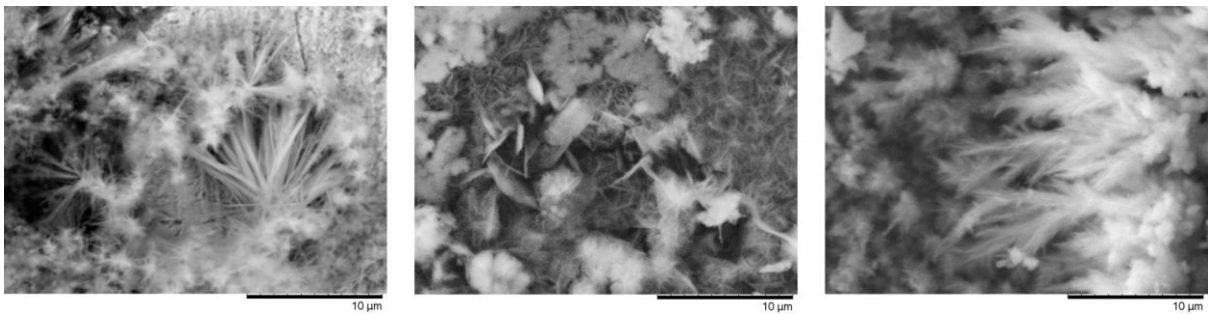

Figure 118, SEM micrographs of oxides formed in the centre of oxide patches showing needle like (left), plate like (centre) and branched / irregular (right) shaped crystal morphologies; comparisons made with a study by Antunes et al. [139]

7.1.2 Different treatments

A new set of samples were cut from railhead steel to allow for a greater surface for testing and XRD analysis. The first of the oxide synthesis programs explored was a selection of treatments as outlined in Table 10 of methodology section 5.2.1 . These are to simulate a dry control, dew, drizzle, a combination of dew and drizzle, and a flooded surface.

Figure 119 shows pictures taken of examples of each of the surfaces with the corresponding applied treatments. The appearance of oxidation on the samples increases with exposure to greater amounts of water. The sample treated with both dew and drizzle displays larger patches of oxide which are more isolated from one another with sections of bare metal surface between; these 'clean' sections between the patches of oxide appear to be larger than those seen on the drizzle only sample. This may be caused by the very small patches of oxide initially formed on the surface

directing the droplets of water into larger patches in contrast to the initial surface which accepted a more homogeneous distribution of oxide over its surface.

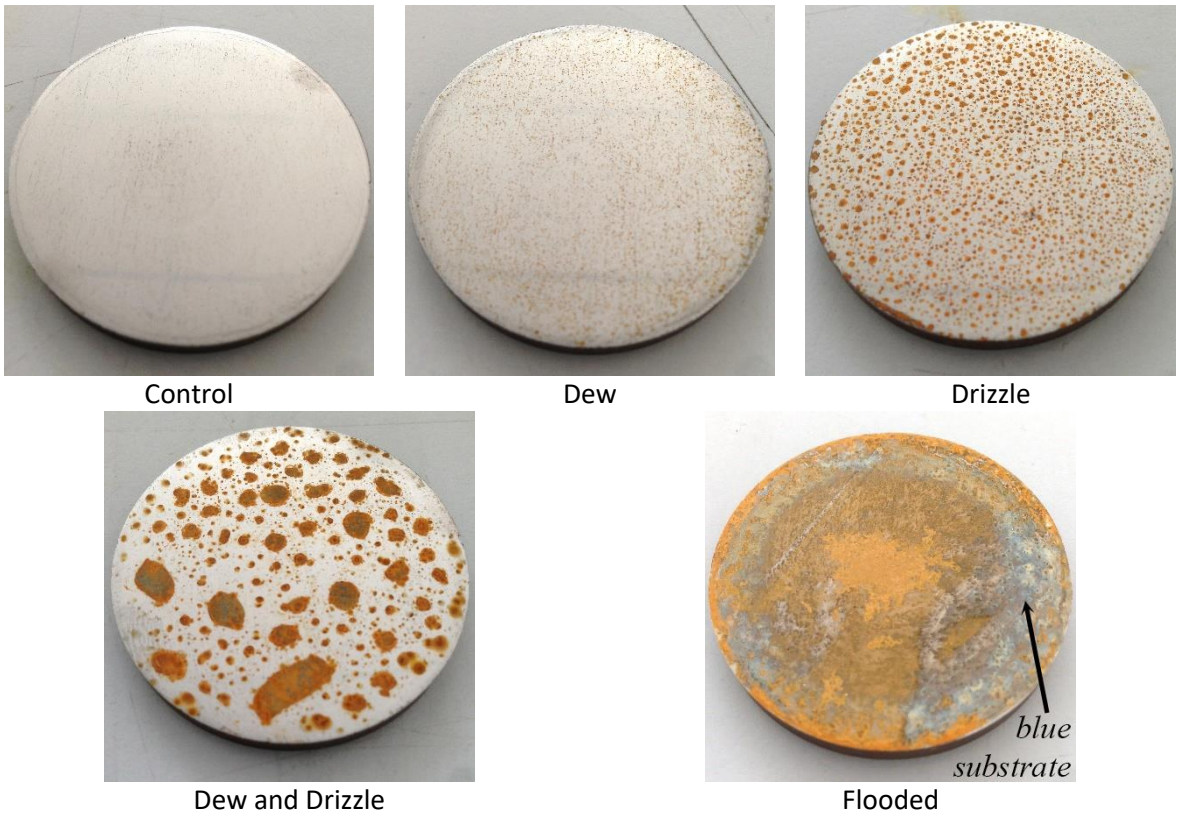

Figure 119, Photographs of rail steel substrate sample surfaces subject to various treatments

The flooded contact in Figure 119 shows a discoloured blue metal substrate surface. This may be caused due to the formation of thin layers of magnetite on the surface diffracting the reflected light. The steel substrate also does not appear to have large patches such as those on the sample with dew and drizzle treatment; after testing and the loose oxide on the surface was removed, the surface was observed to be consistent over the full surface. A loose orange oxide is present on this surface after treatment.

XRD analysis of the control sample shown in Figure 120 reveals the same pattern as seen in the previous control sample: presence of iron carbide and magnetite in addition to the iron peaks.

Figure 121 gives the XRD spectra of a surface after the dew treatment. In addition to that of the control, akaganéite and lepidocrocite are observed. The signals for the iron oxide-hydroxides at this point are weak but present.

Figure 122, the XRD spectra of a sample having undergone the drizzle treatment, displays much stronger peaks. A strong signal for lepidocrocite has emerged as well as trace signals for the other oxides, goethite and akaganéite. A peak corresponding to haematite is also observed.

Samples treated by both flooded treatment and mixed dew and drizzle treatments displayed almost identical XRD spectra, shown in Figure 124 and Figure 123 respectively. The peaks for akaganéite were no longer distinguishable; however, very strong peaks for the iron oxide-hydroxides goethite and lepidocrocite were still present. Magnetite and maghemite were much more more prominent in samples that underwent these treatments. This may be due to a conversion reaction between the iron oxide-hydroxides, ferrous ions and hydroxide in the droplets which precipitates magnetite.

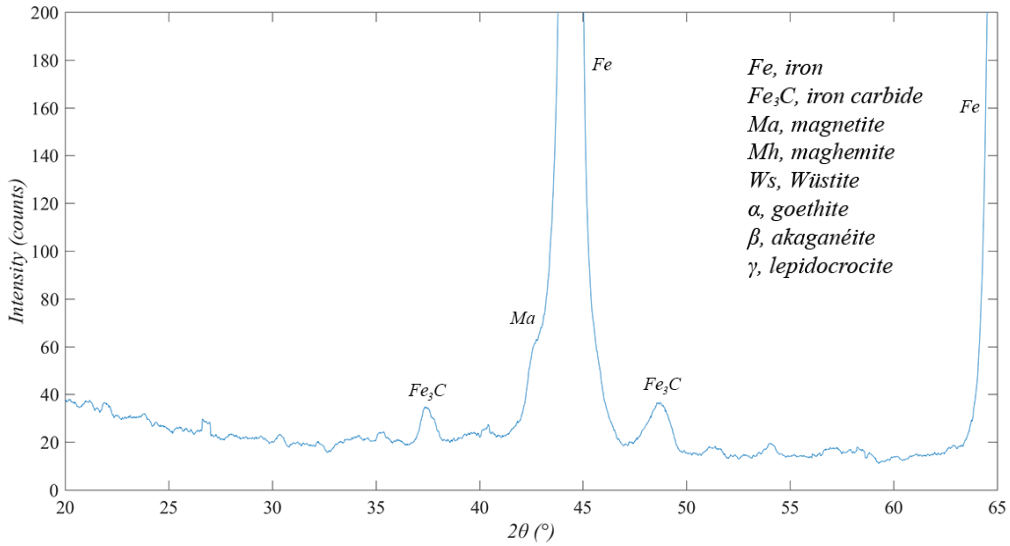

Figure 120, XRD spectra of control sample surface

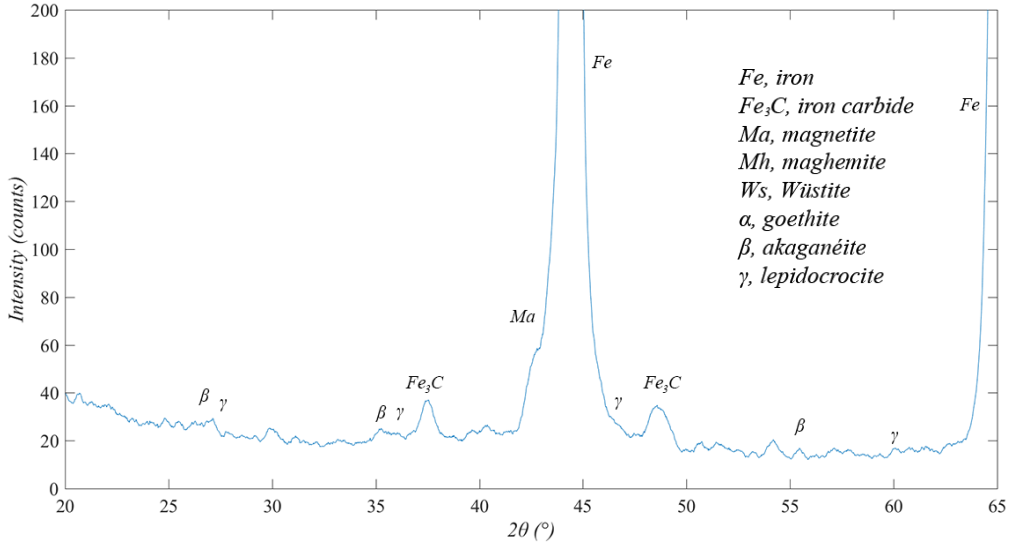

Figure 121, XRD spectra of dew sample surface

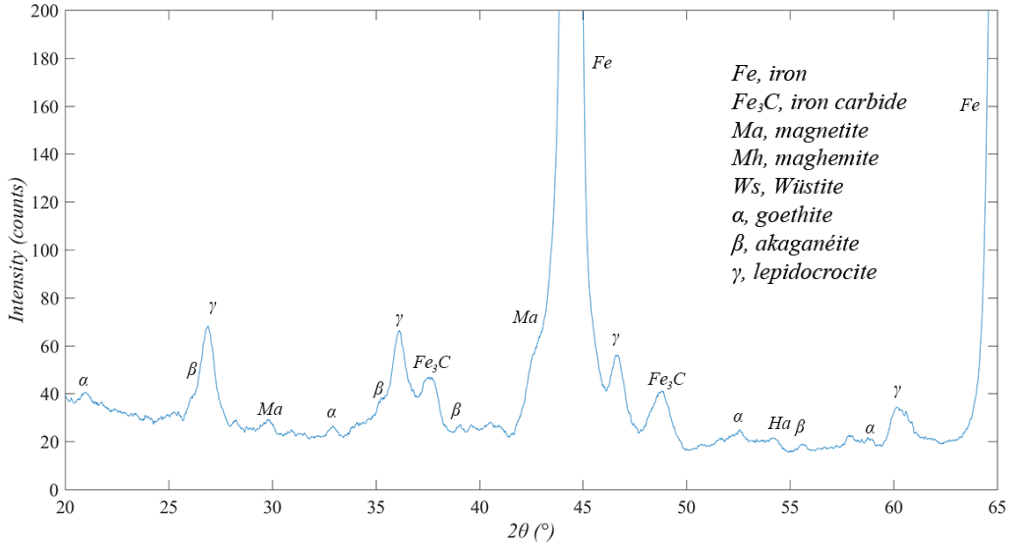

Figure 122, XRD of drizzle sample surface

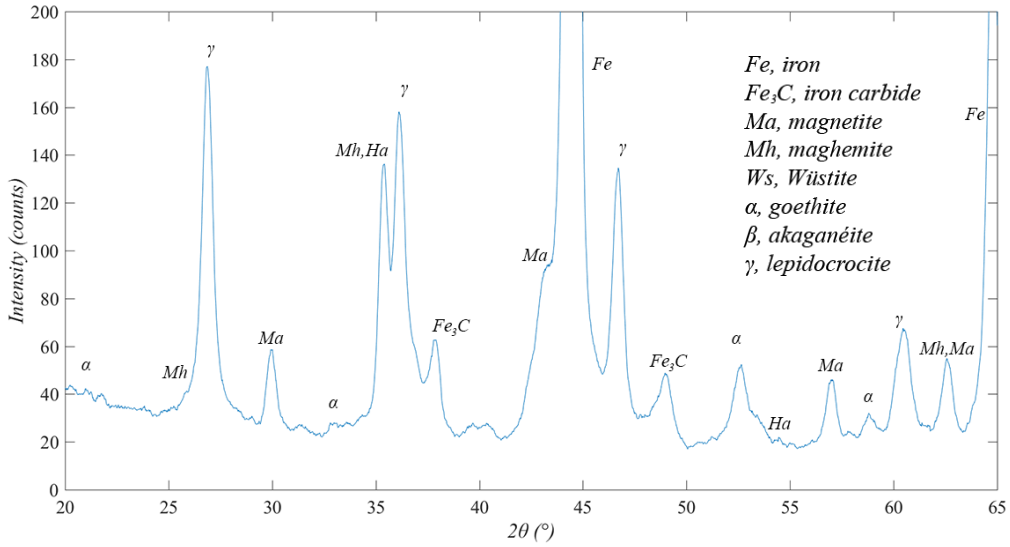

Figure 123, XRD spectra of dew and drizzle mixed sample surface

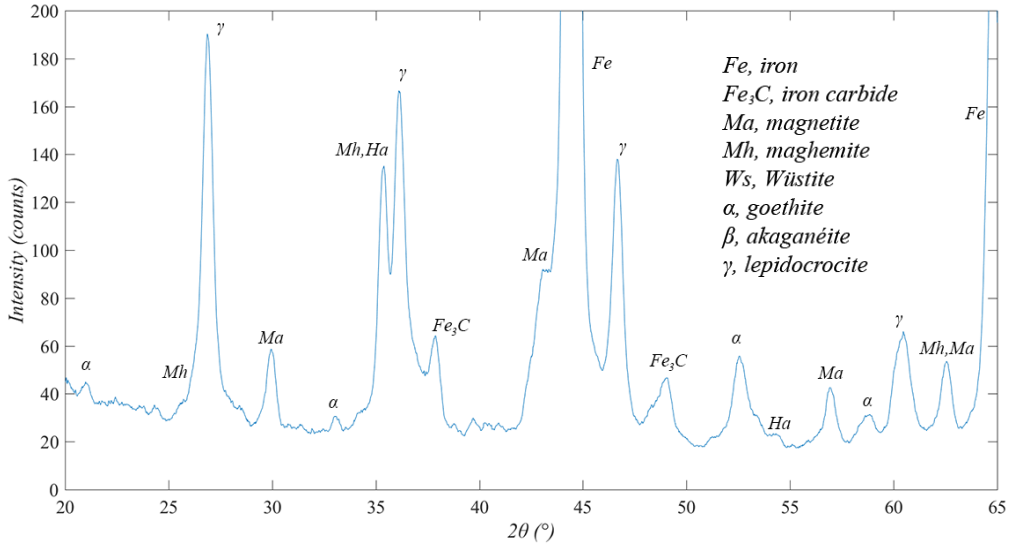

Figure 124, XRD spectra of flooded sample surface

7.1.3 Cycling of conditions

As an extension to the treatments explored in section 7.1.2, the treatments of dew and drizzle were cycled to gradually build up the oxidation on the sample surfaces, simulate repeated weather events and observe how the chemical make-up of the railhead surfaces evolves over time.

The treatment whereby dew was induced on the sample surface was repeated 2, 4, 8, 16 and 32 times. Images of the sample surfaces can be seen in Figure 125 which shows that the build-up of oxide on the surfaces is very gradual and the surface does not appear to change visually between 8 cycles and 32 cycles.

Figure 126 gives the progression of XRD spectra over the cycles. Due to the low intensity of the oxide signals it is difficult to identify many compounds; however, the signal for lepidocrocite is shown to increase with increasing cycles but not increase significantly during the later cycles between 8 and

32 cycles. Haematite was also identified on the sample surfaces of 4 cycles or greater; this implies that the less direct water-exposed surface created by this treatment – as opposed to direct contact of falling droplets of drizzle – leads to conditions where the formation of haematite may be favourable. The signal from the magnetite peak also appears to increase with number of treatments.

Figure 125, Photographic images taken of samples treated with 2, 8 and 32 cycles of dew / condensation treatment

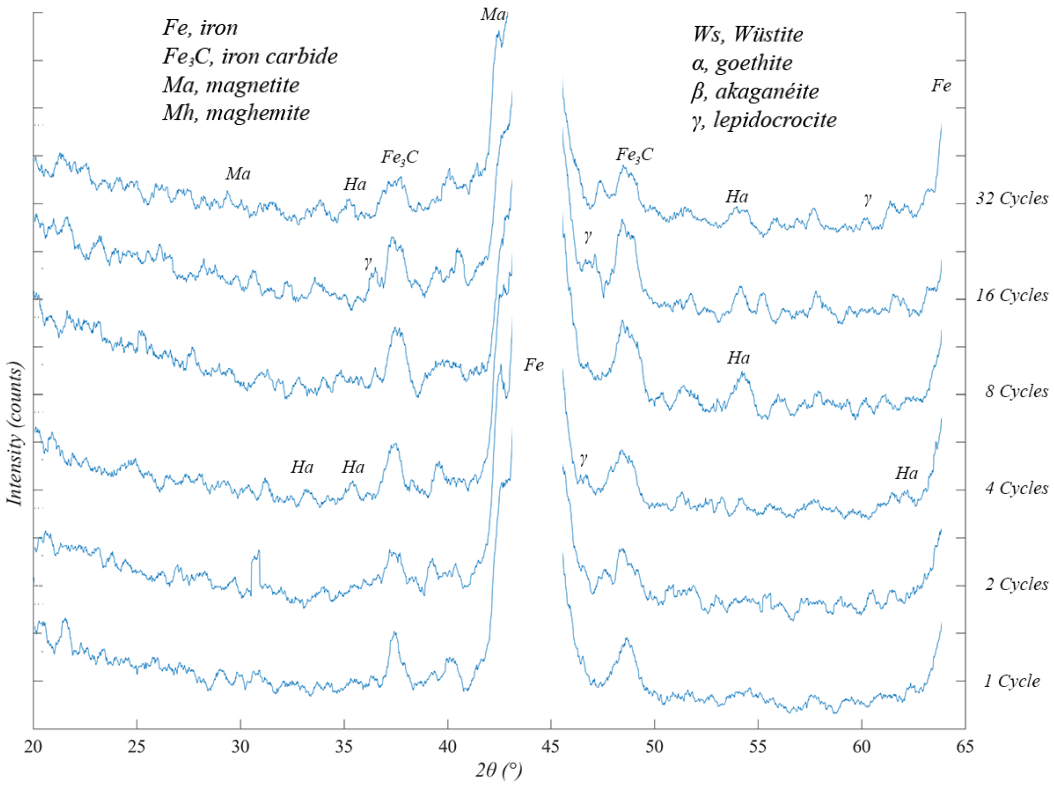

Figure 126, XRD spectra of samples treated with 1, 2, 4, 8, 16, and 32 cycles of dew / condensation treatment

Cycling of the drizzle condition – whereby distilled water was directly sprayed onto the surface of the samples – was repeated 2 and 4 times. Images of these sample surfaces are given in Figure 127. There is a clear visual progression in the surface oxidation achieved through subsequent treatment

cycles. This appears to be caused due to a growth in the size of the oxide patches as opposed to an increase in the number of patches.

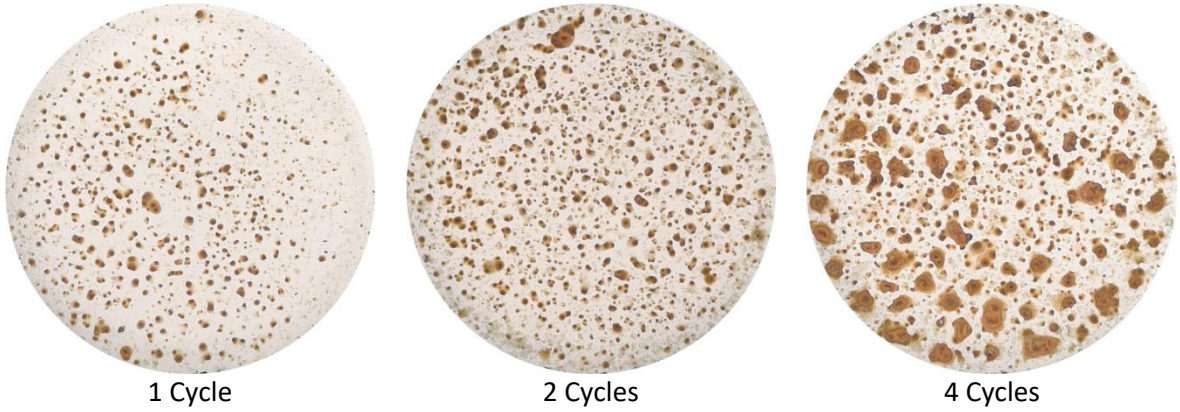

Figure 127, Photographic images taken of samples treated with 1, 2 and 4 cycles of drizzle / spray treatment

In Figure 128 the progression of the drizzle treatment cycles are shown. In all cycles, lepidocrocite can be identified from it's peak and the concentration is shown to increase with each cycle. Goethite is present on the first and second cycle; however, the peaks for this compound are gone by 4 cycles indicating that it has been converted into other compounds after further treatment. Haematite displays an increase in concentration over the cycles and this may be the compound that the goethite in the previous treatments had been converted to. Interestingly, Wüstite was observed on the sample which received 4 cycles of drizzle treatment; this is significant because it has not been observed on any other oxides synthesised in the lab. The signal from the magnetite peak was also shown to increase with number of treatments.

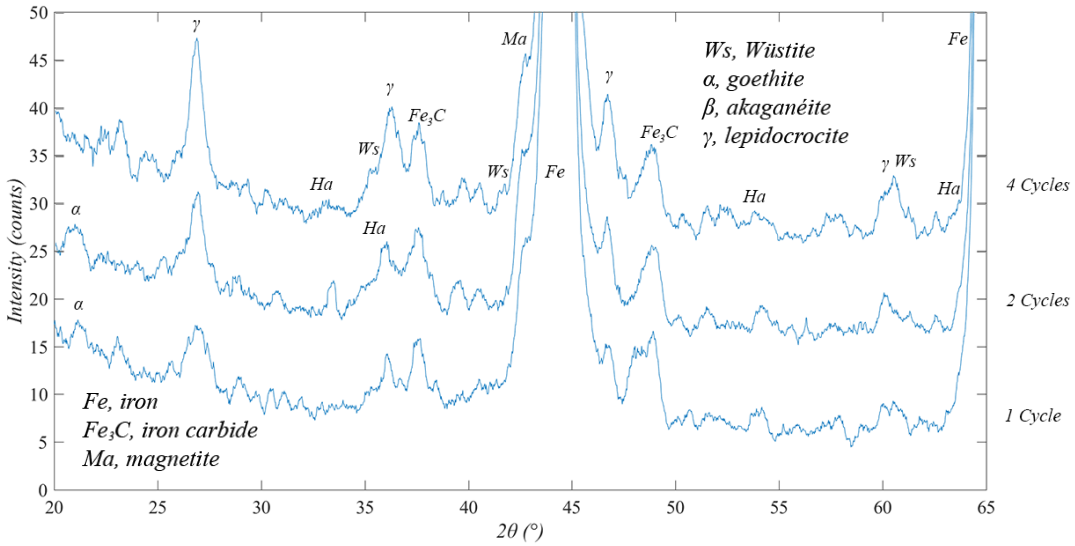

Figure 128, XRD spectra of samples treated with 1, 2, and 4 cycles of drizzle / spray treatment

7.1.4 Influence of mechanical action on oxide composition

The XRD spectra was taken of a sample before and after where the loose material was removed by mechanical action and addition of water during 10 runs. Figure 129 shows the difference observed between a single run and 10 runs; both images were taken after the sample was dried thoroughly in a desiccation chamber. The difference in colour of the surface shows the removal of the lighter

compounds with more yellow / orange hues, but the persistence and revealing of brown / black surfaces. This appears to indicate that iron-hydroxides are removed from the surface, but magnetite and haematite persist.

Debris after run

After removal of debris through 10 runs

Figure 129, Debris photographs on rail steel substrate

Figure 130 gives the XRD pattern of the surface after a single run and after 10 runs. From the peaks observed on the spectra the concentration of iron oxide-hydroxides, notably lepidocrocite, reduces significantly after mechanical action to the surface whereas the concentration of magnetite and haematite appear to be constant.

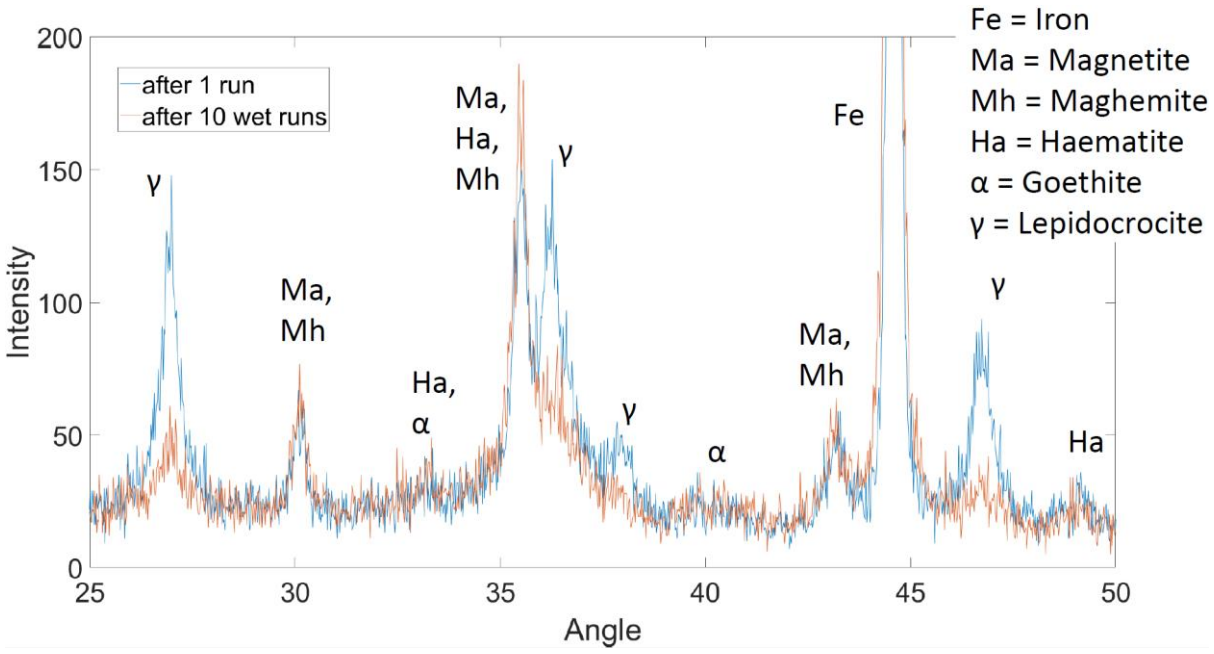

Figure 130, Comparison of XRD spectra of heavily oxidised surface after 1 and 10 passes of mechanical agitation

7.2 Oxide rheology

The flow properties of different oxide paste types and concentrations was tested using a rheometer. 4 compounds were tested: Haematite, Magnetite, Goethite, and Lepidocrocite. Standard powders were obtained through suppliers.

SEM micrographs of the oxide powders were taken and can be seen in Figure 131. The haematite powder has various particle sizes with larger cubic particles up to 10µm but with a large majority of the particles being around a micron in diameter placing the mean particle size around 2µm. Magnetite nano-powder was selected for this testing due to the difficulty of creating pastes and suspensions with larger particle sizes the particles appear to be finely ground uniform sizes and shapes. The goethite obtained appeared to be composed of needle-like particle sizes of 2 to 4µm in length and very uniform in size distribution. The lepidocrocite appears to be composed of needle-like particles around 2µm in length as well as spherical agglomerates of sub-micron particles; these agglomerates are between 2 to 8µm in diameter.

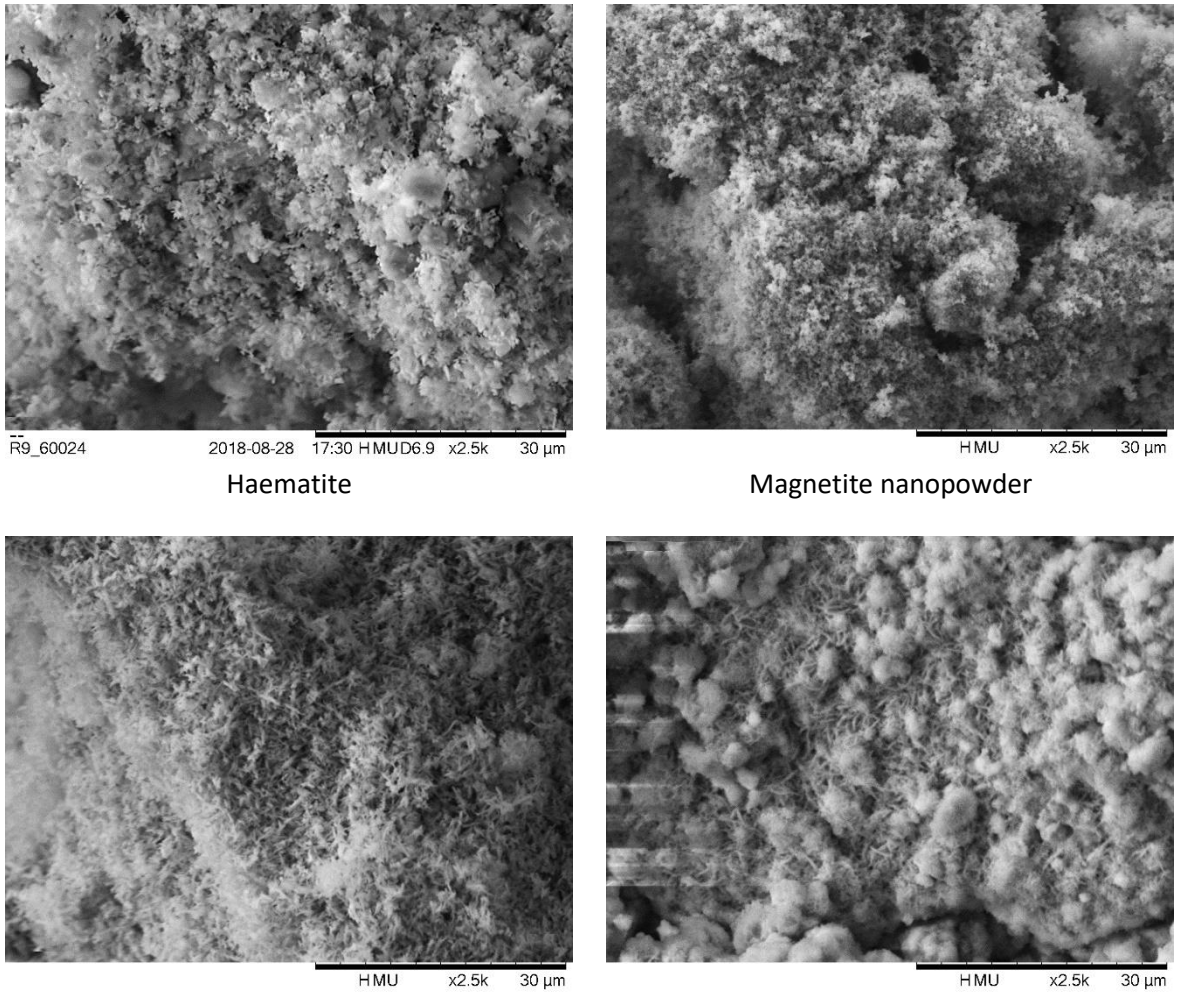

Figure 131, SEM micrographs of powders obtained for the rheology testing

Two additional oxide powders of haematite were obtained of different particle sizes to explore if size is an important factor in the rheological properties of oxide pastes. Powders with particle sizes of less than 50nm and particle sizes of a screen pass size of 100mesh (approximately 150µm) were tested. SEM micrographs of these powders are given in Figure 132. The 100 mesh powder contained very geometric angular crystals whereas the nano-powder contained agglomerations of loosely packed nanoparticles.

A precise volumetric pipette dosed 1ml of water to known measured masses of the powders shortly before the runs then the mixture agitated to form oxide pastes of known oxide concentration. The rheometric data is presented for the oxides in plots of logarithmic viscosity against the material

shear rate. In the figures, the ramp up is presented with points and the ramp down is presented as a solid line.

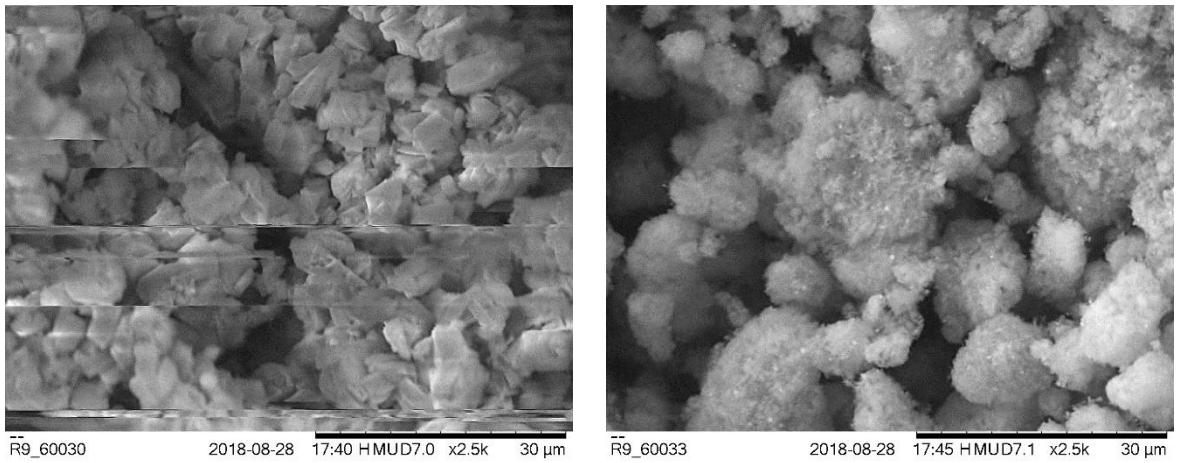

100 Mesh Less than 50 nm

Figure 132, SEM micrographs of additional haematite powders of different particle sizes obtained for the rheology testing

The rheometric charts for haematite, magnetite, goethite, and lepidocrocite are given in Figure 133, Figure 134, Figure 135, and Figure 136 respectively. All pastes behave as Bingham plastic fluids whereby a finite yield stress was required to begin deformation.

Occasionally (on either the up ramp or down ramp or both) there was a drop in viscosity at medium-low shear rates of 10 to 60s^{-1}. This can be observed most clearly on Figure 133 (60% haematite) and Figure 136 (35% and 50% lepidocrocite). The cause of this may be a settling and separation of oxide and water in lower oxide concentration pastes; normal behaviour recovers at higher shear rates.

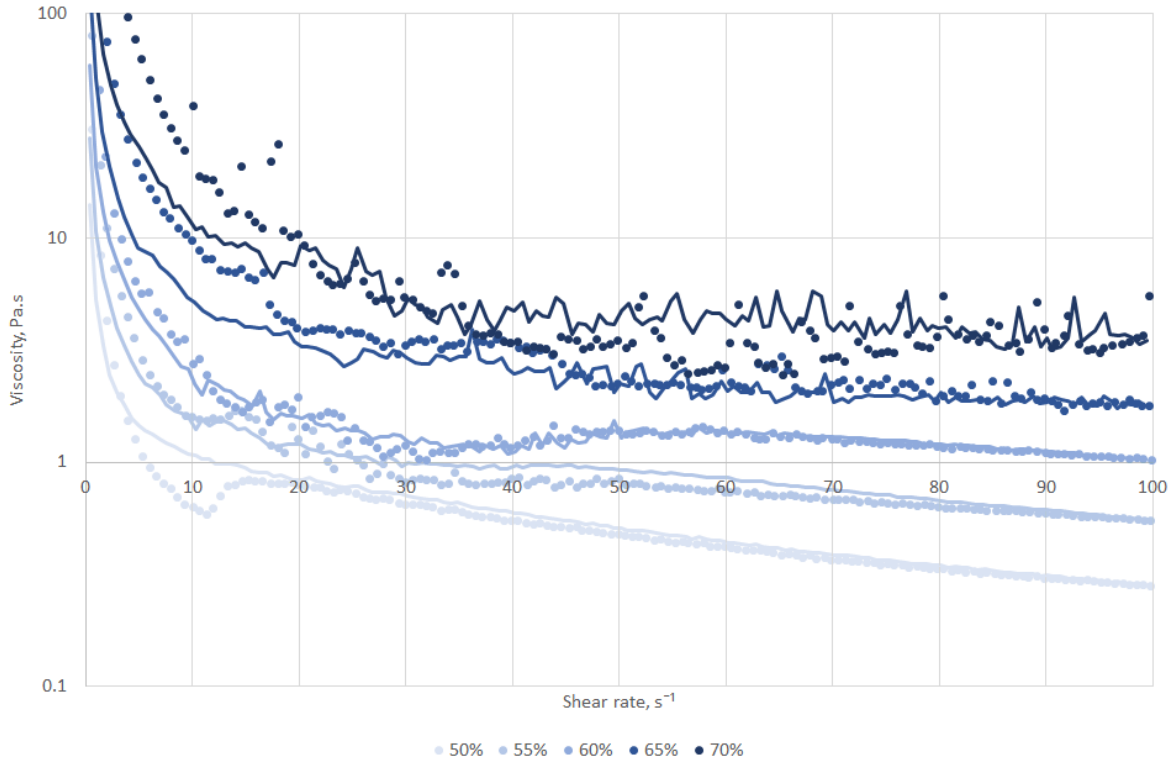

Figure 133, Viscosity / shear rate ramp up and ramp down curves for haematite pastes of varying oxide composition

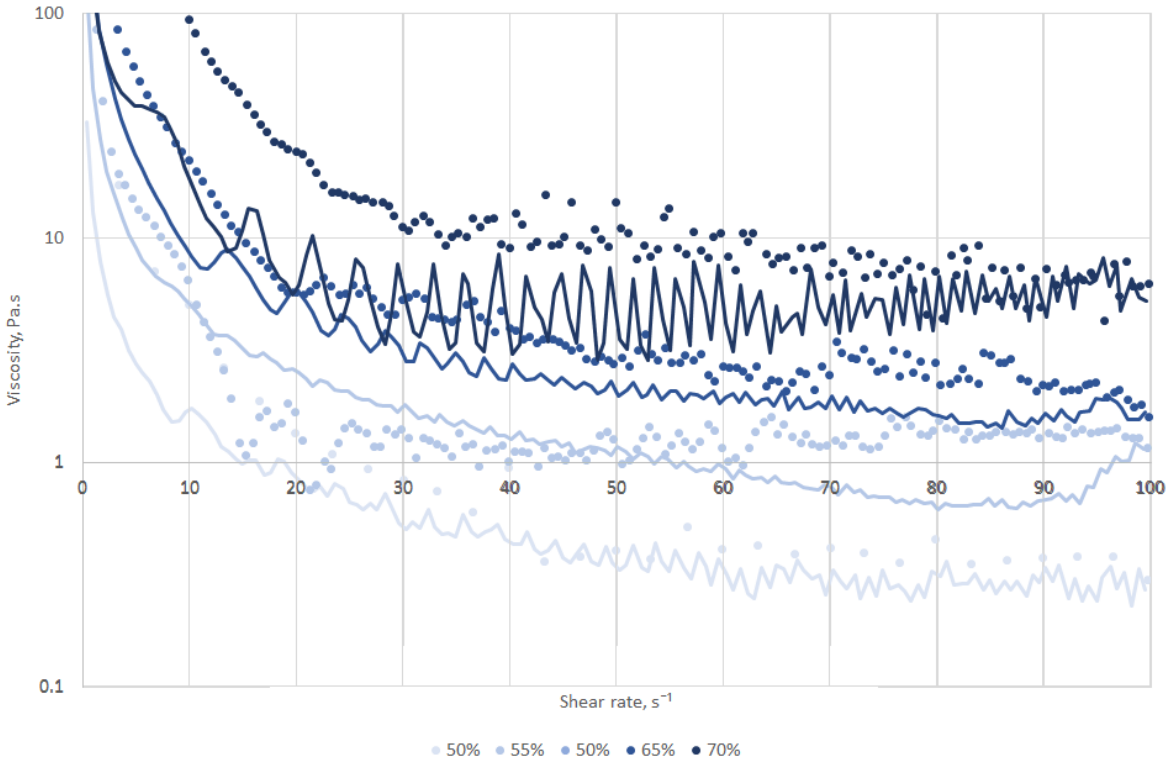

Figure 134, Viscosity / shear rate ramp up and ramp down curves for magnetite pastes of varying oxide composition

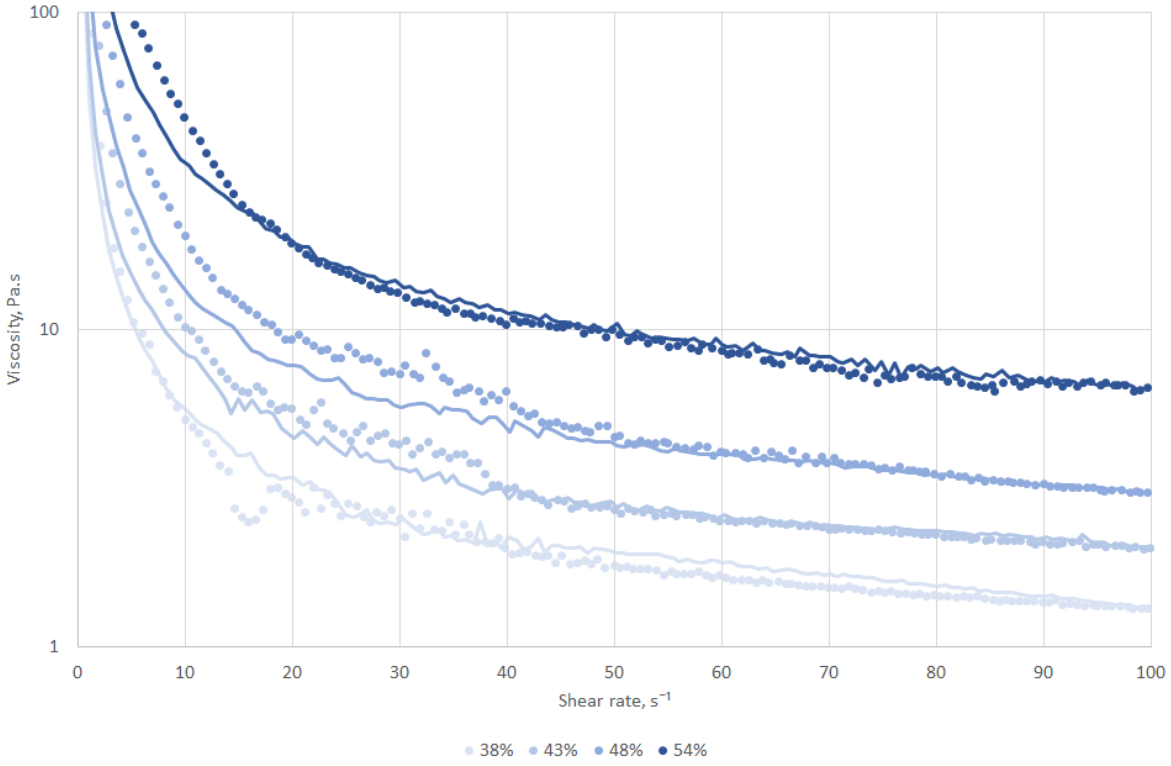

Figure 135, Viscosity / shear rate ramp up and ramp down curves for goethite pastes of varying oxide composition

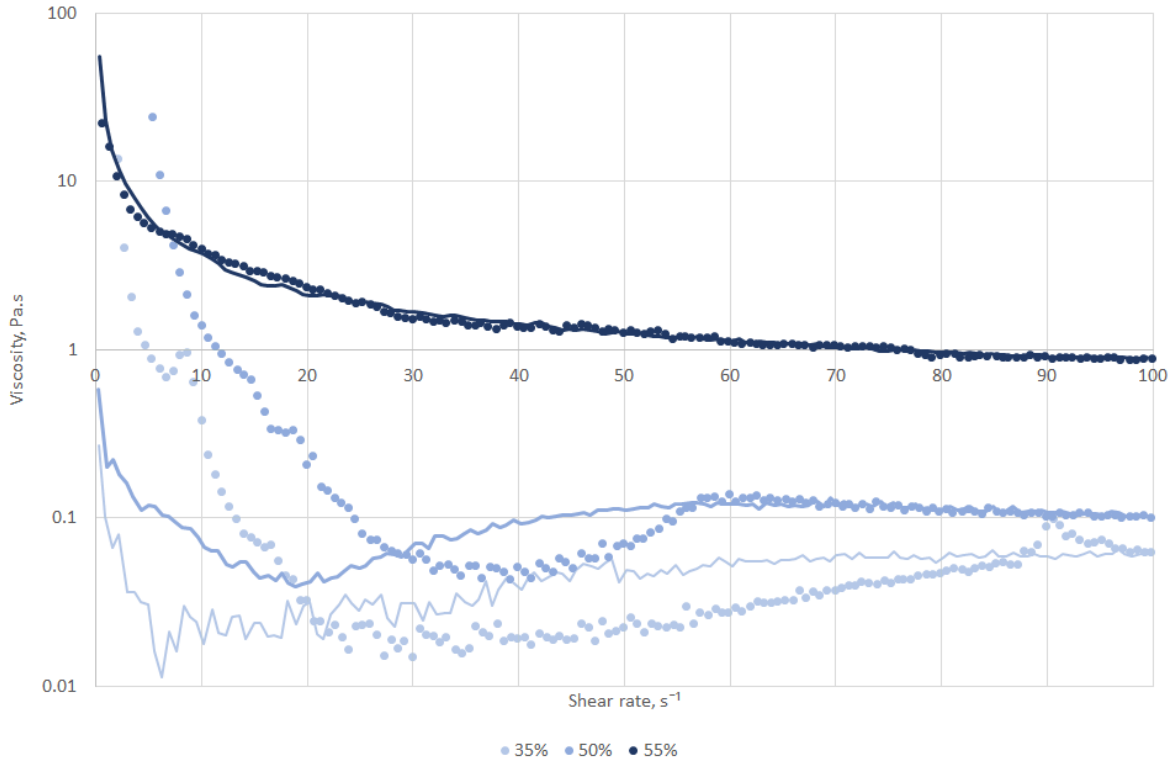

Figure 136, Viscosity / shear rate ramp up and ramp down curves for lepidocrocite pastes of varying oxide composition

Two numerical quantities which describe the behaviour of the oxide pastes during the runs are the initial yield stress and their viscosity at a chosen shear rate of $100s^{-1}$. This shear rate was chosen due to the stable and predictable behaviour of the oxide paste at this value as can be seen in the oxide viscosity / shear rate curves for all compounds investigated.

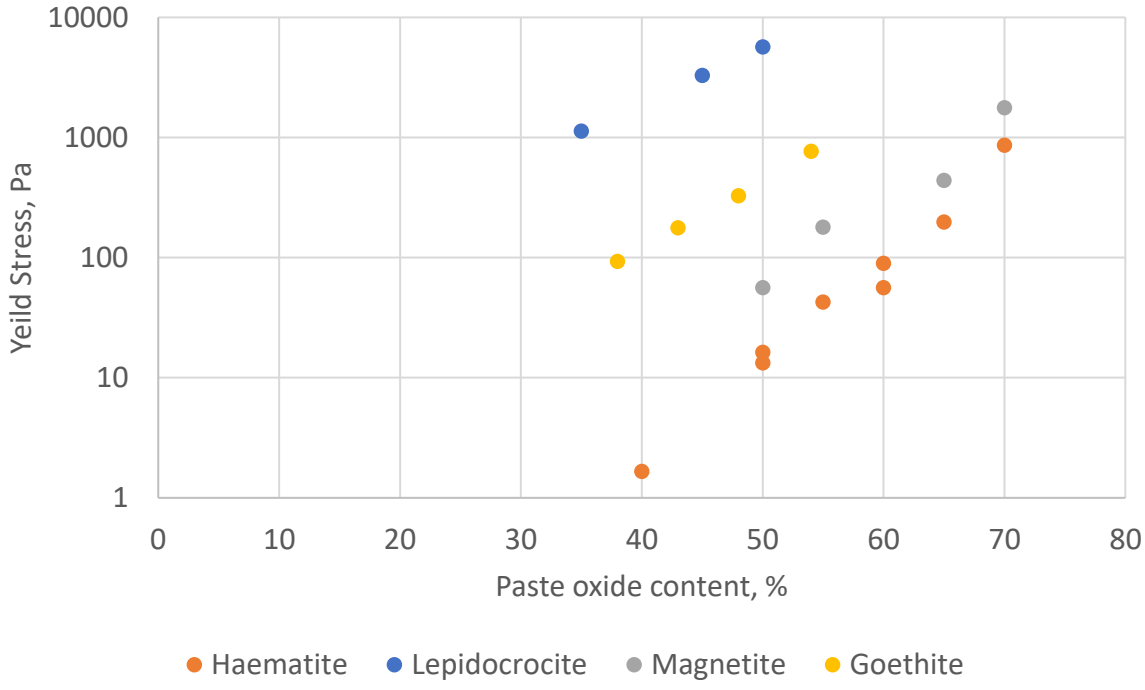

Figure 137, Comparison of yield stresses for different compound aqueous pastes of varying oxide mass composition

The yield stress for different concentrations of aqueous suspensions of the compounds tested are plotted in Figure 137. The yield stresses for the same concentrations of iron oxides (haematite and magnetite) are much lower than the yield stresses of the iron oxide-hydroxides (goethite and lepidocrocite). The highest yield stresses were achieved by lepidocrocite.

Viscosities of the suspensions of 55% mass concentration and at shear rates of $100s^{-1}$ are given in Figure 138. Goethite, at 6.6 Pa.s, is much more viscous as a paste under these conditions than the other compounds explored which exhibit viscosities between 0.5 and 1.2 Pa.s. It is unclear why this is the case; however, it may be attributable to the structure of goethite and the suspension that is possible through the interaction between the particles and water molecules.

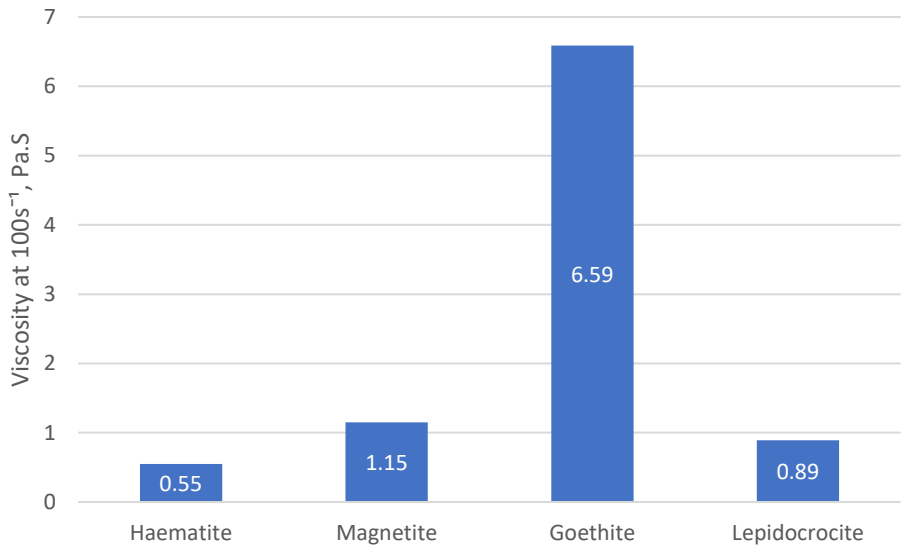

Figure 138, Viscosity at maximum shear rate of different oxides

The rheometric ramp up and ramp down curves are shown in Figure 139 and Figure 140 respectively. Complex behaviour of the lower concentration pastes are seen with some of the compounds including large oscillations in the 100 mesh 50% paste. These oscillations, as seen in some previous curves, may be caused due to the thick material building up in the contact causing a large normal load and allowing the fluid to take on solid characteristics in places and have to overcome a yield stress to allow for further rotation of the rheometer; as a result there is a regular oscillation in viscosity.

Viscosities of the suspensions of 50% mass concentration and at shear rates of $100s^{-1}$ for the haematite suspension are given in Figure 141. The results show that both the 50nm and 100 mesh pastes had higher viscosities than the 2µm paste. The higher viscosity for the smaller, 50nm paste, may be attributable to the relatively high surface area of the particles causing greater adsorption of water molecules to the surface and effectively reducing the amount of water forming the free liquid portion of the paste, thus increasing the apparent oxide concentration. The larger, more geometric particle size of the 100 mesh paste may cause the higher viscosity also due to increased difficulty of the particles flowing over one another as a result of their shape and size.

The yield stresses of the pastes of different haematite particle sizes, given for a variety of oxide concentrations, are shown in Figure 142. For any given concentration, the 100 mesh oxide has a yield stress in the order of two magnitudes higher than that of the other two oxides. This is likely a result of the highly geometric form of the oxides locking together and resisting deformation. The 2µm and 50nm particle size pastes exhibit almost identical yield stresses for the same oxide content.

The yield stresses for the nanoparticle pastes of haematite and magnetite are compared in Figure 143; the oxide content was normalised by density to compare suspensions of the same volumetric composition. The results show that there are no significant differences in yield stresses between the oxide types implying that oxide types are less important than the geometry and size of the particles with respect to the yield shear stresses of their pastes formed.

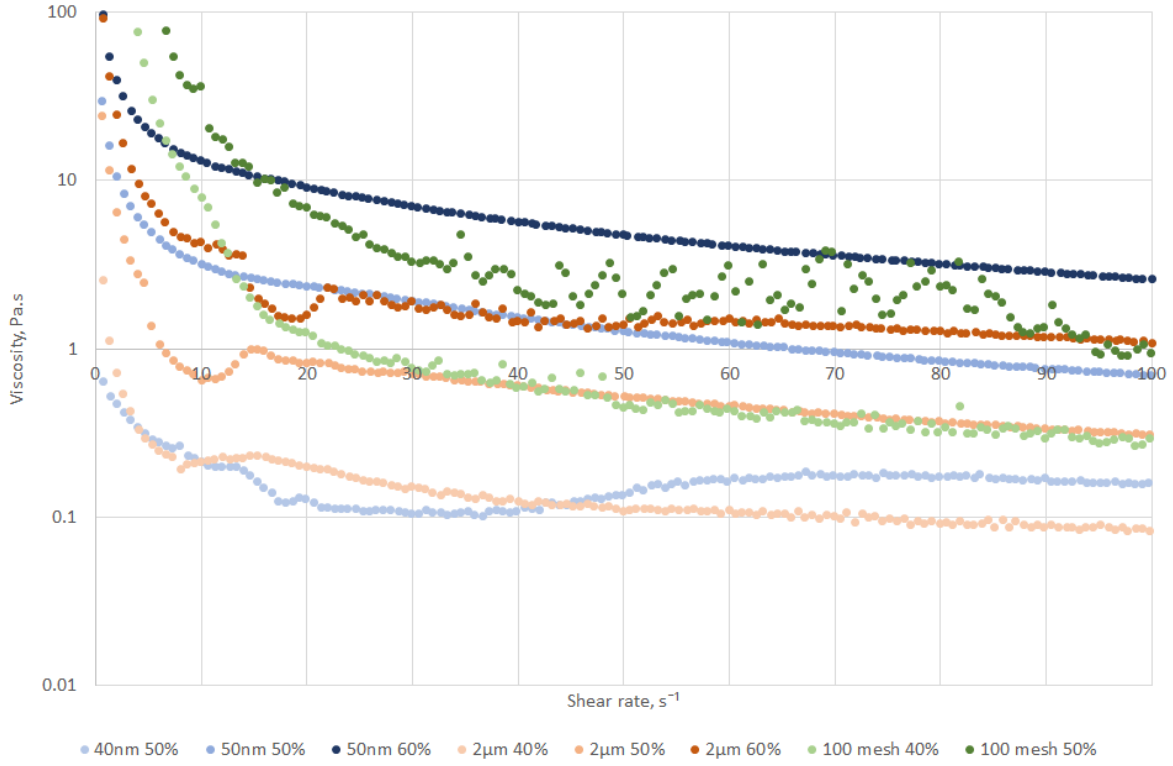

Figure 139, Viscosity / shear rate ramp up curves for haematite pastes of varying oxide composition and particle size

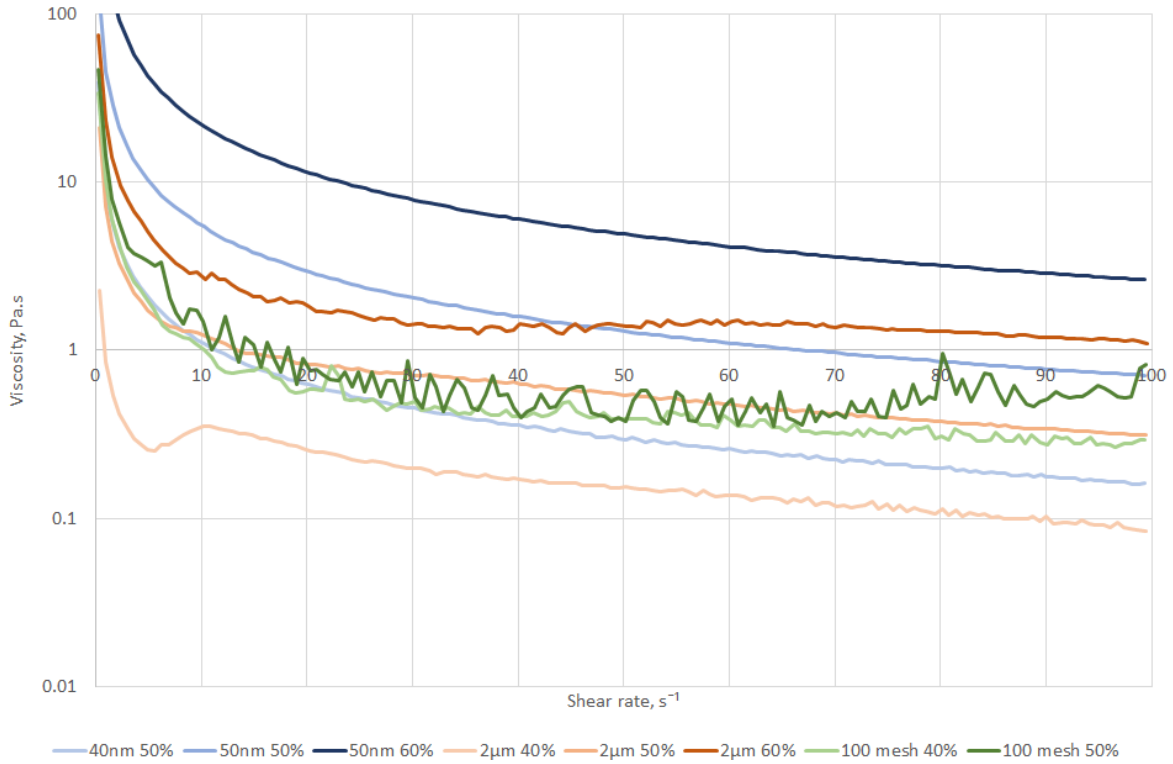

Figure 140, Viscosity / shear rate ramp down curves for haematite pastes of varying oxide composition and particle size

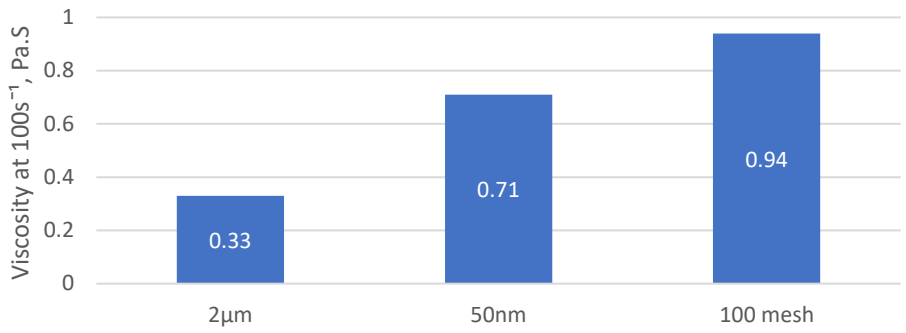

Figure 141, Viscosity at maximum shear rate of different particle sizes of haematite

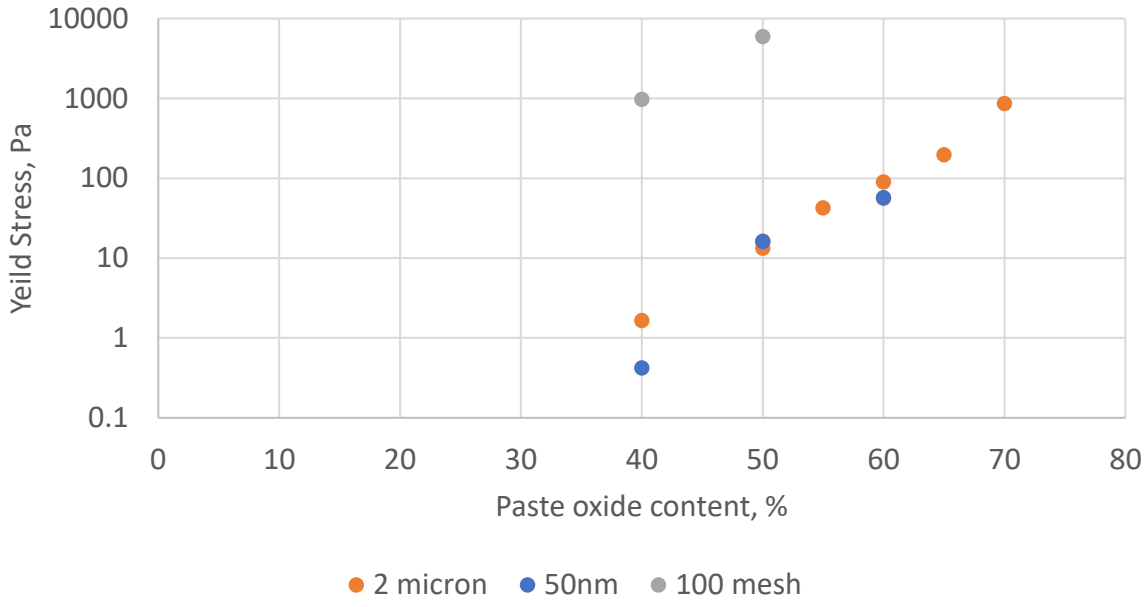

Figure 142, Comparison of yield stresses for haematite aqueous pastes of varying oxide mass and particle size composition

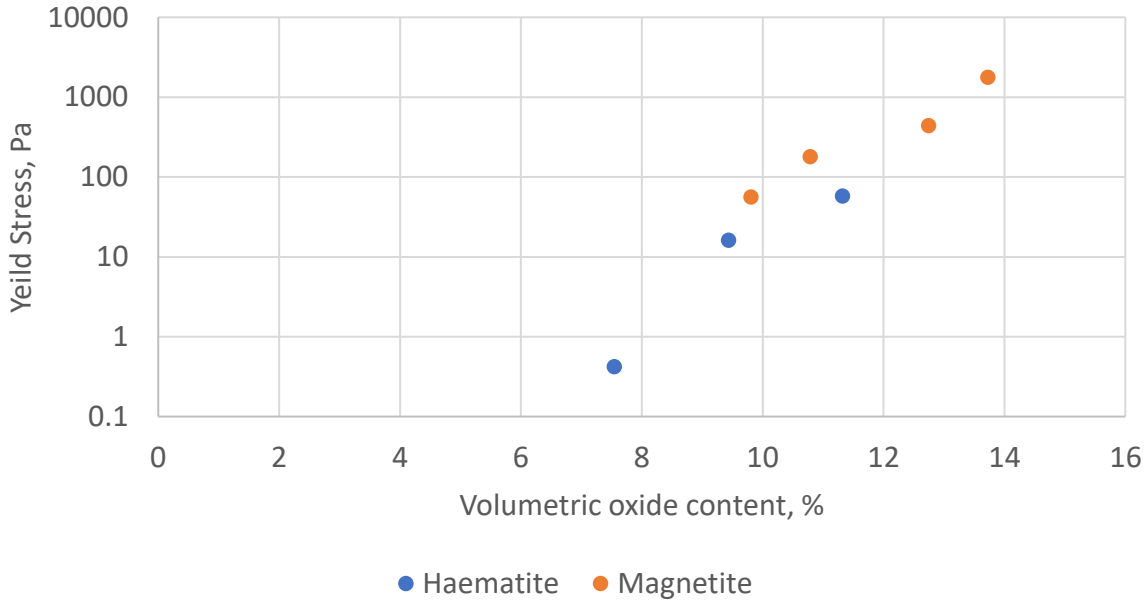

Figure 143, Yeild stress of nano-particles of oxides plotted against the volumetric oxide content of oxide

7.3 Summary

The oxidation and rusting of rail steel is a complex process. Analysis of lab-synthesised surfaces have shown that different oxide compounds are formed at different positions of the railhead surface.

The treatments explored utilising just water allowed for the synthesis of the iron oxides haematite, magnetite, maghemite, wüstite; as well as the iron oxide-hydroxides goethite, akaganéite and lepidocrocite. A major product of both treatments is lepidocrocite. This study recognises the limitation of just using water to induce rusting and oxidation of the sample surface and that with the open system of the railhead expects many other reaction mechanisms leading to varying concentrations and more diverse compounds being formed on the railhead surface.

When the dew cycling treatment was used alone, haematite, magnetite and small amounts of lepidocrocite was formed on the surfaces of the rail steel substrates. This method of treatment typically produced far less oxidation of the surface than the other methods tested.

Simulating drizzle using spray treatment resulted in haematite, magnetite and greater amounts of the iron oxide-hydroxides lepidocrocite as well as goethite. After numerous cycles, this treatment also produced wüstite; however, this mechanism is unclear.

The influence and role of water acting on the railhead surface to produce compounds of iron oxide and iron oxide-hydroxides is clear and appears to indicate that greater quantities of water on the railhead surface produce more oxidation products. Dew produced a more even and distributed oxidation over the surface and drizzle produces a less evenly distribution.

Yield stress may be an important property of solid / liquid suspensions on the railhead surface in addition to the viscosity and influence how much force the material can support. The iron oxide-hydroxides, goethite and lepidocrocite, tested exhibited yield stresses in the region of one to two magnitude greater than that of the iron oxides, haematite and magnetite.

The goethite powder tested displayed a far higher viscosity than all other compounds tested at the same oxide concentrations. This relationship was not observed with other compounds with the high yield stresses paste of lepidocrocite which exhibited a viscosity similar to that of the iron oxides for the same oxide concentration.

The geometry of particles in an aqueous oxide paste is shown to have significant influence on the yield stress of the material with more geometric powders displaying a far greater value. Particle size is shown to have negligible value on this value; however, it can increase the viscosity of the paste which is likely an effect of the high surface area.

The pastes of iron oxides of different types, magnetite and haematite, but similar particle size and shape have been shown to exhibit very similar rheological properties at the same volumetric solid composition suggesting that the hydroxide functional group of iron oxide-hydroxide contributes greatly to their different physical properties and behaviour on the railhead surface.

8 Tribo-chemical properties

The wheel / rail contact is a complex system comprising of several components; tribo-testing is a key element of this research as it provides the stage by which many of these components may be investigated together under conditions representative of real-world operating conditions.

The effects and chemical products of oxidation and corrosion of the railhead surface are key topics of this research and therefore two sample types will be explored: synthesised oxides, which may display the impact of different oxidation treatments surfaces; and deposited oxides, which allow for isolation of each oxide type for individual scrutinization.

Three experimental platforms were used for this testing. The first is a sliding only pin-on-flat test. The second was the use of the SUROS twin-disc rig which simulates a rolling-sliding contact. The final experimental platform was the Full-Scale rig which provides the geometry and conditions of a full-size wheel / rail contact. Overviews of these testing platforms are given in section 5.

8.1 UMT pin-on-flat testing

The pin-on-flat approach uses a pure sliding contact. Two contact sizes were used for this work, a small 10mm diameter steel ball and a bright steel pin of which contact surface is curved to that of a larger 100mm ball were used as the upper samples to provide the different contact sizes. Two sizes of contact were explored as the small specimen may plough / cut through the oxide layers on the sample surface whereas the larger sample projects a greater width in the direction of travel; as a result, it may entrain more oxides within the contact and its behaviour be more representative of the wheel / rail contact.

Two wet runs then a dry run and finally another wet run were performed on each sample specimen to investigate dry and wet contacts. The experimental set-up and test conditions for the runs are described in section 5.5.1.

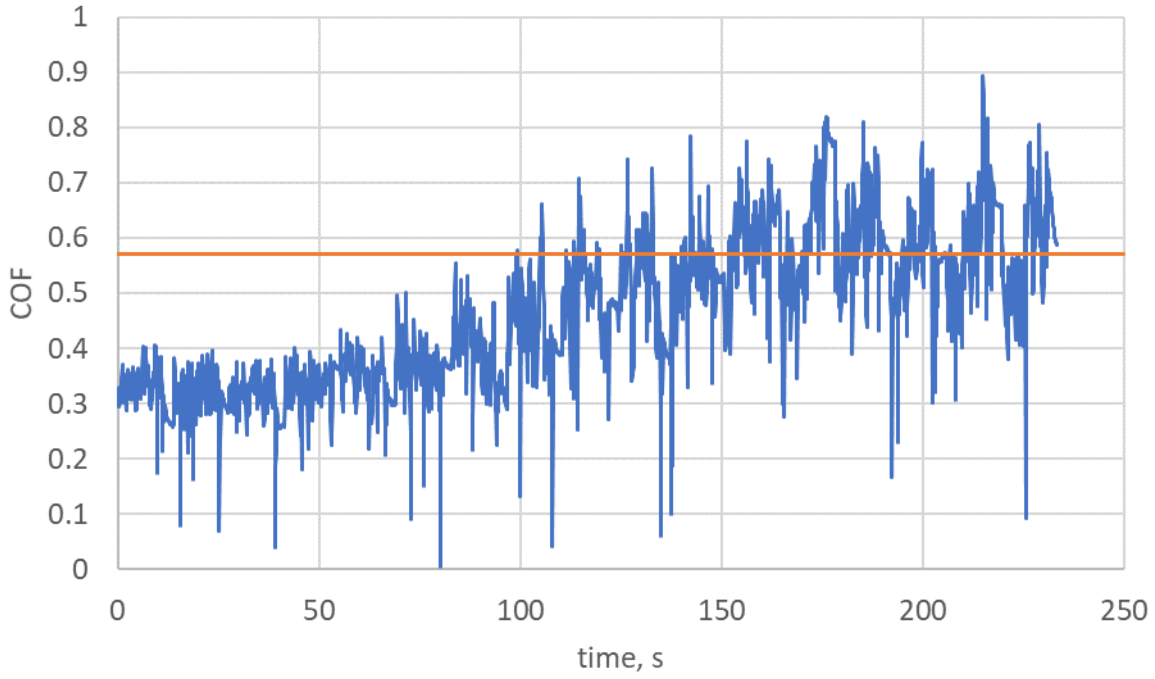

Figure 144, Coefficient friction of 10mm steel ball bearing on rail steel plate under dry conditions; the orange line indicates the kinetic coefficient of friction of mild steel reported in the literature of 0.57

Traction coefficients corresponding to normal, low and ultra-low adhesion levels are defined based on the rolling / sliding contacts of the wheel / rail system. The UMT uses a pure-sliding contact and therefore the equivalent corresponding coefficients of friction will need to be defined. The kinetic COF of mild steel on mild steel is reported as 0.57 [140] in clean dry surfaces. Figure 144 gives the COF of the experimental setup of the trial UMT testing under dry contacts which displays the COF starting around 0.3 and rising during sliding and reaching a value around 0.57 which corresponds well with the value reported in the literature. The rise in friction may be due to the contact surfaces heating up. Average normal adhesion levels reported on the Network Rail network are around 0.3 [9] in reasonably dry conditions; this is a similar level to the COF of the trial test at the start of the run. As a result, the equivalent COF levels corresponding to the levels of low, and ultra-low adhesion levels of 0.1 and 0.05 respectively, will be set to the same. To reduce the effect of contact heating on the results, a short delay was added to the testing programme before each 'stroke'; water within the contact will help to dissipate heat from the contact.

8.1.1 Synthesized oxides

As discussed in section 7.1, numerous simplified treatments of the railhead surface – using just distilled water as a medium – were chosen to simulate conditions experienced at the trackside. Treatments included: 'dew', where the temperature and humidity surrounding the samples were altered in a controlled manner to induce condensation on the surface; and drizzle, which involved spraying distilled water onto the surface and allowing it to dry under controlled conditions. Results from the smaller contact patch runs produced are presented first.

Figure 145 provides surface images, histograms showing the statistical analysis of, and COF maps of the first single-pass tribo-testing runs of samples with different treatments. These COF maps along with the surface images and histograms provide an insight into what is happening during the tests; variations in the COF values over the specimen surfaces reveals that the areas of highest visual corrosion exhibit the highest friction values. This is likely due to a combination of the higher surface roughness created by the surface disturbance and in these areas along with loose oxide providing a three-body abrasive condition which results in long parallel grooves running in the sliding direction.

The histograms in Figure 145 also reveal that large patches of oxidation, such as that created by the 'Drizzle then Dew' treatment, give a wider and occasionally a bi-modal distribution of COF values spread over the clean substrate areas and the heavily oxidised areas. A likely factor influencing this is the size of the contact which, for the smaller 0.12mm contact area diameter, is a similar or smaller order of magnitude in size to that of the heavily oxidised areas for all the treatment. A larger contact was introduced to investigate this and is compared later in this section.

Figure 146 summarises the frictional data from the runs over the surfaces of varying treatments with the smaller contact. The general relationship the data shows is the higher the degree of oxidation of the surface, the higher the mean COF. A control, untreated surface value of 0.23 was recorded and the highest COF values were recorded with the substrates treated with 'Drizzle then Dew' displaying around 0.4 as their average COF. The flooded sample was an exception to this with the highest apparent degree of oxidation yet a COF of 0.35, which is less than the 'Drizzle then Dew' treatment; this may be due to the more even surface oxidation caused by a constant sheet of water as opposed to a patchier distribution of droplets over the surface during the treatment of the samples.

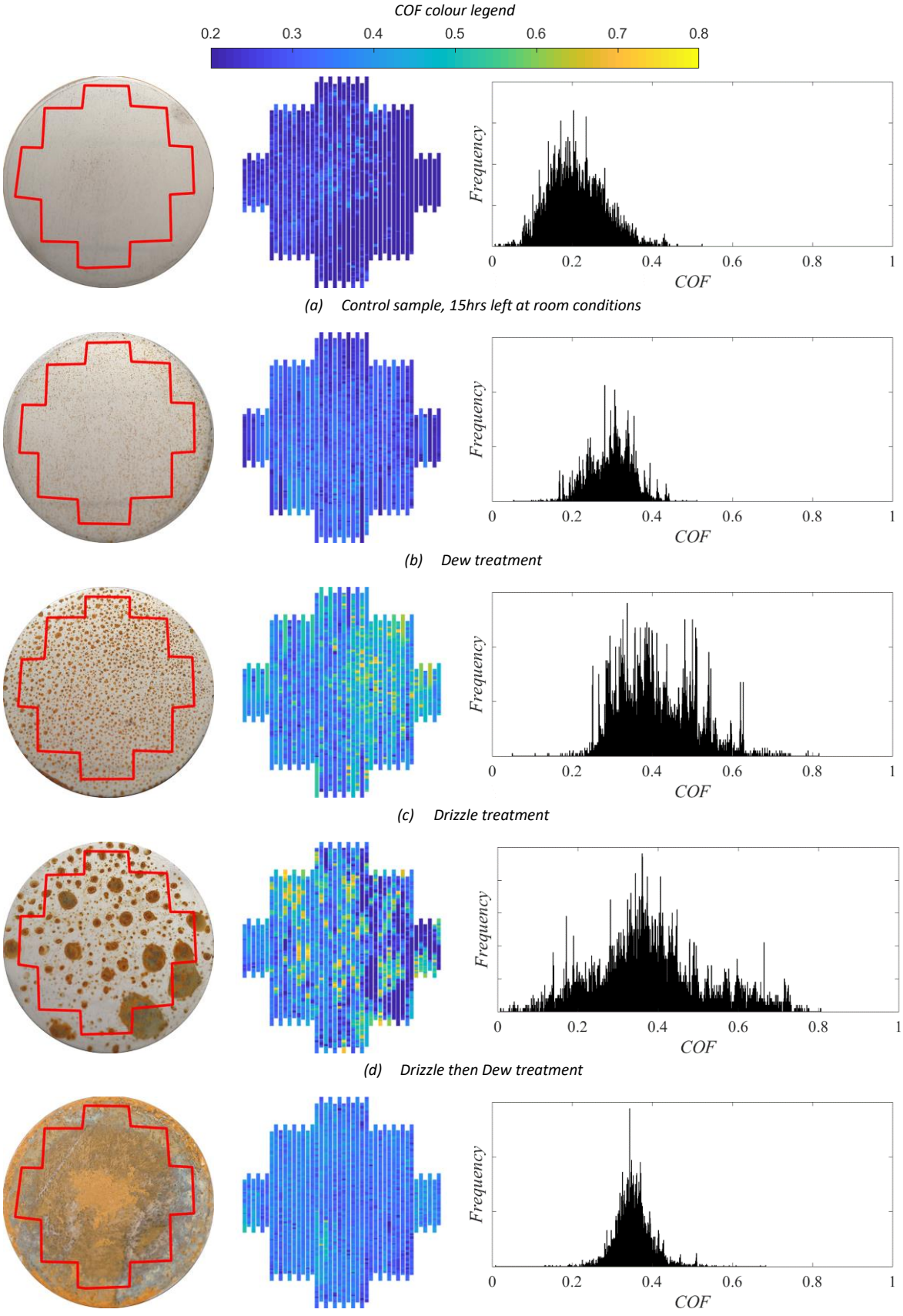

(a) Control sample, 15hrs left at room conditions

(b) Dew treatment

(c) Drizzle treatment

(d) Drizzle then Dew treatment

(e) 5ml water deposition on substrate surface; flooded treatment

Figure 145, Sample surface images, COF maps, and histograms showing the distribution of COF levels for samples of various treatments, tested with the small-contact pin-on-flat testing under wetted conditions. a, control sample; b, dew treatment; c, drizzle treatment; d, drizzle then dew treatment; e, flooded treatment

No average lower COF was achieved by any of the surface treatments lower than the control value; however, areas on the surface treated with the 'Drizzle then Dew' treatment display localised COF values lower than what was experienced on the control sample. It must be noted that railheads currently in service are unlikely to have surfaces which are as clean and as free from oxidation as the control specimen used for this testing and as a result these areas shown on the 'Drizzle then Dew' may indicate areas of low adhesion.

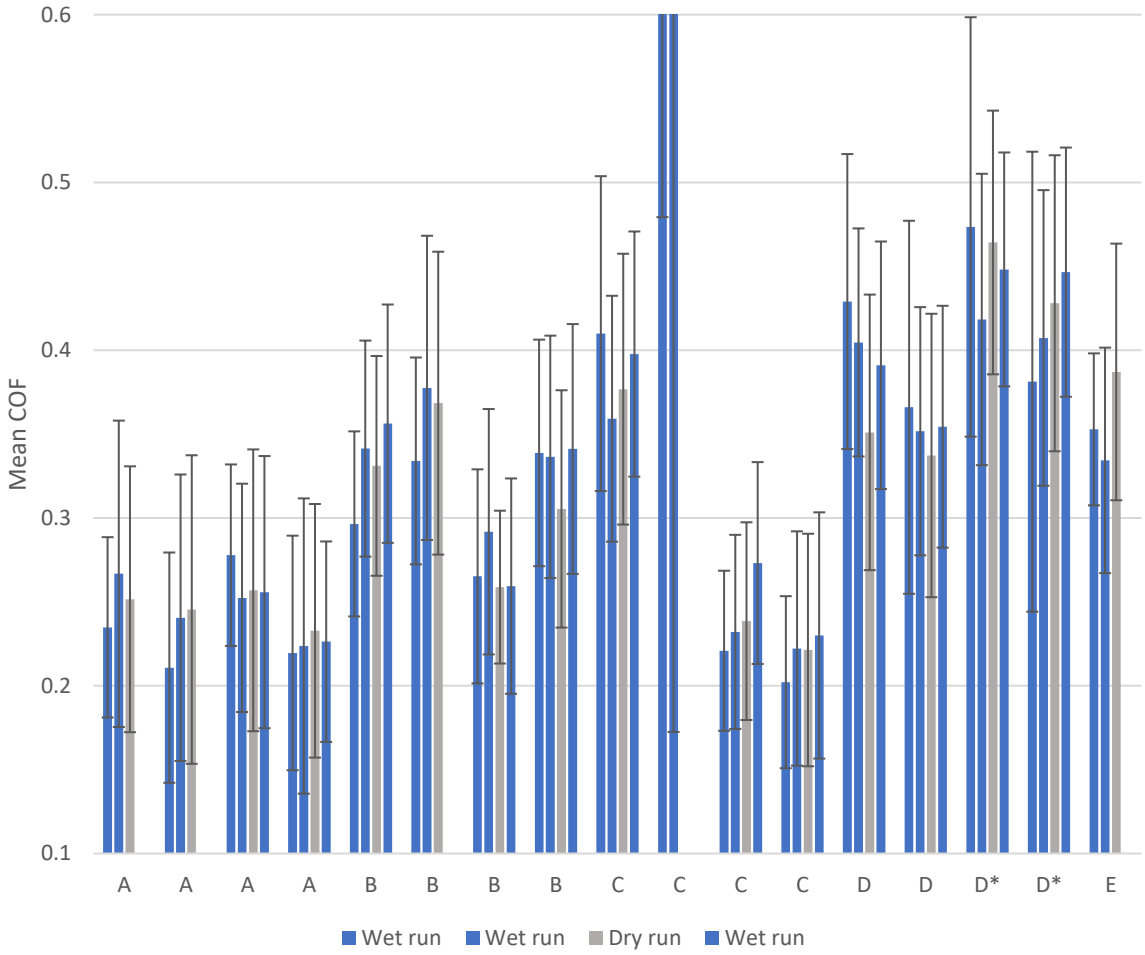

Figure 146, Mean COF of samples of various treatments, tested with the small-contact pin-on-flat testing. A, Control; B, dew treatment; C, drizzle treatment; D, drizzle then dew treatment (D: with additional initial drizzle treatment); E, flooded treatment. Error bars showing one standard deviation from mean. Each group of histograms represents multiple subsequent tests of a single sample*

In the initial experiments, where a smaller specimen was used, it was possible to conduct numerous cycles of tribo-testing over the same patch whilst the sample surface was drying out. Figure 147 presents the mean COF of repeated runs over the same substrate 8 times. Initially the sample surface was sprayed on the first run and the procedure – without re-spraying – was repeated for runs 2 through 4; this was then repeated, with a spraying at the start of run 5, in runs 5 through 8. It can be seen that in run 4 the COF has fallen to its lowest level just when the sample is almost dry; however, this drop in COF is not replicated for the last four runs with the COF rising after the second spraying.

The COF maps, shown in Figure 148, reveal the changes in local areas which contribute to this behaviour. During the first run shown in 'a', there are clear distinctions between the areas of high COF, in the patches of high oxidation, and the areas of low COF which exist between them; this

contrasts with what is seen in ‘b’, showing low contrast between the areas of high COF and low COF. In ‘c’, the contrast between the areas has recovered somewhat and there are once again areas of high COF.

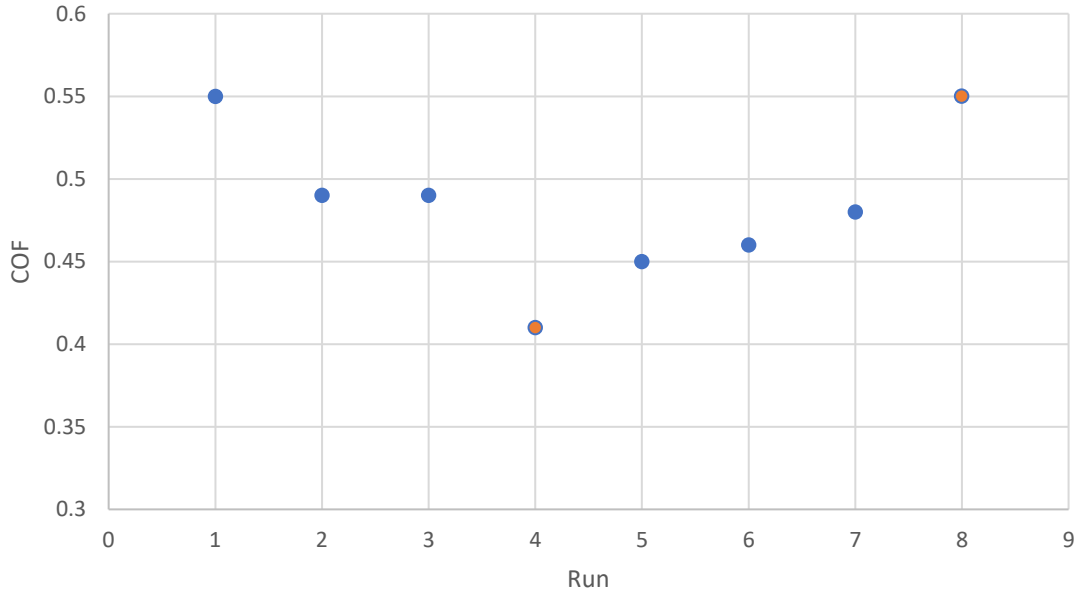

Figure 147, Mean COF of synthesised oxide sample runs plotted against successive run number. Distilled water was sprayed on the sample surface before runs 1 and 5 and allowed to dry out during the runs following. Sample surface was close to being dry on runs 4 and 8.

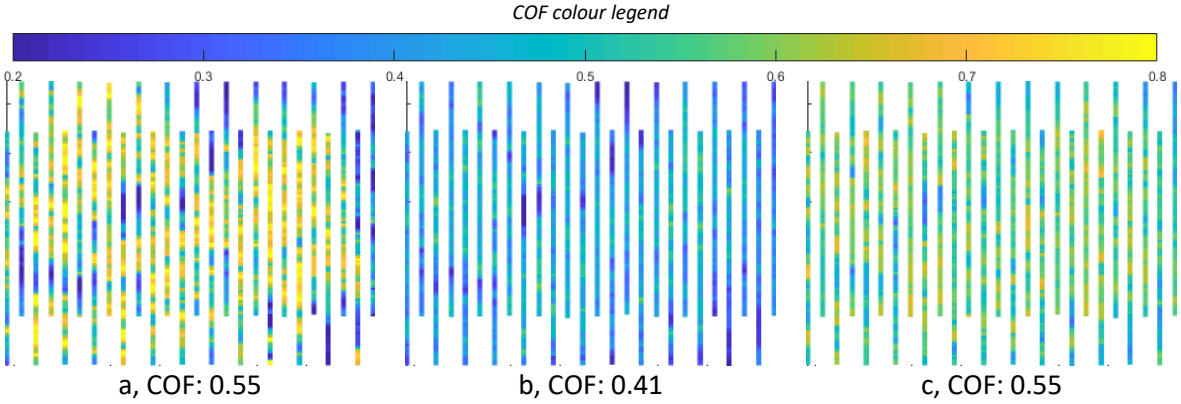

Figure 148, Oxide drying out showing: a, first run after wetting surface; b, fourth run just before surface dries; c, eighth run just before surface dries (water was reapplied on the fifth run)

SEM images were taken of the areas where oxide patches are located on the surfaces after the runs given in Figure 148. These images are displayed in Figure 149 and reveal why there is a reduction in contrast between the areas of high and low COF experienced. The oxide is found to form a cake over these areas of high roughness (left image) which is pressed into a smooth layer where before there would be rough areas. Image ‘b’ in Figure 149 shows the surface at the end of the 8 runs with two applications of water and reveals that the oxide layer has broken up and is no longer as effective at forming a smooth bridge across the roughened surfaces.

As contact size was suspected to be a factor in the contact behaviour due to the relatively small contact diameter in relation to the sizes of the oxide patches, a larger upper sample with the equivalent diameter of 100mm was machined to increase the area of contact between the surfaces.

The resulting contact diameter of 0.37mm is still relatively small in comparison to the sizes of the oxide patches; however, is it over three times the length or greater than nine times the area of the smaller contacts explored.

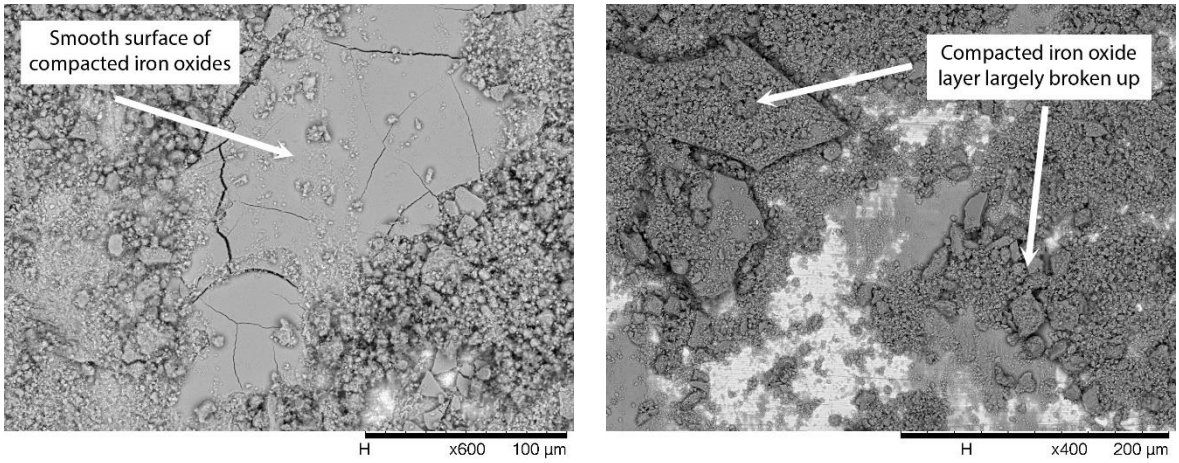

Figure 149, SEM micrographs of debris present on synthesised oxides sample surfaces. a) caked debris forming smooth surface over rough surface, b) debris layer after most loose oxide removed from surface due to mechanical action

The COF maps and histograms alongside the sample surface images are given in Figure 150. The reduced lateral resolution of the COF maps due to the more spread out contact tracks is less effective at picking up surface features; however, they still reveal patchier COF distributions over the surfaces treated with treatments including a 'drizzle' stage. The COF histograms also display the same patterns with wider distribution of COF values and some bi-modal distributions with lower COF values and higher COF values. The samples treated with the 'Dew' treatment exhibited higher and more widely distributed COF values, but unlike the other treatments, did not display a clear separation of the distribution into two modal groups. Once again, none of the treated samples achieved mean COF values lower than that of the control; however, the sample that was treated with 'Drizzle and Dew' displayed some COF values lower than those observed on the control sample supporting that the presence of oxide in some areas may reduce the COF.

Figure 151, summarises the mean COF values of runs with different treatments. The overall relationship is that the higher the oxidation resulting from the treatment, the higher the average COF. The second 'Dew then Drizzle' treatment resulted in COF values of around 0.14 which is comparable to that of the control, but this does not agree with the first 'Dew then Drizzle' run and may be the result of a systematic error caused by the equipment malfunctioning; this is likely due to the next run, a clean control sample repeat, failing and being terminated after which the experimental rig was reset for the following runs.

Due to the mechanical limitations of the testing platform it was necessary to apply lower contact pressures than what the smaller contact experienced; however, studies have found that the average coefficient of friction for pure-sliding tribo-tests is largely unaffected by an increase in contact pressure [141] meaning the results between the different contact size tests are comparable. The tribo-tests with the larger contact when compared with the smaller contact, examining the effect of the various treatments on the sample surfaces, gave lower COF values by around 0.1. This is in line with the belief that the larger contact is less affected by the roughness caused by the areas of oxidation or machining marks on the surface.

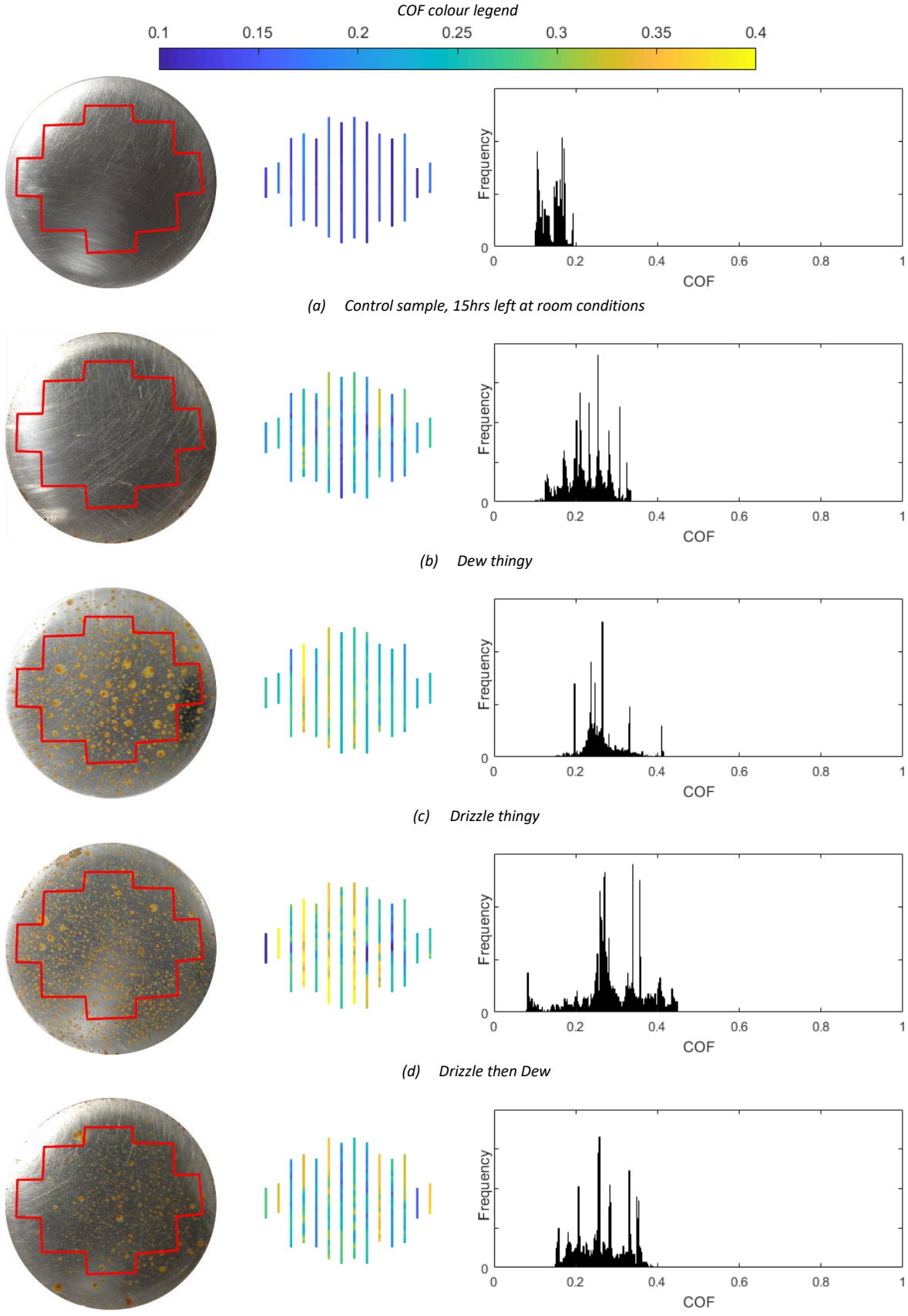

(a) Control sample, 15hrs left at room conditions

(b) Dew thingy

(c) Drizzle thingy

(d) Drizzle then Dew

(e) Dew then Drizzle

Figure 150, Sample surface images, COF maps, and histograms showing the distribution of COF levels for samples of various treatments, tested with the large-contact pin-on-flat testing under wetted conditions. a, control sample; b, dew treatment; c, drizzle treatment; d, drizzle then dew treatment; e, dew then drizzle treatment

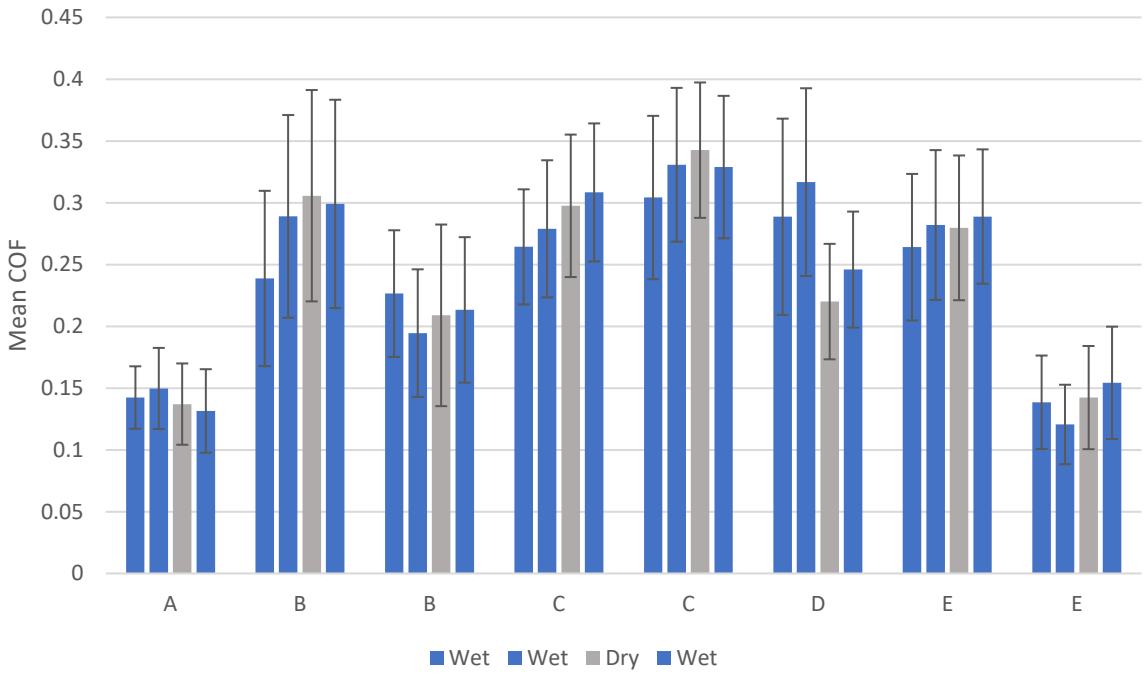

Figure 151, Mean COF of samples of various treatments, tested with the large-contact pin-on-flat testing. A, Control; B, dew treatment; C, drizzle treatment; D, drizzle then dew treatment (D: with additional initial drizzle treatment); E, dew then drizzle treatment. Error bars showing one standard deviation from mean. Each group of histograms represents multiple subsequent tests of a single sample*

Multiple cycles of 'Dew' and 'Drizzle' treatments were applied to samples to build up the oxidation of the sample surfaces. Figure 152 plots the mean COF of samples treated with 1, 2, 4, and 8 cycles of treatment. As both treatments were increased the mean COF initially increased up to 4 cycles where the COF of the 'Dew' and 'Drizzle' treatments were 0.20 and 0.33 respectively the COF then fell with more cycles of treatment.

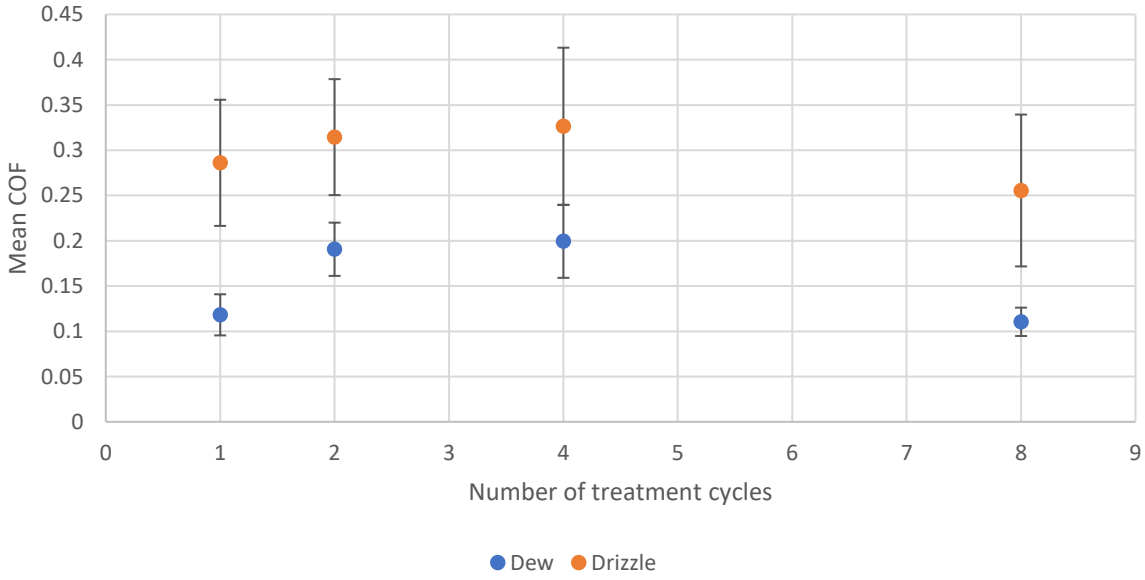

Figure 152, Mean COF of synthesised oxide samples plotted against number of treatment cycles for dew and drizzle treatment; tested using the large-contact pin-on-flat testing under wet conditions. Error bars showing one standard deviation from mean

The treatments were extended further for the 'Dew' treatment and a second set of samples were treated with 4, 8, 16 and 32 cycles, shown in Figure 153. A similar pattern can be seen, and the mean COF reaches a maximum of 0.25 after 8 cycles, but decreases when subjected to further treatments.

Two possible explanations for this pattern observed of increasing then decreasing average COF with number of treatments are, firstly, that an amount of oxide debris in the lower number of cycles is insufficient to form bridging over areas of increased roughness caused by the rusting of the substrate; however, these high roughness areas are still present. Secondly, as the amount of water applied between all the runs was maintained at the same quantity, the concentration of oxide within the water / oxide mixtures on the surface increases with each subsequent treatment cycle of the sample surface; this behaviour has been observed before with oxide-water pastes in rolling-sliding contacts [50].

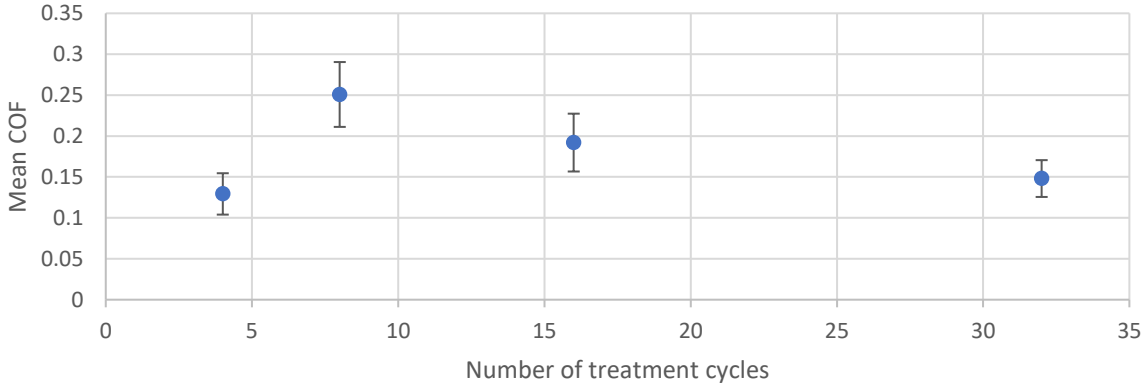

Figure 153, Mean COF of synthesised oxide samples plotted against number of treatment cycles for dew treatment; tested using the large-contact pin-on-flat testing under wet conditions. Error bars showing one standard deviation from mean

8.1.2 Deposited oxides

Oxides were deposited onto the surfaces of the substrates initially via suspensions of distilled water and then suspensions of isopropanol after it was discovered that substantial oxidation of the surfaces of the substrates occurred when distilled water was used as a suspension medium, similar to that of the 'flooded' synthesised oxides sample in section 7.1.2.

All of the tested oxide types in this section were both found to be present on the railhead (section 6.2) and were successfully synthesised on the surfaces of the substrate through controlled oxidation (section 7.1).

After water had dried off the substrates, the layers were explored using the SEM. These micrographs are given in Figure 154 and show haematite and goethite (b and c) formed a consistent surface. The magnetite particles (a) form into clusters, likely due to their magnetic properties. The layer of lepidocrocite (d) showed interesting behaviour as it appeared to form two layers. The lower layer consists of 10 - 20µm agglomerates and the top surface as a smooth plane. XRD depth profiling analysis of this layer revealed almost identical spectra when targeted at both 2° and 10°, suggesting that both layer components are composed of the same material.

Oxides deposited with the isopropanol suspensions 'dried' far quicker and evenly over the surfaces with the exception of goethite which agglomerated into patches 20 – 100µm across, it is unclear why this occurred but upon applying water at the start of the tribo-testing runs, the layer returned to being continuous over the surface of the substrate. Layer thicknesses and mass coverage densities are given in Table 14 for the oxides deposited via isopropanol solutions.

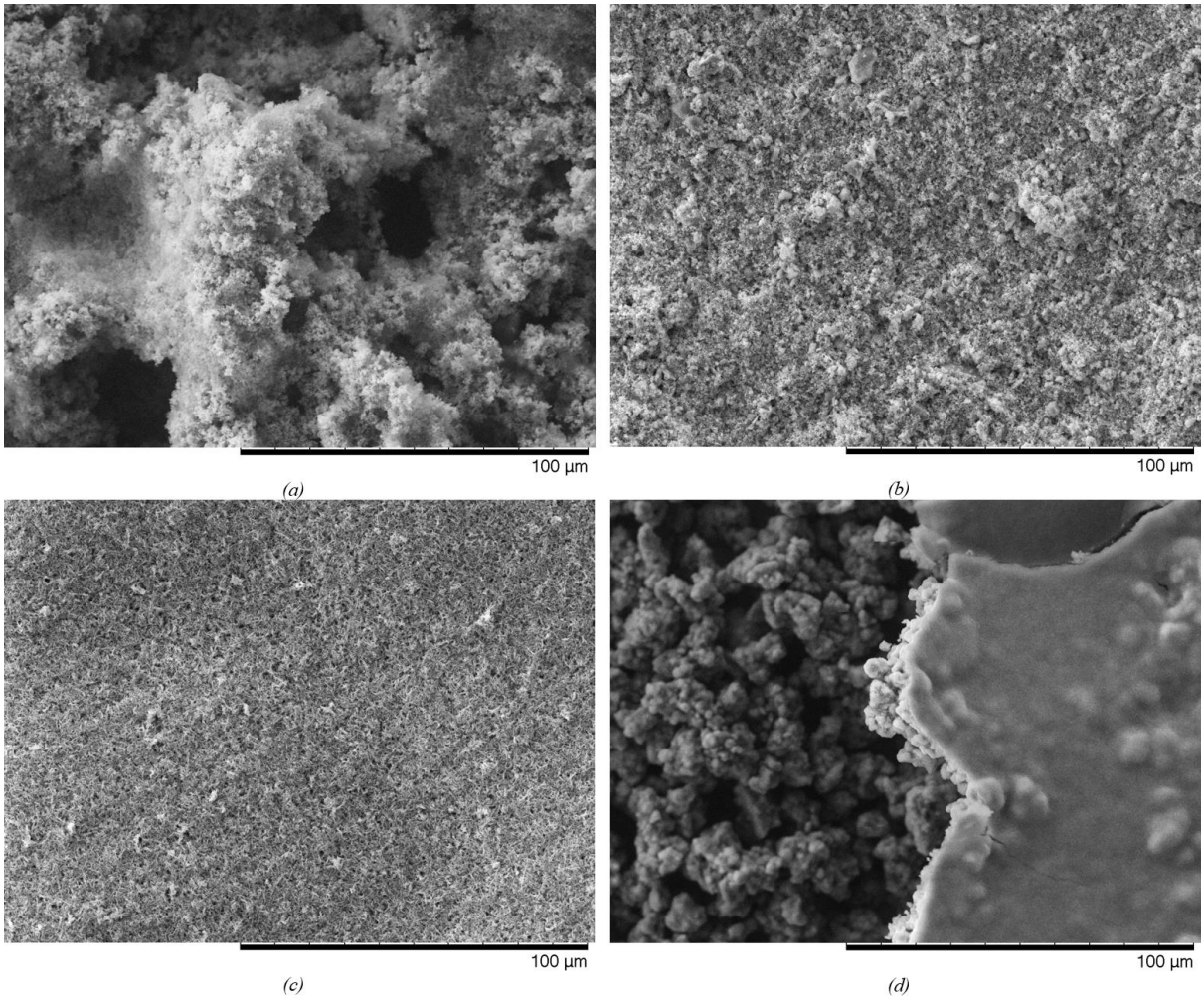

Figure 154, SEM micrographs of iron oxide powder layers of different types deposited on rail-steel substrates using drop deposition in aqueous suspensions a: magnetite, b: haematite, c: goethite, d: lepidocrocite

The mean COF of each of the samples tested with each oxide for the smaller contact sizes are given in Figure 156 for substrates deposited using suspensions in both water (left set) and isopropanol (right set). The mean COF of the oxides deposited via the water are 0.1 to 0.2 higher than those deposited via isopropanol, this is likely due to the increased roughness of the surfaces due to the oxidation during the exposure to water when the substrates were drying.

Table 14, Thicknesses and mass density of isopropanol deposited oxide layers. Goethite base layer thickness (A), average layer thickness (B), and average height of agglomerates

Layer Material	**Magnetite**		**Haematite**		**Goethite**		**Lepidocrocite**	
Density, $g.cm^{-2}$	0.87	0.79	1.31	1.53	1.34	1.44	1.01	0.92
Thickness, µm	0.9	0.8	5.6	5.8	A) 1.3, B) 3.8, C) 17.0	A) 1.0, B) 4.2, C) 17.0	3.5	3.6

The impact of the oxide layers on the samples is an almost doubling in mean COF from a control sample value of approximately 0.25 to around 0.5; and higher for the oxides deposited using water. As can be clearly seen in the isopropanol-deposited samples, there is no discernible difference

between the oxide types in their effect on COF other than the magnetite layer which is lower than that of the other oxides; however, this can be attributed to the less dense and thinner layer that was deposited on the surfaces. The SEM micrograph of the deposited oxide layer surface, Figure 155, shows that little oxide was left in the contact path after the runs. This suggests that oxide was pushed out of the contact path rather than being entrained within it.

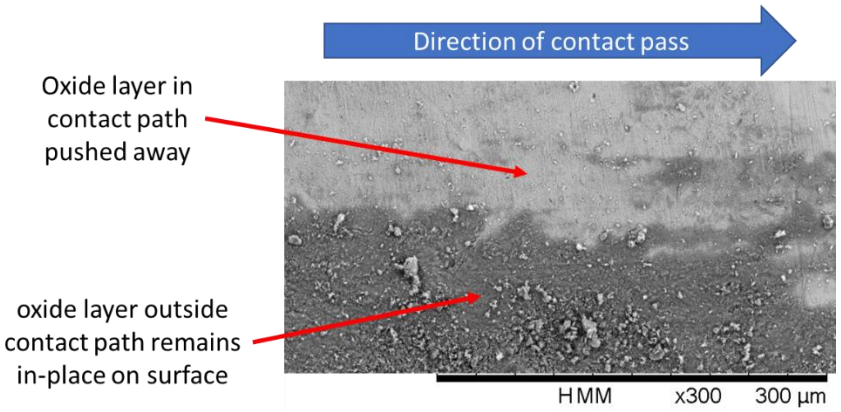

Figure 155, SEM micrograph of deposited oxide showing surfaces inside and outside the contact path after a single wet run

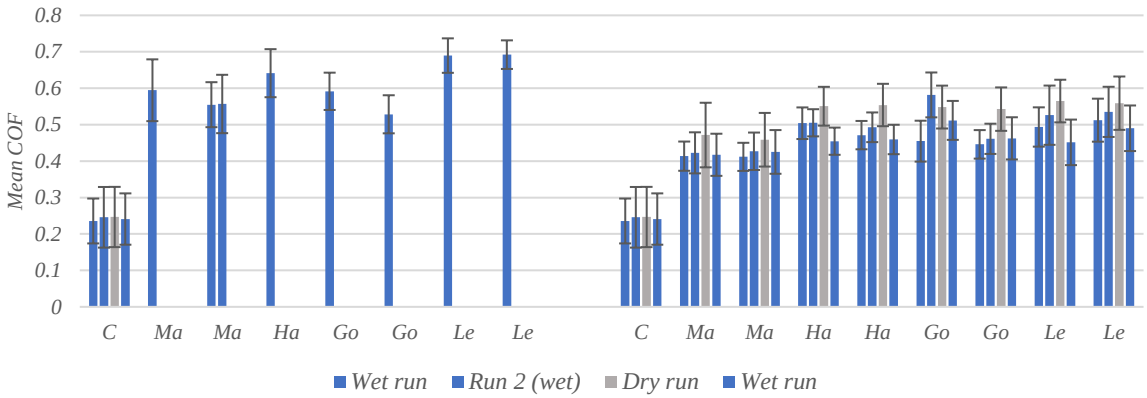

Figure 156, Mean COF of samples with deposited layers of different oxides, tested with the small-contact pin-on-flat testing. Left group: oxides deposited on substrate by distilled water; right group: oxides deposited on substrate in isopropanol suspension. C, control; Ma, magnetite; Ha, haematite; Go, goethite; Le, lepidocrocite. Error bars showing one standard deviation from mean. Each group of histograms represents multiple subsequent tests of a single sample

When the same experimental procedure was carried out with a larger contact, the same relationships between the oxides and increase in mean COF were observed as can be seen in Figure 157. The COF of these oxide layers using the larger contact geometry, similar to the tests observed with the synthesised oxides, were around 0.1 lower than the smaller geometry tests.

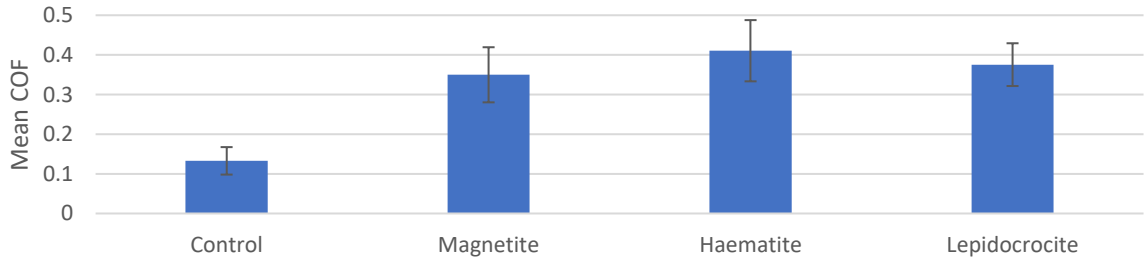

Figure 157, Mean COF of samples with isopropanol-suspension deposited layers of different oxides, tested with the large-contact pin-on-flat testing. Error bars showing one standard deviation from mean

8.2 SUROS testing

The SUROS experimental platform was used to explore oxide pastes of different types in rolling / sliding contacts. This was performed by testing oxides of magnetite, haematite, goethite, and lepidocrocite in various oxide content aqueous paste concentrations for the runs along with controls of dry and wet contacts. The grouped raw data of these runs are given in Figure 181 to Figure 186 in appendix D.

The pastes were applied in known oxide concentrations into the contact; however, due to drying in the contact and expulsion of material from the disc contact, the actual concentration of the pastes in the contact are unknown.

After the oxide paste being deposited was expended, the system was then allowed to dry out and the run ended when the COT increased rapidly to minimise damage to the discs. This drying out behaviour was shown to vary depending on the type of oxide tested and a compiled chart of these behaviours is given in Figure 158. Tests which explored water alone showed a slow increase of traction as the contact dried. Haematite and goethite pastes displayed a drop in COT whilst drying out. This behaviour was not noticed with magnetite which mostly mimicked the effect of water in its behaviour; however, there is a slight but insignificant drop towards the very end of the run when the sample is almost completely dry. Testing with the lepidocrocite pastes was problematic due to small quantities of powder available, this resulted in the drops of paste being less frequently applied to the contact and the surface almost drying out in-between application and thus shows sharp drops in the COT on multiple occasions of the run presented; a more extreme effect than that of the goethite or haematite pastes. When the oxide pastes had dried out completely, the COT returned to values comparable to the dry contact runs. This drying behaviour, which allowed for the exploration of oxide pastes of concentrations far higher than what was practical to deposit into the twin-disc contact directly, demonstrated that the proportion of water in the wheel / rail system with respect to the amount of oxides is of critical significance to levels of traction formed; lowest traction levels are experienced when the oxide content is very close to 100% but not completely dry.

The summary of the twin disc testing is given in Figure 159 through to Figure 164 showing the mean COT of the runs as well as the minima recorded when the oxides were in the process of drying out. Under the condition tested the dry contact control had a traction coefficient of around 0.28 and the water only having a traction coefficient of around 0.09. It is very clear from the results that all oxide pastes reduced the traction coefficient below that of water alone. Ultra-low adhesion was not achieved for the mean data of any run; however, all oxides except magnetite displayed minima values when they dried out within the <0.05 ultra-low adhesion range. Lepidocrocite experienced the lowest minima of 0.024. The results for haematite pastes are comparable to the values recorded by White and Lewis [50] for pastes of similar concentrations. The relationship that the higher the oxide concentration of the paste applied, the lower the COT was observed with haematite and magnetite; however, this is not clear with the goethite or lepidocrocite.

The difference between the mean COT and the minima experienced when drying out varies between the oxide types and concentrations. Magnetite experienced the lowest drop, falling only around 0.015 and similar to that of water (0.010). Goethite and haematite both experienced significant drops in COT of 0.026 and 0.029 respectively whilst lepidocrocite experienced the highest, falling by an average of 0.037. Lower concentrations such as the 29.7% goethite paste and smaller volumes of material which was noted when testing the 49.9% lepidocrocite oxide paste resulted in smaller drops in the coefficient of traction when drying out; this is likely caused by there being insufficient material to sufficiently cover the surfaces or form the low-traction surface conditions.

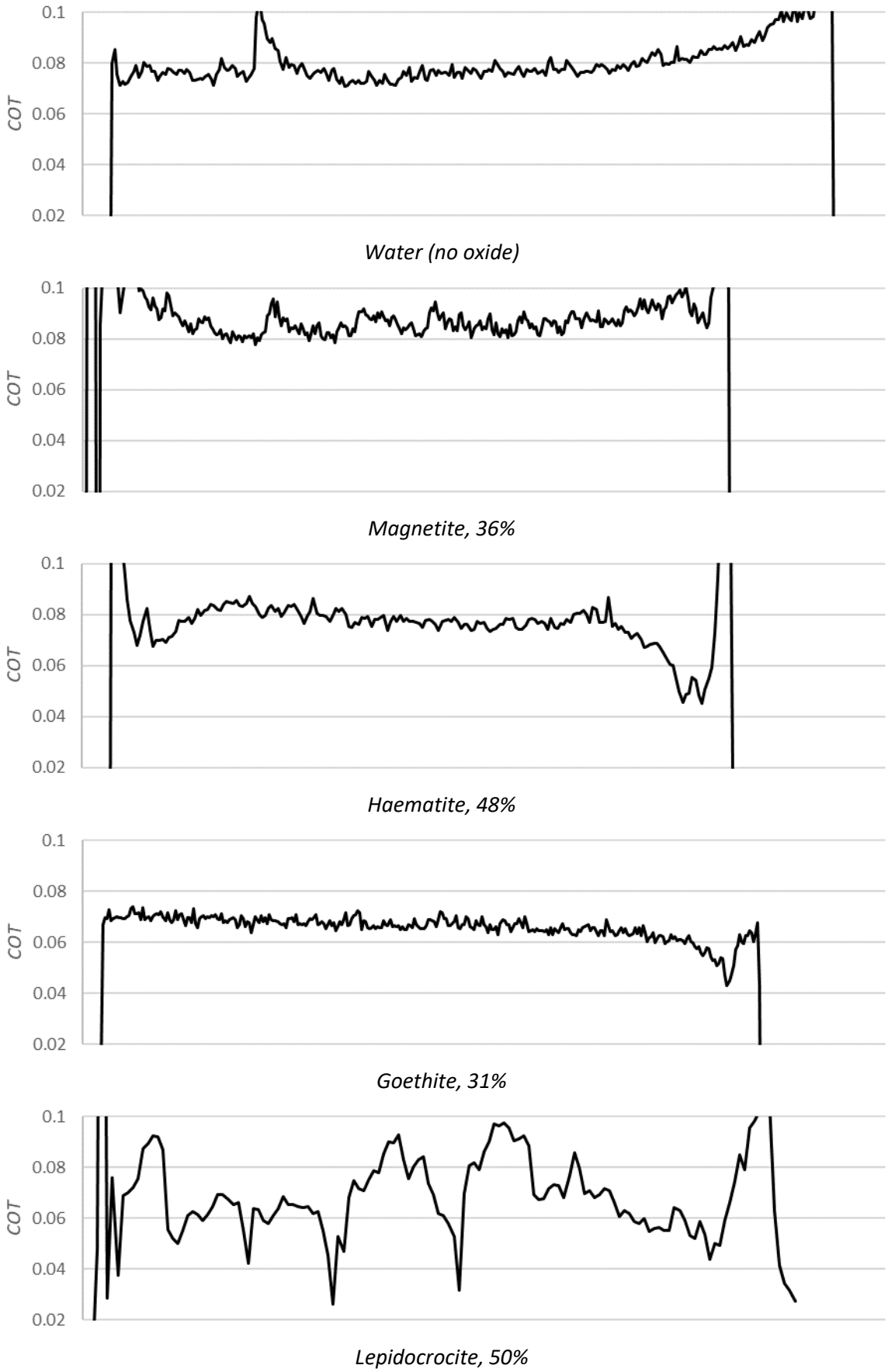

Figure 158, Comparison of traction behaviours of twin-disc experimental tests showing the effect of different oxide pastes as they dry out in the contact; COT is plotted against the number of cycles (x-axis for number of cycles is omitted for brevity)

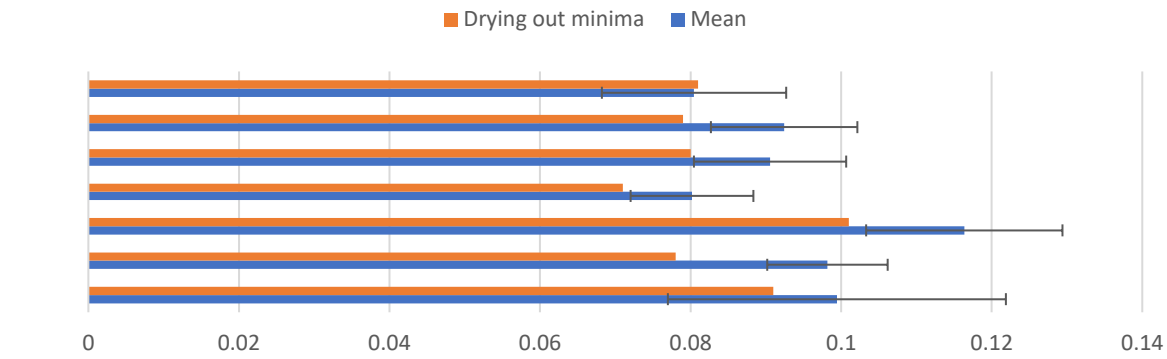

Figure 159, Mean and minima COTs of wet twin disc test runs. Error bars show one SD from mean

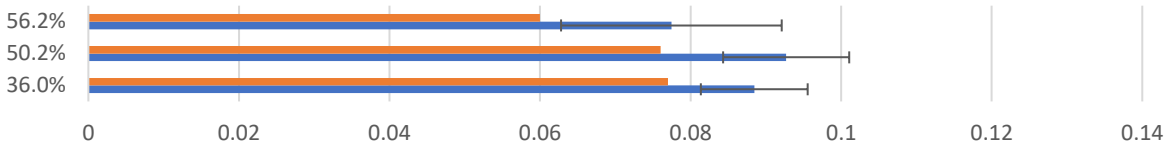

Figure 160, Mean and minima COTs of magnetite-water pastes twin-disc test runs. Error bars show one SD from mean

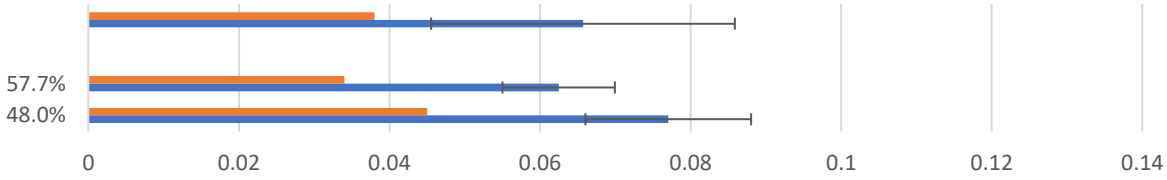

Figure 161, Mean and minima COTs of haematite-water pastes twin-disc test runs. Error bars show one SD from mean

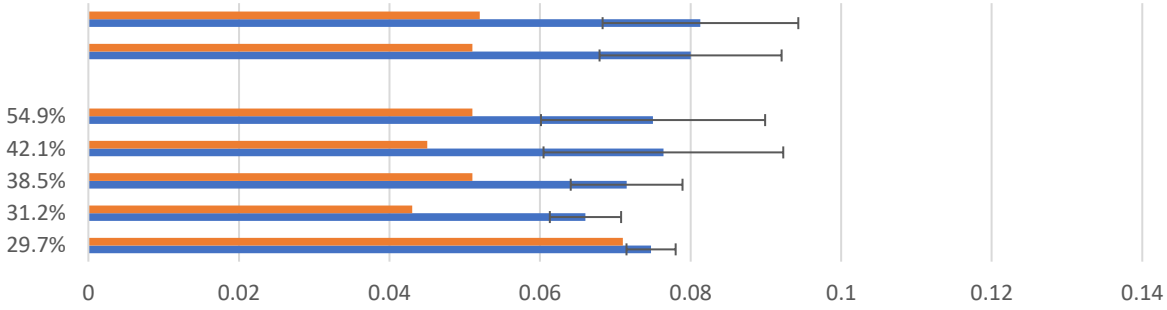

Figure 162, Mean and minima COTs of goethite-water pastes twin-disc test runs. Error bars show one SD from mean

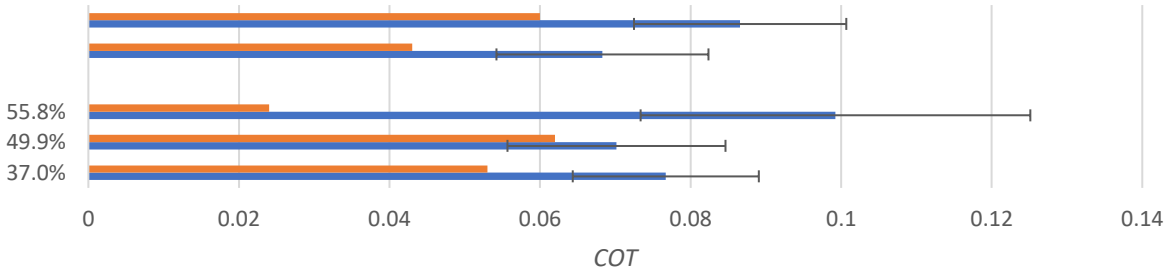

Figure 163, Mean and minima COTs of lepidocrocite-water pastes twin-disc test runs. Error bars show one SD from mean

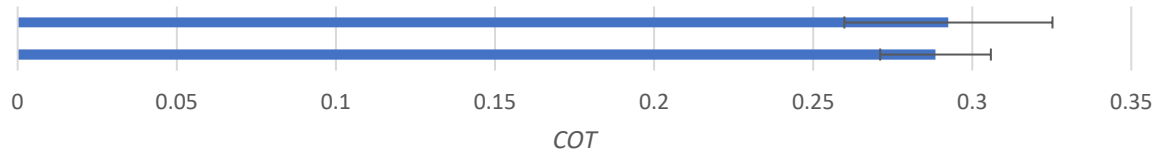

Figure 164, Mean COTs of dry twin-disc test runs. Error bars show one SD from mean

Low adhesion levels (<0.1) were achieved throughout most of the runs where there was an addition of liquid or paste into the twin-disc contact, including water alone; however, ultra-low adhesion levels were only achieved as the oxide pastes of haematite, goethite and lepidocrocite dried out and approached close to 100% oxide concentration. In section 7.2 it was revealed that the rheological yield stress of aqueous oxide pastes increase exponentially with their oxide concentration; therefore, as the oxide pastes dried out and their yield stresses increased, this may have enabled them to resist the initial shearing caused, become more entrained in the contact, and ultimately affected the traction more. The goethite pastes, with a much higher yield stress for the same oxide concentration, would be expected to give a greater reduction in traction by this reasoning whilst it exhibits a similar reduction in traction than haematite but this may be explained by the viscosity findings of the pastes shown in Figure 138 in section 7.2 where the goethite paste is shown to have a far higher viscosity than the other oxides; this infers that, whist the goethite paste may be more entrained in the contact, it requires a greater force to shear and therefore the traction force can be transferred more efficiently through the layer than a lower viscosity paste.

8.3 Full Scale Rig testing

Exploration of the different oxide pastes on the Full Scale Rig is important for this testing as it provides the most representative contact geometry to the true wheel / rail contact. This may be significant as the larger contact may allow for the pastes to become more entrained in the contact during operation.

50% oxide pastes of haematite and goethite were explored through this testing as well as a dry contact control and a water alone control. The procedure of rolling over the patches with an induced slip was cycled 20 times whilst the contact was drying out. Data was statistically analysed for runs 2, 6, 10, 14 and 18.

The individual run traction coefficients are given in Figure 165 and the overall averages given in Figure 166. The presence of water in the contact reduced the experienced traction coefficient from a dry level of 0.21 to a level of 0.18. Both haematite and goethite had the effect of increasing the traction coefficient to 0.22 and 0.25 respectively. The second run of the first haematite test experienced a low COT comparable to that of the wet contact, but this was not repeated in the second test.

Under the contact conditions of the Full Scale Rig, it is apparent that oxide in the contact increases traction rather than reducing it and as the contact dries out there is very little change in traction. This is likely caused by either the contact ploughing through the oxide or third-body abrasion in the contact. Goethite increased the COT higher than that of the haematite; the goethite paste suspension was particularly “messy” and appeared to remain in the contact better which possibly enabled the paste to be better entrained in the contact leading to the higher traction experienced. It should also be noted that the rig operates at relatively slow rolling and sliding velocities which, like the UMT testing, may not allow significant mechanisms mixed lubrication by the oxides to develop.

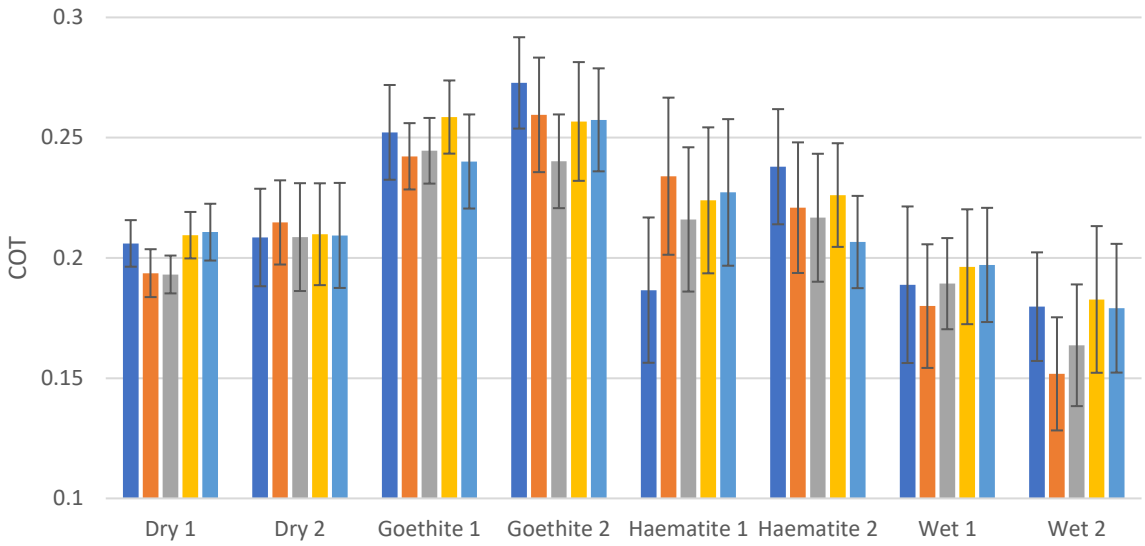

Figure 165, Mean traction coefficients of passes 2, 6, 10, 14 and 18 of Full Scale Rig testing of dry, wet, haematite paste, and goethite paste runs, Error bars showing one standard deviation from mean

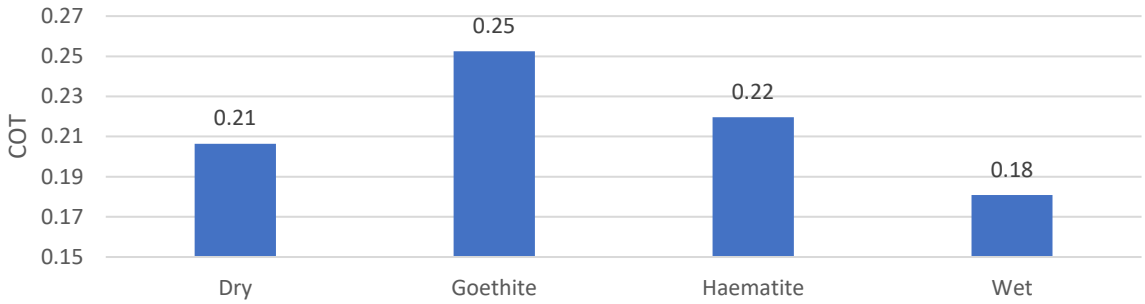

Figure 166, Average mean traction coefficients of Full Scale Rig tests of the contact modifications with dry, wet, haematite paste, and goethite paste

Unlike the SUROS twin-disc experimentation, levels of low adhesion were not achieved during this testing. There are many suspected reasons for this: firstly, once the oxide material was pushed in front of the contact path it would no longer be able to be re-entrained into the contact as the wheel would lift up and transverse the same section again making it impossible to maintain oxide on the contact surfaces; secondly, the rolling and sliding velocities of the rig are slow and may not have been able to get to a speed which would allow for the oxides to lubricate the surface effectively; and thirdly, the rig was unable to log the data for the first cycle resulting in little control over the concentration of oxide paste on the surface during the logged cycles as well as little ability to maintain the quantities of oxide pastes that may be required to observe the phenomena observed in the twin-disc testing.

8.4 Summary

The effectiveness of the novel pin-on-flat COF mapping experimental platform has been demonstrated in this work and provides useful insights into heterogeneous surfaces, as well as enabling single-pass tribo-data to be captured; it's potential as a useful technique extends much beyond the subject of railway tribology. The maps reveal that the COF varies across the oxidised railhead surfaces, displaying much increased resistance in the heavily oxides patches – suspected due to the higher surface roughness – and lower resistance where there has been less formation of oxides.

The COF maps, along with SEM micrographs of the debris present on the railhead surface, also show how the overall COF may be reduced by the presence of the oxides on rough surfaces by the mechanism of oxide-bridging in which rust builds up around areas of high roughness resulting in a smoother surface. The results also reveal that the surface created by this mechanism, which may result in lower friction, is fragile and rapidly worn away by mechanical action.

The general pattern observed with the low velocity sliding or rolling / sliding tests of the UMT and the FSR is that the more oxidation – whether synthesised or deposited – the higher the traction or friction coefficient. The main reasons surrounding this increase appear to be the increased surface roughness, ploughing of the contact through oxide layers, and potential third-body abrasive wear within the contact.

The powdered oxides appeared to interact with water in different ways and, when deposited on the substrate surfaces using distilled water, showed different layer structures. Deposited oxides on both the pin-on-flat testing and the FSR had the effect of increasing the friction and traction; thicker layers were shown give greater increases in friction with SEM imagery supporting that the layers were ploughed through on the UMT rather than being entrained within the sliding contact. Loose oxide was better retained on the surfaces of samples which underwent treatment to synthesised oxides than the deposited oxides suggesting that rougher substrate surfaces provide a better purchase for the oxide pastes than smooth contacts and increase entrainment of oxides within the contact.

Twin-disc testing showed a markable decrease in traction coefficient with the application of oxide pastes, resulting in values lower than what was seen with water. As the oxide pastes dried in the contact during the testing, the traction coefficients decreased towards their lowest level just before they had dried completely followed by a sharp increase in traction towards that of dry contact traction. The drop in traction as the pastes dried out varied between oxide types with haematite, goethite and lepidocrocite displaying a far more pronounced drop in levels than that of magnetite which was comparable to that of water alone. Higher concentration oxide pastes, when applied to the contact typically displayed lower COT values; however, due to material being squeezed through the contact, it was not possible to determine the actual concentration of the oxide pastes in the contact.

Ultra-low adhesion levels of less than 0.05 were achieved by oxide pastes of all types, during the twin-disc runs except for the magnetite pastes. The haematite pastes and goethite pastes were shown to have similar minimum COT levels which was initially unexpected due to the rheological testing of the pastes (section 7.2) which showed that goethite had a higher yield shear stress than the haematite at the same oxide content levels; however, this revealed that there is likely a second material property which impacts the traction modifying properties of the pastes which, in this case, appears to be the viscosity. These results support the hypotheses presented in section 4.2.4 and it is proposed that higher yield shear stresses increase the entrainment of material within the contact, but the traction-diminishing effects are reduced by higher viscosities.

Application of iron oxide pastes to the full-scale rig contact resulted in higher COT than the clean dry contact condition for both the iron oxide, haematite, and the iron oxide hydroxide, goethite. This result is likely due to the amount of oxide present on the surface of the rail being insufficient to cause any substantial degree of separation between the wheel and rail on the rig, yet the presence of the paste on the railhead may still have been present in the contact outside of the areas of direct contact between the wheel and rail; therefore increasing the COT due to the additional work of its shearing and wear between the wheel and rail.

Out of the three test platforms used, the twin-disc testing of the oxides resulted in the opposite effect on the COF / COT to the other platforms. The twin-disc creates a rolling-sliding contact which is the same type as the FSR and, as such, highlights the importance of higher rolling velocities in order to achieve the mechanisms by which low adhesion is caused by oxides and water. The result that higher rolling velocities are required implies that the mechanism of oxide-water induced low adhesion is due to a mixed micro elasto-hydrodynamic lubrication effect. The testing of the SUROS showed that, in addition to very high oxide concentration pastes being required, sufficient material was necessary to reduce traction to very low levels; this suggests that a thick solid shearing layer is likely and may act as a solid lubricant within the wheel / rail interface.

9 Discussion

Low adhesion and loss of traction in the wheel / rail system continues to be poorly understood, but this work contributes towards identifying how changeable environmental situations lead to undesirable surface conditions as well as some of the mechanisms by which traction may be lost due to various surface contaminants. Managing and understanding traction is of great importance to the railway industry for operations to run safer and more effectively; therefore, the work undertaken in this study may add value through:

- Consolidating and appraising scientific knowledge from the disciplines of process, chemical, materials, and mechanical engineering which has previously been largely unexplored when considering the wheel / rail interface
- Presenting physical and chemical relationships between railhead surface conditions and recent environmental conditions, including identifying trackside environmental condition trends
- Observations highlighting the importance of various oxide properties through tribo-testing
- Providing experimental test platforms for combined chemical, physical, and tribological analysis of oxides on the railhead

This chapter discusses outputs of this work, their significance, and practical implications of the findings. It is presented in two sections which underly the two areas of investigation in this work: subjects relating to the formation of low adhesion surface conditions, and those relating to the mechanisms of traction loss. Recommendation of future research areas is also given.

9.1 Low adhesion formation mechanisms

The railhead, being open to the trackside environment, presents a diverse and complex chemical system with many present chemical species.

Chemically active organic compounds on the railhead originate from two major sources: oils and greases, and leaves. These chemicals have been shown to possess the ability interact with the railhead surface in numerous ways including physical and chemical adsorption onto the surface to form thin molecular layers. Organometallic compounds such as ferrous- and ferric-soaps may also be formed as thicker layers which may build up on the railhead. Due to the wide variety of compounds present on and around the railhead surface, complex layers may build up on top of the railhead aided by the surface modifying properties of surfactant layers; incorporating larger molecules into a lattice providing for stronger and more robust layer structures.

Leaves present both a solid fibrous structure as well as chemically active substances within. Through the research, cutin in the plant cuticle and polyphenols (including tannins) within the plant cell vacuoles appear to be the most abundant sources of chemically active species within the leaves. Many of these reactive species within the leaves are ‘locked up’ either chemically – in the case of cutin – or physically, in the case of tannins in the cell vacuoles; however, mechanisms by which they may be released are possible and presented in the hypotheses given in section 4.1.2.

Two main forms of interaction between chemicals and the railhead surface are proposed in the hypotheses presented in sections 4.1.1 and 4.1.3, and the bonding mechanisms in the formation of complex leaf layers are given in hypotheses 4.1.2. These hypotheses were not explored further in this study; however, potential chemical species thought to be responsible for these processes are identified in this work. Further research exploring these hypotheses could be made by experimentation, with the omission or addition of the proposed chemical species, to observe their effects on boundary lubrication and / or leaf bonding strength.

Low adhesion events have been connected to times of the day where dew forms on the railhead surface. Results from the environmental monitoring campaigns undertaken in this work have revealed new trends in trackside conditions which largely occur on a daily basis; leading to the railhead temperature dipping below that of the environment dew-point temperature and resulting in condensation. A major component of the patterns observed is a disconnection between the railhead temperature and the environmental temperature due the bulk mass of the railhead causing a thermal lag of its temperature behind that of the environment and, during humid conditions, the dew-point. Local trackside features have been shown to influence these patterns in two ways: features that shade the track accentuate the thermal lag of the railhead; and vegetation surrounding the railhead greatly increase local humidity levels. Both effects lead to longer and more frequent drops of the railhead temperature below the dew-point and the findings of the environmental monitoring campaigns may be used to expand and improve upon adhesion level forecasting climate models.

Light rainfall and condensation / dew formation on the railhead lead to not only the characteristic conditions of low adhesion events, whereby a very slight amount of water is present on the railhead, but also the conditioning of the railhead surface through oxidation to form surfaces which can produce low adhesion. Surface analysis of the railhead through XRD identified nine compounds, more than have been previously detected through XRD of the railhead surface. Two reasons which allowed for the detection of more oxide types are that: firstly, through sampling during different environmental conditions as well as in different locations, a wider variety of surface conditions and oxides were present; and secondly, ex-situ analysis of the samples allowed for longer and higher resolution scans enabling the detection of trace compounds and those without strong XRD spectra.

Hypotheses 4.1.4 proposes that drier conditions lead to the formation of more iron oxide compounds and wet environments lead to the formation of iron oxide-hydroxide compounds. This hypothesis is largely supported by the railhead analysis where the wet and humid conditions of QRTC in the UK produced swabs with large signals for lepidocrocite whereas swabs taken from British Columbia during dry conditions show very little presence of iron oxide-hydroxide, but still display the presence of iron oxide components. Controlled synthesis of the oxides in the laboratory was only able to generate surfaces with both iron oxides and iron oxide-hydroxides; however, the mechanical action of tribo-testing effectively removed the iron oxide-hydroxides preferentially. This suggests that iron oxides and iron oxide-hydroxides are synthesised simultaneously on the railhead and that dry railhead conditions merely display products of past oxidation remaining after being worn down by train passes. Since low adhesion due to oxides and water (the wet-rail phenomena) appears to be most problematic during the first trains of the day, it can be inferred that the problematic fraction of oxides are the loose oxides on the railhead: the iron oxide-hydroxides. The distinct discovery of wüstite on the railhead at QRTC during a morning where the conditions were reported to be causing very poor traction by the train driver was unexpected. Its appearance suggests that its behaviour on the railhead is like that of the loose iron oxide-hydroxides and itself may lead to low adhesion conditions. Due to the scope of this work, a very limited sample set of locations and times were possible to be analysed; however, the new knowledge of patterns in trackside conditions and oxide composition of the railhead surface, brought by the combined analysis of environmental conditions and chemical composition of the railhead surface through the use of external XRD profiling, is significant and justifies more extensive research.

9.2 Traction loss mechanisms

Three testing platforms were used to evaluate tribo-properties: the UMT, a sliding-only pin on flat tester; the SUROS, a twin-disc rolling-sliding tester; and the Full Scale Rig, a rolling-sliding full size

contact tester. These differed by contact mechanism between rolling-sliding and sliding-only, contact size, and speed. The UMT pin-on-flat testing demonstrated a novel analysis technique developed in this work, which enables the COF over a surface to be mapped onto visual surface images. Examples of this visualisation and it's clarity in identifying frictional effects of surface features can be seen in Figure 145 and Figure 150. This technique has clear applications beyond this project in the broader fields of surface analysis and tribology; however, in this project it allowed for distinction between tribological effects within and outside-of heavily oxidised areas on the surfaces of substrates as well as enabling a statistically significant amount of data to be determined from single-path transverses of the substrate surface.

Influence of oxides on the railhead surface was the primary focus of tribological analysis for this work. Boundary lubrication, presented in hypotheses section 4.2.1, is likely to have been the most likely form of contact due to the high contact pressures involved. Applying water to clean surfaces on all the testing platforms, regardless of sliding velocity, reduced the COF and COT showing that water does act as a boundary lubricant on the surfaces; this, however, was insufficient to produce friction or traction levels in the ultra-low adhesion range. The presence of oxide on the surface of the metal may have reduced the coefficient of friction due to less steel-steel contact; however, in section 8.1.1 it is seen that even slight oxidation of the surface increases the COF and, as a result, the friction increasing effects of higher surface roughness and / or abrasive three body wear associated with the formation of iron oxides are likely to outweigh any friction loss resulting from this mechanism.

If traction is not capable of being reduced by boundary lubrication alone, alternative mechanisms which may account for the loss of traction involve separation, in part or in full, of the contact surfaces transmitting the forces through the contact. Hypotheses section 4.2.3 postulates how the viscosity of a lubricating liquid film, whether that be water or a paste slurry, may decrease the coefficient of friction between the wheel and rail. Unfortunately, due to the slow operating speed of the UMT and FSR rig tests, the sliding velocities were too low for any noticeable effect. In the twin-disc testing, a reduction in COT was observed with an increasing concentration of oxides in the paste applied to the contacts, supporting that the higher the viscosity of an applied fluid, the lower the traction.

An issue with the hypotheses regarding enhanced viscosity liquids given in section 4.3.2 regarding oxide pastes, is that it is not clear within the twin-disc contact whether the material is a liquid or a solid layer of paste due to the unknown water or solid content or properties of the solid/liquid mixtures under the compression within the wheel / rail contact. The hypotheses in section 4.2.2, presents the oxide layer as a solid body which shears under the wheel preferentially to transmitting the traction force between the wheel and rail. Results of the deposited oxides on the sliding-only tribo-tests given in section 8.1.2, revealed that the layer was pushed away from the contact rather than being entrained within the contact resulting in an increase in friction with the thickness of the layer deposited. Some entrainment of oxides within the sliding contact was, however, observed on the synthesised oxide layers in the heavily oxidised areas suggesting that the roughness of the surfaces caused by oxidation increases entrainment of the oxide layers into the contact. The oxides are however, shown to be entrained to some extent in rolling-sliding contacts. A reduction of COT and the presence of some solid layer can be seen on the surface of the twin-discs during testing with oxides when compared to water alone.

Pastes composed of highly concentrated suspensions of fine solid particles, such that of fine iron oxides, display the rheological properties of Bingham-plastic fluids. Materials with such properties act as a rigid body at low stresses – below the yield stress – but flow as a viscous fluid under high

stress. The significance of this material property, which led to the development of the hypotheses presented in section 4.2.4, is that the oxide / debris pastes may behave like both solids and fluids. We can see from the results presented in section 7.2 that the oxide pastes do exhibit a yield shear stress characteristic of Bingham-plastic materials. Iron oxide-hydroxides were shown to exhibit significantly higher yield stresses for their oxide concentration than the iron oxides, likely due to their greater bonding potential with the water molecules. Significantly higher yield stresses were also observed with more irregular and angular particle sizes of haematite. The viscosity of the pastes was shown to be largely the same between the pastes with the exception of the goethite powder which exhibits viscosities around a magnitude higher than that of the other materials for pastes of the same solid concentration. The significance of theses parameters, are:

- High yield shear stresses give the material an ability to resist flow when the wheel rolls onto them, allowing them to enter the contact.
- Low viscosities reduce the force capable of being transmitted through the layer and therefore reduce the force transmitted between the wheel and rail.

Currently, oxide pastes are postulated to produce 'stable low shear pastes' in the contact which reduce the traction coefficient; however, the findings of this work suggest that the easily sheared layers may only be half of the mechanism of traction loss caused by these oxides. In a study which investigated iron oxide pastes under pressures comparable to that of the wheel rail contact [55] a stick-slip behaviour is observed which is characteristic of Bingham-plastic materials which build up stress in them until reaching their yield shear stress after which stress is released through deformation until the stress drops below that of the yield shear stress.

The twin-disc testing showed that the least effective oxide pastes at reducing the COT was pastes of magnetite. This may be explained by its relatively low yield shear stress causing low entrainment in the contact and moderate viscosity meaning that any paste that is present within the contact still transmits reasonable force between the wheel and rail during shearing. The haematite powder pastes tested have equivalent yield shear stress as the magnetite at the same solid concentration and therefore will likely be entrained within the contact to a similar degree; however, with a lower viscosity, the paste in the contact is not capable of transferring as much of the force between the wheel and rail during shearing leading to a lower COT. Lepidocrocite and goethite both have higher yield shear stresses and will be entrained more within the contact as a result. Because of this, lepidocrocite exhibited the lowest minimum COT of the group at only 0.02; however, goethite exhibited minimum COT values higher on average than that of the haematite which is likely due to its much higher viscosity causing the force to be effectively transmitted through the contact even with a high degree of paste entrainment.

The twin-disc test results, in combination with the rheological testing, supported the hypothesis given in section 4.2.4 well. It can be inferred from this research that aqueous material pastes capable of causing the lowest adhesion are those which have high yield stresses, enabling them to enter into the wheel / rail contact; and low viscosities, capable of shearing without transmitting force to the surfaces within the contact. The result concerning goethite pastes also shows great commercial potential for the development of friction modifiers as it shows how the traction coefficient may be controlled by high yield shear stress materials, enabling them to enter the contact more effectively, but maintain moderate COT values due to its high viscosity. Friction modifiers displaying these properties would both enable the control of adhesion levels but also provide for a degree of separation of the wheel and rail surfaces; reducing wear and potentially forming a less

damaging, yet less effective, alternative to sanding. The search for materials bearing such qualities is therefore a highly recommended cause of further research in this area.

The rheological tests concerning different haematite powders revealed that particle shape and size have significant effects on the yield shear stress and viscosity of the pastes produced; the more crystalline and angular particle shapes produced much higher yield shear stresses. These powders were not explored in the twin-disc tribo-testing due to very little material available after the rheological testing; however, testing of such materials to characterise the effects of particle shape and size in the wheel / rail interface would be useful directions for future research.

The amount of oxide used in this testing is high when compared to the amounts present on the railhead, therefore providing the material to allow for more stable films to develop. Whilst capable of varying significantly over a short distance, the surface coverage of oxides on the railhead is occasionally not insignificant, as shown in Figure 84, but may only be able to form much thinner films than what is observed during the tribo-testing of this work; as a result the films may collapse and adhesion recover more easily after slip, as described in hypotheses section 4.2.4. This may explain why sustained low adhesion due to the wet rail phenomena is rare and difficult to replicate.

10 Conclusions

10.1 Thesis conclusions

The work in this thesis has successfully led towards greater understanding of how environmental conditions effect both the chemical development of the railhead surface as well as the conditions capable of resulting in low adhesion conditions. The study also proposes a new mechanism of traction loss, made possible due to the complex rheological behaviour of oxide or debris pastes, supported by experimental findings in this research.

A diverse and complex variation of compounds capable of interacting with the railhead and themselves in numerous ways have been found to be present in the trackside environment as well as on the railhead itself. 8 different iron compounds carbon were discovered from track swabs in this work, a greater variety than what has previously been identified on the railhead, which are shown to vary greatly with environment conditions and location.

Daily variation in environmental conditions leads to a lag in the railhead temperature behind that of the environment, particularly in shaded areas, occasionally causing it to fall below that of the dew point temperature and result in condensation on the railhead surface.

Conditions associated with wet and humid environments developed iron oxide-hydroxides on the railhead surface in addition to iron oxides. Dry conditions were shown to have iron oxides present on the surfaces of the railhead likely due to the wear of the iron oxide-hydroxides from the surface by train passes. The presence of iron oxide-hydroxides and wüstite, as well as dew on the railhead, were linked to low adhesion conditions through the testimony of a train driver in combination with environmental and railhead chemistry analysis.

Three testing platforms were used to explore the tribo-properties of iron oxides: a pin-on-flat, a twin-disc, and a Full Scale Rig. The twin-disc rig was most suitable for simulating low adhesion conditions from iron oxide pastes; however, testing on the UMT allowed for closer analysis of traction loss mechanisms but was largely unable to allow for entrainment of oxide pastes within the contact due to its pure sliding contact mode.

A newly proposed mechanism of traction loss concerning debris and oxides on the railhead is supported by the combination of rheological testing of the oxides and twin-disc tribo-testing. Oxide pastes were shown to exhibit the properties of Bingham-plastic fluids with two parameters significant to their influence on wheel / rail traction: yield shear stress and viscosity. Pastes were shown to exhibit higher viscosities and higher yield shear stresses with increasing solid concentration.

Materials with higher yield shear stresses were better entrained within the rolling-sliding twin disc contact. Materials with higher viscosities transmitted force through their layer in the contact more effectively. Pastes capable of achieving lowest traction coefficients had high yield shear stresses and low viscosities. It may be possible to control the traction coefficient of the wheel / rail contact to reasonable levels using pastes with high yield shear stresses, for good contact entrainment, and high viscosities allowing highly efficient force transmission through them during shearing.

10.2 Future work

The work presented in this thesis affords opportunities for a number of avenues of further research and development of the ideas and concepts given, including:

- More extensive combined environmental monitoring and railhead analysis campaigns, preferably on live operational track, to enable the identification of more relationships between environmental patterns and railhead conditions.
- Exploration of a wider variety of oxide / debris pastes using rheometric analysis and twin-disc tribo-testing, including those with distinctly different particle shape and size characteristics. Such testing would allow for better understanding of their behaviours in the wheel / rail contact in addition to the search for and appraisal of high yield shear stress - high viscosity pastes which potentially may be used to control traction to acceptable levels.
- Investigation of the synthesis of railhead surface conditions under a broader range of environmental influence factors including introducing other contaminants, such as salt or oils, which may give different rusting or composition profiles.

10.3 Publications

R. Kempka, R. Falconer, D. Gutsulyak, R. Lewis, “Effects of oxide and water on friction of rail steel – new test method and friction mapping”, in *Contact Mechanics (CM2018)*, Delft, 2018.

D.T. Eadie, H. Harrison, R. Kempka, R. Lewis, A. Keylin, N. Wilson, “Field assessment of friction and creepage with a new tribometer”, in *Contact Mechanics (CM2018)*, Delft, 2018.

11 References

[1] Network Rail Limited, “Annual report and accounts 2015,” Network Rail, 2015.

[2] Network Rail Limited, “Long Term Planning Process: Freight Market Study,” Network Rail, 2013.

[3] Network Rail Limited, “Technical Strategy 2013,” Network Rail, 2013.

[4] Network Rail Limited, “The value and importance of rail freight,” Network Rail, 2013.

[5] R. Lewis and R. Dwyer-Joyce, “Industrial Lubrication Practice - Wheel/Rail Tribology,” in *STLE Handbook of Lubrication and Tribology - Volume 1*, CRC Press, 2006.

[6] Network Rail, “CP6 Enhancements Delivery Plan,” Network Rail, 2019.

[7] R. Lewis and U. Olofsson, “Basic tribology of the wheel-rail contact,” in *Wheel-Rail Interface Handbook*, CRC Press, 2009, pp. 34-57.

[8] W. Wang, T. Liu, H. Wang, Q. Liu, M. Zhu and X. Jin, “Influence of friction modifiers on improving adhesion and surface damage of wheel/rail under low adhesion conditions,” *Tribology International,* vol. 75, pp. 16-23, 2014.

[9] C R Fulford Associates, “CRF04002: Review of Low Adhesion Research,” RSSB, 2004.

[10] D. Fletcher and S. Lewis, “Creep curve measurement to support wear and adhesion modelling, using a continuously variable creep twin disc machine,” *Wear,* Vols. 298-299, pp. 57-65, 2013.

[11] G. Vasic, F. Franklin, A. Kapoor and V. Lucanin, “Laboratory simulation of low-adhesion leaf film on rail steel,” *Int. J. Surface Science and Engineering,* vol. 2, no. 1/2, pp. 84-97, 2008.

[12] A. Meierhofer, C. Hardwick, R. Lewis, K. Six and P. Dietmaier, “Third body layer-experimental results and a model describing its influence on the traction coefficient,” *Wear,* vol. 314, pp. 148-154, 2014.

[13] S. Descartes, C. Desrayaud, E. Niccolini and Y. Berthier, “Presence and role of the third body in a wheel-rail contact,” *Wear,* vol. 258, pp. 1081-1090, 2005.

[14] O. Arias-Cuevas, “Disseration, Low Adhesion in the Wheel-Rail Contact: Investigations towards a bettwe understanding of the problem and its possible countermeasures,” Delft University of Technology, Delft, 2010.

[15] Y. Berthier, S. Descartes, M. Busquet, E. Niccolini, C. Desrayaud and L. Baillet, “The role and effects of the third body in the wheel-rail interaction,” *Fatigue and Fracture of Engineering Materials and Structures,* vol. 27, pp. 423-436, 2004.

[16] C. Hardwick, S. Lewis and R. Lewis, “The effect of friction modifiers on wheel/ rail isolation at low axle loads,” *Proceedings of the Institution of Mechanical Engineers, Part F,* vol. 228, no. 7, pp. 768-783, 2013.

[17] Y. Berthier, S. Descartes, M. Busquet, E. Niccolini, C. Desrayaud, L. Balillet and M. Baietto-Dubourg, “The role and effects of the third body in the wheel-rail interaction,” *Fatigue & Fractrue of Engineering Materials & Structures,* vol. 27, pp. 423-436, 2003.

[18] R. Aghababaei, “On the origins of third-body particle formation during adhesive wear,” *Wear,* Vols. 426-427, pp. 1076-1081, 2019.

[19] C. B. Jan, E. Gucciardi and S. Cavallaro, “Principles of lubrication,” in *Biolubricants; Science and technology*, Cambridge, Woodhead Publishing Limited, 2013, pp. 10-23.

[20] W. Wang, H. Wang, H. Wang, J. Gu, Q. Liu, M. Zhu and X. Jin, “Sub-scale simulation and measurement of railroad wheel/rail adhesion under dry and wet conditions,” *Wear,* vol. 302, pp. 1461-1467, 2013.

[21] B. Bhushan, “Fluid Film Lubrication,” in *Introduction to Tribology*, New York, John Wiley & Sons, 2002, pp. 423-532.

[22] H. Chen, M. Ishida, A. Namura, K.-S. Baek, T. Nakahara, B. Leban and M. Pau, “Estimation of the wheel/rail adhesion coefficient under wet condition with measured boundary friction coefficient and real contact area,” *Wear,* vol. 271, pp. 32-39, 2011.

[23] H. Chen, T. Ban, M. Ishida and T. Nakahara, “Adhesion between rail / wheel under water lubricated contact,” *Wear,* vol. 253, pp. 75-81, 2002.

[24] J. Williams, “Boundary Lubrication and Friction,” in *Engineering Tribology*, Cambridge, Cambridge University Press, 2005, p. Chapter 9.

[25] K. Six, “Physical processes in wheel-rail contact and its implication on vehicle-track interaction,” *Vehicle System Dynamics: International Journal of Vehicle Mechanics and Mobility,* vol. 53, pp. 635-650, 2014.

[26] M. Masjedi and M. Khonsari, “Theoretical and experimental investigation of traction coefficient in line-contact EHL of rough surfaces,” *Tribology International,* vol. 70, pp. 179-189, 2014.

[27] M. R. Tyagi and A. Sethuraamiah, “Asperity level conformity in partial EHL Part I: its characterization,” *Wear,* vol. 197, pp. 89-97, 1996.

[28] M. R. Tyagi and A. Sethuramiah, “Asperity level conformity in partial EHL Part II - Its influence in lubrication,” *Wear,* vol. 197, pp. 98-104, 1996.

[29] X. Jin, W. Zhang and J. Zeng, “Adhesion experiment on a wheel-rail system and its numerical analysis,” *Proceedings of the IMechE, Part J,* vol. 218, no. 1, pp. 293-303, 2004.

[30] C. Hardwick, R. Lewis and D. Eadie, “Wheel and rail wear-Understanding the effects of water and grease,” *Wear,* vol. 314, pp. 198-204, 2013.

[31] H. Chen, T. Ban, M. Ishida and T. Nakahara, “Experimental investigation of influential flactors on adhesion between wheel and rail under wet conditions,” *Wear,* vol. 265, pp. 1504-1511, 2008.

[32] T. Ohyama and H. Maruyama, “Traction and slip at high rolling speeds-some experiments under dry friction and water lubrication,” *Proceedings of the International Symposium on Contact Mechanics and Wear of Rail/Wheel Systems,* pp. 395-418, 1982.

[33] RSSB, “T1077: Modelling & quantifying the influence of water on wheel/rail adhesion levels,” RSSB, 2015.

[34] T. Beagley, I. McEwen and C. Prichard, “Wheel/Rail adhesion - boundary lubrication by oily fluids,” *Wear,* vol. 31, pp. 77-88, 1975.

[35] P. Cann, “The "leaves on the line" problem - a study of leaf residue film formation and lubricity under laboratory test conditions,” *Tribology Letters,* vol. 24, no. 2, pp. 151-158, 2006.

[36] E. Gallardo-Hernandez and R. Lewis, “Twin disc assessment of wheel/rail adhesion,” *Wear,* vol. 265, pp. 1309-1316, 2008.

[37] Z. Li, O. Arias-Cuevas, R. Lewis and E. Gallardo-Hernández, “Rolling-Sliding Laboratory Tests of Friction Modifiers in Leaf Contaminated Wheel-Rail Contacts,” *Tribology Letters,* vol. 33, pp. 97-109, 2009.

[38] W. Poole, “Characteristics of Railhead Leaf Contamination Summary Report,” RSSB, 2007.

[39] O. Arias-Cuevas, Z. Li, R. Lewis and E. Gallardo-Hernándes, “Laboratory investiagion of some sanding parameters to improve the adhesion in leaf-contaminated wheel-rail contacts,” *Proceedings of the Institute of Mechanical Engineers, Part F: J.,* vol. 224, pp. 139-157, 2010.

[40] Y. Zhu, U. Olofsson and R. Nilsson, “A field test study of leaf contamination on railhead surfaces,” *Submitted to the first International conference on Railway Technology,* 2012.

[41] K. Suberkropp, G. Godshalk and M. Klug, “Changes in the Chemical Composition of Leaves During Processing in a Woodland Stream,” *Ecology,* vol. 57, no. 4, pp. 720-727, 1976.

[42] K. Ishizaka, S. R. Lewis and R. Lewis, “The low adhesion problem due to leaf contamination in the wheel/rail contact: Bonding and low adhesion mechanisms,” *Wear,* Vols. 378-379, pp. 183-197, 2017.

[43] P. Cann, “The "leaves on the line" problem - a study of leaf residue film formation and lubricity under laboratory test conditions,” *Tribology Letters,* vol. 24, pp. 151-158, 2006.

[44] K. Ishizaka, S. R. Lewis, D. Hammond and R. Lewis, “Investigation of leaf chemistry and leaf layer: low adhesion mechanism,” in *Contact Mechanics (CM2018)*, Delft, 2018.

[45] K. BoHoon, M. Ramoun and P. B. Aswath, “Properties of tribofilms formed with ashless dithiophosphate and zinc dialkyl dithiophosphate under extreme pressure conditions,” *Wear,* vol. 268, pp. 579-591, 2010.

[46] J. Suzumura, Y. Sone, A. Ishizaki, D. Yamashita, Y. Nakajima and M. Ishida, “In situ X-ray analytical study on the alteration process of iron oxide layers at the railhead surface while under railway traffic,” *Wear,* vol. 271, pp. 47-53, 2011.

[47] Y. Sone, J. Suzumura, T. Ban, F. Aoki and M. Ishida, “Possibility of in situ spectroscopic analysis

for iron rust on the running band of rail," *Wear,* vol. 265, pp. 1396-1401, 2008.

[48] P. Dillmann, F. Mazaudier and S. Hœrlé, "Advances in understanding atmospheric corrosion of iron. I. Rust characterisation of ancient ferrous artefacts exposed to indoor atmospheric corrosion," *Corrosion Science,* vol. 46, pp. 1401-1429, 2004.

[49] F. Genuzio, A. Sala, T. Schmidt, D. Menzel and H. J. Freund, "Phase transformations in thin iron oxide films: Spectromicroscopic study of velocity and shape of the reaction fronts," *Surface Science,* vol. 648, pp. 177-187, 2015.

[50] B. White and R. Lewis, "Simulation and understanding the wet-rail phenomenon using twin disc testing," *Tribology International,* vol. 136, pp. 475-486, 2019.

[51] Y. Zhu, Y. Lyu and U. Olofsson, "Mapping the friction between railway wheels and rails focusing on environmental conditions," *Wear,* Vols. 324-325, pp. 122-128, 2015.

[52] Y. Zhu, X. Chen, W. Wang and H. Yang, "A study on iron oxides and surface roughness in dry and wet wheel - rail contacts," *Wear,* Vols. 328-329, pp. 241-248, 2015.

[53] T. Nakahara, K.-S. Baek, H. Chen and M. Ishida, "Relationship between surface oxide layer and transient traction characteristics for two steel rollers under unlubricated and water lubricated conditions," *Wear,* vol. 271, pp. 25-31, 2011.

[54] B. White, P. Laity, C. Holland, K. Six, G. Trummer and R. Lewis, "Iron oxides and water paste rheology and its effect on low adhesion in the wheel/rail interface," in *Contact Mechanics (CM2018)*, Delft, 2018.

[55] L. Buckley-Johnstone, G. Trummer, A. Voltr, A. Meierhofer, K. Six, D. Fletcher and R. Lewis, "Assessing the impact of small amounts of water and iron oxides on adhesion in the wheel/rail interface using High Pressure Torsion testing," in *Contact Mechanics (CM2018)*, Delft, 2018.

[56] Y. Lyu, Y. Zhu and U. Olofsson, "Wear between wheel and rail: A pin-on-disc study of environmental conditions and iron oxides," *Wear,* Vols. 328-329, pp. 277-285, 2015.

[57] S. Abbasi, U. Olofsson, Y. Zhu and U. Sellgren, "Pin-on-disc study of the effects of railway friction modifiers on airborne wear particles from wheel-rail contacts," *Tribology International,* vol. 60, pp. 136-139, 2013.

[58] Y. Zhu, U. Olofsson and K. Persson, "Investigation of factors influencing wheel-rail adhesion using a mini-traction machine," *Wear,* Vols. 292-293, pp. 218-231, 2012.

[59] R. Galas, D. Kvarda, M. Omasta, I. Krupka and M. Hartl, "The role of consituents contained in water-based friction modifiers for top-of-rail application," *Tribology International,* vol. 117, pp. 87-97, 2018.

[60] Y. Zhu, U. Olofsson and K. Persson, "Investigation of factors influencing wheel-rail adhesion using a mini-traction machine," *Wear,* Vols. 292-293, pp. 218-231, 2012.

[61] M. Osmasta, M. Machatka, D. Smejkal, M. Hartl and I. Křupka, "Influence of sanding parameters on adhesion recovery in contaminated wheel-rail contact," *Wear,* Vols. 322-323,

pp. 218-225, 2015.

[62] S. Lewis, R. Lewis, G. Evans and L. Buckley-Johnstone, “Assesment of railway curve lubricant performance using a twin-disc tester,” *Wear,* vol. 314, pp. 105-212, 2014.

[63] M. D. Evans, R. Lewis, C. Hardwick, A. Meierhofer and K. Six, “High Pressure Torsion testing of the Wheel/Rail Interface,” *Contact Mechanics: Conference Paper,* Vols. 10th International Conference on Contact Mechanics, CM2015, 2015.

[64] L. Buckley-Johnstone, G. Trummer, P. Voltr, A. Meierhofer, K. Six, D. Fletcher and R. Lewis, “Assessing the impact of small amounts of water and iron oxides on adhesion in the wheel/rail interface using High Pressure Torsion testing,” *Tribology International,* vol. 135, pp. 55-64, 2019.

[65] X. S. Jin, W. H. Zhang, J. Zeng, Z. R. Zhou, Q. Y. Liu and Z. F. Wen, “Adhesion experiment on a wheel/rail system and its numerical analysis,” *Proc. Instn Mech. Engrs,* vol. 218, pp. 293-303, 2003.

[66] M. Burstow, “Rolling Contact Fatigue Laboratory Testing - AEATR-ES-2004-907,” RSSB, Derby, 2004.

[67] S. Lewis, D. Fletcher, A. Beagles, K. Ishizaka, L. Buckley-Johnstone, B. White, M. Harmon, C. Grigson, H. Brunskill, L. Zhou, T. Kempka and R. Lewis, “A re-commissioned flexible full-scale wheel/rail test facility,” in *Contact Mechanics (CM2018)*, Delft, 2018.

[68] D. T. Eadie, H. Harrison, R. Kempka, R. Lewis, A. Keylin and N. Wilson, “Field assessment of friction and creepage with a new tribometer,” in *Contact Mechanics (CM2018)*, Delft, 2018.

[69] S. Lewis, R. Lewis, P. Richards and L. Buckley-Johnstone, “Investigation of the isolation and frictional properties of hydrophobic products on the rail head, when used to combat low adhesion,” *Wear,* vol. 314, pp. 213-219, 2014.

[70] P. Somasundaran and P. Purohit, “Effect of Surfactand and Polymer Nanostructures on Frictional Properties,” in *Surfactants in Tribology*, Boca Raton, CRC Press, 2008, pp. 431-436.

[71] H. Spikes and P. Cann, “The development and application of the spacer layer imaging method for measuring lubricant film thickness,” *Proc Instn Mech Engrs,* vol. 215, pp. 261-277, 2001.

[72] R. Kapadia, R. Glyde and Y. Wu, “In situ observation of phosporous and non-phosphorous antiwear films using a mini traction machine with spacer layer image mapping,” *Tribology International,* vol. 40, pp. 1667-1679, 2007.

[73] H. L. Costa and H. A. Spikes, “Impact of ethanol on the formation of antiwear tribofilms from engine lubricants,” *Tribology International,* vol. 93, pp. 364-376, 2016.

[74] M. Broster, C. Pritchard and D. A. Smith, “Wheel/Rail Adhesion: its relation to rail contamination on british railways,” *Wear,* vol. 29, pp. 309-321, 1974.

[75] T. Nakahara, K.-S. Baek, H. Chen and M. Ishida, “Relationship between surface oxide layer and transient traction characteristics for two steel rollers under unlubricated and water lubricated

conditions," *Wear,* vol. 271, pp. 25-31, 2011.

[76] Y. Zhu, U. Olofsson and H. Chen, "Friction Between Wheel and Rail: A Pink-On-Disc Study of Environmental Conditions and Iron Oxides," *Tribology Letters,* vol. 52, pp. 327-339, 2013.

[77] G. Shuatak, A. J. Domb and D. Mandler, "n-Alkanoic Acid Monolayers on 316L Stainless Steel Promote the Adhesion of Electropolymerized Polypyrrole Films," *Langmuir,* vol. 22, pp. 5237-5240, 2006.

[78] G. Shustak, A. J. Domb and D. Mandler, "Preparation and Characterization of n-Alkanoic Acid Self-Assembled Monolayers Adsorbed on 316L Stainless Steel," *Langmuir,* vol. 20, pp. 7499-7506, 2004.

[79] A. Raman, M. Dubey, I. Gouzman and E. S. Gawalt, "Formation of Self-Assembled Monolayers of Alkylphosphonic Acid on the Native Oxide Surface of SS316L," *Langmuir,* vol. 22, pp. 6469-6472, 2006.

[80] E. Vollebregt, "Numerical modeling of measured railway creep versus creep-force curves with CONTACT," *Wear,* vol. 314, pp. 87-95, 2014.

[81] O. Polach, "Creep forces in simulations of traction vehicles running on adhesion limit," *Wear,* vol. 258, pp. 992-1000, 2005.

[82] C. Tomberger, P. Diermaier, W. Sextro and K. Six, "Friction in wheel-rail contact: A model comprising interfacial fluids, surface roughness and temperature," *Wear,* vol. 271, pp. 2-12, 2011.

[83] Z. Shen and Z. Li, "A fast non-steady state creep force model based on the simplified theory," *WEAR,* vol. 191, pp. 242-244, 1996.

[84] M. Spiryagin, O. Polach and C. Cole, "Creep force modelling for rail traction vehicles based on the Fastsim algorithm," *Vehicle System Dynamics,* vol. 51, pp. 1765-1783, 2013.

[85] T. Beagley, "The rheological properties of solid rail contaminants and their effect on wheel / rail ashesion," *Proceedings of the institute of mechanical engineers,* vol. 190, pp. 419-430, 1976.

[86] H. Chen, M. Ishida and T. Nakahara, "Analysis of adhesion under wet conditions for three-dimensional contact considering surface roughness," *Wear,* vol. 258, pp. 1209-1216, 2005.

[87] R. I. Popovici, "PhD Thesis: Friction in Wheel - Rail Contacts," University of Twente, Enschede, The Netherlands, 2010.

[88] B. Wu, Z. Wen, H. Wang and X. Jin, "Numerical analysis on wheel/rail adhesion under mixed contamination of oil and water with surface roughness," *Wear,* vol. 314, pp. 140-147, 2014.

[89] G. Trummer, L. Buckley-Johnstone, P. Voltr, A. Meierhofer, R. Lewis and K. Six, "Wheel-rail creep force model for predicting water induced low adhesion phenomena," *Tribology International,* vol. 109, pp. 409-415, 2017.

[90] D. I. Fletcher and T. A. Battashi, "Adhesion dependence on water dispersion and rail

wettability," *10th International Conference on Contact Mechanics and Wear of Rail/Wheel System,* 2015.

[91] S. Lewis, R. Lewis, P. Richards and L. Buckley-Johnstone, "Investigation of the isolation and frictional properties of hydrophobic products on the rail head, when used to combat low adhesion," *Wear,* vol. 314, pp. 213-219, 2014.

[92] N. Somashekara, Z. Saiyed and C. Ramchand, "Biochemistry of railhead leaf film formation," RSSB, 2006 (2007 Issue 2).

[93] U. Olofsson and R. Lewis, "Tribology of the Wheel - Rail Contact," in *Handbook of Railway Vehicle Dynamics*, Boca Raton, CRC Press, 2006, pp. 121-142.

[94] R. Lewis, R. Dawyer - Joyce and J. Lewis, "Disk Machine Study of Contact Isolation During Railway Track Sanding," *Proc. IMechE Part F: J. Railway and Rapid Transit,* vol. 217, pp. 11-24, 2003.

[95] R. Galas, M. Omasta, I. Krupka and M. Hartl, "Laboratory investigation of ability of oil-based friction modifiers to control adhesion at wheel-rail interface," *Wear,* Vols. 368-369, pp. 230-238, 2016.

[96] J. Lundberg, M. Rantatalo, C. Wanhainen and J. Casselgren, "Measurements of friction coefficients between rails lubricated with a friction modifier and the wheels of an IORE locomotive during real working conditions," *Wear,* Vols. 324-325, pp. 109-117, 2015.

[97] S. Lewis, R. Lewis, J. Cotter, X. Lu and D. Eadie, "A New Method for the Assessment of Traction Enhancers and the Generation of Organic Layers in Twin-Disc Machine," *10th International Conference on Contact Mechanics,* 2015.

[98] W. Callister, "Phase transformations in Metals," in *Materials science and engineering: an introduction - 7th ed.*, John Wiley & Sons, Inc., 2007, pp. 311-352.

[99] Committee, Iron and Steel Standards Policy, "BS 5892-3," British Standards Institution, London, 1992 , 2009.

[100] D. Godfrey, "Iron oxides and rust (hydrated iron oxides) in tribology," *Journal of the society of tribologists and lubrication engineers,* vol. 55, pp. 33-37, 1999.

[101] R. Cornell, The iron oxides: structure, properties, reactions, occurrence and uses, Cambridge: Wienheim, 1996.

[102] N. Somashekara, Z. Saiyed and C. Ramchand, "Biochemistry of railhead leaf film contamination," RSSB, 2006.

[103] Ministry of Defence, "MOD UK Railways - Permanent Way Design and Maintenance Policy and Standards," Defence Movements & Transportation Policy Division, Bristol, 2009.

[104] B. G. Delgado, A. Viana da Fonseca, E. Fortunato and P. Maia, "Mechanical behaviour of inert steel slag ballast for heavy haul rail track: Laboratory evaluation," *Transportation Geotechnics,* vol. 20, p. 100234, 2019.

[105] C. Ditzler, K. Scheffe and H. Monger, “Chapter 3: Examination and Description of Soil Profiles,” in *Soil Survey Manual*, Washington, D.C., United States Department of Agriculture, 2017, pp. 83-233.

[106] S. W. Buol, R. J. Southard, R. C. Graham and P. A. McDaniel, “Modern Soild Classification Systems,” in *Soil Genesis and Classification*, Sixth Edition ed., New Jersey, John Wiley & Sons, Inc., 2011, pp. 181-205.

[107] S. Descartes, A. Saulot, C. Godeau, S. Bondeux, C. Dayot and Y. Berthier, “Wheel flange/rail gauge corner contact lubrication: Tribological investigations,” *Wear,* vol. 271, pp. 54-61, 2011.

[108] H. Chen, S. Fukagai, Y. Sone, T. Ban and A. Namura, “Assessment of lubricant applied to wheel/rail interface in curves,” *Wear,* vol. 314, pp. 228-235, 2014.

[109] B. White, R. Nilsson, U. Olofsson, A. Arnall, M. Evans, T. Armitage, J. Fisk, D. Fletcher and R. Lewis, “A Study into the effect of the Presence of Moisture at the Wheel/Rail Interface During Dew and Damp Conditions,” *Proceedings of the Institution of Mechanical Engineers. Part F: Journal of Rail and Rapid Transit,* 2017.

[110] L. Taiz, E. Zeiger, I. Møller and A. Murphey, “Plant and Cell Architecture,” in *Plant Physiology and Development*, Sunderland, MA, Sinauer Associates, Inc, 2015, pp. 1-50.

[111] A. Smith, G. Coupland, L. Dolan, N. Harberd, J. Jones, C. Martin, R. Sablowski and A. Amey, “Cells,” in *Plant Biology*, New York, Garland Science, 2010, pp. 91-166.

[112] X. Yang, J. Tang, J. Mustard, J. Wu, K. Zhao, S. Serbin and J.-E. Lee, “Seasonal variability of multiple leaf trates captured by leaf spectroscopy at two temperate diciduous forests,” *Remote Sensing of Environment,* vol. 179, pp. 1-12, 2016.

[113] A. Ravve, “Naturally Occuring Polymers,” in *Principles of Polymer Chemistry*, New York, Springer, 2000, pp. 357-565.

[114] K. Mesa, S. Serra, A. Masia, F. Gagliardi, D. Bucci and S. Musacchi, “Seasonal trends of starch and soluble carbohydrates in fruits and leaves of 'Abbé Fétel pear trees and their relationship to fruit quality parameters,” *Scientia Horticulturae,* vol. 211, pp. 60-69, 2016.

[115] W. Forsythe, M. Garrett, C. Hardacre, M. Nieuwenhuyzen and G. Sheldrake, “An efficient and flexible synthesis of model lignin oligomers,” *Green Chemistry,* vol. 15, pp. 3031-3038, 2013.

[116] P. Schofield, D. Mbugua and A. Pell, “Analysis of condensed tannins: a review,” *Animal Feed Science and Technology,* vol. 91, pp. 21-40, 2001.

[117] A. Smith, G. Coupland, L. Dolan, H. N., J. Jones, C. Martin, R. Sablowski and A. Amey, “Development,” in *Plant Biology*, New York, Garland Science, 2010, pp. 301-375.

[118] A. Gellman and N. Spencer, “Surface chemistry in tribology,” *Proceedings of the Institute of Mechanical Engineers, Part J: Engineering Tribology,* vol. 216, no. 1, pp. 433-461, 2002.

[119] S. Jahanmir, “Chain Length Effects in Boundary Lubrication,” *Wear 102,* pp. 331 - 349, 1985.

[120] J. Gregory, “Report A74,” C.S.I. Tribophysics Division, Australia, 1943.

[121] F. P. Bowden and F. Tabor, “Boundary Friction of Lubricated Metals,” in *The Friction and Lubrication of Solids*, Oxford, Clarendon Press, 1950, pp. 176-199.

[122] S. Yazawa, I. Minami and P. Braham, “Reducing Friction and Wear of Tribological Systems through Hybrid Tribofilm Consisting of Coatings and Lubrication,” *Lubricants,* vol. 2, pp. 90-112, 2014.

[123] M. A. Nicholls, T. Do, P. R. Norton, M. Kasrai and G. M. Bancroft, “Review of the lubrication of metallic surfaces by zinc dialkyl-dithiophosphates,” *Tribology International,* vol. 38, pp. 15-39, 2005.

[124] G. Parkinson, “Iron oxide surfaces,” *Surface Science Reports,* vol. 71, pp. 272-365, 2016.

[125] O. Gamba, H. Noei, J. Pavelec, R. Bliem, M. Schmid, U. Diebold, A. Stierle and G. Parkinson, “Adsorption of Formic Acid on the Fe3O4(001) Surface,” *Journal of Physical Chemistry C,* vol. 119, pp. 20459-20465, 2015.

[126] J. N. Tilton, R. H. Perry, D. E. Ackers and D. W. Green, “Fluid and Particle Dynamics,” in *Perry's Chemical Engineers' Handbook*, 8th ed., New York, McGraw-Hill, 2008, pp. 6-4 - 6-9.

[127] J. W. Anthony, R. A. Bideaux, K. W. Bladh and M. C. Nichols, “Handbook of Mineralogy,” Mineralogical Society of America, Chantilly, VA 20151-1110, USA, 2003.

[128] D. P. Kalman, B. A. Rosen and N. J. Wagner, “Effects of Particle Hardness on Shear Thickening Colloidal Suspension Rheology,” *The XVth International Congress on Rheology,* pp. 1408-1410, 2008.

[129] D. V. Gutsulyak, L. J. Stanlake and H. Qi, “Twin Disc evaluation of third body materials in the wheel/rail interface,” in *11th International Conference on Contact Mechanics and Wear of Rail/Wheel Systems*, Delft, 2018.

[130] M. Ratoi, V. Anghel, C. Bovington and H. Spikes, “Mechanisms of oiliness additives,” *Tribology International,* vol. 33, pp. 241-247, 2000.

[131] G. Stachowiak and A. Batchelor, “Boundary and Extreme Pressure Lubrication,” in *Engineering Tribology*, Oxford, Butterworth-Heinemann, 2013, pp. 371-428.

[132] T. Beagley, I. McEwen and C. Pritchard, “Wheel/Rail Adhesion - The influence of railhead debris,” *Wear,* vol. 33, pp. 141-152, 1975.

[133] R. W. Binkley and E. R. Binkley, “Radical Reactions of Carbohydrates: Volume II Radical Reactions in Carbohydrate Synthesis,” LibreTexts, 5th June 2019. [Online]. Available: https://chem.libretexts.org/Bookshelves/Organic_Chemistry/Book%3A_Radical_Reactions_of_Carbohydrates_(Binkley)/II%3A_Radical_Reactions_of_Carbohydrates/07%3A_Unprotected_Carbohydrates/VII._Reactions_of_Polysaccharides. [Accessed 20 July 2019].

[134] X. Kong, P. Zhu, Z. Sui and J. Bao, “Physicochemical properties of starches from diverse rice cultivars varying in apparent amylose content and gelatinisation temperature combinations,” *Food Chemistry,* vol. 172, pp. 433-440, 2015.

[135] T. Fawcett, F. Needham, C. Crowder and S. Kabekkodu, “ICDD: PDF-4+ (Database),” *Proceedings of the 10th National Conference on X-Ray Diffraction and ICDD Workshop,* pp. 1-3, 2009.

[136] L. K. Bogart, C. Blanco-Andujar and Q. A. Pankhurst, “Environmental oxidative aging of iron oxide nanoparticles,” *Applied Physics Letters,* vol. 113, no. 13, 2018.

[137] Ordinance Survey, *Online Standard Map, Grid Ref: SP 150 466 to SP 160 479,* Southampton: Ordinance Survey Limited, 2019.

[138] H. Lin, H. Sakamoto, W. Seo, K. Kuwabara and K. Kumoto, “Crystal growth of lepidocrocite and magnetite under Langmuir monolayers,” *Journal of Crystal Growth,* vol. 192, pp. 250-256, 1998.

[139] R. A. Antunes, I. Costa and D. L. Araújo de Faria, “Characterisation of Corrosion Products Formed on Steels in the First Months of Atmospheric Exposure,” *Materials Research,* vol. 6, no. 3, pp. 403-408, 2003.

[140] D. R. Lide, “Section 15: Practical Laboratory Data: Coefficients of Friction,” in *CRC Handbook of Chemistry and Physics*, Boca Raton, CRC Press, 2005, pp. 15-50.

[141] C. Jessop and J. Ahlström, “Friction between pearlitic steel surfaces,” *Wear,* Vols. 432-433, pp. 1-9, 2019.

[142] L. Buckley-Johnstone, G. Trummer, P. Voltr, A. Meierhofer, K. Six, D. Fletcher and R. Lewis, “Assessing the impact of small amounts of water and iron oxides on adhesion in the wheel/rail interface using High Pressure Torsion testing,” *Tribology International,* vol. 135, pp. 55-64, 2019.

[143] W. Wang, T. Liu, H. Wang, L. Q.Y., M. Zhu and X. Jin, “Influence of friction modifiers on improving adhesion and surface damage of wheel/rail under low adhesion conditions,” *Tribology International,* vol. 75, pp. 16-23, 2014.

Appendix A – quantitative paper evaluation form

Paper reference number: _____

Quantitative Paper Evaluation

Paper Title:

Authors:

Publisher:

Date:

Categories:

Primary	Secondary	Tertiary

Notes / Comments:

Scoring:

Peer reviewed publication	Theory tested and supported	Conclusions in paper evidenced	Scale test	Full size test

Score: _____

Appendix B – paper scoring table

	Topic Categories			Scoring Criteria*					
Paper Ref.	**Primary**	**Secondary**	**Tertiary**	**A**	**B**	**C**	**D**	**E**	**Score**
[23]	Causes	Water	-	Y	Y	Y	Y	Y	5
[20]	Causes	Water	-	Y	Y	Y	Y		4
[29]	Causes	Water	-	Y	Y	Y	Y	Y	5
[30]	Causes	Water	-	Y	Y	Y	Y		4
[22]	Causes	Water	-	Y	Y	Y	Y	Y	5
[32]	Causes	Water	-	Y	Y	Y	Y		4
[34]	Causes	Oil & Grease	-	Y	Y	Y	Y		4
[88]	Causes	Oil & Grease	-	Y	Y	Y		Y	4
[30]	Causes	Oil & Grease	-	Y	Y	Y	Y		4
[52]	Causes	Oxides/Debris	-	Y	Y	Y	Y		4
[30]	Causes	Oxides/Debris	-	Y	Y	Y	Y		4
[132]	Causes	Oxides/Debris	-	Y	Y	Y	Y		4
[51]	Causes	Oxides/Debris	-	Y	Y	Y	Y		4
[46]	Causes	Oxides/Debris	-	Y	Y	Y	Y	Y	5
[36]	Causes	Leaves	-	Y	Y	Y	Y		4
[37]	Causes	Leaves	-	Y	Y	Y	Y		4
[38]	Causes	Leaves	-	Y	Y	Y			3
[39]	Causes	Leaves	-	Y	Y	Y	Y		4
[40]	Causes	Leaves	-	Y	Y	Y		Y	4
[43]	Causes	Leaves	-	Y	Y	Y	Y		4
[118]	Surface Chemistry	Boundary Lubrication	-	Y	Y	Y	Y		4
[24]	Surface Chemistry	Boundary Lubrication	-	Y	Y	Y			3
[119]	Surface Chemistry	Boundary Lubrication	-	Y	Y	Y			3
[120]	Surface Chemistry	Boundary Lubrication	-	Y	Y	Y			3
[121]	Surface Chemistry	Boundary Lubrication	-	Y	Y	Y			3
[130]	Surface Chemistry	Viscous near-surface effects	-	Y	Y	Y	Y		4
[118]	Surface Chemistry	Viscous near-surface effects	-	Y	Y	Y	Y		4
[131]	Surface Chemistry	Viscous near-surface effects	-	Y	Y	Y			3
[122]	Surface Chemistry	Complex layer formation	-	Y	Y	Y			3
[123]	Surface Chemistry	Complex layer formation	-	Y	Y	Y			3
[69]	Surface Chemistry	Complex layer formation	-	Y	Y	Y	Y		4
[80]	Numerical Modelling	CONTACT	-	Y	Y	Y		Y	4
[84]	Numerical	Spiryagin	-	Y	Y	Y	Y	Y	5

	Modelling								
[83]	Numerical Modelling	FASTSIM	-	Y	Y	Y	Y	Y	5
[82]	Numerical Modelling	Tomberger	-	Y	Y	Y	Y	Y	5
[12]	Numerical Modelling	ECF	-	Y	Y	Y	Y	Y	5
[85]	Numerical Modelling	Beagley	-	Y	Y	Y	Y	Y	5
[86]	Numerical Modelling	Chen	-	Y	Y	Y	Y	Y	5
[87]	Numerical Modelling	Popovici	-	Y	Y	Y	Y	Y	5
[88]	Numerical Modelling	Wu	-	Y	Y	Y	Y	Y	5
[69]	Abatement	Prevention	Hydrophobic	Y	Y	Y	Y		4
[90]	Abatement	Prevention	Hydrophilic	Y	Y	Y	Y		4
[14]	Abatement	Prevention	Trackside Management	Y	Y	Y			3
[92]	Abatement	Prevention	Chemical Treatment		Y	Y			2
[61]	Abatement	Mitigation	Sand	Y	Y	Y	Y	Y	5
[14]	Abatement	Mitigation	Sand	Y	Y	Y	Y		4
[94]	Abatement	Mitigation	Sand	Y	Y	Y	Y		4
[8]	Abatement	Mitigation	Friction Modifiers	Y	Y	Y	Y		4
[97]	Abatement	Mitigation	Traction Gels	Y	Y	Y	Y		4
[93]	Abatement	Mitigation	Railhead Cleaning	Y	Y	Y	Y		4
[73]	Test Methods	Tribotests	MTM-SLIM	Y	Y	Y	Y		4
[56]	Test Methods	Tribotests	Pin-on-Disc	Y	Y	Y	Y		4
[57]	Test Methods	Tribotests	Pin-on-Disc	Y	Y	Y	Y		4
[58]	Test Methods	Tribotests	MTM	Y	Y	Y	Y		4
[63]	Test Methods	Tribotests	HPT	Y	Y	Y	Y		4
[65]	Test Methods	Tribotests	Full-Scale	Y	Y	Y	Y	Y	5
[56]	Test Methods	Tribotests	Twin-Disc	Y	Y	Y	Y		4
[61]	Test Methods	Tribotests	Twin-Disc	Y	Y	Y	Y	Y	5
[69]	Test Methods	Tribotests	Field	Y	Y	Y	Y		4
[71]	Test Methods	Analysis	UFI	Y	Y	Y			3
[72]	Test Methods	Analysis	SLIM	Y	Y	Y			3
[73]	Test Methods	Analysis	SLIM	Y	Y	Y			3
[34]	Test Methods	Analysis	ESR	Y	Y	Y	Y		4
[35]	Test Methods	Analysis	IR	Y	Y	Y	Y		4
[52]	Test Methods	Analysis	SEM	Y	Y	Y	Y		4
[52]	Test Methods	Analysis	EDS	Y	Y	Y	Y		4
[46]	Test Methods	Analysis	XRD	Y	Y	Y	Y	Y	5
[47]	Test Methods	Analysis	Raman	Y	Y	Y	Y		4
[40]	Test Methods	Analysis	GE-DOS	Y	Y	Y	Y		4
[40]	Test Methods	Analysis	XPS	Y	Y	Y	Y		4
[78]	Test Methods	Analysis	CA	Y	Y	Y	Y		4

*Scoring Criteria: Peer reviewed publication, A; Theory tested and supported, B; Conclusions in paper evidenced, C; Scale test, D; Full size test, E.

Appendix C – Environmental monitoring data overview

Unless stated otherwise:

- RED lines indicate railhead temperatures
- YELLOW lines indicate environment temperatures
- BLUE lines indicate dew-point temperatures

QRTC, 10th October – 12th October 2017:

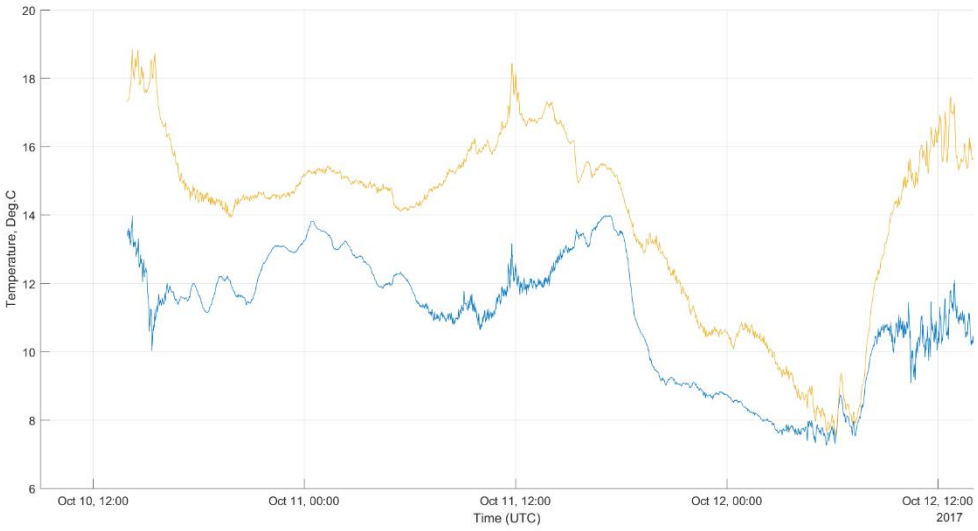

Figure 167, Station 1 (raised steps) environment and dew point temperatures

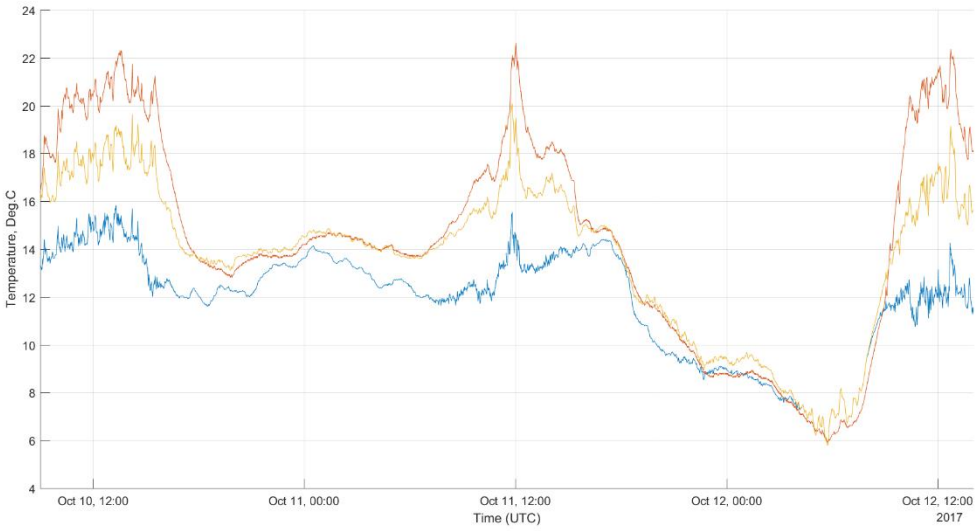

Figure 168, Station 2 (on grass by testing area) railhead, environment and dew point temperatures

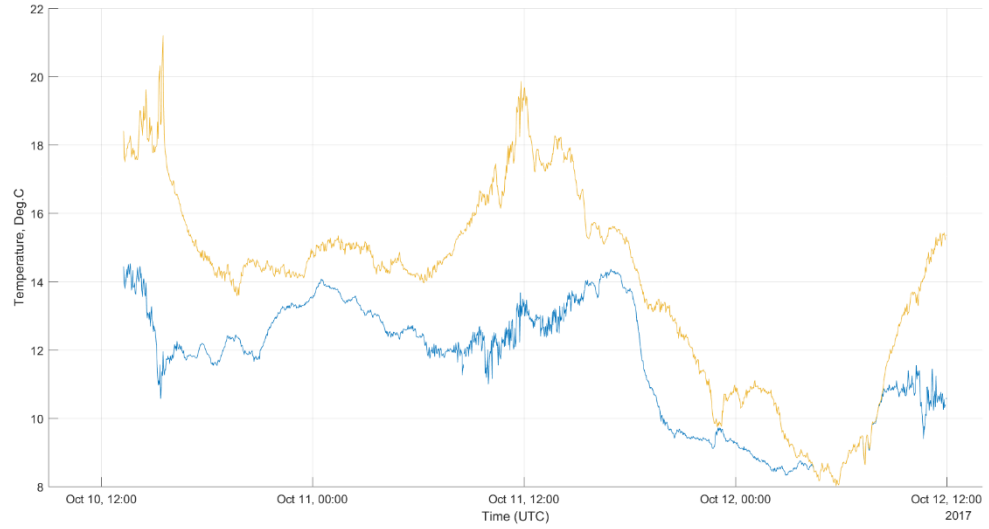

Figure 169, Station 3 (in the tree clearing) environment and dew point temperatures

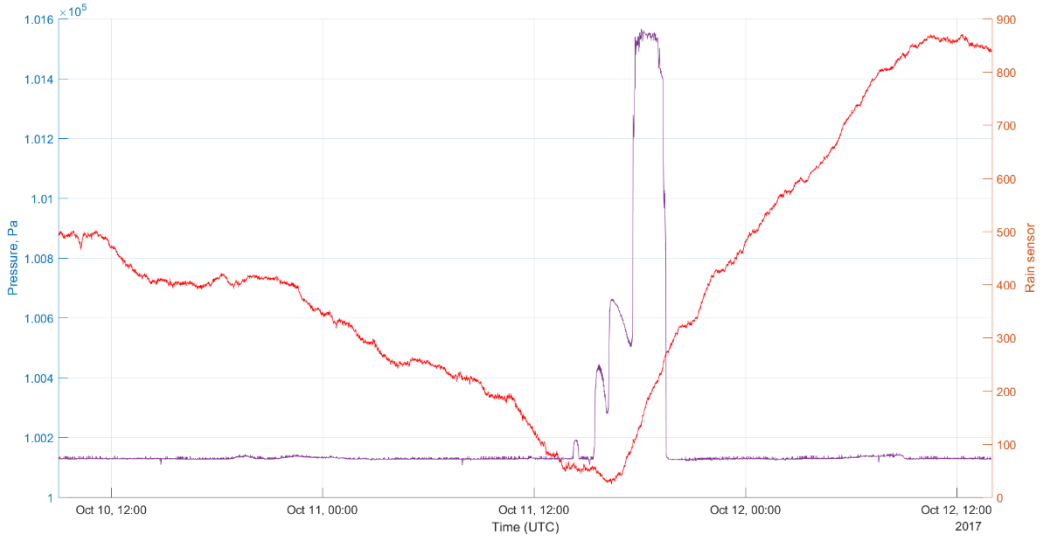

Figure 170, All stations pressure (Pa, red line) and rainfall (arbitrary units, purple line) measurements

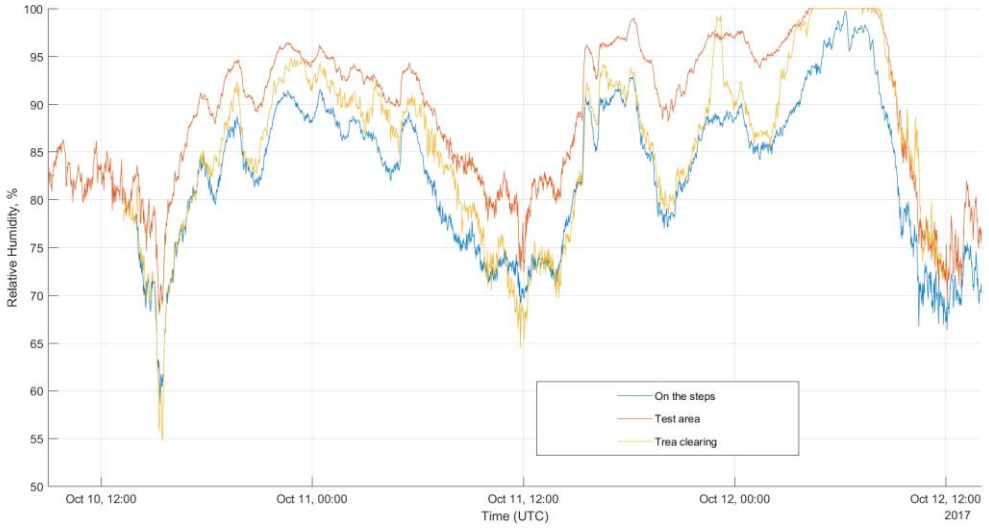

Figure 171, Relative humidity at stations 1, 2 and 3

QRTC, 22nd January – 11th February 2018:

Note: Station 1, on the raised steps, was not set up for this period.

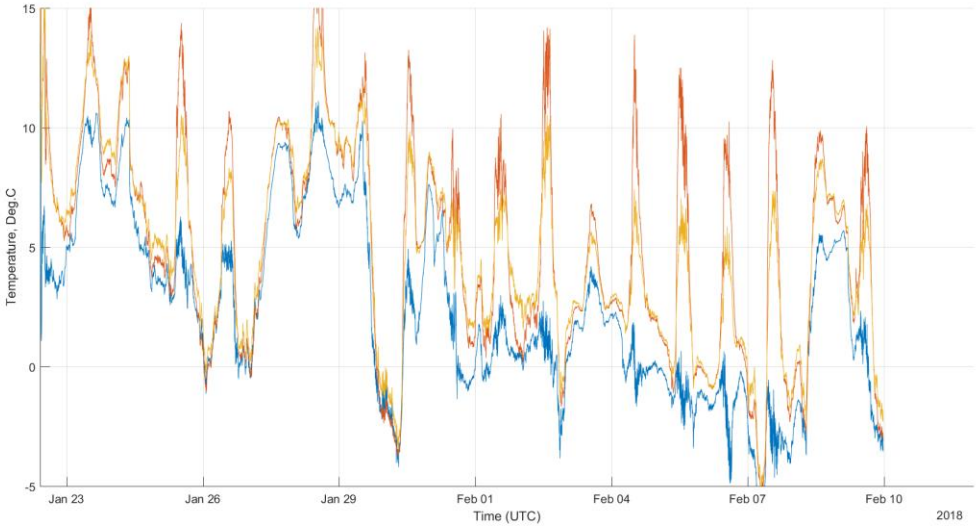

Figure 172, Station 2 (on grass by testing area) railhead, environment and dew point temperatures

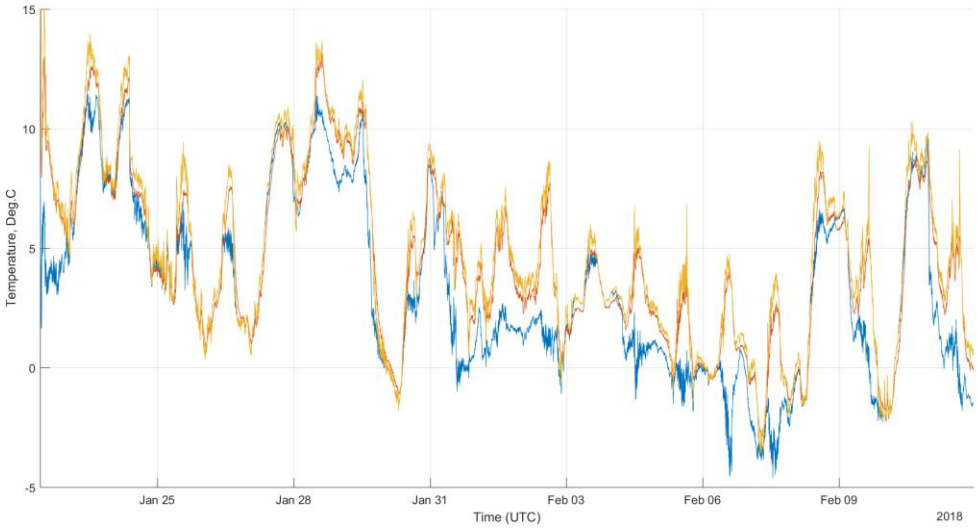

Figure 173, Station 3 (in the tree clearing) railhead, environment and dew point temperatures

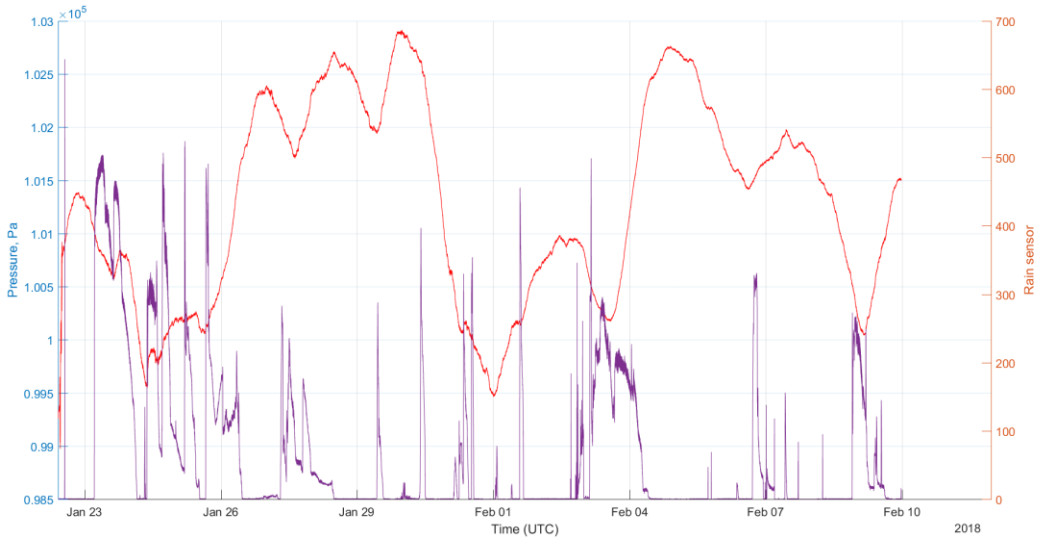

Figure 174, All stations pressure (Pa, red line) and rainfall (arbitrary units, purple line) measurements

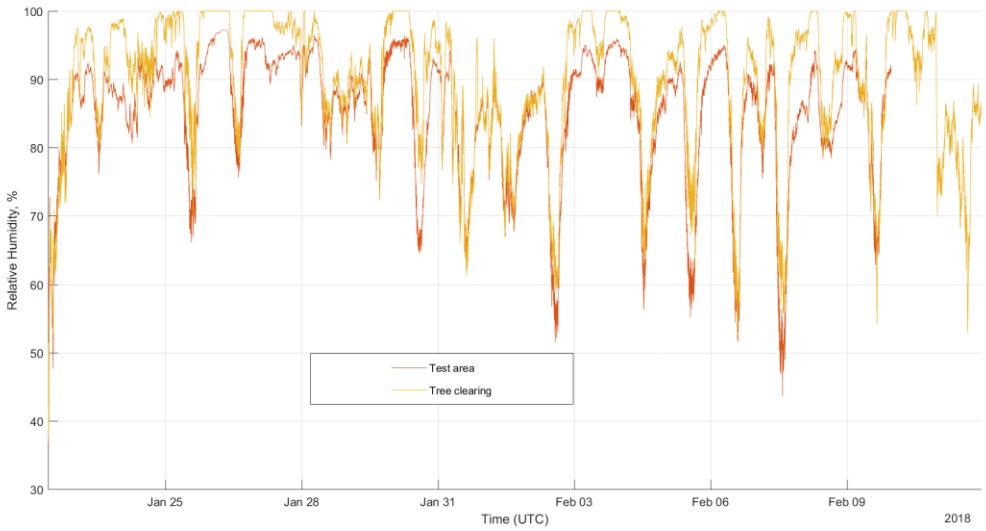

Figure 175, Relative humidity of stations 2 and 3

Royston, Barnsley, Rail Bridge 194, 10th October – 19th December 2017:

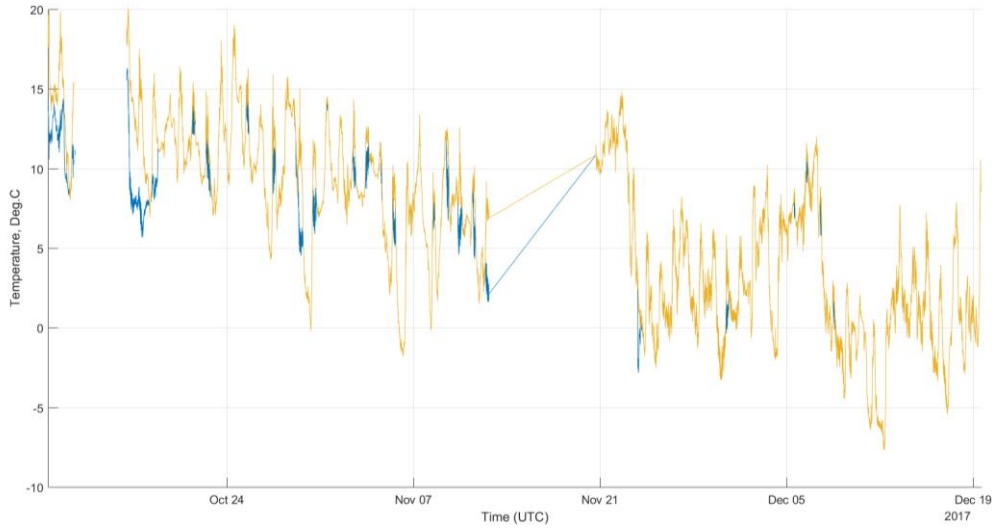

Figure 176, Environment and dew point temperatures

Figure 177, Pressure

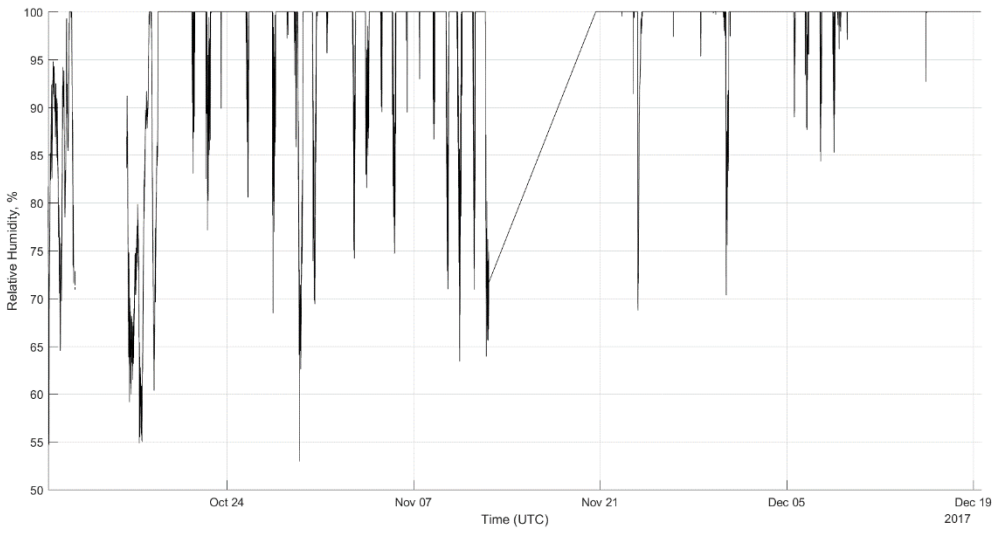

Figure 178, Relative humidity

Surrey B.C. Canada, 13th February 2018 17 – 3200hrs UTC (09 – 1500hrs local):

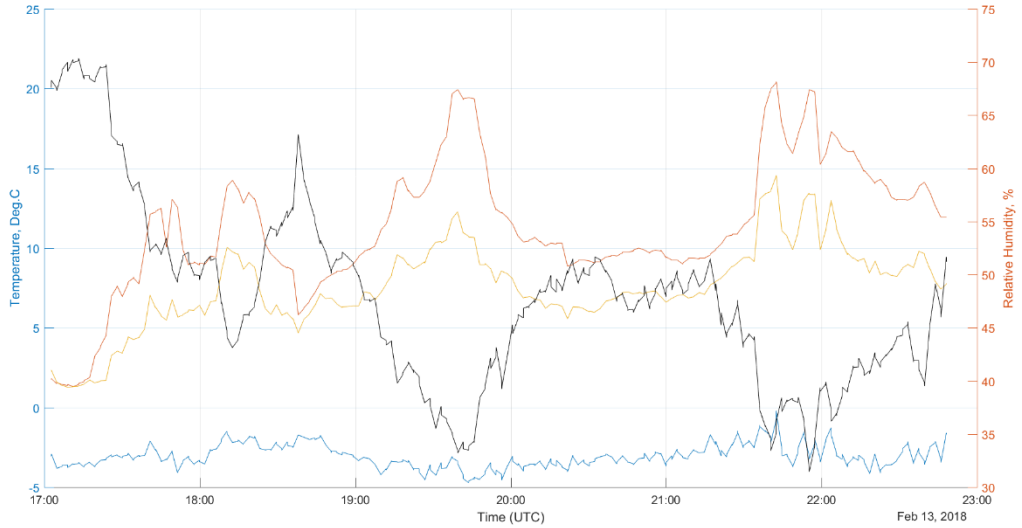

Figure 179, Temperatures (railhead, environment and dewpoint) and relative humidity (black line)

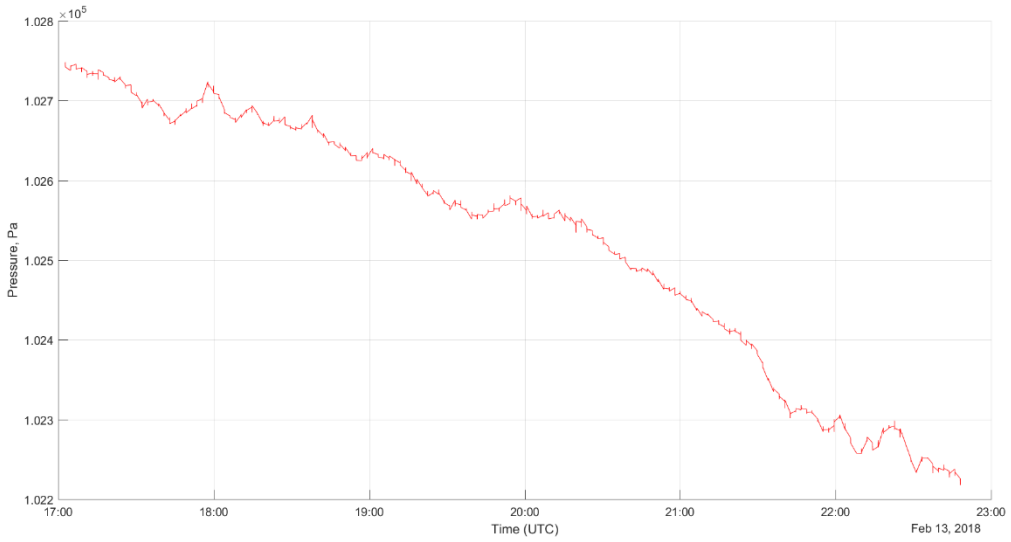

Figure 180, Pressure

Appendix D – SUROS runs

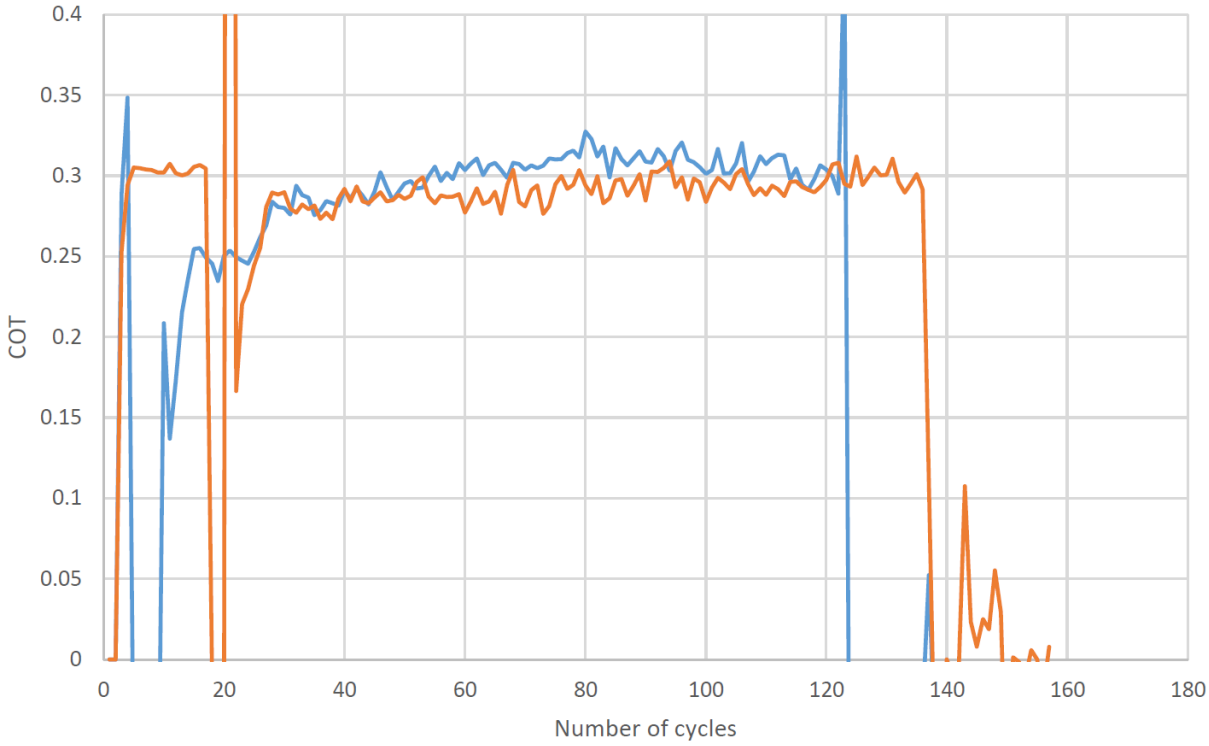

Figure 181, SUROS twin-disc tribo-testing runs, dry contact

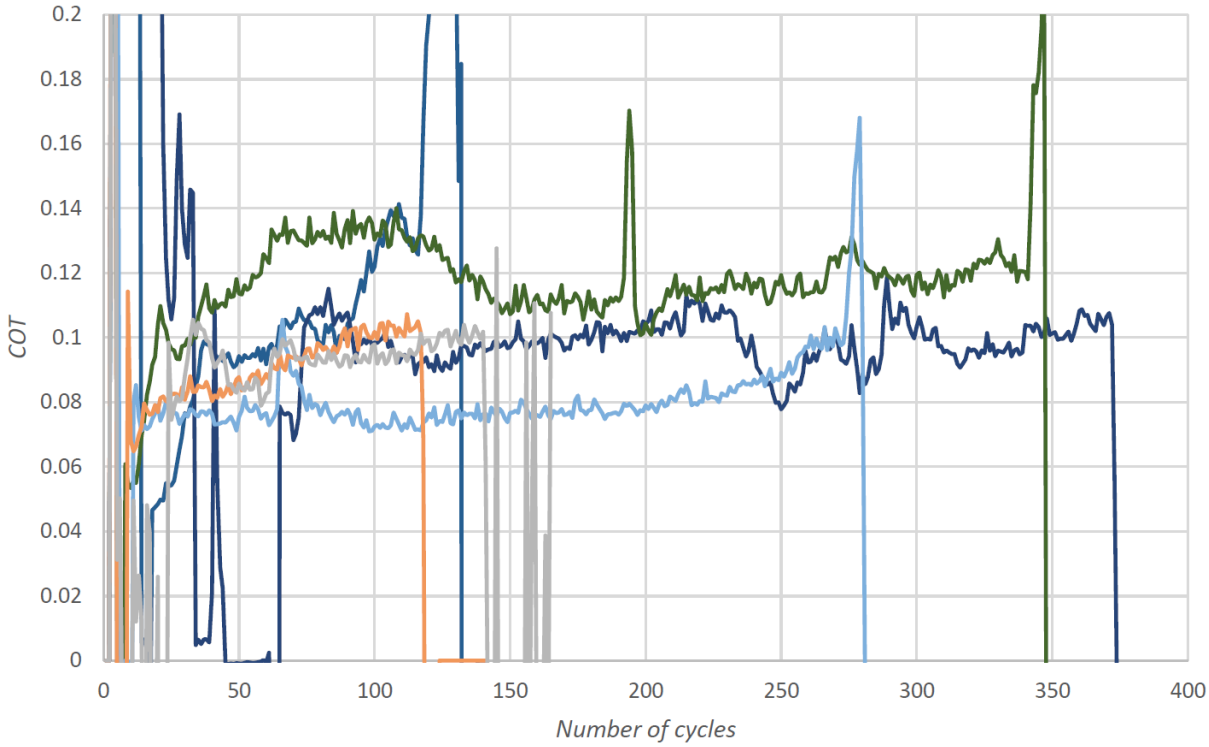

Figure 182, SUROS twin-disc tribo-testing runs, wet contact

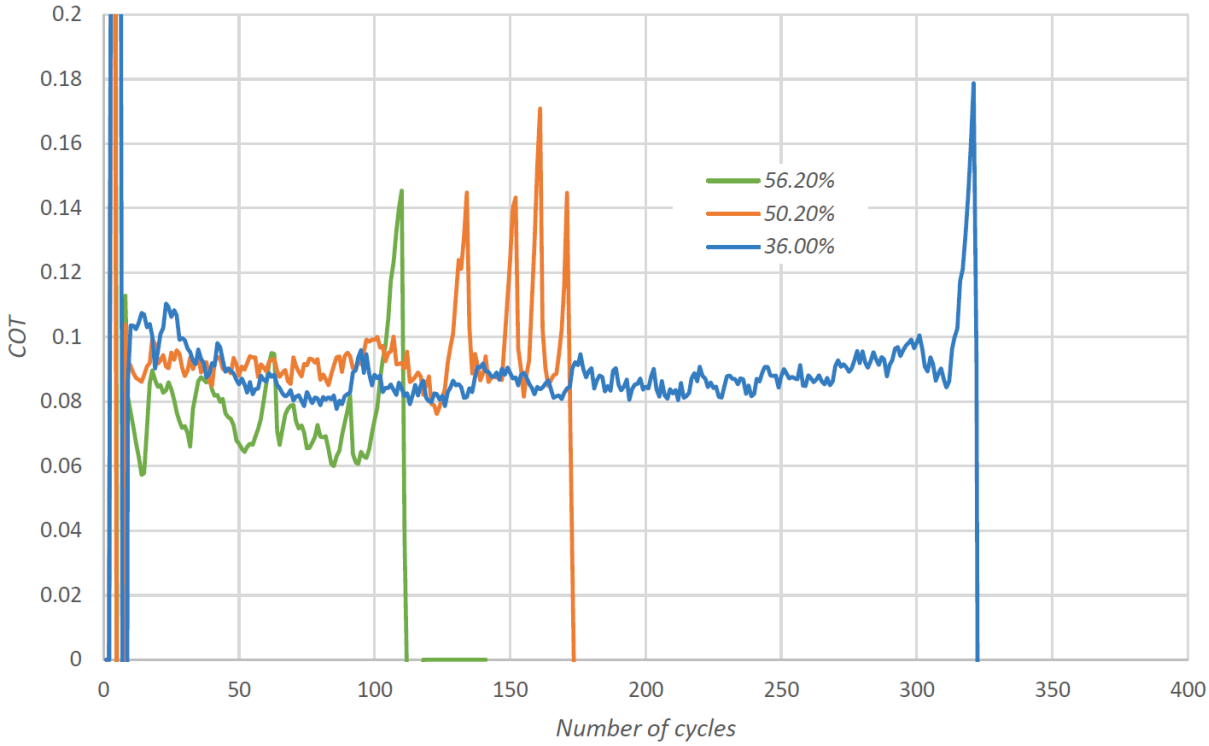

Figure 183, SUROS twin-disc tribo-testing runs, magnetite-water pastes of various oxide concentrations

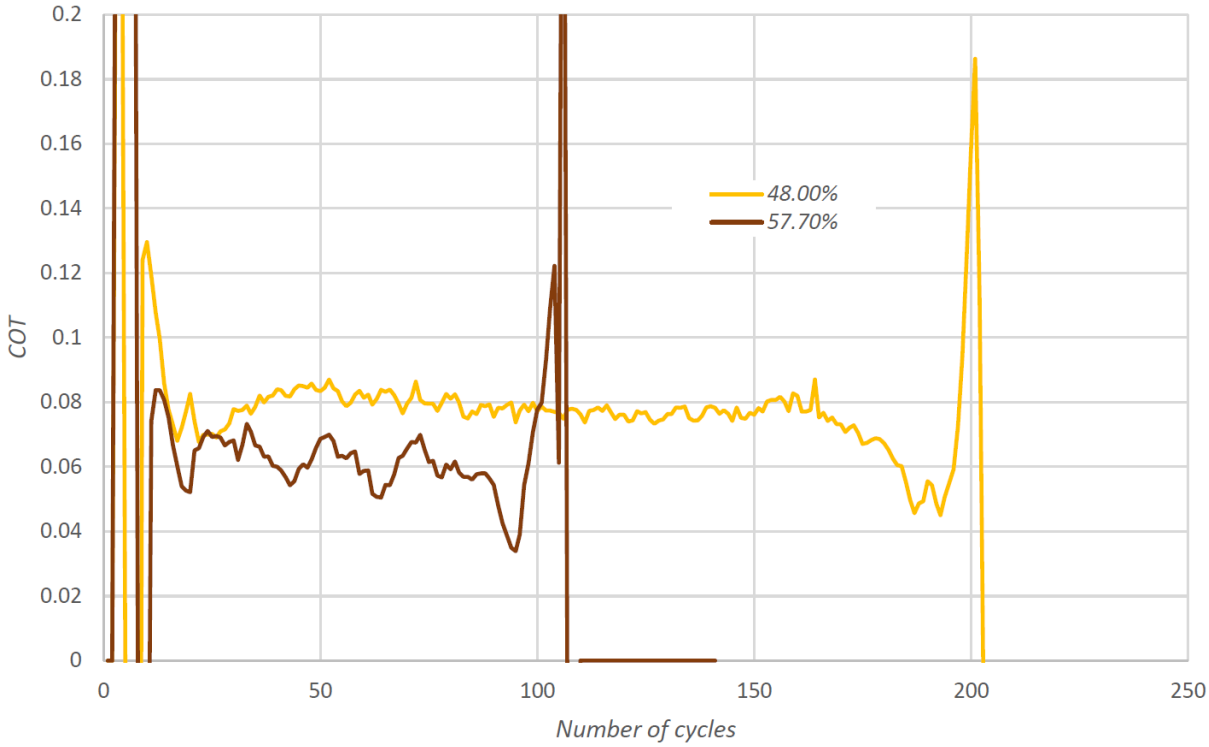

Figure 184, SUROS twin-disc tribo-testing runs, haematite-water pastes of various oxide concentrations

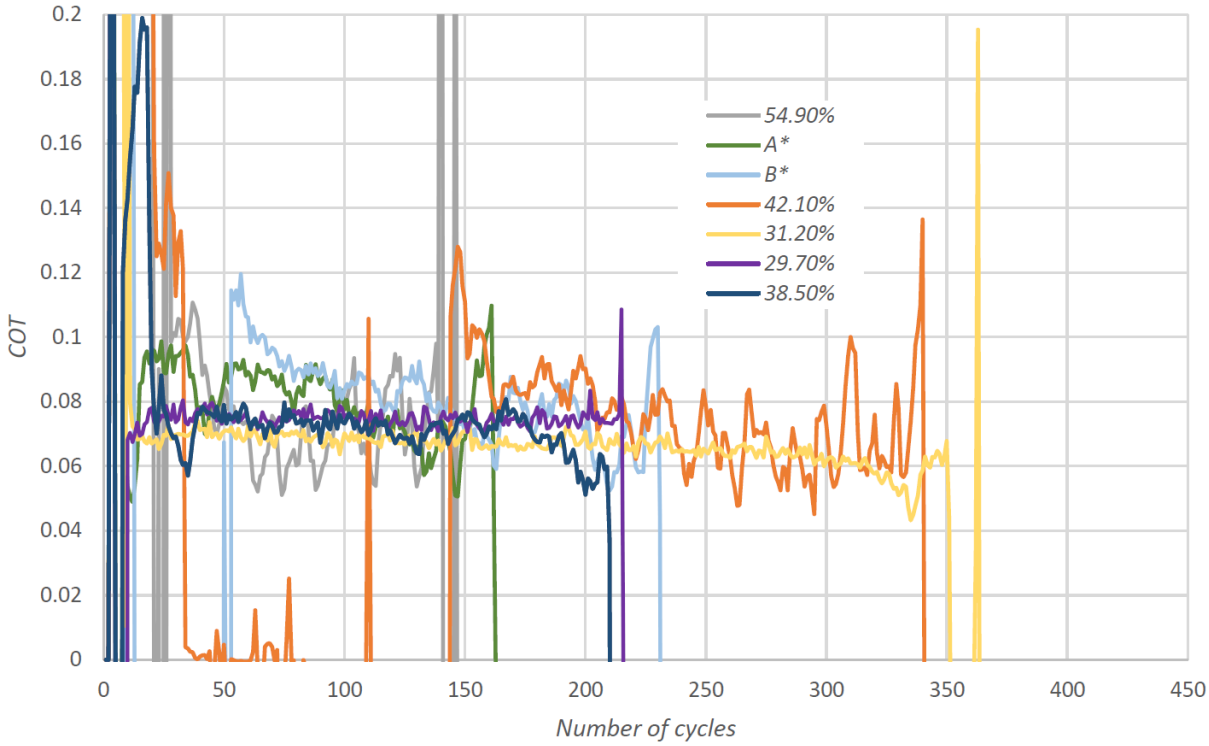

*Figure 185, SUROS twin-disc tribo-testing runs, goethite-water pastes of various oxide concentrations; *unknown oxide concentrations*

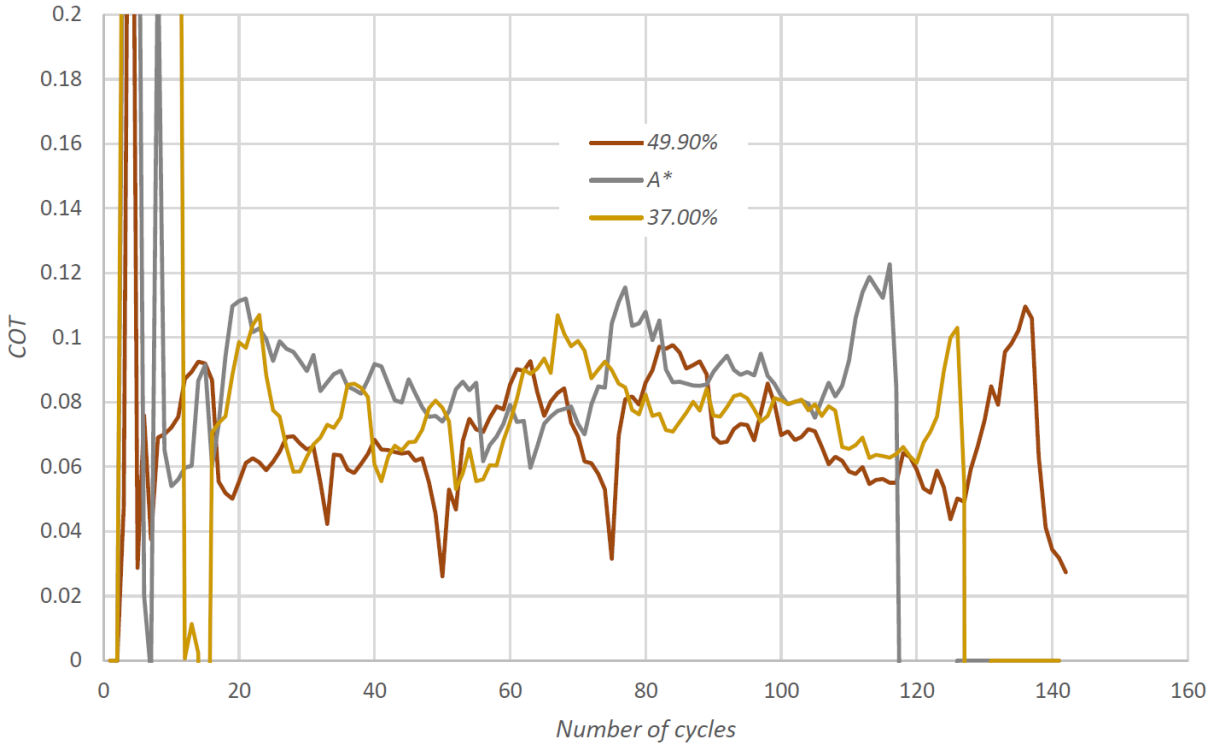

*Figure 186, SUROS twin-disc tribo-testing runs, lepidocrocite-water pastes of various oxide concentrations, *unknown oxide concentrations*